Implementation and Accuracy of Continuous Hybrid Simulation with Geographically Distributed Substructures

By

Gilberto Mosqueda
SUNY Buffalo

Bozidar Stojadinovic
University of California, Berkeley

Stephen Mahin
University of California, Berkeley

A Report on Research Conducted under Grant No. CMS-0086621
from the National Science Foundation

Earthquake Engineering Research Center
University of California, Berkeley

UCB/EERC 2005-02

Abstract

The hybrid simulation test method is a versatile technique for evaluating the seismic performance of structures by seamlessly integrating physical and numerical simulations of substructures into a single model. This test method has advanced considerably since its inception 30 years ago, moving from ramp-and-hold specimen loading to more realistic continuous and real-time loading histories. Further advancements are necessary to fully utilize the potential of the hybrid simulation test method. Specifically, larger and more complex structures can be tested by integrating advanced analytical modeling tools and physical models using a geographically distributed hybrid simulation testing method.

A control system is presented that supports the implementation of computationally demanding hybrid simulation algorithms including: continuous algorithms, real-time algorithms, and hybrid testing with geographically distributed substructures. The controller is based on an event-driven scheme, as opposed to a real-time clock-based scheme, that supports the implementation of continuous algorithms on distributed models where network communication, numerical integration and other tasks may have random completion times. The advantage of an event-driven approach is that logic can be included to minimize, if not eliminate, the adverse effects of random completion times on the stability and accuracy of the test. This procedure is demonstrated by computing the earthquake response of a two-story shear building model with two remote physical substructures connected using the Internet.

A rigorous investigation is carried out to evaluate the validity and reliability of the results from the hybrid simulations with geographically distributed substructures. The test results are compared to the results from a conventional local testing configuration and a pure numerical simulation. Both evaluation procedures indicate that reliable results can be obtained from network experiments and that the proposed distributed control system is effective. Additionally, a method is developed to estimate the reliability of the simulation results based on energy errors that accumulate in the experimental substructures. The proposed error indicators can be used to monitor experimental errors during a hybrid simulation, and provide a measure of confidence that assesses the quality of the results.

Acknowledgements

Support of this work through an NSF grant CMS-0086621 made within the George E. Brown Jr. Network for Earthquake Engineering Simulation (NEES) Program of the National Science Foundation is gratefully acknowledged. The authors also acknowledge the assistance of University of California, Berkeley graduate student Mr. Andreas Shellenberg and EERC laboratory personnel Mr. Don Clyde, Mr. Wes Neighbor and Mr. David McLam during experiment setup and hybrid testing. Any opinions, findings, and conclusions or recommendations expressed in this paper are those of the authors and do not necessarily reflect those of the National Science Foundation.

Table of Contents

List of Figures

List of Tables

1 Introduction

1.1 EXPERIMENTAL METHODS FOR STRUCTURES

In order to reduce the existing vulnerabilities of our nations infrastructure to seismic hazards, the earthquake engineering community needs to improve the current knowledge of the behavior of civil structures subjected to severe earthquake shaking. The experimental evaluation of existing and new seismic design methodologies provides the most effective means for the profession to understand, accept and utilize the new technologies in their design. For example, the widespread use of seismic isolation occurred only after a thorough examination of the technology through theoretical and experimental research (Kelly 1985).

There are three main experimental methods to evaluate the seismic performance of structures and components: shake table tests, quasi-static tests, and hybrid simulation. Shake table tests provide the most realistic means of subjecting a model structure to simulated earthquake loading. However, shake tables, especially with multi-degree of freedom capabilities, are expensive to build and limited in payload (Shing et al. 1996). The substantial reduction in scale required of models to be tested on shake tables remains as one of the major drawbacks to these types of tests. Quasi-static testing is a much simpler testing method that can be used to test structural members at large scales, but these tests require a predefined displacement history, that can later be difficult to relate to the seismic demands on the structure (Shing and Mahin 1984).

Hybrid simulation offers an alternative cost-effective solution for large-scale laboratory testing of structures under simulated earthquake loading. This test method can be used to evaluate the seismic performance of structures by smoothly integrating physical and numerical simulations of substructures into a single model. The principles of the hybrid simulation test method are rooted in the pseudo-dynamic testing method developed over the past 30 years (Takanashi 1975, Taka-

nashi and Nakashima 1987, Mahin et al. 1989, Shing et al. 1996, Magonette and Negro 1998, Royal Society 2001).

The research proposed herein seeks to increasing the complexity and scale-size of structural systems that can be evaluated using hybrid simulation with the George E. Brown Jr. Network for Earthquake Engineering Simulation (NEES) infrastructure. With NEESGrid, the network component of NEES, the capabilities of numerous equipment sites can be seamlessly combined to simulate the dynamic response of structural systems by simultaneously testing multiple large-scale experimental substructures. The developments presented in this report focus on reliable and efficient techniques for distributed testing.

1.2 HYBRID SIMULATION

Hybrid simulation combines numerical and experimental modeling techniques for the efficient and realistic evaluation of the seismic performance of structural systems. The hybrid simulation method comprises numerical simulations and simultaneous experimental testing of substructured components by integrating the dynamic equation of motion for the hybrid model. Typically, the subassemblages tested experimentally are portions of the structure that are difficult to model numerically, while components with predictable behavior are modeled on the computer. One significant advantage of hybrid simulation is that it removes a large source of uncertainty compared to pure numerical simulations by replacing structural element models that are not well understood with physical specimens on the laboratory test floor. Laboratory space and equipment are the only limits to the scale size and number of substructures that can be tested simultaneously for a single simulation.

The hybrid simulation test method is useful for modeling structures exhibiting complex non-linear behavior, especially if the non-linear behavior is concentrated in specific regions of the structure. For example, a base isolated building typically has non-linear isolation bearings at its base while the protected superstructure remains linear during strong earthquake shaking. In this case, substructuring techniques (Dermitzakis and Mahin 1985) can be used with the hybrid simulation method to experimentally model the isolation bearings in the laboratory and simultaneously capture the response of the linear structure using a simple computer simulation model (Nakashima and Masaoka 1999, Magonette 2001). Such tests are more economical than shake table tests, given

that a physical model of the entire building is not required. Moreover, the bearings can be tested at large- or full-scale using the hybrid simulation approach.

1.2.1 Advancements in Hybrid Simulation

The procedures for conducting a hybrid simulation test have advanced considerably since the method was first developed. The first experiments operated at a very slow rate (over 100 times slower than real time) and utilized a ramp-and-hold loading procedure on the experimental elements. Since the dynamic interaction of the inertial loads is modeled in the computer, tests can be carried out at an extended time scale for rate-independent experimental substructures. Under slow loading conditions, the servo-hydraulic actuators used to load the test specimen can apply larger forces compared to similar equipment at fast testing rates. The slow rates of testing permit for the economical seismic evaluation of experimental elements at larger scales.

Recently developed techniques, along with advancements in computers and testing hardware, have improved the execution of the hybrid simulation test method by achieving continuous tests at slow and fast rates. Applying a continuous load history, rather than the ramp-and-hold load history, has been shown to provide improved results in capturing the behavior of the experimental substructures (Magonette 2001, Section 6.5.5). These improvements are largely based on the elimination of the hold phase and the associated force relaxation in the experimental specimens. The continuous testing techniques are based on algorithms running on a real-time platform to insure the commands for the servo-hydraulic controller are updated at deterministic rates. Constant update rates allows for the control of velocity, thus allowing for a continuous load history on the experimental specimen. In the case of rate-dependent experimental substructures, the hybrid simulation test method has been extended to real-time applications where the experimental elements can be loaded at realistic seismic rates (Nakashima et al. 1992, Darby et al. 1999, Horiuchi et al. 1999, Nakashima and Masaoka 1999, Darby et al. 2001, Shing et al. 2002).

The potential of the hybrid simulation test method has been further extended by proposing to geographically distribute experimental substructures within a network of laboratories, then linking them through numerical simulations using the Internet (Campbell and Stojadinovic 1998). While various NEES facilities are individually equipped with the capacity to test one or more structural subassemblages at large scales, an increased number of experimental substructures can be tested simultaneously by integrating this network of laboratories. The NEES infrastructure pro-

vides the experimental equipment, the analytical modeling tools and the network communication between the sites to engage in the simultaneous testing of multiple large-scale experimental substructures and more complex numerical models using the distributed hybrid simulation approach.

Geographically distributed hybrid simulation using the Internet has already been carried out jointly between Japan and Korea (Watanabe et al. 2001), in Taiwan (Tsai et al. 2003) and in the US as part of the NEES efforts (MOST 2003). However, these previous applications of distributed hybrid simulation have used the ramp-and-hold procedure to load the experimental substructures. As such, they are not benefiting from the improved continuous testing methods.

1.3 RESEARCH OBJECTIVES

A current challenge facing hybrid simulation lies in increasing the complexity of the structural models that can be tested while, at the same time, utilizing advanced methods for continuous testing. Geographically distributed substructures present a challenge in that the required communication over the Internet can be randomly delayed at some steps. The difficulty in applying real-time based algorithms for continuous hybrid simulation stems from their lack of suitability with tasks that involve random completion times. Alternatively, the ramp-and-hold loading procedure can be readily applied when dealing with random delays since the hold period can be arbitrarily long. To maintain the benefits of continuous testing, an event-driven controller is presented to conduct continuous tests over the network by minimizing, if not eliminating, the hold phase at each integration step. A distributed hardware architecture utilizing the proposed event-driven controllers is also presented and verified experimentally. The experiments presented here are the first-ever attempt to conduct a continuous hybrid simulation distributed over multiple facilities that are linked through the Internet.

A second objective of this report is to investigate procedures for evaluating the reliability of the results obtained from hybrid simulations. Analytical models of a simple experimental setup are first derived and used to illustrate the effects of errors on the seismic response of structures. Then, Hybrid Simulation Error Indicators (HSEI) are proposed to monitor and evaluate the results of a hybrid simulation based on the energy errors in the experimental substructures. This procedure is applied to the results of the geographically distributed hybrid simulations to verify that reliable results were obtained using the proposed distributed control architecture. Further, the relationship

between the HSEI and the accuracy of the simulation results is established using pure numerical simulations of hybrid simulations with various levels of induced experimental errors. The benefit of HSEI is that they can be used to estimate the quality of the simulation results using information that is readily available during a test. Another advantage of HSEI is that they allow for the early detection of the unacceptable growth of errors, possibly before the test specimen is damaged. Early warning signals allows for the appropriate corrective steps to be taken prior to continuing with an experiment.

1.4 ORGANIZATION OF THE REPORT

The remainder of this report is divided into seven chapters and conclusions. The next chapter describes the hybrid simulation test method in technical detail and presents various procedures for slow continuous testing and real-time testing. Integration algorithms used to compute the response of structures in the numerical simulations are also summarized. Chapter 3 examines sources of error in a hybrid simulation and derives new analytical tools for examining the effects of errors in dynamic tests. Chapter 4 presents the distributed hardware architecture for coordination and control of a geographically distributed hybrid simulation. The distributed control system with the event-driven scheme for continuous testing over the Internet is described. In Chapter 5, the experimental equipment for conducting hybrid simulations is presented and characterized to determine its limitations. The extension of the test system to geographically distributed applications is also described. Chapter 6 presents the testing protocol and experimental results from a series of hybrid simulations with the numerical simulation located in a different geographical location from two experimental substructures. The simulation results are compared to a local testing configuration to validate the network configuration. In Chapter 7, the results from the distributed hybrid simulation are evaluated. The experimental results are compared to a pure numerical simulation and the experimental errors are examined. A simple formulation is proposed to characterize the severity of experimental errors in terms of energy that is introduced into the structural model. Finally, in Chapter 8, the use of HSEI is proposed as an effective method for monitoring the quality of the results during an experiment. The relationship between HSEI and performance parameters describing the accuracy of simulation is examined.

2 Numerical Methods for Hybrid Simulation

2.1 INTRODUCTION

The hybrid simulation test method is an experimental technique for evaluating the seismic performance of civil structures. Since the method was first developed 30 years ago, there have been vast improvements in the algorithms and hardware used to conduct such experiments. Algorithms with improved stability for integration of the equation of motion and procedures for fast continuous testing have been proposed. Recent advancements in experimental testing hardware have allowed for easier implementation and deployment of these new algorithms.

In this chapter, the hybrid simulation test method and procedures for testing are presented. Numerical methods used for the integration of the equation of motion and methods for fast continuous testing are summarized.

2.2 HYBRID SIMULATION TEST METHOD

The problem statement posed in hybrid simulation is to determine the seismic response of a structural model composed of experimental and numerical elements. To this end, the complete structural model is idealized as a discrete parameter system with a finite number of degrees of freedom. The governing equation of motion for the structural system is expressed as

$$Ma(t) + Cv(t) + R(d(t)) = F(t) \tag{2.1}$$

where M and C are the mass and damping matrices, $a(t)$, $v(t)$ and $d(t)$ are the time-dependent acceleration, velocity and displacement response vectors, respectively, $R(d)$ is the vector of nodal restoring forces, and $F(t)$ is the applied load vector.

The challenge in modeling a structure numerically using Equation (2.1) is in determining the restoring forces $R(d)$ for complex structural elements. If a linear elastic analysis is sufficient,

the problem is simplified by letting $R(d)=Kd$, where K is the stiffness matrix, and the problem is reduced to a linear second order equation. However, if it is necessary to model the response of a structure to severe loading, the non-linear restoring force behavior can become increasingly difficult to model for some structural elements. Robust analytical models do not exist for many structural members with complex behaviors. For these cases, hybrid simulation can be used to partially eliminate the uncertainty in modeling by replacing the element restoring force models with measured data from an experiment.

The concept of the hybrid test method is illustrated in Figure 2-1. Similar to a conventional numerical analysis in the time-domain, a prototype structure is modeled in the computer to conduct a dynamic structural analysis. The governing equation of motion (2.1) is solved using forward-marching time-stepping integration algorithms. The main difference in hybrid simulation is that the computer analysis program is linked to one or more physical subassemblages of the structure. For example, in Figure 2-1, one column of the multi-story frame is modeled experimentally on the laboratory floor. The experimental element is incorporated into the digital model by means of substructuring techniques for on-line testing (Dermitzakis and Mahin 1985). A dynamic analysis of the complete structure is carried out whereby the experimental subassemblage is considered as an element of the numerical model.

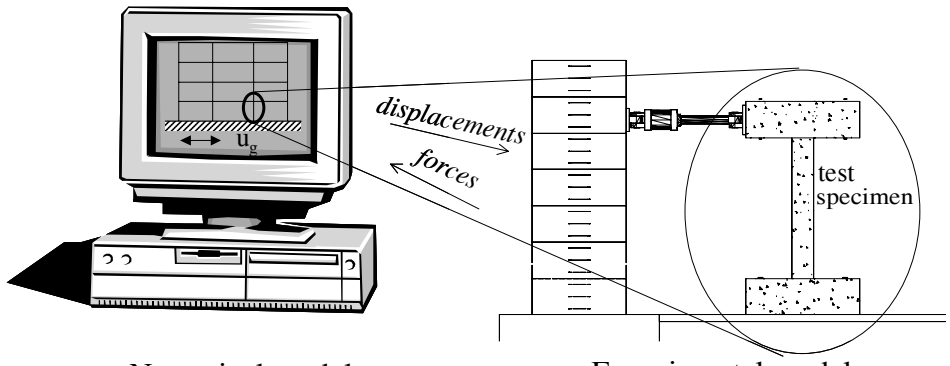

Figure 2-1. Experimental and numerical models for hybrid simulation

2.3 TESTING PROCEDURE

The equipment used for quasi-static testing in most structural testing facilities can be utilized to conduct hybrid tests. The basic components of a hybrid simulation test setup and their interconnections are illustrated in block diagram form in Figure 2-2. The required tools are: (1) a servo-hydraulic system consisting of controller, servo-valve, actuator and pressurized hydraulic oil supply; (2) a test specimen with the actuators attached at the degrees of freedom where the displacements are to be imposed, (3) instrumentation to measure the response of the test specimen and (4) an on-line computer capable of computing a command signal based on feedback from the transducers. The last item is the major addition from standard equipment typically available in structural testing laboratories. As demonstrated in Chapter 5, the on-line computer can be easily integrated with the servo-hydraulic controller. Further, an on-line computer with real-time computation capabilities allows for the implementation of real-time algorithms and provides the actuator with continuous commands updated at deterministic time intervals. To support fast rates of testing, a communication link with fast data transfer rates between the controller and the on-line computer is required.

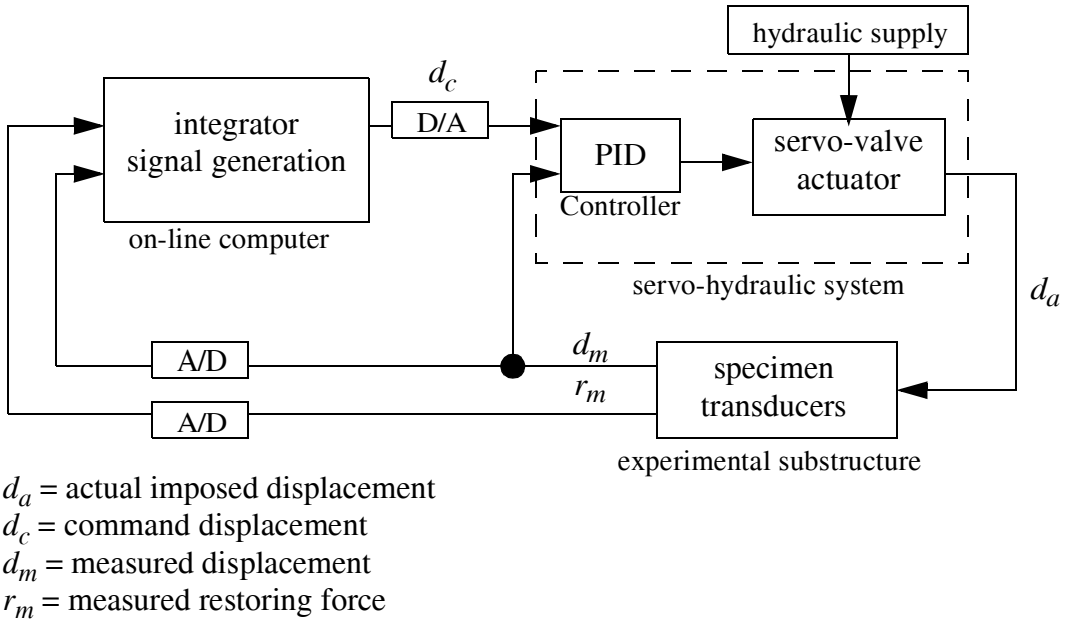

Figure 2-2. Block diagram showing equipment layout for hybrid simulation

The primary task of the on-line computer is to integrate the equation of motion utilizing the restoring force data measured from an experiment. The solution method is based on a time-stepping integration procedure, which enforces the discretized equation of motion

$$Ma_i + Cv_i + r_i = f_i \tag{2.2}$$

at time intervals $t_i = i\Delta t$ for $i=1$ to N. The subscript i denotes the time-dependant variables at time t_i, Δt is the integration time step and N is the number of integration steps. Numerical methods used to solve the equation of motion are discussed in the sections that follow. For now, an explicit solution scheme is assumed such that the displacement response at time step t_{i+1} is computed based on the response at step t_i. The procedure shown in Figure 2-3 is used to advance the hybrid simulation experiment by one time step.

The procedure described in Figure 2-3 is conducted for each integration step until the simulation time has elapsed. Traditionally, the pseudodynamic testing procedure has been carried out at slow rates, typically rates 100 or more times slower than real time. That is, for each second of earthquake simulation, the pseudodynamic test consumes 100 seconds of actual time. The long duration of the test is mostly due to the ramp-and-hold nature of conventional implementation techniques. In each step, the target displacement is first computed and sent as a command to the actuator (step 1). The actuator applies the commanded displacement in a ramp-wise manner from its current position (step 2). After reaching the target displacement, the actuator holds at a constant displacement while the force measurements are taken and computations are carried out (steps 3-5) to compute the next target displacement (step1). Figure 2-4 tracks the motion of the actuator with respect to actual time for one load step.

In addition to the slow rates of testing, there are other shortcomings to the ramp-and-hold loading procedure. One consequence of the hold phase is that test specimens can exhibit force relaxation, resulting in the introduction of erroneous force readings into the numerical algorithm. Static friction in the actuator piston from the stop and go motion can result in small oscillations in the applied load history. The discontinuity in velocity at the transition from the ramp to the hold phase is also a challenge for the servo-controller and can result in overshooting of the target displacements for poorly tuned gain settings (Thewalt and Mahin 1987).

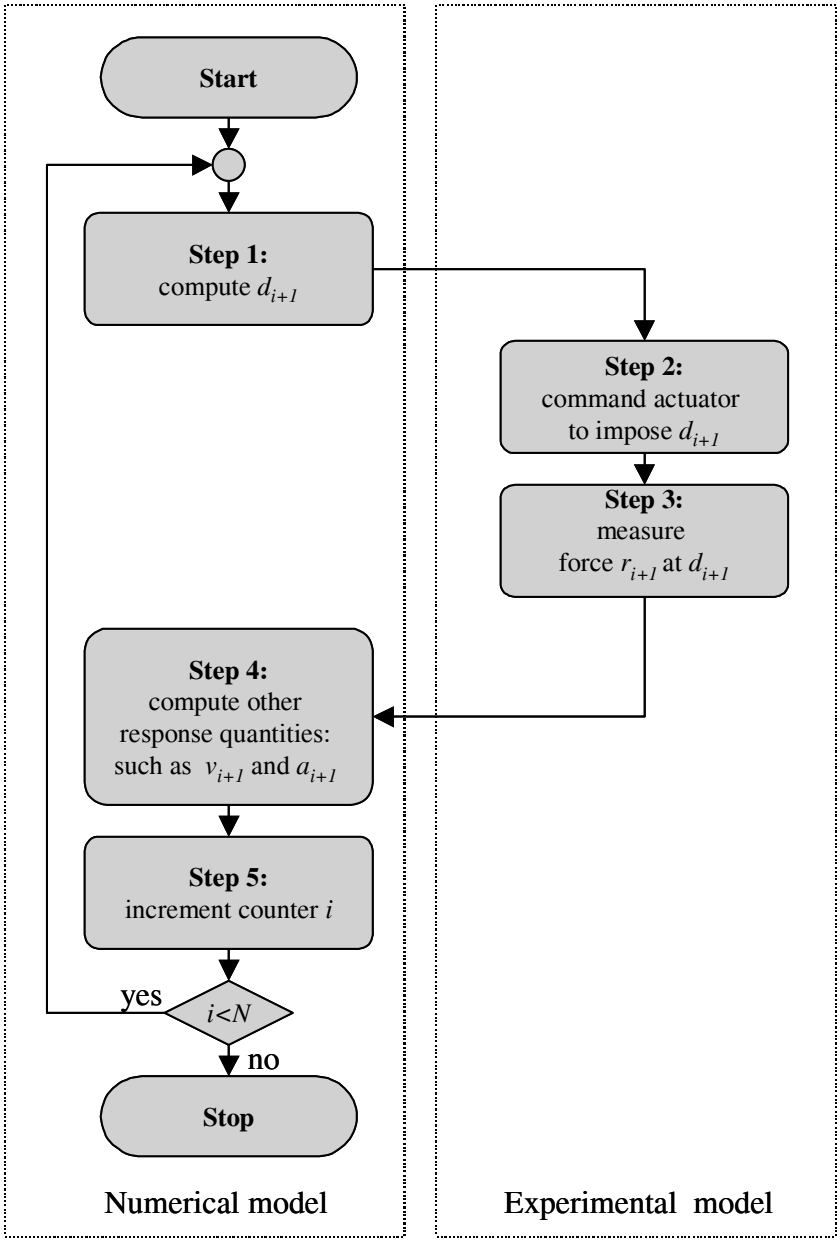

Figure 2-3. Flow chart of procedure for hybrid simulation

Faster and more efficient techniques for hybrid simulation have been introduced in the last decade. Recent developments in hybrid testing algorithms have focused on achieving a continuous motion of the actuators (Magonnete 2001) and increasing the speed of the test to approach real-time rates of loading (Nakashima et al. 1992, Horiuchi et al. 1996, Darby et al. 1999, Nakashima and Masaoka 1999; Darby et al. 2002, Shing et al. 2002). The use of techniques for continuous loading can improve the performance and accuracy of the experiment by eliminating the hold phase

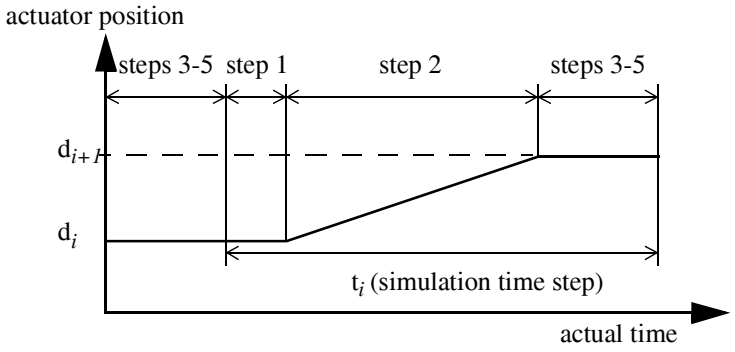

Figure 2-4. Ramp-and-hold load history in conventional hybrid tests

and associated force relaxation. Also, better control of the actuator is achieved through a continuous command signal. High performance actuators coupled with fast hybrid test methods can capture the rate-dependent behavior of materials for applications to viscous material. Techniques for achieving a continuous load history are presented after the discussion of numerical integrators.

It is important to note that as higher velocities are demanded from hybrid tests, the capacity and performance of the hydraulic actuators limit the scale size of the experimental model. The flow capacity of the hydraulic pumps and accumulators become critical to achieve the velocities required during a test. Similar limitations prevent the use of shaking tables for large scale testing. One advantage of the hybrid test method is that the specimen is not required to include additional dead weight, reducing the inertial forces on the actuators. In this case, the inertial forces can be modeled in the computer.

2.4 INTEGRATION ALGORITHMS FOR HYBRID SIMULATION

Both explicit and implicit time-stepping integration algorithms have been applied for hybrid simulation. Explicit methods compute the response of the structure at the end of the current step based on the state of the structure at the beginning of the step. The solution is determined by predicting the node displacements, determining the element restoring forces at those displacement, and computing the remaining response parameters to satisfy the equilibrium equation (2.2). This is an attractive property for hybrid testing because the actuator command displacement can be computed without prior knowledge of the specimen response at the target displacement.

Implicit methods require knowledge of the structural response at the displacement target in order to satisfy equilibrium at the end of the step. Usually, the displacement is prescribed as a function of other unknown response parameters at the end of the step, such as the acceleration. Iteration is required to satisfy both the imposed kinematic conditions and the equilibrium conditions at the end of the time step.

While explicit methods are easier to implement in hybrid simulations, implicit integration algorithms provide improved stability characteristics and permit the use of larger integration time steps. Better accuracy can be achieved with implicit methods, but iteration on experimental models is not practical since structural materials are path dependent. Mainly for this reason, explicit integration methods are preferred for hybrid simulation when the stability limits are satisfactory for the structural model under investigation.

2.4.1 Explicit Integration Algorithms

The most widely applied methods for solving the equation of motion in hybrid tests are explicit methods. A limiting factor of explicit methods is their stability criteria. For example, the Central Difference Method described below has a stability criterion

$$\Delta t \leq \frac{T_n}{\pi} \tag{2.3}$$

limiting the maximum allowable integration step size Δt based on the lowest natural period of the structure, T_n. For multi-degree of freedom systems, these requirements can become stringent.

Central Difference Method

One of the simplest algorithms for hybrid testing involves integration of the equation of motion using the Central Difference Method. The method was used for the original implementation of the on-line computer experiment by Takanashi et al. (1975) because of its efficiency and accuracy. Japanese (Nakashima 1999) and European researchers (Magonette 2001) consider the Central Difference Method as the basic integration method for simple to moderate applications of hybrid tests. These applications include structural models with few degrees of freedom such that the stability conditions imposed by Equation (2.3) are satisfied.

The Central Difference Method is based on the following finite difference approximations of velocity and acceleration:

$$v_i = \frac{d_{i+1} - d_{i-1}}{2\Delta t}, \; a_i = \frac{d_{i+1} - 2d_i + d_{i-1}}{\Delta t^2} \tag{2.4}$$

Combining these two approximations within the discretized equation of motion (2.2), the target displacement at the end of the step $i+1$ can be expressed explicitly as

$$d_{i+1} = \left(\frac{1}{\Delta t^2}M + \frac{1}{2\Delta t}C\right)^{-1}\left[\frac{2}{\Delta t^2}Md_i - \left(\frac{1}{\Delta t^2}M - \frac{1}{2\Delta t}C\right)d_{i-1} - r_i + f_i\right] \tag{2.5}$$

Note that the displacement at t_{i+1} is only dependent on the state of the structure at time t_i.

Newmark-Beta Method

Newmark's method (1959) and modified forms of this method have also served as popular numerical integrators in hybrid testing. Newmark's method is based on the discretized equation of motion at time t_{i+1} and the following approximations for displacement and velocity:

$$Ma_{i+1} + Cv_{i+1} + r_i = f_{i+1} \tag{2.6}$$

$$d_{i+1} = d_i + \Delta t v_i + \Delta t^2\left[\left(\frac{1}{2} - \beta\right)a_i + \beta a_{i+1}\right] \tag{2.7}$$

$$v_{i+1} = v_i + \Delta t[(1-\gamma)a_i + \gamma a_{i+1}] \tag{2.8}$$

The factor β provides a weighting distribution of the accelerations at the beginning and end of the time step on the change of displacement. Similarly, the factor γ provides weighting between the initial and final acceleration on the change of velocity. Further, the factor γ controls the amount of artificial damping provided in the algorithm, where $\gamma=1/2$ provide no artificial damping (Clough and Penzien 1993). Two well-known forms of Newmark's method are the constant average acceleration method with parameters $\beta=1/4$ and $\gamma=1/2$ and the linear acceleration method with parameters $\beta=1/6$ and $\gamma=1/2$. The constant average acceleration method is an unconditionally stable implicit algorithm. For linear elastic structures, this method can be manipulated to obtain a non-iterative formulation by taking advantage of the substitution $r_i=Kd_i$ in the equation of motion.

Setting the parameter $\beta=0$ results in an explicit formulation of Newmark's method since the term at $i+1$ vanishes from Equation (2.7). With parameters $\beta=0$ and $\gamma=1/2$, Newmark's method is numerically identical to the Central Difference Method.

Modified Newmark's Method

Shing and Mahin (1983) proposed an alternate form of Newmark's explicit method with dissipative properties suited for hybrid testing of multi-degree of freedom systems. The modified numerical method provides artificially damping such that the modal damping ratio increases monotonically with $\omega\Delta t$, where ω is the natural frequency of the corresponding mode. The large amount of damping suppresses the spurious response of high modes that can be excited by the noise in the experimental measurements and other sources of experimental error. The propagation of experimental and numerical errors has a more pronounced effect on the higher modes because the cumulative errors increase with the product of the natural frequency and the integration time step (Shing and Mahin 1983).

The numerical formulation for the Modified Newmark's method is

$$Ma_{i+1} + \left[(1+\alpha)K + \frac{\rho}{\Delta t^2}M\right]d_{i+1} = f_{i+1} + \left(\alpha K + \frac{\rho}{\Delta t^2}M\right)d_i \tag{2.9}$$

$$d_{i+1} = d_i + \Delta t v_i + \frac{1}{2}\Delta t^2 a_i \tag{2.10}$$

$$v_{i+1} = v_i + \frac{1}{2}\Delta t(a_i + a_{i+1}) \tag{2.11}$$

where the parameters $\rho < 0$ and $\alpha \geq 0$ can be selected to determine the amount of numerical dissipation in the structural modes of vibration. Note that the viscous damping term has been omitted from the equation of motion since the initially specified damping properties change substantially as the structure yields.

The γ-function Pseudodynamic Algorithm

Another dissipative algorithm based on Newmark's method is the γ-function pseudodynamic algorithm. This integration algorithm was recommended for hybrid testing by Chang (1997) because it offers better control in assigning damping parameters for the natural modes of vibration of the structural model. The Modified Newmark's method presented previously assigns damping

ratios that increases monotonically with the modal frequency, which can lead to high damping in lower modes important to the response. The γ-function pseudodynamic algorithm also provides increasing damping with frequency, but better control is offered in assigning realistic damping ratios to the lower modes that contribute to the structural response. This method is based on Newmark's explicit method with properly selected values for γ to obtain the desired damping characteristics. For multi-degree of freedom structures, the numerical algorithm consists of the discretized equation of motion (2.6) with the following assumptions:

$$d_{i+1} = d_i + \Delta t v_i + \frac{1}{2}\Delta t^2 a_i \tag{2.12}$$

$$v_{i+1} = v_i + \Delta t[(I-\gamma)a_i + \gamma a_{i+1}] \tag{2.13}$$

where

$$\gamma = \frac{1}{2}I + \sum_{k=1}^{\infty} c_k[\Delta t^2 M^{-1} K_0]^k \tag{2.14}$$

I is the identity matrix, c_k is a constant and K_0 is the initial structural stiffness matrix.

Unconditionally Stable Explicit Method

Chang (2002) also proposed an unconditionally stable explicit pseudodynamic algorithm of the form

$$Ma_{i+1} + Cv_{i+1} + r_{i+1} = f_{i+1} \tag{2.15}$$

$$d_{i+1} = d_i + \beta_1 \Delta t v_i + \beta_2 \Delta t^2 a_i \tag{2.16}$$

$$v_{i+1} = v_i + \frac{1}{2}\Delta t(a_i + a_{i+1}) \tag{2.17}$$

where the parameters β_1 and β_2 are coefficient matrices for multi-degree of freedom systems defined as

$$\beta_1 = \left[I + \frac{1}{2}(\Delta t)M^{-1}C + \frac{1}{4}(\Delta t)^2 M^{-1}K_0\right]^{-1} \times \left[I + \frac{1}{2}(\Delta t)M^{-1}C\right] \tag{2.18}$$

$$\beta_2 = \frac{1}{2}\left[I + \frac{1}{2}(\Delta t)M^{-1}C + \frac{1}{4}(\Delta t)^2 M^{-1}K_0\right]^{-1} \tag{2.19}$$

These parameters are based on the initial stiffness matrix of the structure and only need to be computed once prior to testing.

Chang's method appears to be similar to Newmark's implicit method expressed explicitly for linear systems. In fact, unconditional stability is proved (Chang 2002) by showing that the algorithm has the same characteristic equation as Newmark's constant average acceleration method. Similar results can be expected from both numerical algorithms when applied to linear systems. In a non-linear analysis, Chang's method uses the initial stiffness matrix to estimate the post-yield behavior of the structure whereas iterations are recommended for the constant average acceleration method (Bathe 1996). Chang's stiffness approximation is evident by the use of the initial stiffness matrix in Equations (2.18) and (2.19). Consequently, this approach is similar to using an implicit integration method limited to one iteration with the tangent stiffness matrix set to the initial stiffness matrix.

2.4.2 Implicit Integration Algorithms

Implicit integration algorithms can be designed to be unconditionally stable, but iteration is required for a non-linear dynamic analysis. Iterations on experimental elements are not practical since the restoring force behavior is dependent on the load path. The predicted displacements in an iterative scheme can overshoot the target displacements after which the test specimen has to be unloaded to return to the target displacement. Furthermore, implicit methods require a tangent stiffness matrix, which can be difficult to obtain from experimental measurements. An estimate of the tangent stiffness matrix using data available at the end of the time step has been proposed by Thewalt and Roman (1994), but its applications to implicit integration algorithms has not been demonstrated.

Despite these difficulties, implicit integration algorithms have been successfully applied to hybrid simulations in the past. Although the use of implicit integrators has been limited, the extra effort to apply these algorithms is necessary when explicit integrators cannot capture the structural response with sufficient accuracy. Implicit techniques for hybrid simulation are described below, but first, an implicit integration method with numerical dissipation is presented.

Newmark-Alpha Method

The Newmark-Alpha method (Hilber et al. 1977) increases the numerical damping in higher modes while maintaining low numerical damping in the lower modes that are important in capturing the response. The formulation for this implicit integrator is as follows:

$$Ma_{i+1} + Cv_{i+1} + (1+\alpha)r_{i+1} - \alpha r_i = f_{i+1} \tag{2.20}$$

$$d_{i+1} = d_i + \Delta t v_i + \Delta t^2 \left[\left(\frac{1}{2} - \beta \right) a_i + \beta a_{i+1} \right] \tag{2.21}$$

$$v_{i+1} = v_i + \Delta t[(1-\gamma)a_i + \gamma a_{i+1}] \tag{2.22}$$

The practical ranges of interest for the scalar parameters are

$$\frac{1}{3} \le \alpha \le 0\,,\ \gamma = \left(\frac{1}{2} - \alpha \right),\ \beta = \frac{(1-\alpha)^2}{4} \tag{2.23}$$

resulting in a second-order accurate method with unconditional stability.

Hybrid Implicit Algorithm

Recognizing the need for hybrid simulation integrators with unconditional stability, Thewalt and Mahin (1987) constructed a creative implementation of an implicit integrator through a mixed analog and digital algorithm. In their application, the Newmark-Alpha method was used because of its desirable numerical dissipative properties and stability.

The basic idea is that in an implicit integration algorithm, the displacement d_{i+1} in Equation (2.21) is expressed as the sum of an explicit part and an implicit part containing the term a_{i+1}. The explicit portion can be readily solved since all the variables are known at the beginning of the time step. Solving for a_{i+1} by eliminating the viscous damping terms in Equation (2.20), the following is obtained

$$a_{i+1} = M^{-1}[f_{i+1} - (1+\alpha)r_{i+1} + \alpha r_i] \tag{2.24}$$

Substituting this expression into Equation (2.21), the remaining unknown implicit term is r_{i+1}.

$$d_{i+1} = d_i + \Delta t v_i + \Delta t^2 \left(\frac{1}{2} - \beta \right) a_i + \Delta t^2 \beta M^{-1}[f_{i+1} + \alpha r_i] - \Delta t^2 \beta M^{-1}(1+\alpha) r_{i+1} \tag{2.25}$$

Thewalt and Mahin modified the servo-controller displacement command for each integration step as the analog sum of the constant explicit portion plus an analog function of the measured restoring force constituting the implicit part. A feedback control loop was incorporated into the algorithm so that the analog target displacement signal was continuously updated with the measured force feedback until the restoring force and target displacement satisfied Equation (2.25). In this approach, the target displacement is corrected based on the most current restoring force measurements.

Newton Iterations

Shing et al. (1991) also applied an implicit integration algorithm for hybrid testing based on the Newmark-Alpha method. This procedure uses modified Newton iterations with a displacement reduction factor to avoid overshooting the load path of the experimental specimen. The implicit method demonstrated improved error propagation characteristics over explicit methods and contained the growth of spurious roots in the numerical models.

2.4.3 Operator Partitioning Algorithms

Another earlier approach to overcome the stability limitations associated with explicit methods was proposed by Dermitzakis and Mahin (1985). A combined implicit-explicit integration algorithm (Hughes and Liu 1978) was applied for integration of the equation of motion by dividing the degrees of freedom (DOF) of a structure into two substructures: one containing experimental DOF and the other containing analytical DOF. An explicit method was employed for the integration of the experimental substructure and an implicit method was used for the analytical substructure. This division allows for the application of unconditionally stable implicit algorithms to solve for the response of the numerical substructure. The equation of motion for the implicit-explicit scheme is expressed in the following form

$$Ma_{i+1} + C^I v_{i+1} + C^E \bar{v}_{i+1} + K^I d_{i+1} + R_{i+1} = f_{i+1} \tag{2.26}$$

where C^I and C^E are the damping matrices corresponding to the analytical and experimental substructure, respectively, K^I is the stiffness matrix of the analytical substructure and $\bar{d}_{i+1}$ and $\bar{v}_{i+1}$ are the predictor displacement and velocity vectors, respectively. The above equation can then be solved using the explicit predictor-corrector method for the substructures with nonlinear behavior

and the unconditionally stable Newmark's method can be applied for the numerical integration associated with the linear substructures to obtain

$$\bar{d}_{i+1} = d_i + \Delta t v_i + \left(\frac{1}{2} - \beta\right)\Delta t^2 a_i \tag{2.27}$$

$$\bar{v}_{i+1} = v_i + (1-\gamma)\Delta t a_i \tag{2.28}$$

$$d_{i+1} = \bar{d}_i + \Delta t^2 a_{i+1} \tag{2.29}$$

$$v_{i+1} = \bar{v}_{i+1} + \gamma \Delta t a_{i+1} \tag{2.30}$$

In a hybrid simulation, the predicted displacements $\bar{d}_{i+1}$ are applied on the experimental substructures to obtain the measured force vector. The acceleration, a_{i+1}, is determined from Equation (2.26) and used to correct the predicted displacements based on Equation (2.29).

Nakashima et al. (1990) used a predictor-corrector integration scheme (Hughes et al. 1979) in their implementation of the operator splitting method for pseudodynamic testing. The numerical procedure is similar to the implicit-explicit formulation described previously, with the exception that only the stiffness matrix is divided into linear and non-linear substructures. The advantage of using the operator splitting predictor-corrector method is that unconditional stability is guaranteed for non-linear structures of the softening type. Additionally, the Newmark-Alpha operator splitting method has been shown to provide improved error propagation characteristics and stability as compared to explicit methods (Combescure and Pegon 1997). The operator-splitting formulation is non-iterative; thus this method can be applied with the same simplicity of explicit methods.

In both applications discussed above, an implicit integration algorithm was used to solve the response of the numerical substructure. However, the numerical models were limited to linear elastic systems that can be solved using non-iterative implicit methods. Dermitzakis and Mahin considered a non-linear analytical model, but a fully explicit method was used for both the analytical and experimental substructures in this case.

2.5 SUBSTRUCTURING TECHNIQUES

Using hybrid simulation, it is not necessary to construct and test a model of the complete structure when major damage or unpredictable behavior is only expected in a few structural elements. A more economical approach is to model the substructures with predictable behavior in the computer and test experimentally the key elements where damage is expected to occur. Using substructuring techniques from conventional dynamic analysis, hybrid simulation with substructured experimental elements is feasible and has been investigated by Dermitzakis and Mahin (1985), Shing et al. (1994), Schneider and Roeder (1994) and Pegon and Pinto (2000).

Properly specified boundary conditions between the physical and experimental substructures are necessary to insure force equilibrium and displacement compatibility. Actuators need to be strategically positioned to enforce these boundary conditions on the experimental substructures. To simplify the experimental apparatus, points of inflection may be assumed at the boundary degrees of freedom (Schneider and Roeder 1994) or rotations may be omitted.

An algorithm with substructuring techniques for hybrid testing has already been demonstrated in the implicit-explicit integration method. The equation of motion is divided into analytical and experimental substructures and the resisting force terms are separated to include contribution from these two components. In the case of the mixed implicit-explicit integration algorithm, the equation of motion is written as in (2.26) where the explicit restoring forces, R_{i+1}, corresponds to the forces measured in the experimental substructure and, $K^I d_{i+1}$, corresponds to the restoring forces of the analytical substructure.

A more general equation of motion for substructuring applications may be expressed as

$$M^A a_{i+1} + C^A v_{i+1} + R^A{}_{i+1} + R^E{}_{i+1} = f_{i+1} \tag{2.31}$$

where the superscript A denoted the contributions from the analytical substructure and the superscript E denotes contribution from the experimental substructures. The measured forces, $R^E{}_{i+1}$, are not limited to element restoring forces, but can also include contributions from viscous elements and inertial loads in dynamic tests. For example, a portion of the nodal mass may be located on the experimental element. In a real-time test, the inertial forces are included in the load cell measurements. Similarly, viscous dampers may be included in the physical substructure in a real-time hybrid simulation.

For linear analytical substructures, the substitution $R^A_{i+1}=K^A d_{i+1}$ may be made in Equation (2.31). The notation R^A_{i+1} is used to demonstrate that substructuring techniques are not limited to linear restoring force models. Non-linear models have been included in the analytical substructures by Dermitzakis and Mahin (1985). Further, Schneider and Roeder (1994) proposed a substructuring technique for non-linear structures where the measured restoring forces were treated as unbalanced forces. This formulation does not require a tangent stiffness matrix for the experimental substructure but the measured forces lag one time step behind the analysis, effectively introducing a time delay in the restoring force feedback.

2.6 FAST CONTINUOUS TESTING

Current research on hybrid simulation has focused on developing algorithms that update the command signal to the actuator at fast rates. The fast update rates provide for a continuous motion of the actuators having two benefits: the speed of testing is improved and a continuous load history, as opposed to the ramp-and-hold procedure, eliminates force relaxation of structural materials. Capabilities for real-time or near real-time testing also allows for the seismic performance evaluation of rate-dependent materials through hybrid simulation. These new techniques for fast hybrid testing are built upon the same integration algorithms and principles developed for pseudo-dynamic testing described earlier. As faster rates of testing are achieved, new challenges arise in solving the equation of motion within the allotted time and dealing with the inherent control error and response lag of servo-hydraulic systems.

The first implementation of a real-time hybrid test was achieved by improved hardware, namely, upgrading from a static to a dynamic actuator with a digital servo-mechanism for accurate displacement and velocity control of the actuators (Nakashima et al. 1992). The procedure for hybrid testing remained essentially the same. This system was only applicable to single degree of freedom systems because of the limitations in the speed of the hardware.

Horiuchi et al. (1996, 1999) developed a more sophisticated procedure for real-time hybrid test of multi-degree of freedom systems. In particular, a method was devised to compensate for actuator delay using a polynomial extrapolation procedure. As described by Horiuchi et al., the hardware configuration and programming involved appears difficult to implement in structural testing facilities. Nakashima and Masaoka (1999) improved upon the idea of polynomial approxi-

mation procedures and developed a more practical procedure for real-time testing of multi-degree of freedom systems using a Digital Signal Processor (DSP).

Darby et al. (1999, 2001) also implemented a real-time hybrid test of a multi-degree of freedom structure having one experimental substructure with a single actuator. These tests combined the actuator compensation technique of Horiuchi et al. and modified the explicit central difference method integration algorithm using a first-order hold discretization to obtain a smooth output command signal to the experimental substructure. Blakeborough et al. (2001) executed a real-time substructure test of a multi-degree of freedom structure where both translational and rotational degrees of freedom where considered in their physical cantilever model. In this study, problems were encountered in accurately controlling the two coupled actuators enforcing the boundary conditions on the two-degree of freedom experimental substructure.

Shing et al. (2002) further developed the implicit integration algorithm of Thewalt and Mahin (1987) and proposed a fast implicit integration algorithm. In this method, the analog implicit loop is replaced by a fixed number of numerical iterations within each integration step.

From the real-time hybrid testing algorithms that were reviewed, the methods developed by Nakashima and Masaoka and Shing et al. appear to be the most promising. These two algorithms provide substantial modifications to the conventional hybrid test procedure and are further discussed below.

Nakashima and Masaoka (1999)

In their algorithm for real-time testing, Nakashima and Masaoka separate the computations of the on-line computer into two tasks running at different sampling rates: (1) the response analysis task, which carries out the integration of the equation of motion and (2) a signal generation task, which provides a continuously updated displacement command to the servo-hydraulic actuator at a rate faster than the integration time step. These two tasks run on a DSP in real-time using a multi-rate approach.

The response analysis task deals with the typical numerical algorithms for solving the equation of motion. The signal generation task is based on predicting the displacement path of the actuator using polynomial approximation procedures. Nakashima and Masaoka showed that third order polynomial interpolation and extrapolation of known displacement values provide accurate dis-

placement and velocity predictions. The key to the polynomial approximation procedure is that the computation time is small and actuator commands can be continuously generated at short time intervals.

During each integration step, the actuator is kept in motion after reaching the target displacement by predicting a command signal based on polynomial extrapolation of the previous target displacement values. Meanwhile, the integrator task is carrying out computations for the next target displacement. Once the integration task has been completed and the target displacement in known, the algorithm begins to interpolate and corrects the path of the actuator towards the target value.

The *n-the* order polynomial extrapolation procedure is of the form

$$d_i^j = \sum_{k=0}^{n} a_{jk} d_{i-k} \tag{2.32}$$

where the displacements d_i^j are predicted values between d_i and d_{i+1}. The constants a_{jk} are based on Lagrangean polynomial approximations of known displacement data from previous steps. For an m step corrector method, i.e., j=1 to m, the servo-hydraulic controller command is updated at the time interval $\delta t = \Delta t / m$ where Δt is the integration step size. Figure 2 shows an example of the real-time output computed by the signal generation task.

Once the integrator algorithm has completed the computation of the target displacement, d_{i+1}, the signal generation task includes the new displacement data in the polynomial interpolation scheme. The interpolation command is of the form:

$$d_i^j = \sum_{k=0}^{n} a_{jk} d_{i+1-k} \tag{2.33}$$

This procedure provides a smoother displacement trajectory on the experimental substructures by updating the actuator commands at a more frequent rate than the integration algorithm alone. The polynomial computations are simple and can easily be handled by a DSP for each channel of a system with multiple actuators.

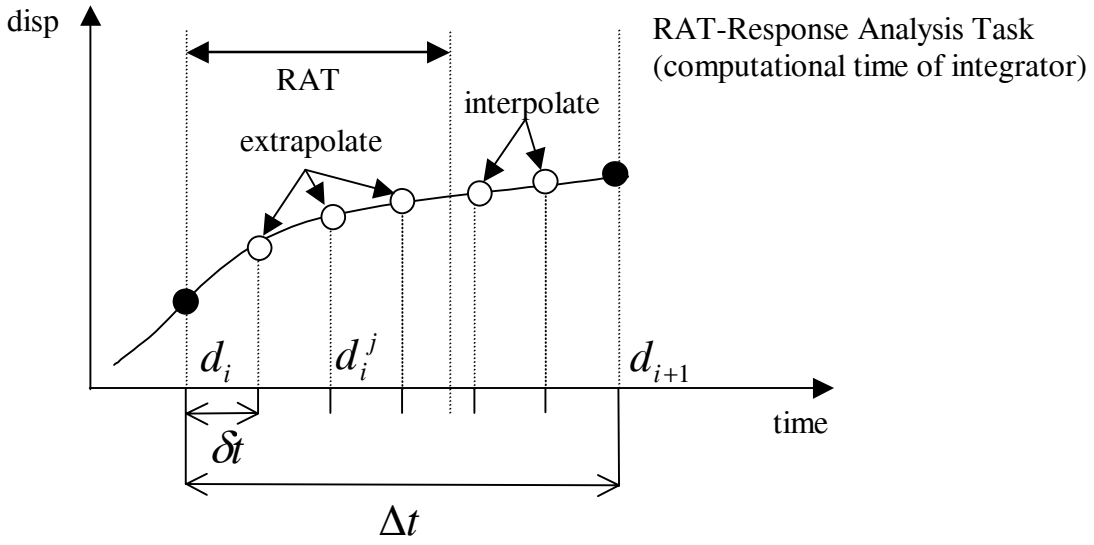

Figure 2-5. Extrapolation and interpolation of the command signal during one integration step (after Nakashima and Masaoka 1999)

Shing, Spacone and Stauffer (2002)

The implicit integration algorithm method developed by Thewalt and Mahin (1987) was modified by Shing et al. (2002) for fast applications with an error corrections scheme. The analog correction loop implemented by Thewalt and Mahin was replaced by a digital real-time algorithm. The digital implementation of the iterative displacement correction loop can provide similar results to Thewalt and Mahin's analog loop since the iterations run at a rate an order of magnitude faster than the integrator. The advantage of the digital implementation is the flexibility in modifying the mathematical procedure to incorporate an error correction scheme for lag and error compensation.

To enable the application of this implicit algorithm for fast hybrid testing, Shing et al. modified the displacement iterations to provide a more uniform incremental correction in each iteration. This was done by normalizing the displacement correction by the number of iterations remaining in each step. Without this normalization, the initial increments to the displacement command are much larger than the final corrections. Additionally, to account for errors in the position of the actuator, the final displacement and forces computed by the algorithm are corrected based on the measured displacement error and the initial stiffness matrix. Using the initial stiffness matrix to correct the measured forces can increases the magnitude of the errors in the post-yield phase, particularly for an element with negative stiffness.

2.7 SUMMARY

Integration algorithms applicable to hybrid simulation were presented. While implicit integration algorithms with improved stability have been suggested and applied, explicit methods remain more popular because they are much easier to implement. Implicit methods typically require iteration where care must be taken not to overshoot the final target displacement of the structure in each step. Operator partitioning integration algorithms offer improved stability and accuracy with the simplicity of non-iterative methods. For superior accuracy and stability in simulations of complex structural models, implicit methods are necessary. More work is needed in developing techniques to simplify the application of implicit methods for hybrid simulation.

In the last decade, the research focus in hybrid simulation has concentrated on improving the execution of the test. Continuous testing method, both at slow and fast rates, provide a more realistic load history on the experimental specimens and mitigate force relaxation errors. Algorithms for fast hybrid testing have been proposed for testing of rate-dependent materials such as fluid viscous dampers. The end result of continuous testing methods is improved measurements of the experimental substructure behavior and more accurate simulation results.

To achieve geographically distributed testing, the implementation techniques and numerical algorithms need to be extended to applications within distributed substructures. For remote applications, where communication over the Internet is not efficient, algorithms with minimal communication between the integration algorithm and the remote experimental substructures are necessary. In non-iterative methods, the integrator sends and receives data from the experimental substructures only once per integration step. Current applications of implicit methods require several sub-steps to exchange information between the integrator and the experiments. The multiple exchanges of information within each step may hamper the application of implicit methods for network tests.

Internet communication also poses a challenge for continuous and real-time algorithms. These algorithms rely on the fast exchange of information between the real-time actuator controller and the integrator. The communication task time cannot be guaranteed for Internet applications. The distributed control scheme presented in Chapter 4 is designed to implement a continuous test in the presence of random communication delays.

3 Errors in Hybrid Simulation

3.1 INTRODUCTION

Reliable results can be obtained from a hybrid simulation if the errors introduced into the numerical algorithms are reasonably small. In this chapter, the different sources of error are discussed, including errors based on modeling, implementation techniques, and the experimental setup. From these various sources of errors, experimental errors can have the most substantial impact on the simulation results, mostly because these errors are not known prior to testing and can be large for improperly tuned experimental setups. The other types of errors are inherent of the assumptions in the numerical modeling techniques.

Experimental errors in hybrid tests are examined herein by demonstrating their effect on the computed response of structures. This is accomplished through numerical simulations with controlled errors induced into the numerical models of simulated experimental specimens. A more rigorous investigation of the effects of errors follows using an analytical approach. The analytical studies focus on errors relevant to fast dynamic testing, although these errors also need to be considered for slow testing methods.

3.2 SOURCES OF ERROR

Errors are introduced into the hybrid simulation algorithms through the structural model idealization, the approximate numerical methods used to solve the equation of motion, and the experimental setup. Modeling and numerical errors have been described in detail by Shing and Mahin (1983, 1984). Thewalt and Mahin (1987) provide a thorough discussion on hardware components involved in a hybrid test and sources of experimental errors. A brief summary of the different sources of error is provided here.

3.2.1 Modelling and Implementation Techniques

The numerical and experimental models selected to represent the prototype structure determine the ability of the test method to capture the structural characteristics under investigation. The algorithms used to implement the hybrid simulation test method also influence the accuracy of the results.

3.2.1.1 Structural Model

The structural idealizations set forth in the numerical modelling of structures are present in hybrid testing. The structural model is described by the equation of motion in discrete parameter form, which is only an approximate representation of the continuous prototype structure. A course discretization of the experimental substructure is required so that its degrees of freedom can be controlled with the limited number of available actuators.

3.2.1.2 Numerical Methods

In the implementation of a hybrid simulation, the idealized equation of motion describing the prototype structure is solved using approximate numerical integration algorithms. The integration methods also introduce errors into the model and can become significant if the algorithm parameters are not properly selected. It is necessary to insure that the dynamic response of the structural model can be accurately captured by the integration method and the integration time step selected. Further, for non-linear analysis, energy can be introduced into the model by the linearization of the force-displacement relationship at each step (Shing and Mahin 1984).

3.2.1.3 Load History on Experimental Elements

The implementation technique can also impact the results of a hybrid simulation. The various forms of hybrid simulation were discussed in Chapter 2, including the ramp-and-hold loading procedures, slow continuous testing methods, and real-time tests. These different method influence the behavior of the experimental specimen because many structural materials are rate dependent and exhibit force relaxation. The technique for testing should be selected to insure that the measured response of the experimental substructure is representative of the material behavior under realistic seismic loading rates.

3.2.2 Experimental Setup

In a hybrid simulation, the experimental setup introduces various source of error that can influence the computed structural response. Errors result from the displacement control of the hydraulic actuators, calibration errors in the instrumentation, and noise generated in the instrumentation and analog to digital converters. Experimental errors can be classified as either random or systematic in nature. Random errors have no distinguishable pattern while a regular patterns of occurrence can be identified for systematic errors. For example, a lag in the displacement response of the actuator produces systematic errors since the resulting displacement control errors have a magnitude and direction proportional to the velocity demand.

When compared to other experimental techniques, hybrid simulation is more sensitive to actuator control errors. Experimental measurements contaminated by errors are used to compute future commands in the time-stepping hybrid simulation algorithms. Errors can propagate throughout the test, possibly resulting in an unstable response. In contrast, errors do not accumulate in shake table and quasi-static testing since the command displacement history is predefined. Additionally, the final structural response can be evaluated based on the measured load history as opposed to the command input. For example, the results of a shake table test can be evaluated based on the measured table acceleration to remove the uncertainty associated with control errors in applying the reference command signal. However, for a hybrid test, the measured forces are assumed to be taken exactly at the command displacement. Care should be take to properly tune the actuator controllers and calibrate the measurement devices.

The displacement control of hydraulic actuators becomes increasingly important for fast hybrid simulations. One critical factor is the time lag inherent of servo-hydraulic systems, partly due to a delay in the response of the servo-valve (Horiuchi et al. 1999, Conte and Trombetti 2000). The effects of actuator lag on the structural response are further discussed in Section 3.4.

Systematic errors can also result from improper tuning of the experimental setup. These sources of error include improper calibration of instrumentation and flexibility in the reaction frame. To minimize the effects of systematic errors, the testing equipment needs to be properly tuned and calibrated prior to testing.

3.3 TECHNIQUES FOR EXPERIMENTAL ERROR REDUCTION

The sensitivity of hybrid simulation algorithms to experimental errors has been investigated by Shing and Mahin (1983), Thewalt and Mahin (1987) and Thewalt and Roman (1994). Methods have been proposed to minimize the effects of experimental errors on the results of a test. Some of these techniques are presented below.

3.3.1 Random Errors

Random noise generated by the measurement instrumentation can be problematic in the evaluation of multi-degree of freedom systems using hybrid simulation. The noise in the measured forces can excite spurious response in the lightly damped high frequency modes of the structure that would otherwise remain dormant under the simulated earthquake load. To overcome this problem, integration algorithms with artificial numerical dissipation have been used to suppress the response of the higher modes. Several integration algorithms with numerical dissipation, particularly with increased damping for the higher frequency modes, are discussed in Chapter 2.

A second approach to minimize the effects of random errors on a hybrid simulation was recommend by Chang (1998). In this procedure, the momentum equation of motion is solved as the governing equation as opposed to the force equilibrium equation of motion. The momentum equation of motion is obtained by integrating the force balance equation with respect to time as show below.

$$\int m\ddot{u}dt + \int c\dot{u}dt + \int rdt = \int fdt \tag{3.1}$$

$$m\dot{u}dt + cudt + \int rdt = \int fdt \tag{3.2}$$

The integration of the force signal filters the noise in the measurements prior to being introduced into the numerical algorithms. The same numerical procedures, such as Newmark's method, can be applied to solve Equation (3.1) for the time integral of displacement, displacement, and velocity as opposed to displacement, velocity, and acceleration.

3.3.2 Systematic Errors

Improvements in the execution of the test method have been successful in reducing the effects of systematic errors on hybrid simulations. These procedures include compensation techniques for load history effects and actuator time delay.

3.3.2.1 Load History Compensation

The traditional ramp-and-hold approach to hybrid simulation result in systematic experimental errors due to force relaxation and rate effects in the experimental substructures. The hold phase maintains the test specimens at a constant displacement for a period of time. During this time, the resisting force of the specimen may be reduced due to material relaxation, then reloaded in the next step. From observations of the load history, the specimen appears to be subjected to small amplitude cycles of loading and unloading. Continuous testing methods mitigate this effect and can provide improved measurements of the experimental specimen behavior under the simulated loading.

It is important to consider the strain-rate sensitivity of the material being tested and select the rate of testing accordingly for continuous hybrid simulations. Shing and Mahin (1988) investigated the sensitivity of the earthquake response of structures using a rate-dependent restoring force model representative of steel. The results showed that the rate of loading in a slow hybrid simulation affects the response of structures in the short period range (less than 0.5 seconds). Real-time test methods can be applied to evaluate experimental substructures that are sensitive to the rate of loading.

A numerical technique to compensate for rate effects was proposed in Molina et al. (2002), to allow for the slow continuous testing of rate-dependent materials. Molina et al. tested rate-dependent elastomeric bearing using a slow continuous hybrid simulation technique by mathematically compensating for the rate effects. In their approach, the measured restoring forces from the elastomeric bearings were modified based on a predetermined compensation function.

3.3.2.2 Actuator Delay Compensation

There is an inherent lag in the displacement response of servo-hydraulic actuator versus the command displacement. Consequently, the measured restoring forces are delayed relative to the command signal. This actuator delay becomes critical as the rate of testing is increased, especially for

real-time rates. To compensate for this lag, Horiuchi et al. (1999) measured the time lag of the actuator response and by the polynomial extrapolation procedure in Equation (2.32), predicted the command of the actuator by advancing the current time in the algorithm by the delay time. This was accomplished by selecting the appropriate constants a_{jk} in Equations (2.32) to predict a command several sub-steps ahead of the current simulation time.

3.3.3 Other Techniques

European researchers (Stoten and Magonette 2001) have made an effort to improve the hardware components in the laboratory to achieve better experimental results. One such improvement is the use of digital controllers to reduce the displacement control error in the actuator. A second improvement is the use of digital transducers for improved accuracy and less noise in the experimental measurements. A third recommendation is the use of the adaptive minimal control synthesis (MCS) algorithm as opposed to the proportional-integral-velocity (PID) control algorithm typically used for the servo-hydraulic actuators. The MCS control scheme provides adaptive gain settings that adjust to improve the performance of the actuators as the test specimen properties change due to degradation.

3.4 SIMULATION OF EXPERIMENTAL ERRORS

The effects of experimental errors on the results of a hybrid simulation can be observed by modeling a hybrid simulation algorithm and introducing controlled errors into the simulation. Errors representing the effects of random noise in load cells and displacement control errors such as actuator lag are demonstrated below. Both linear and non-linear structural response is investigated

3.4.1 Random Noise in Load Cells

The Simulink (Mathworks 2003) diagram in Figure 3-1 simulates the dynamic response of a single degree of freedom system subjected to an external excitation. The inertial and damping forces are modeled in the integrator algorithm and the spring element restoring force is included as feedback from the ‘Experimental Specimen’ block. The restoring force feedback is computed as the sum of a linear or non-linear spring force and an error source. The error, modeled as band-limited white

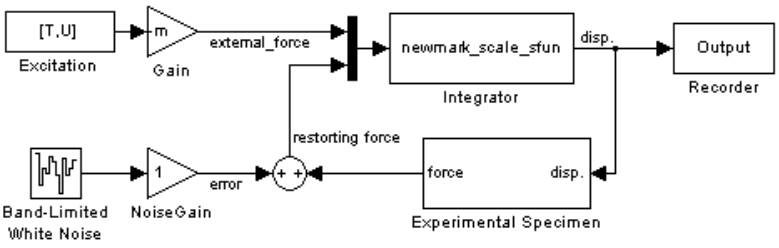

Figure 3-1. Simulink model with random noise added to restoring force feedback

noise, is intended to represent the random noise in the load cell measurements associated with the instrumentation and analog to digital converters.

The structural model consists of a single degree of freedom system with a natural period of 1.0 seconds and 5 percent of critical damping. The stiffness of the "Experimental Specimen' is set to 10 kip/in. for the linear simulations. The mass and damping constants are selected to obtain the desired natural period and damping ratio. For the non-linear simulations, the spring constant is replaced by an elastic-perfectly plastic model with the same initial stiffness and a yield displacement of 1 in. Newmark's explicit method is used to integrate the equation of motion with a time step of 0.01 seconds. The input excitation is the 1940 El Centro N-S component with a peak acceleration of 0.32 g. The amplitude of the ground motion is scaled by 20 percent for the linear simulations and 100 percent for the non-linear simulations.

The white noise error source covers a frequency range from 0 to 50 Hz and the 'Noise Gain' block is adjusted to introduced different levels of noise into the simulation. The magnitude of the error signal is characterized by the peak-to-peak value of the error signal normalized by the peak measured force. A second method to characterize the magnitude of the errors is the signal to noise ratio (SNR), which relates the error signal to the restoring force signal in terms of the root-mean-square (RMS). The SNR is computed as

$$SNR = \frac{RMS(r)}{RMS(e)} \tag{3.3}$$

where r is the restoring force feedback signal and e is the error signal. The RMS of the signal $e(t)$ in the time interval 0 to T is computed as

$$RMS(e) = \left[\frac{1}{T} \int_0^T e^2(t)\,dt \right]^{\frac{1}{2}} \tag{3.4}$$

Figure 3-2a shows the computed displacement response of a single degree of freedom system subjected to the 1940 El Centro N-S component. The 'exact' response without errors is compared to the resulting displacement histories with errors in the restoring force feedback. The modified force feedback is displayed in Figure 3-2b as a function of displacement and the resulting error signal is shown in Figure 3-2c. The peak-to-peak noise level of the error signal is approximately one percent of the value of the restoring force signal. The resulting SNR is 78 for this case.

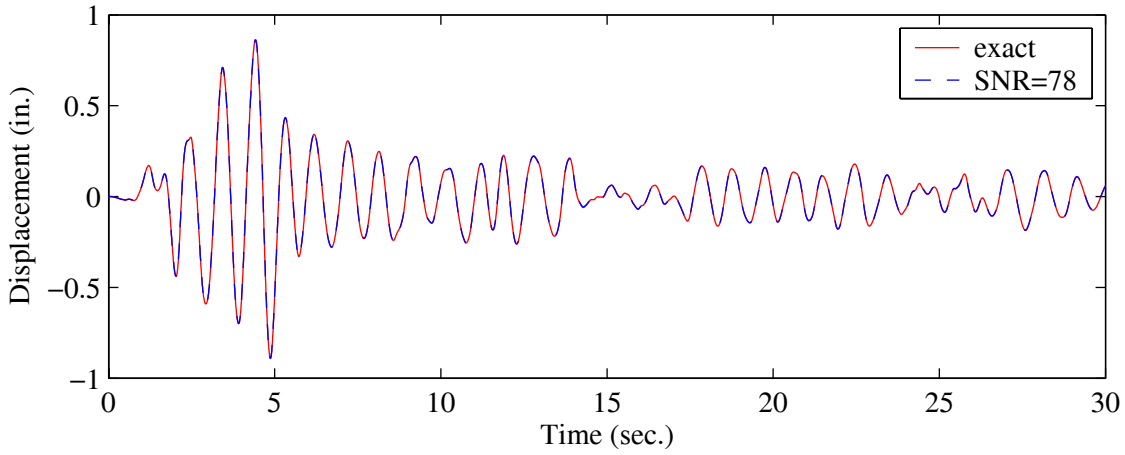

a. displacement history

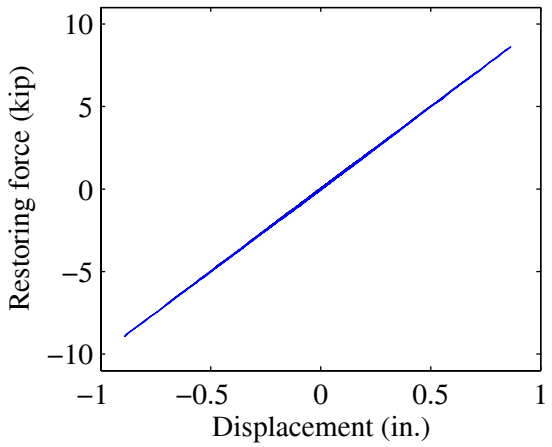

b. modified force-displacement

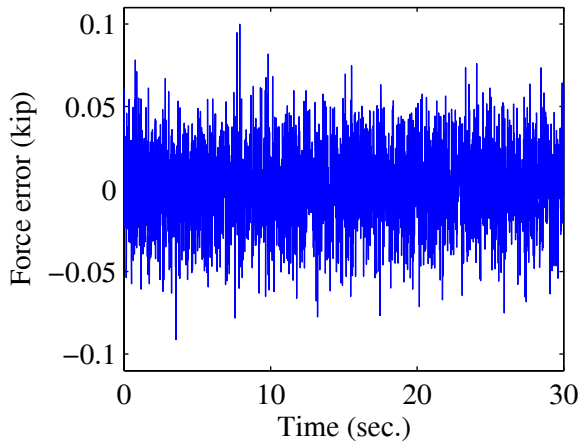

b. generated error signal

Figure 3-2. Simulation of linear structure with moderate random errors in force feedback

The magnitude of the error signal can be considered as a moderate level of noise for load cells. (The load cells used in the test setup described in Chapter 5 have peak-to-peak noise levels under 0.5 percent compared to the total range.) The results show that there is a negligible effect on the structural response for random errors in this moderate range.

Figure 3-3 shows the single degree of freedom system response with a larger amplitude random error signal added to the restoring force feedback. For this case, the SNR is computed as 7.8, with the peak-to-peak value of the error signal at approximately 10 percent of the magnitude of the restoring force. These noise levels are much larger than expected for reliable load cell measurements. The simulation results in Figure 3-3a show that relatively large random errors have a

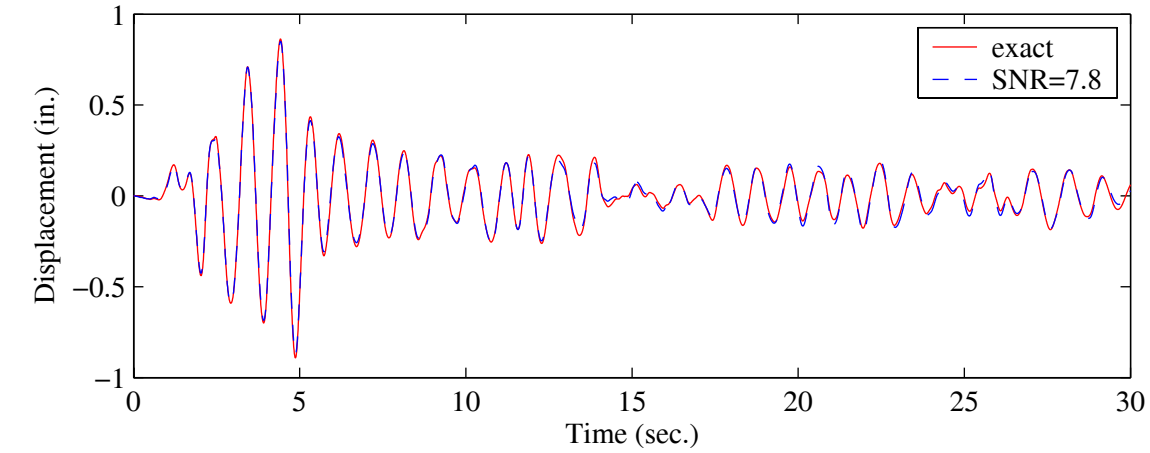

a. displacement history

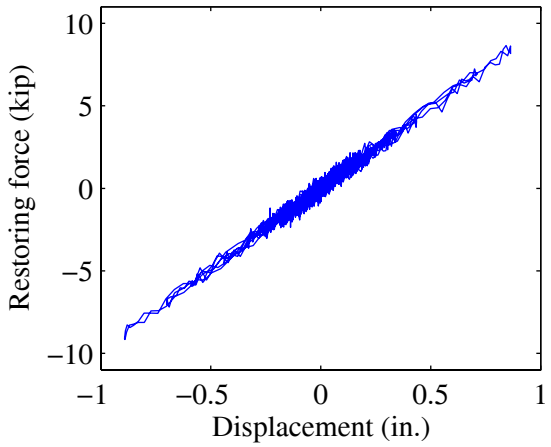

b. modified force-displacement

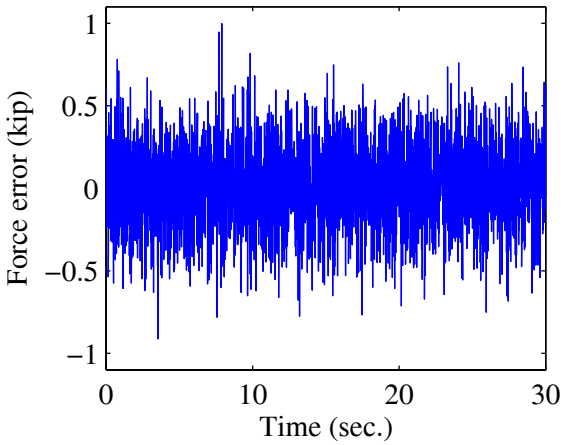

b. generated error signal

Figure 3-3. Simulation of linear structure with large random errors in force feedback

small effect on the overall structural response. The trends of both displacement histories are similar, with apparently no significant propagation or amplification of the random load cell measurement error.

To investigate the effects of random noise on the response of non-linear systems, Figure 3-4a shows the simulated response of a single degree of freedom system where the restoring force is determined using the non-linear elastoplastic model. The resulting restoring force, including noise, is shown in Figure 3-4b as a function of displacement. The noise amplitude is maintained at slightly under 10 percent of the restoring force signal based on peak-to-peak values with a SNR of 21.This noise level is relatively large compared to the maximum forces. Similar to the linear systems, the large amplitude random noise has a negligible effect on the overall structural response.

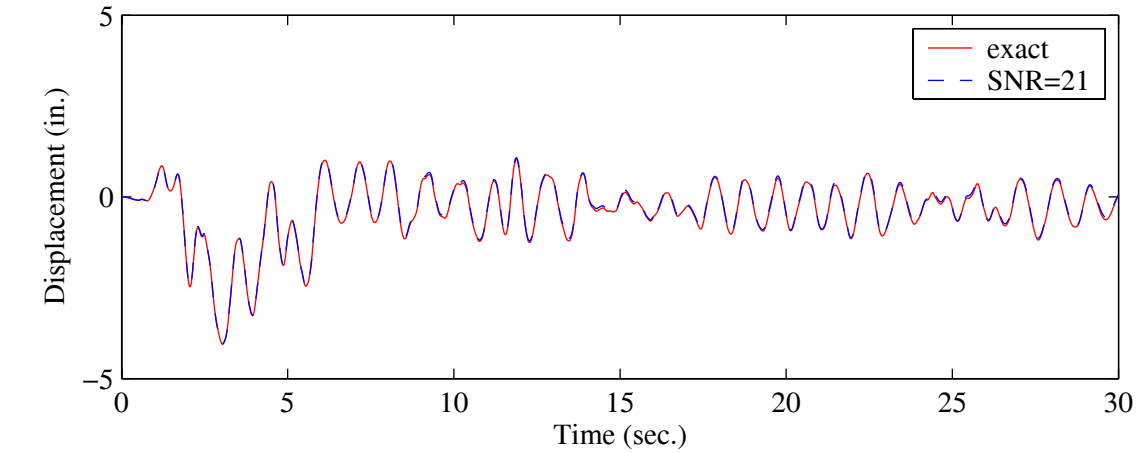

a. displacement history

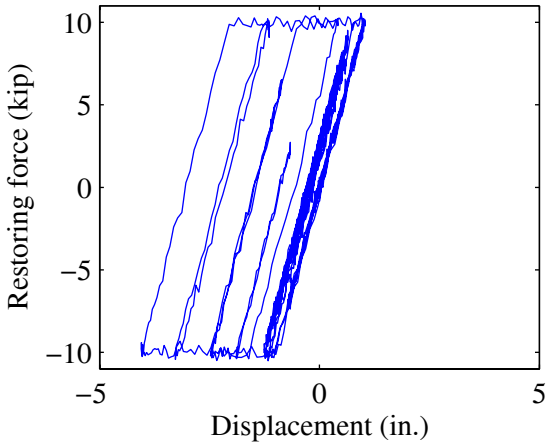

b. modified force-displacement

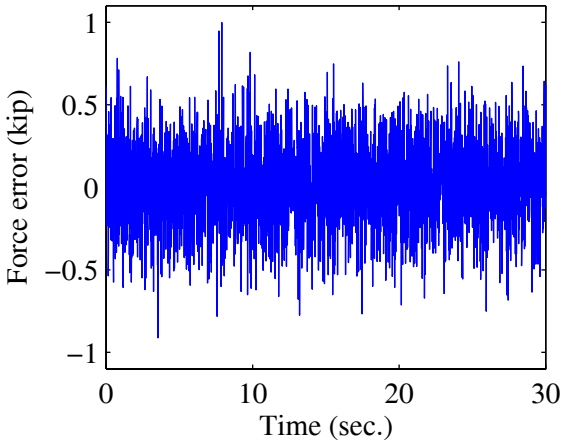

b. generated error signal

Figure 3-4. Simulation of non-linear structure with large random errors in force feedback

3.4.2 Displacement Control Error

Another source of error in an experimental setup is in the displacement control of servo-hydraulic actuators. This error can be measured as the difference between the command displacement and the measured displacement. Random errors in the position control of the actuator are likely to have an effect similar to random noise in the force feedback signal, the difference being that the displacement error is amplified by the stiffness of the specimen. Here an attempt is made to model systematic errors, where the position of the actuator is consistently lagging behind the target displacement command signal.

In the Simulink model shown in Figure 3-5, an error is introduced into the displacement prior to being applied to the specimen model. The error is defined as a normally distributed random signal multiplied by the displacement increment, where the displacement increment serves as a first order approximation to velocity. The generated systematic errors, with direction and magnitude proportional to velocity, result in an approximately constant time lag in the displacement signal. This simplified model is based on the observed relationship between the error signal and the velocity demand on the actuator from actual experimental data. The response of the actuator is also sensitive to the changes in force and stiffness of the specimen and these factor are not included in the model (Merritt 1967).

For the simulation model in Figure 3-5, the severity of the errors is dependent on the statistical distribution assigned to the 'random number' generator and the displacement increment. The

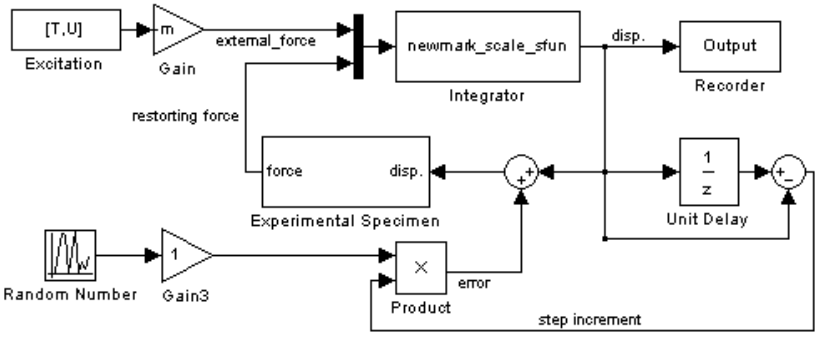

Figure 3-5. Simulink model with systematic displacement control errors

random signal is determined based on a normal distribution where the mean determines the average magnitude of the error or the effective time delay in the restoring force measurements. The variance is kept constant at 0.01. The severity of the error signal is characterized in terms of the effective time delay since this definition is more meaningful here. The SNR used in the previous section is more appropriate for random signals.

Results of a simulation using the same linear structural model as before are shown in Figure 3-6, where the errors are now introduced into the displacement prior to computing the restoring force. A plot of the resulting command displacement vs. restoring force is shown in Figure 3-6b.The generated error signal in Figure 3-6c with a mean of 0.2 causes an effective time delay of 2 milliseconds. Evidently, these delays do not cause significant changes in the structural response

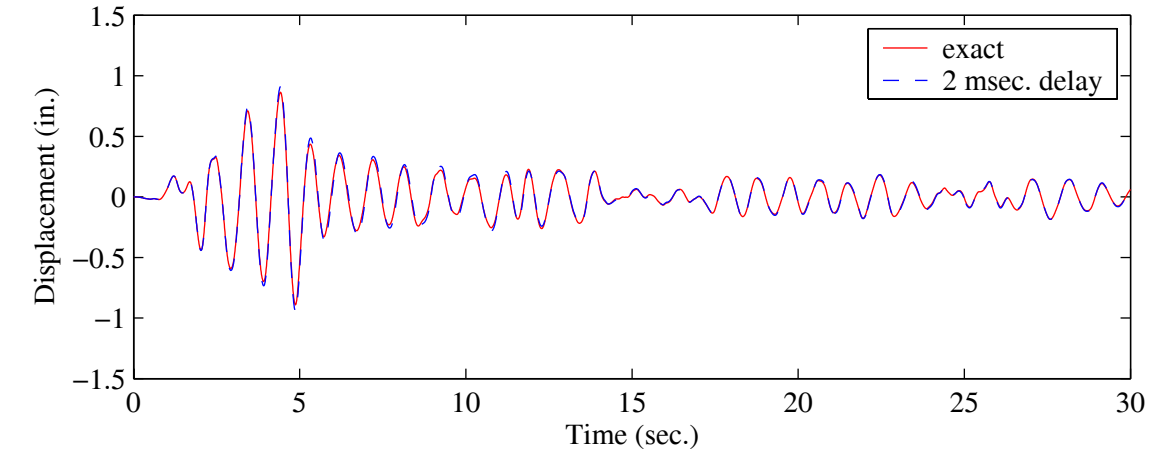

a. displacement history

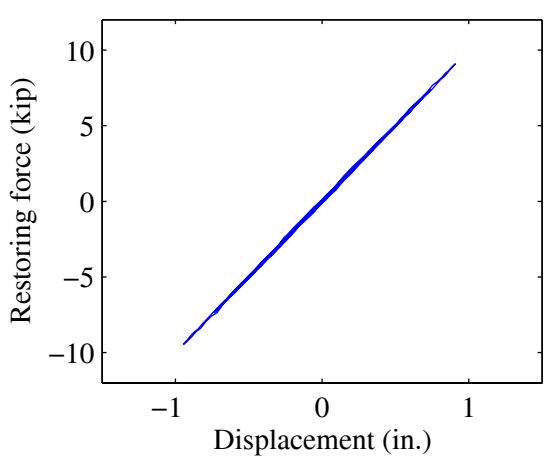

b. modified force-displacement

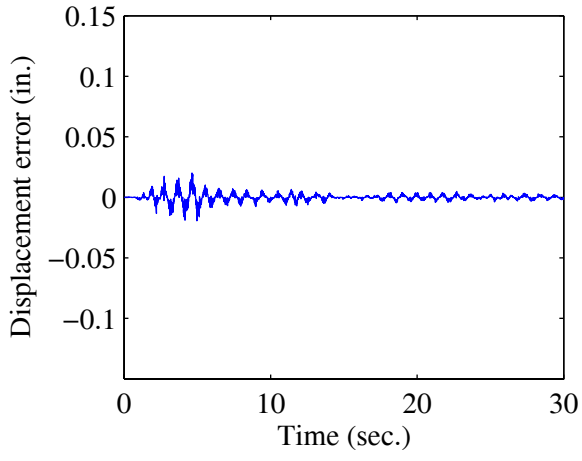

b. generated error signal

Figure 3-6. Simulation of linear system with 2 msec. displacement control lag

when compared to the exact solution. The force-displacement response with errors included in Figure 3-6b shows that the expected behavior for a linear system is maintained by the model.

The mean of the random error generator is increased to 1.0 for the simulation results shown in Figure 3-7, also for a linear system. The effective time delay is approximately 9.9 milliseconds, which is slightly less than the integration time step and almost one percent of the natural period of the structure. The displacement histories in Figure 3-7a show that delays of this magnitude amplify the structural response as compared to the simulation without errors. The force-displacement plot in Figure 3-7b shows a reverse hysteresis effect in the presumed linear element as a result of the delayed displacement used to compute the restoring force. The net effect of the hysteresis is that

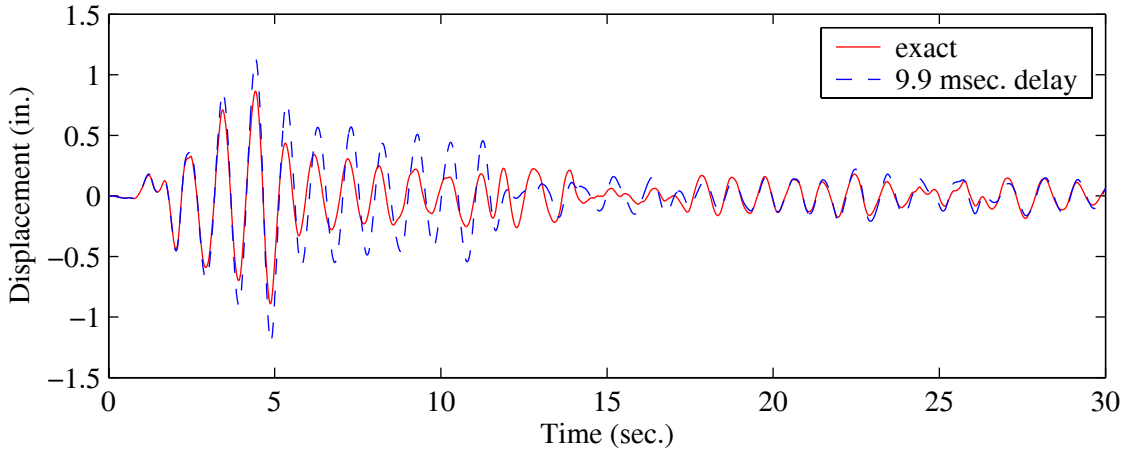

a. displacement history

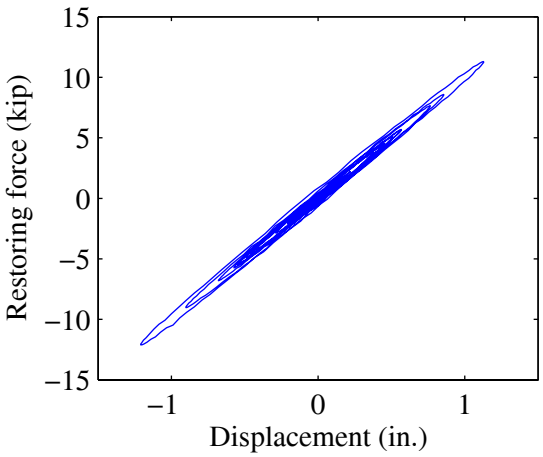

b. modified force-displacement

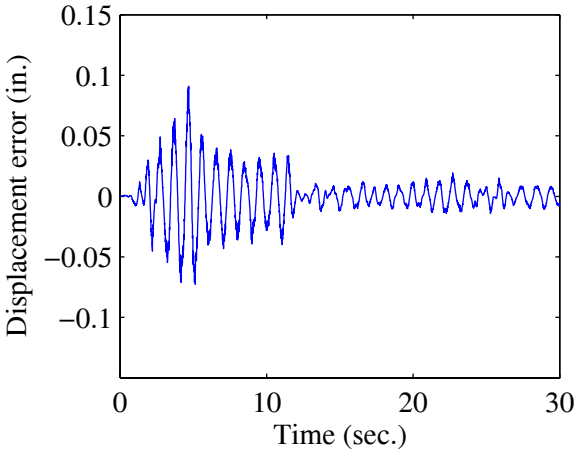

b. generated error signal

Figure 3-7. Simulation of linear system with 9.9 msec. displacement control lag

energy is added to the structural model and the displacement response is amplified, especially at the peak displacements.

The effects of actuator response lag is also simulated for a non-linear structural systems, where the linear spring is again replaced by an elastoplastic model. The errors introduced into the non-linear models are of similar magnitude compared to the linear models. First, the displacement errors are generated with a mean of 0.2 to produce a 2 milliseconds lag. This lag does not cause significant changes to the structural response as shown in Figure 3-8.

In Figure 3-9, the errors generated with a mean of 1.0, resulting in a 9.7 millisecond lag, show a modest change in the structural response. The simulation with errors shows good displacement correlation with the exact model for the first seven seconds of simulation. Thereafter, the two

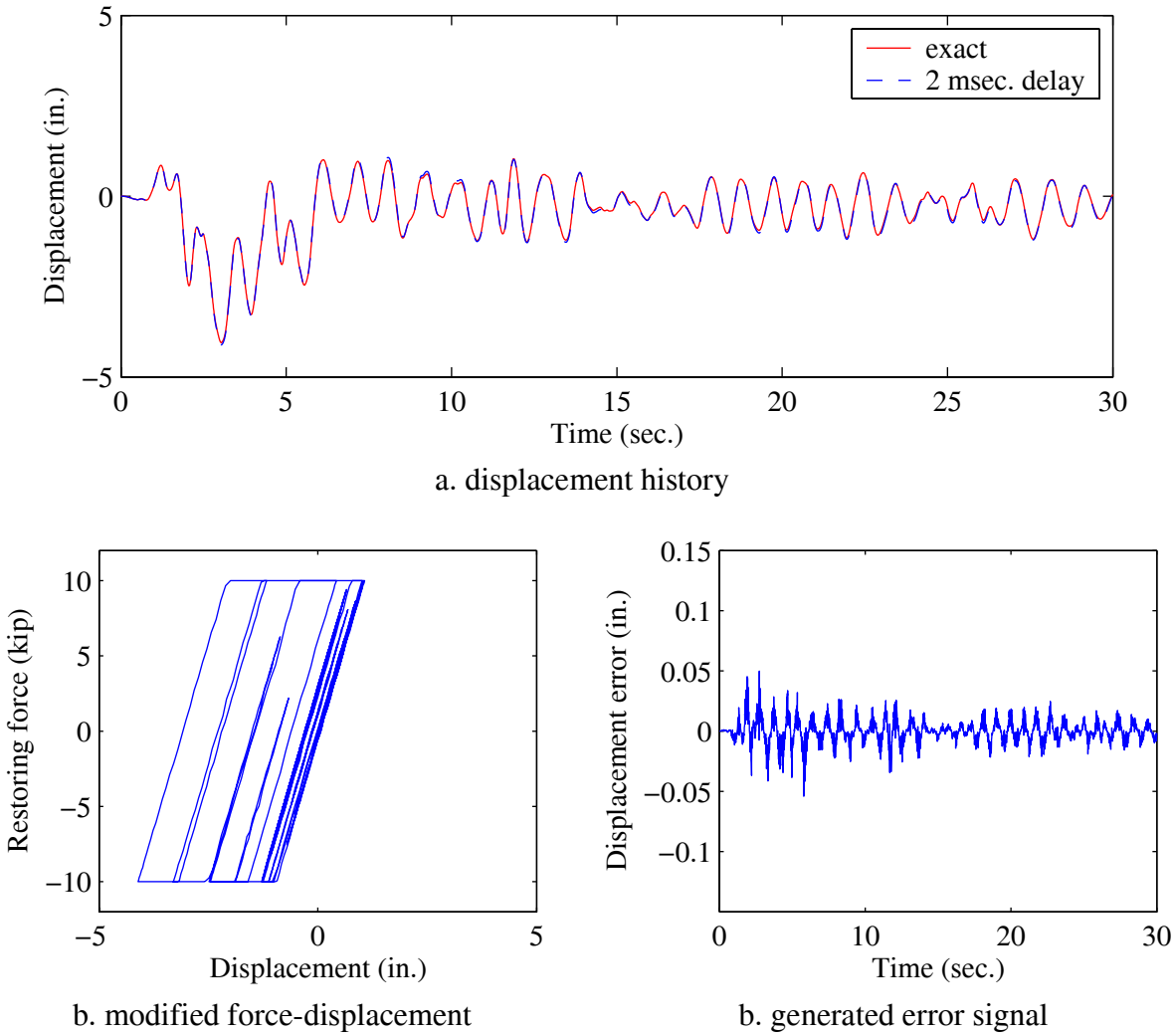

a. displacement history

b. modified force-displacement

b. generated error signal

Figure 3-8. Simulation of non-linear system with 2 msec. displacement control lag

displacement histories deviate as the response of the structure oscillates for several cycles within the linear stiffness range at an offset near the peak positive displacement. Delays in the response of the actuator appear to be less sensitive for non-linear systems, particularly during the non-linear excursions. In this region, errors in the applied displacement have a small effect on the measured restoring force because the tangent stiffness is reduced to the post-yield value. Additionally, the structural response is less sensitive to the reverse hysteresis effect since energy is dissipated at a much faster rate by the hysteretic non-linear model and viscous damping compared to the energy generated by the errors. The energy errors can be observed from the force displacement plot in Figure 3-9b, particularly at the two unloading/reloading cycles near a displacement of (-2) in. In

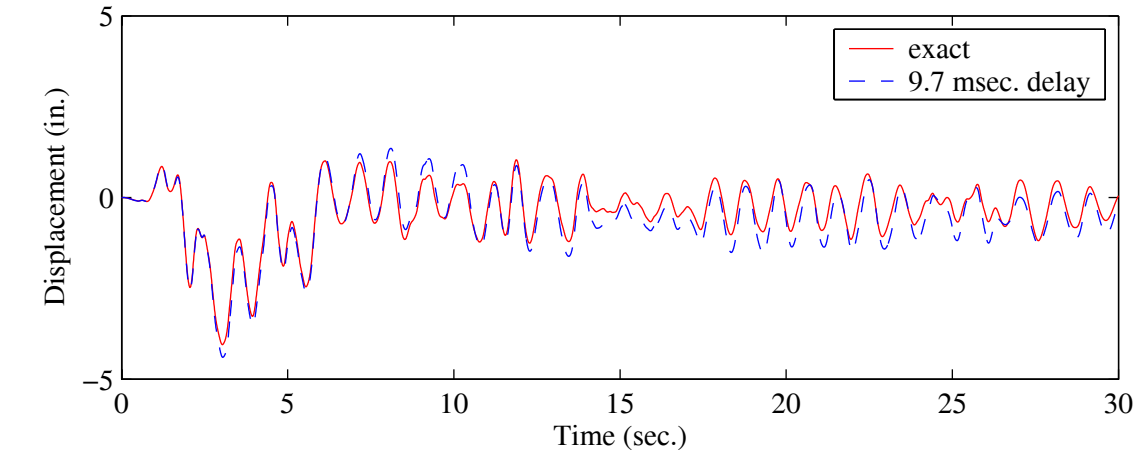

a. displacement history

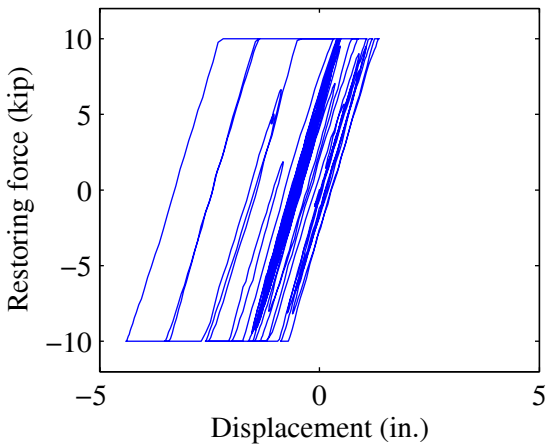

b. modified force-displacement

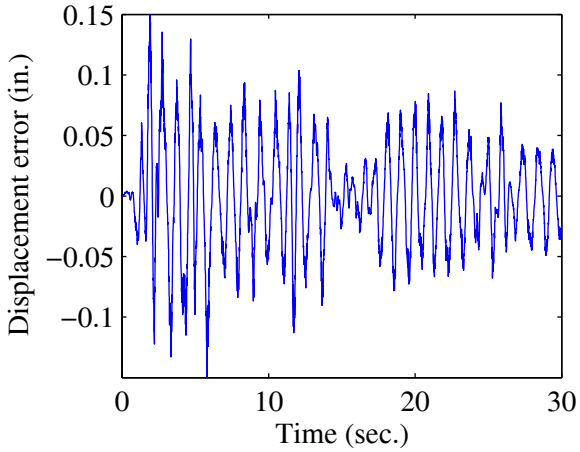

b. generated error signal

Figure 3-9. Simulation of non-linear system with 9.7 msec. displacement control lag

these low amplitude cycles, the reloading branch does not coincide with the unloading branch as is expected for an elastoplastic model and illustrated in Figure 3-8b with smaller time delay.

3.5 EFFECTS OF ACTUATOR LAG ON STRUCTURAL RESPONSE

During a hybrid tests, errors in the displacement control of the actuators result in force measurements at the incorrect displacements. The measured force are introduced into the numerical integration algorithm assuming they correspond to the target displacements. The simulations in Section 3.4 showed that random errors produced a negligible effect on the structural response, but systematic errors such as actuator lag can modify the response considerably. (See also Shing and Mahin 1983 and Thewalt and Roman 1994.)

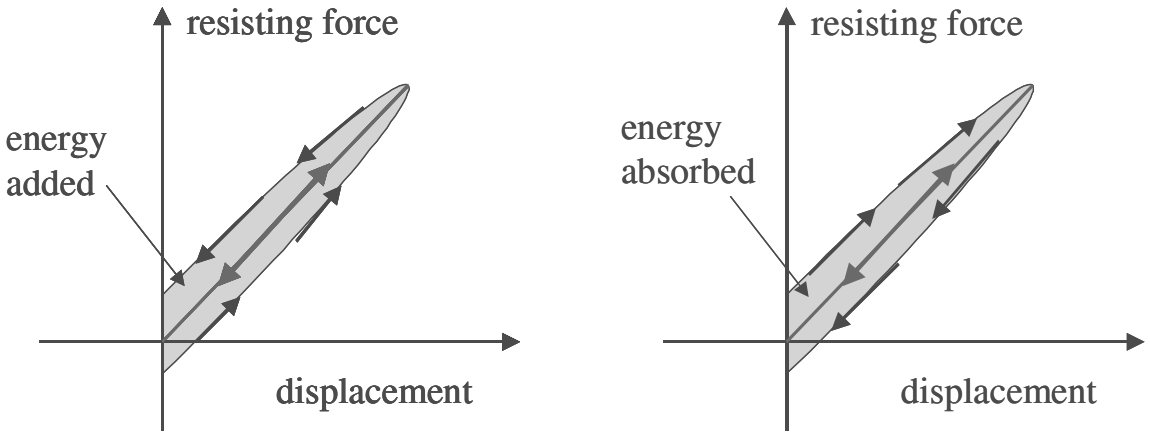

a. undershooting (lag) b. overshooting

Figure 3-10. Loading and unloading of a linear-elastic element with actuator error.

In a hybrid simulation, the numerical integrator observes the experimental specimen behavior as the command displacement versus the measured force. However, the true behavior of the structural specimen is given by the measured displacement versus the measured force. The modification to the observed structural behavior as a result of displacement control errors is demonstrated in Figure 3-10. The expected results from loading and unloading a linear-elastic element is given by the straight bold line shown in Figure 3-10a. However, if there is a lag present in the actuator response, a plot of the command sinusoidal displacement vs. measured force will produce the oval-shaped reverse hysteresis shown in Figure 3-10a. The modification to the expected element

behavior results from the time lag in the measured force vs. the commanded displacement. The shaded area in the figure represents the energy that is added to the structural system by the experimental element, thus having the effect of negative damping. If the actuator is overshooting, or ahead of the commanded response, the linear elastic element absorbs energy similar to a linear-viscous element. The case of undershooting is more common in continuous hybrid simulation since servo-hydraulic actuators have an inherent lag in their response.

3.5.1 Restoring Force Delay in Structural Systems

To further examine the effects of actuator lag on structural response, the response of a structural system with a time delay in the restoring force is examined. An analytical model is derived in the form of a transfer functions for linear systems. It is important to note that this model provides an approximation to the behavior of the actuators, and serves to provide an understanding of the effects of experimental errors on the seismic response of structures. Errors in the actuator are not only constituted by a time delay, but also by other factors affecting the performance of the actuator and controller.

In a hybrid simulation, the dynamic response of a structural system to a random excitation *f(t)* is determined by solving for the governing equation of motion

$$m\ddot{u}(t) + c\dot{u}(t) + r(u(t)) = f(t) \tag{3.5}$$

where the restoring force term *r(u(t))* is measured from an experiment. A time delay, τ, in the response of the actuator is reflected in the measured restoring force by modifying the equation of motion to the following

$$m\ddot{u}(t) + c\dot{u}(t) + r(u(t-\tau)) = f(t) \tag{3.6}$$

If the restoring force response is assumed to be linear elastic, the following substitutions can be made

$$r(u(t-\tau)) = ku(t-\tau) \tag{3.7}$$

$$\omega_n = \sqrt{\frac{k}{m}} \tag{3.8}$$

and

$$\xi = \frac{c}{2m\omega_n} \tag{3.9}$$

Equation 3.6 may be expressed as

$$\ddot{u}(t) + 2\xi\omega_n\dot{u}(t) + \omega_n^2 u(t-\tau) = \frac{1}{m}f(t) \tag{3.10}$$

Assuming zero initial conditions for displacement and velocity, the Laplace Transform of Equation 3.10 is

$$s^2U(s) + s2\xi\omega_n U(s) + \omega_n^2 e^{-\tau s}U(s) = \frac{1}{m}F(s) \tag{3.11}$$

where *U(s)* and *F(s)* are the Laplace Transforms of *u(t)* and *f(t)* respectively. Further, in the Laplace Domain, the transfer function *T(s)* between the input excitation and the displacement response of the single degree of freedom system including time delays in the restoring force is

$$T(s) = \frac{U(s)}{F(s)} = \frac{1/m}{s^2 + s2\xi\omega_n + \omega_n^2 e^{-\tau s}} \tag{3.12}$$

A graphical representation of the transfer function, *T(s)* may be obtained by substituting $s = i\bar{\omega}$, where $\bar{\omega}$ is the excitation frequency and $i = \sqrt{-1}$. Further, the natural frequency is normalized by the excitation frequency

$$\rho = \frac{\omega_n}{\omega} \tag{3.13}$$

and the time delay parameter is expressed as a phase delay, ϕ_d, of the natural frequency

$$\phi_d = \tau\omega_n \tag{3.14}$$

The resulting transfer function is

$$T(i\bar{\omega}) = \frac{u_{static}}{(\cos(\rho\phi_d) - \rho^2) + i(2\xi\rho + \sin(\rho\phi_d))} \tag{3.15}$$

where

$$u_{static} = \frac{f_o}{k} \tag{3.16}$$

under the presumed harmonic loading $f(t) = f_o \sin(\bar{\omega} t)$.

Figure 3-11 plots the transfer function $T(i\bar{\omega})$ of a single degree of freedom system with 10 percent of critical damping and a time delay in the restoring force. Figure 3-11a shows the results for small values of time delay corresponding to phase delays of 1, 2, 3, and 5 degrees based on the natural frequency of the structure. For example, a single degree of freedom system with a natural frequency of 1 Hz and restoring force time delay of 0.01 seconds corresponds to a phase delay of $0.01(2\pi)$ radians or 3.6 degrees. It is interesting to note that for a linear system, the effects of actuator lag are similar to a reduction in viscous damping. The constant time lag in the measured restoring force increases the amplitude of the resonant peak in the transfer function. There is a negligible change in response amplitude for excitation frequencies away from the natural frequency of the structure. This behavior is confirmed in Figure 3-10, which shows that a restoring force delay transforms the behavior of a linear elastic element into the oval shaped response representative of a linear-viscous element under sinusoidal loading.

Figure 3-11b shows the transfer function response for larger values of time delay, which may be reasonable for higher modes in a multi-degree of freedom structure. Recall from Equation (3.14) that the phase delay is proportional to the natural vibration frequency, hence only a very small time delay is necessary to reduce the effective damping ratio for the high frequency modes. These plots provide some insight into the sensitivity of higher modes to systematic errors. Consequently, higher modes in a structure need to be suppressed with high amounts of artificial damping. The effective damping in the single degree of freedom system continues to decrease with an increasing lag up to 10 degrees. As the phase lag is increased beyond 10 degrees, the response amplitude of the resonant peak begins to decrease, with a slight reduction in vibration period of the single degree of freedom system. For large phase delays of 30 degrees, the resonant response amplitude is less than a structural model without delay. However, the approximate linear model used here may not be reliable for large values of delay.

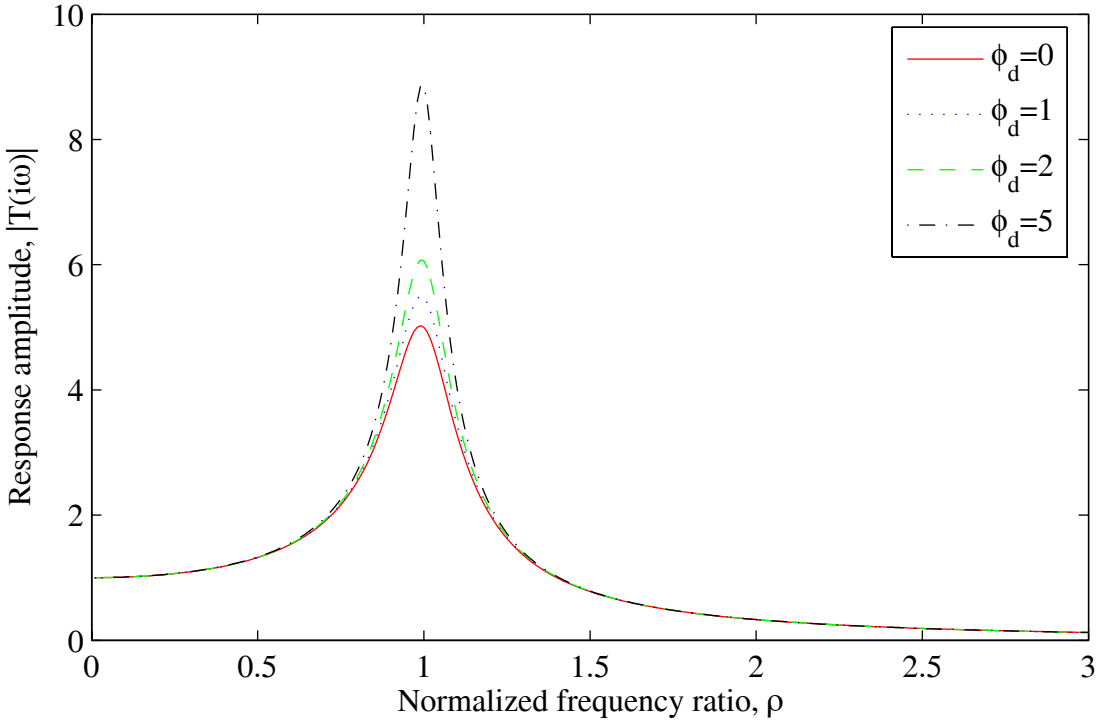

a. small values of delay

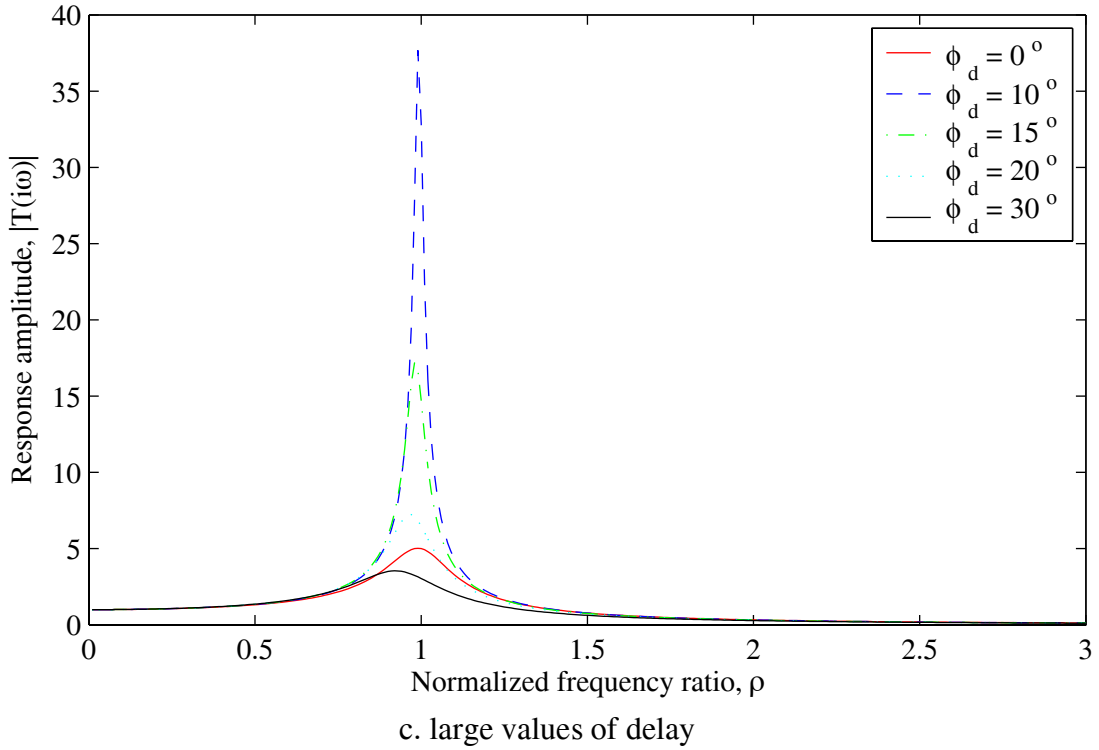

c. large values of delay

Figure 3-11. Transfer function of SDF system with restoring force delay $\phi_d = \tau\omega_n$

3.6 SUMMARY

The effects of errors on hybrid simulation algorithms were demonstrated. It was shown that random error have a negligible influence on the results of a test, but systematic errors can have a substantial impact. One major source of systematic errors in the experimental setup is in the response lag of the actuator, which produces an effective delay in the measured restoring force. An analytical investigation of delays in the restoring force showed that this error has a similar effect on the response of linear systems as a reduction in viscous damping. Further, numerical simulations showed that systematic errors are more critical for linear systems compared to non-linear systems of the softening type. These results indicate that a linear analysis may provide an upper-bound of the effects of errors expected during a non-linear analysis.

4 Versatile Hardware Architecture for Hybrid Simulation

4.1 INTRODUCTION

The NEES facilities provide the equipment necessary for the civil engineering community to engage in the large-scale testing of complex structures. NEES facilities combined with the hybrid simulation test method allow for next-generation experiments to evaluate the seismic performance of complex civil structures and components at large scales. To fully utilize the facilities, the hybrid test method can be used to: (1) test structural components at large- or full-scale; (2) increase the number of physical and numerical substructures within a single simulation by conduction a geographically distributed test; and (3) refine analytical models using state-of-the-art modeling tools and advanced numerical algorithms.

As the complexity of the structural models increase, the standard algorithms for hybrid testing become more difficult to implement. In particular, for geographically distributed testing or the use of implicit integration algorithms, randomness is introduced into the simulation due to uncertainties in task completion times. Variable task times can be problematic for improved continuous algorithms running on real-time processors. In order to fully utilize the infrastructure provided by NEES with the state-of-the-art algorithms for hybrid testing, test controllers at the NEES facilities need to be equipped to efficiently deal with the uncertainties of next-generation hybrid simulations.

After describing the next-generation of applications using hybrid simulation and sources of problems associated with such tests, a versatile hardware architecture for hybrid simulation is presented. This framework provides a distributed control scheme for an extensible network of earthquake testing facilities while facilitating the implementation of algorithms for continuous testing and geographically distributed testing.

4.2 NEXT GENERATION HYBRID SIMULATION

Pseudo-dynamic testing on structural models with few degrees of freedom and a single experimental substructure having one or more actuator degree of freedom has been successfully implemented in the past. (Mahin et al 1989, Shing et al. 1996) More recent studies have experimentally executed hybrid test in real-time to account for the rate-dependent behaviors of materials (Nakashima et al. 1992, Darby et al. 1999, Horiuchi et al. 1999, Nakashima and Masaoka 1999, Darby et al. 2001, Shing et al. 2002). These experiments on simple structural models have been useful in the development and testing of algorithms for hybrid simulation. Only recently has the hybrid test method been applied to verify the performance of large-scale experimental substructures (Molina et al. 1998, Pinto et al. 2002).

The infrastructure of NEES provides for further improvements in the sizes and complexity of numerical models and the number of experimental substructures that can be tested. Some notable efforts making use of the advanced capabilities in hybrid simulation include geographically distributed testing between Japan and Korea (Watanabe et al. 2001), the Internet-based Simulation for Earthquake Engineering (Tsai et al. 2003) in Taiwan and the Multi-Site On-Line Simulation Test (MOST 2003) demonstrations in the US. All of these distributed tests have made use of ramp-and-hold loading procedures to load the experimental substructures and the duration of the test has been exhaustive.

Improved analytical modeling techniques can be included in hybrid tests by integrating major structural analysis software packages with experimental equipment and adapting the software for hybrid simulation. The OpenSees (Fenves 2004) software is an attractive option since the source code is available and is designed for parallel processing applications. Its expandable architecture also allows for the addition of user specified integrators and element models specific to hybrid testing. Using such software, numerical structures can be analyzed using state-of-the-art modeling tools. In concentrated regions of the structure where damage is expected to be greatest and modeling uncertainty is not known with confidence, then experimental substructures can be combined with the analytical models. For example, testing of a multi-span bridge is typically limited to 1/4 scale models on shake tables (Kelly et al. 1985, Constantinou et al. 1993, Anderson and Mahin 2002). Using the hybrid approach, full scale testing of components can be achieved by phys-

ically testing the piers individually whereas the deck, consisting of the massive portion of the structure with predictable behavior, can be modeled on the computer (Pinto et al. 2002).

Further advancements to the hybrid test method include an increase in the length scale of experimental models that can be tested and increasing the number of substructures than can be tested simultaneously. The slow rates of loading in conventional pseudodynamic tests allows for specimens to be tested at large scales. The increased capacity in the number of experimental models is realizable through a fast and reliable network of laboratories for collaborative testing; this network infrastructure is available through NEES. The networked large-scale structural testing facilities enable the testing of complex structural systems by distributing experimental substructures throughout the laboratories then combining them into a global hybrid model between the substructures. The simulation is coordinated by the numerical component, which also enforces the boundary conditions. In addition, the numerical simulation components can be anywhere on the Internet, allowing for the use of supercomputing facilities. In the bridge example noted above, one NEES laboratory could likely handle two concurrent large-scale pier tests, being limited to a single span bridge. Distributing the piers within the networked laboratories can result in the performance evaluation of multi-span bridges, including the experimental evaluation of several piers. (Tsai et al. 2003)

4.3 IMPROVED HARDWARE ARCHITECTURE

In order to realize the potential of applications realizable through NEES, it is necessary to examine the test controllers at facilities enabled for hybrid simulation. Current control methodologies can be adapted to conduct such tests, but an improved hardware architecture as recommended here can allow for a faster and continuous execution of tests. The versatility of this hardware layout is first described for local real-time test and then expanded for network applications.

4.3.1 Multi-Tasking in Real-Time Applications

The typical architecture of a hybrid simulation controller consists of the integration loop commanding the inner servo-hydraulic controller loop as shown in Figure 4-1. A Digital Signal Processor (DSP) is used to compute the hybrid simulation algorithm in this setup. In their algorithm for real-time testing, Nakashima and Masaoka (1999) separated the on-line computer tasks into the

two tasks of integration of the equation of motion and signal generation. These two tasks were implemented within a single processor where the computational time is shared between the low priority task of integration (larger time step) and the higher priority task of signal generation (smaller time step). The separation of tasks allows for a large time step to be used for integration of the equation of motion. The faster time step for signal generation is selected to provide the controller with fast update rates, ideally this rate should equal the update rate of the controller.

Figure 4-2a demonstrates the division of the processor time during the execution of Nakashima and Masaoka's real-time algorithm. For each integration time step, Δt, the processor first handles the task of signal generation. Once completed, the integration task is executed until the smaller time interval δt has elapsed. At this instant, the processor interrupts the low priority task to handle the signal generation task for the next sub-step. This process continues until the integration task has been completed and is repeated at the next integration time step.

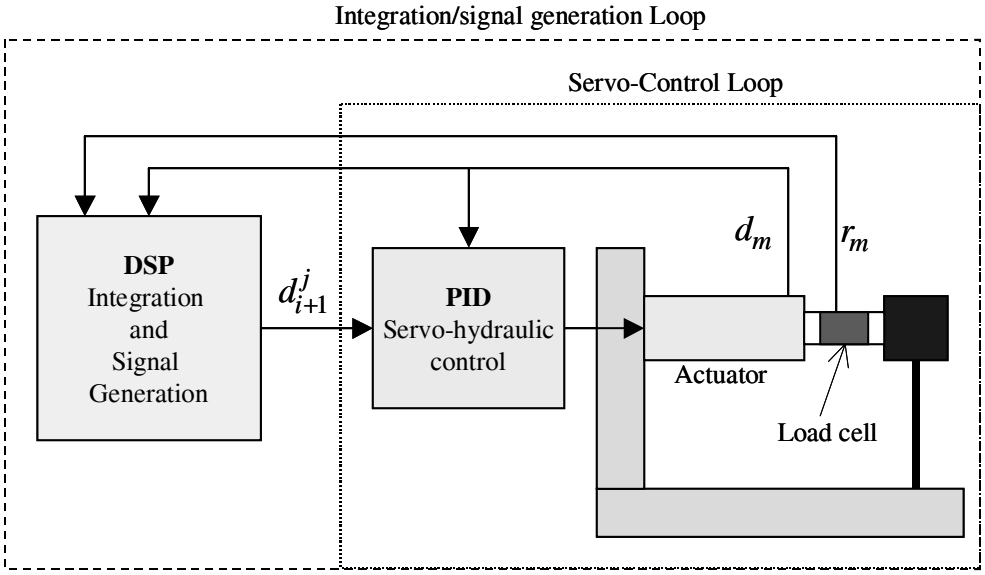

Figure 4-1. Two-loop architecture for hybrid testing

The execution of this hybrid simulation algorithm can benefit by separating these two tasks into different processors. The two processors application avoids interruption of the integration task, resulting in a faster computational time. A dedicated processor can facilitate the analysis of more complex analytical substructures within the same time step. Figure 4-2b illustrates the polynomial approximation procedure using a two-processor approach. The increase in computational

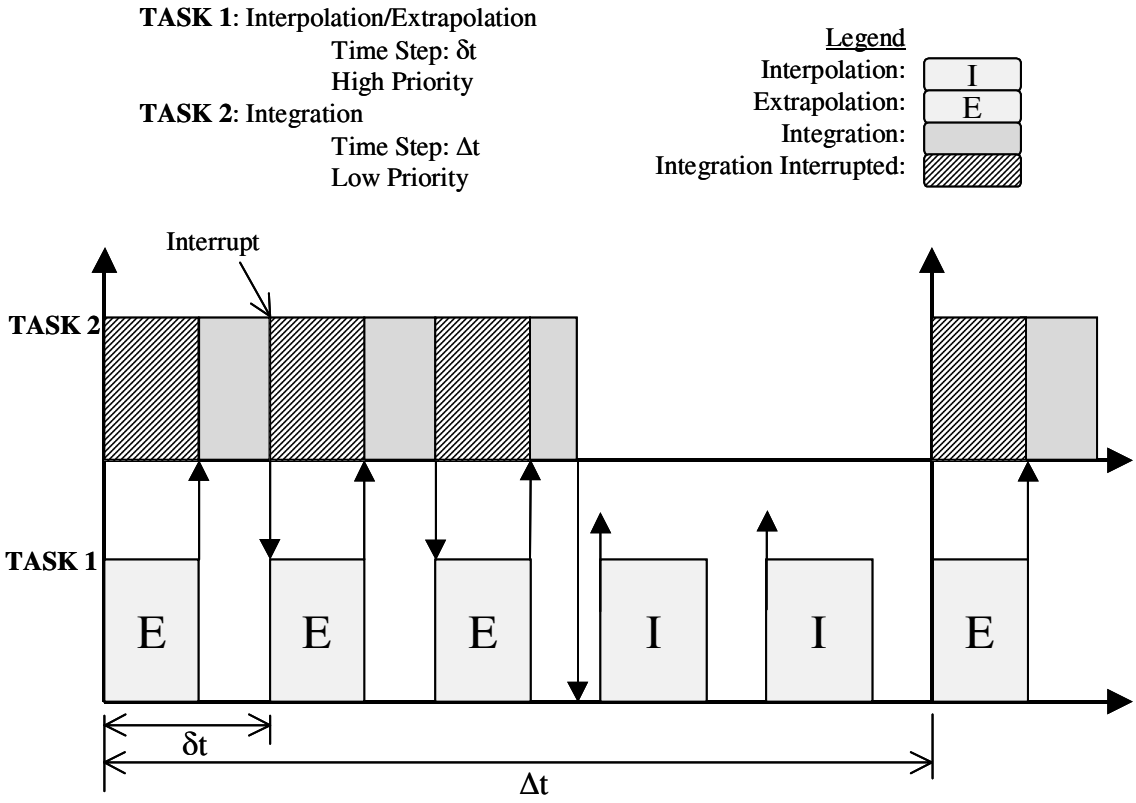

(a) single processor

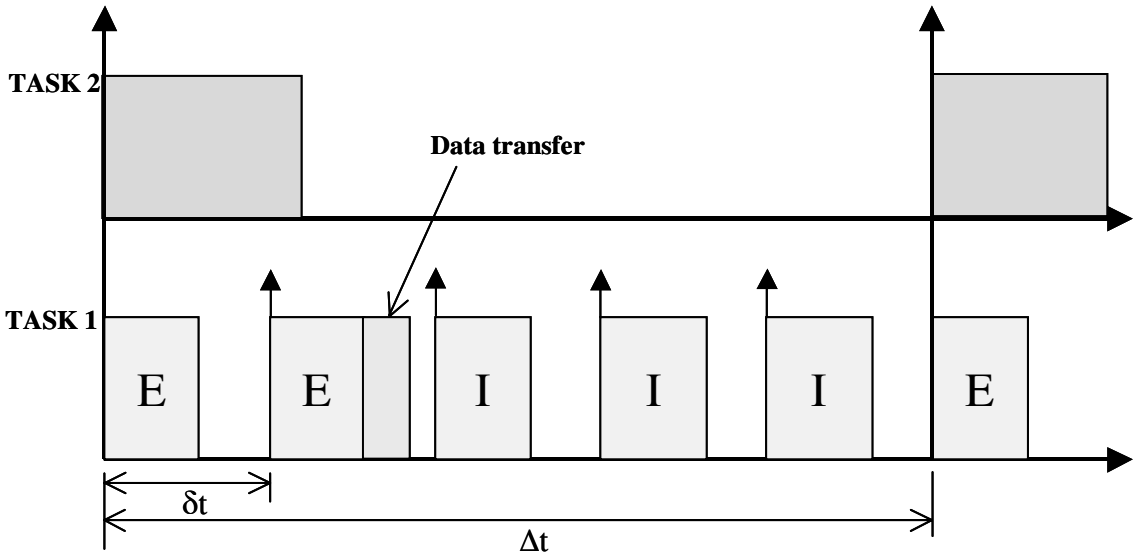

(b) two processors

Figure 4-2. Hybrid simulation extrapolation and interpolation task on one and two processors

time reduces the number of predictive commands based on polynomial extrapolation and increases the number of corrective interpolation steps. Alternatively, a larger analytical model can be analyzed using the same time step. The two-processor approach is especially beneficial as the number of actuators is increased and more time is required to complete the signal generation task.

Separating the two closely coupled tasks of integration and signal generation using two processors raises the issue of communication time between the two components. Note that for this particular method, there only needs to be one exchange of data between the two processors per integration time step, Δt. A shared memory resource (Systrans 2003) between the two processors can provide for fast data transfer rates on the order of or faster than the typical 1000 Hz rate for the signal generation task.

4.3.2 Three-Loop Hardware Architecture

Multi-tasking algorithms can benefit in execution speed by dividing tasks into different processors. This is particularly true when the exchange of information between the two tasks is small as is the case for the procedure previously described. The proposed controller for hybrid simulation is designated as a multiprocessor system running the three nested loops shown in Figure 4-3.

A close examination of the proposed hybrid test controller demonstrates the benefits of additional processors in an organized architecture. For the controller in Figure 4-3, the innermost loop is a PID servo-hydraulic controller tuned for optimal performance with the available actuators. This task is implemented on a dedicated processor for the servo-controller. The outer loop, or the integration loop, carries out the numerical integration of the equation of motion for a structure composed of analytical and experimental components. This task runs on a local or remote processor, different from the servo-controller and the DSP. The integration algorithm is a forward-marching time-stepping algorithm with a typical time step size on the order of 0.01 seconds. For real-time hybrid testing, the integration loop operates at a rate of approximately 100 Hz. On the other hand, the servo-control loop is executed at a rate of about 1000 Hz (Thoen 2003) or ten times faster than the outer loop running in real time. To synchronize the inner and the outer loops, an intermediate loop, labeled here the corrector loop, can buffer the exchange of data and, more importantly, guarantee that servo-hydraulic commands are updated at deterministic sampling rates. It is important

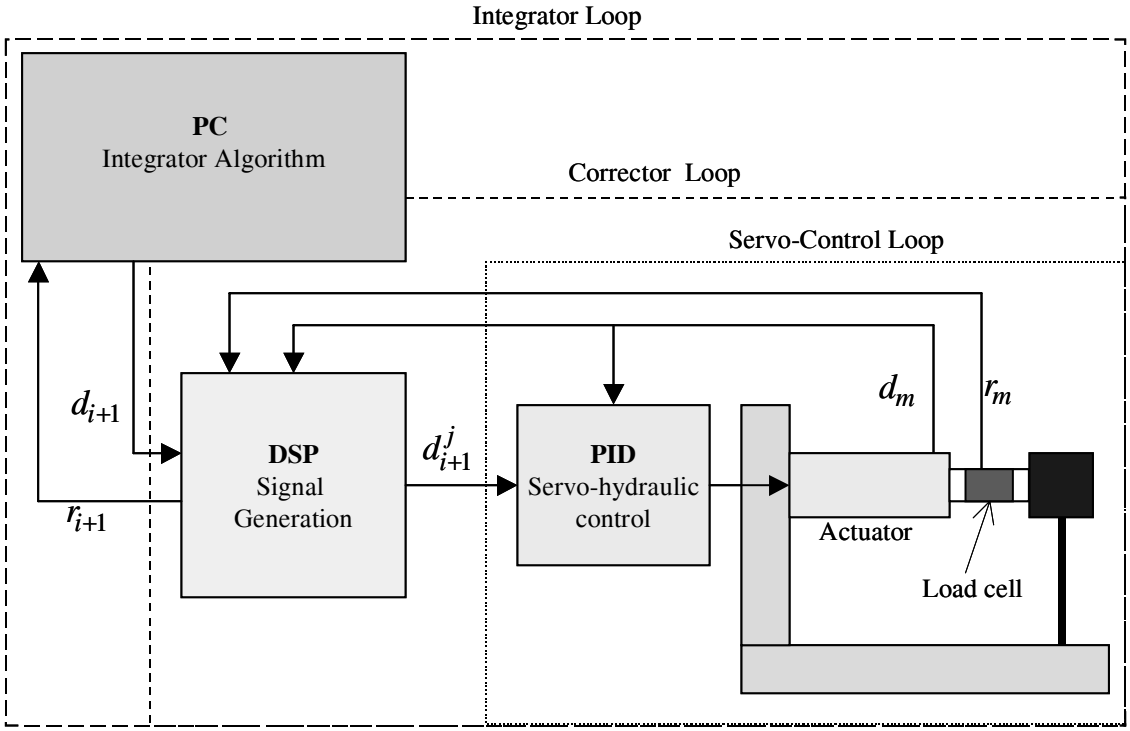

Figure 4-3. Three-loop architecture for hybrid test controller

for the real-time servo-hydraulic controller to receive command updates at constant time intervals to enable control of the actuator velocity.

The servo-control loop in Figure 4-3 runs on a real-time platform to insure stability of the servo-hydraulic control system. The integration loop may or may not be running in a real-time platform, depending on the testing protocol. In order for the corrector loop to generate updated commands at deterministic time intervals for each controller cycle, the corrector loop is also required to operate on a real-time platform. When the integration algorithm is not running in real-time, the corrector loop can be programmed to deal with uncertainties associated with the integration task.

The intermediate corrector loop also serves to separate the tasks of integration and generating a signal calibrated to the servo-hydraulic actuators. This allows for easier programming and implementation of the two tasks. For a slow pseudo-dynamic test, the corrector loop can simply generate the ramp loading command for each actuator. For fast continuous tests, this loop can carry out interpolation or extrapolation of the displacements based on Nakashima and Masaoka's cubic interpolation procedure. Other pseudo-dynamic test algorithms, such as displacement corrections

using the current restoring force feedback for implicit integration (Shing et al. 2002) or force correction using displacement feedback, can also be implemented in this intermediate loop. Furthermore, general multi-rate control approaches can be implemented and tested for use in this hybrid simulation environment.

4.3.3 Distribution for Network Testing

The three-loop architecture for the hybrid test controller also facilitates multiple-substructure experimental testing in local or remote sites. In a local testing configuration, a fast connection can be achieved between the integration loop and servo-hydraulic controller through a SCRAMNET interface (Systrans 2002). With consideration for longer delays, the integration PC can be remotely located and linked with the local signal generation DSP via the Internet. Similar links can be established with other remote experimental facilities having a network-enabled DSP commanding the servo-hydraulic system as shown in Figure 4-4.

4.3.4 Task Execution Timing

A distributed control scheme based on the three-loop architecture maintains a local command generator at each experimental site while conducting a geographically distributed test. The advantage to this approach can be seen in Figure 4-2b. For an experiment over the internet, random delays are likely to occur in the communication between the integrator and remote substructure. The communication time can simply be added to the integration task time and the additional processor is still beneficial. The local real-time DSP can generate continuous commands to the experimental setup regardless of delays in the integration and communication tasks. The next section presents an event-driven controller that replace the local signal generation task to deal with random communication delays.

4.4 EVENT-DRIVEN SIMULATION

Real-time based algorithms are not suitable for testing over the Internet (See Section 5.4.2 for characteristics of the network). In cases where task execution times are random, a clock-based control scheme could fail if the required processes are not completed within the allotted time. As an alternative to the clock-based scheme used for real-time applications, an event-driven reactive system

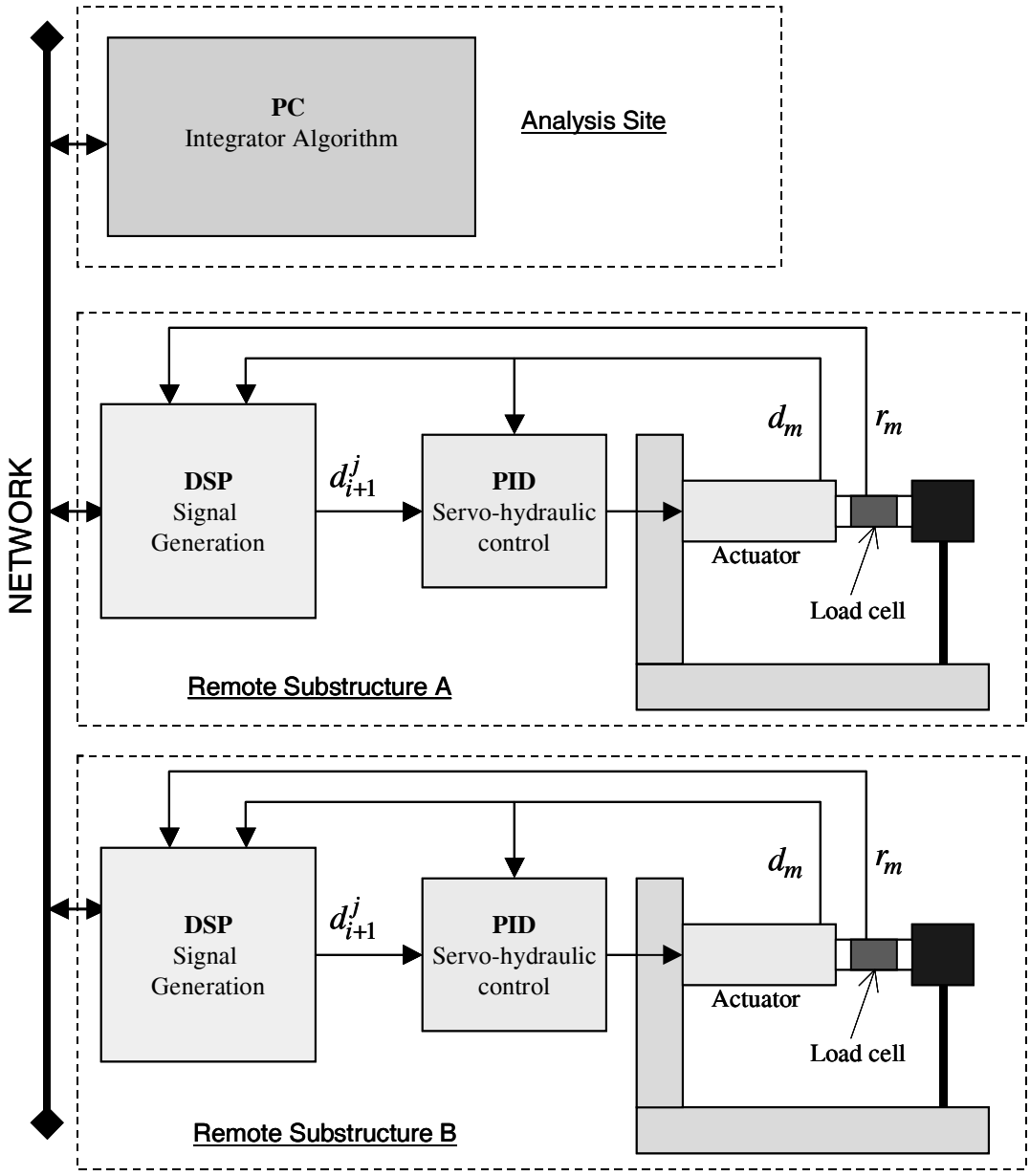

Figure 4-4. Distribution of hardware for geographically distributed testing

based on the concepts of finite state machines (Harel 1987) can respond to events based on the state of the hybrid simulation system. The event-driven controller can be programmed to account for the complexity and randomness of real systems and take action to minimize the effect of randomness on the experimental substructures. The programming procedure is based on defining a number of states in which the program can exist and transitions between these states that take place when specified events occur.

Nakashima and Masaoka's algorithm reacts to events in the sense that the algorithm switches from extrapolation to interpolation when the integration task has been completed. However, the variance in task completion times for their example application was very low. An explicit integration method was used and the DSP running these tasks had a dedicated and reliable connection to the servo-hydraulic controller. However, Nakashima and Masaoka's real-time hybrid simulation algorithm was not designed to handle iterative solvers for the equation of motion or remote substructures linked via the Internet.

4.4.1 Uncertainties in Hybrid Simulation

The use of advanced analytical tools may require the use of iterative solvers to integrate the equation of motion. The solution time for non-linear analytical sub-structures using implicit solvers can vary randomly from time-step to time-step. Factors influencing the number of iterations per step include the specified tolerance for convergence, the iteration algorithm selected, the non-linear models used in the analysis, and the degrees of freedom of the analytical model. There is also the likelihood that the integration method does not converge in a given step.

Similarly, for geographically distributed hybrid test, network transmission time is not known beforehand and can also limit the rate of testing. The internet, however, is less predictable than the integration algorithms and less control is offered in terms of assuring a maximum time for completion of the network transmission task.

4.4.2 Continuous Testing Using Event-Driven Controllers

Traditionally, hybrid tests have been conducted using a ramp-and-hold loading procedure for each integration step. This procedure is effective when dealing with random delays since the hold period can be extended arbitrarily. However, the hold period subjects the test specimen to force relaxation and should be avoided. Improved results can be obtained from a hybrid simulation if the actuators are commanded to load the specimen in a continuous fashion (Magonette 2001). The event-driven procedure presented here attempts to minimize, if not eliminate, the hold phase in each integration step.

A state transition diagram in Figure 4-5 shows the implementation of an event-driven version of Nakashima and Masaoka's polynomial approximation method. This algorithm continuously

updates the actuator commands under normal operation conditions and takes action for excessive delays. This diagram consists of five states: *extrapolation*, *interpolation*, *slow*, *hold* and *free_vibration*. The default state is *extrapolation*, during which the controller commands are predicted based on previously computed displacements while the integrator computes the next target displacement. The state changes from *extrapolation* to *interpolation* when the controller receives the next target displacement and generates the event *D_update*. Once this target displacement has been realized by the physical sub-structure, an event *D_target* is generated, and subsequently transitions back to the extrapolation state after sending updated measurement to the integrator.

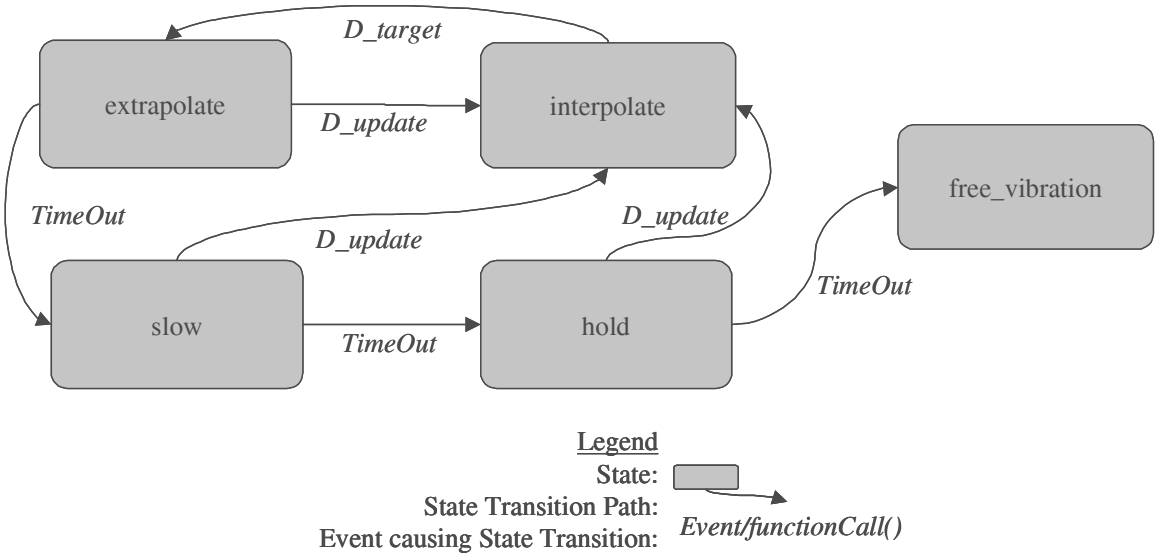

Figure 4-5. Finite state chart implementation of the polynomial extrapolation and interpolation algorithm with delay adjusting features.

Under normal operation conditions, the controller will continuously command the actuator to move based on extrapolation or interpolation of know displacement values. The smooth execution of this procedure is then dependent on having a reliable network connection and selecting the run time of each integration step sufficiently large for all required tasks to finish. Small variations in completion times for these tasks will only affect the total number of extrapolation steps versus interpolation steps.

The advantage of the event-driven approach is that logic can be programmed to account for excessive delays. For example, if the system is in the *extrapolate* state over a specified time interval, the actuator can deviate substantially or even exceed its target (Nakashima and Masaoka

1999). Limits need to be placed on the number of steps allowed to extrapolate. A simple solution is ordering a state change by throwing the event *TimeOut* to *slow* down the actuator. The *slow* state continuous to extrapolate at a reduced velocity, thereby allowing more time to receive an update from the integrator. Upon receiving the updated displacement, the *interpolation* state is activated. If updated displacements are not received after a specified number of steps, the *slow* state needs to *TimeOut* as well, placing the actuator on *hold* until the displacement is updated. Longer delays, possibly due to the integrator crashing or a network failure, could indefinitely delay the controller receiving an updated displacement, hence the *hold* state can also time out and force the system into *free_vibration* or any other desirable state to dissipate the energy in the system and end the test. The *free_vibration* state is intended to fully unload the structure based on locally stored mass and damping ratio for the test specimen.

The sample finite state machine discussed above attempts to carry out a continuous hybrid simulation and hold the actuator only if excessive delays are experienced during the experiment. Different methods can be explored to deal with delays, or other complexities that may occur during a hybrid simulation experiment. Other events, such as limit-detects and hydraulic interlocks, are handled by the servo-hydraulic controller hardware and need not be dealt with here at this time.

4.4.3 Reduction in Simulation Time

In addition to applying a continuous load trajectory on the experimental specimens, there is another advantage to the proposed event-driven method. The run-time of the test can be controlled to some extent, and in many cases reduced as compared to the traditional ramp-and-hold procedure. The polynomial extrapolation procedure moves the actuator towards the predicted target while the network transmission and integration tasks are carried out. Once the local controller receives the displacement target, the actuator should be approaching the target if the predictor scheme is successful. Given limits on actuator velocities, as is the case for loading large scale specimens, much less time is required to reach the target displacements after the advancements made by the predictor scheme. In addition, the ramp-and-hold loading procedures requires some settling time at the target displacement.

4.5 SUMMARY

A control scheme was presented for the implementation of hybrid simulation algorithms. The controller features a configurable architecture that allows for multiple-substructure testing on site or through the network. Test can be conducted at slow rates or approach real-time rates, where the speed is limited by the size of the numerical model and the rate capacity of the servo-hydraulic actuators.

The control scheme is also able to include logic developed through visual state chart programming to deal with uncertainties associated with implicit integration algorithms and network latencies. The effectiveness of state chart programming was demonstrated through a simple example that handled delays while minimizing force relaxation in the experimental test specimen. This example serves as a starting point in finding effective ways to deal with problems that may arise during a complex hybrid simulation experiment. More advanced methods are being explored to deal with complexities that can occur during a real-time hybrid experiment.

5 Facilities for Hybrid Simulation

5.1 INTRODUCTION

In this chapter, the experimental facilities used for the hybrid simulation conducted as part of this research are described. The testing system was designed for the implementation, testing and evaluation of hybrid simulation algorithms using a reduced scale apparatus. An on-line computer with real-time capabilities for hybrid simulations using slow continuous testing procedures and methods approaching real-time testing rates is included in this system. Methods for integration of the equation of motion, substructuring techniques, and techniques for error reduction can be implemented and verified experimentally. Additionally, the test system can be configured for multi-substructure testing, either locally or remotely distributed through the network.

Two identical experimental specimens and supporting hardware form part of the hybrid testing setup. Each specimen can be loaded by a dedicated actuator controlled by a computer that can also execute the hybrid simulation algorithms. The components of the test setup are described in Section 5.2 and the overall system architecture enabled for hybrid simulation is described in Section 5.3. The extension of this system for distributed testing applications and the network protocol is described in Section 5.4. The integrated hybrid simulation testing system is characterized in Section 5.5 to determine its limitations.

5.2 EXPERIMENTAL SETUP

The test setup consists of a PC with the dSPACE ACE 1104 Hardware Kit (dSPACE 2001), a servo-control and data acquisition system, two 12-kip hydraulic actuators, two test specimens and two reaction frames. A picture of the experimental setup is shown in Figure 5-1. Each reaction frame supports an actuator and cantilever specimen. The instrumentation frame to the right of the setup provides a fixed point of reference for measuring the absolute displacements.

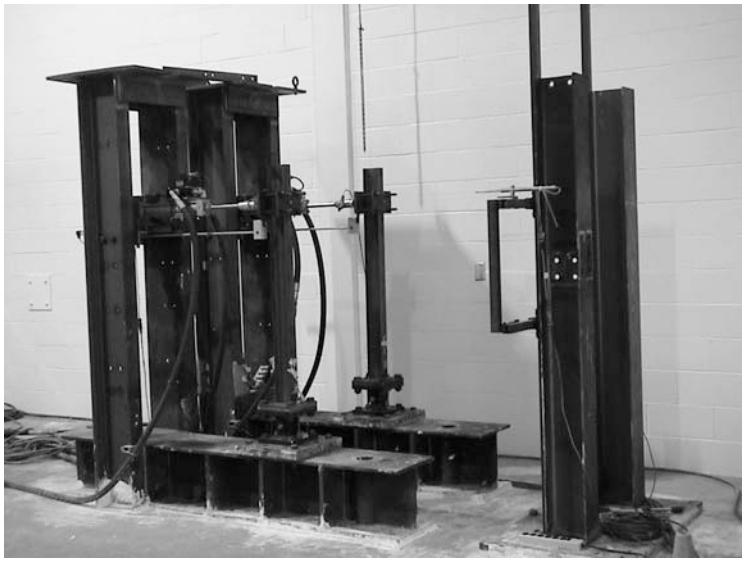

Figure 5-1. Small scale experimental setup for hybrid simulation

5.2.1 Test Specimens

Each identical test specimens consist of a cantilever column with an idealized plastic hinge connection at the base (van Dam 2000). The S4X7.7 column is 50 in. in length and welded all around at the base to a 9 in. by 9 in. plate of 1 in. thickness. The actuator is attached to the strong axis of the column at a distance of 42 in. from the base plate. The base plate is bolted to a specially designed clevis, which behaves as a plastic hinge zone of a steel beam.

A close-up photograph of the plastic hinge connection is shown in Figure 5-2a. The dimensions of the clevis and the coupons are shown in Figures 5-2b and 5-2c, respectively. The coupons are bolted to the clevis at both the top and bottom plates. The bottom attachment consists of the 1.5 in. threaded end of the coupon inserted into the 1-in. deep threaded hole of the clevis plate. The remaining 1/2-in. thread is used to tighten the connection with a nut. At the top end, the coupon is fastened both under and above the two bolted plates by nuts. The center-to-center distance between the coupons is 5.75 in.

The non-linear moment-rotation response at the clevis is obtained by a pin bridged with a pair of off-centered coupons. The pin connection provides the resistance to shear and axial load at the base while the coupons form a moment resisting couple. The pair of coupons emulate the behavior of column flanges. When loaded beyond the elastic limit, the coupons yield in tension or

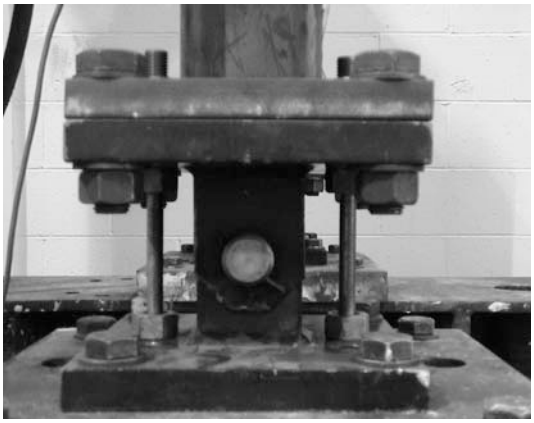

a. non-linear connection

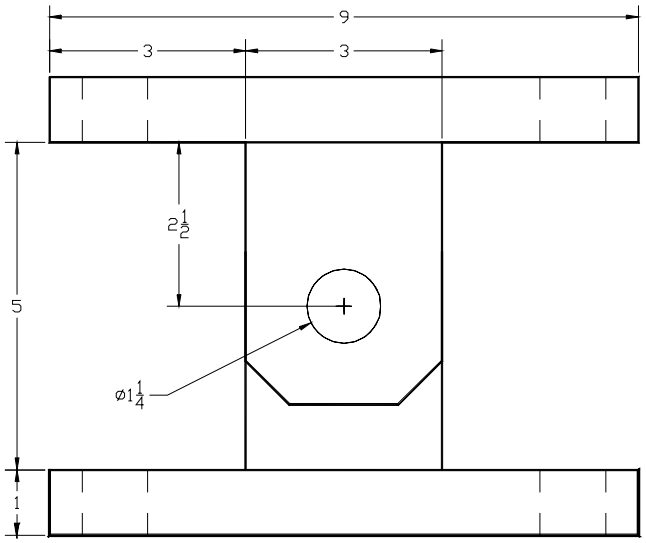

b. dimensions of clevis (in.)

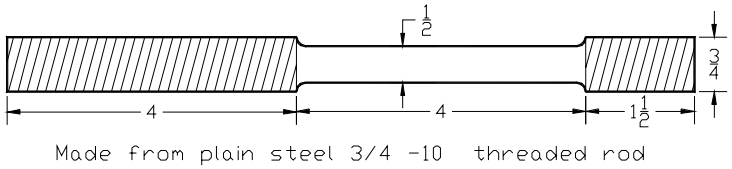

c. dimensions of coupon (in.)

Figure 5-2. Non-linear connection of cantilever column specimen

buckle in compression under the moment couple. The rest of the cantilever column remains within the elastic deformation range based on a capacity design approach. After a non-linear test, the inexpensive coupons can be easily replaced to begin a new test. The specimens provide good repeatability from tests to test and allow for the modeling of many types of behavior including brittle or ductile behavior with strength and stiffness degradation. Additionally, shake table tests data of a moment resisting frame utilizing these idealized plastic hinge connections is available to confirm their behavior under seismic loading (Rodgers and Mahin 2002).

The combined behavior of the beam and clevis was characterized by subjecting the specimen to cyclic loading at various amplitudes. Based on an approximate yield displacement, u_y, of 0.5 in., the load history consists of two cycles at each of the following amplitudes: $0.5u_y$, u_y, $2u_y$, u_y, $3u_y$, $4u_y$, $5u_y$, u_y. The applied load history is shown in Figure 5-3a with a cyclic loading rate of 0.02 Hz. This rate of loading is representative of the slow rates of testing expected for hybrid

tests over an Ethernet network. The displacements applied to the cantilever specimen were less than three inches in each direction to conform with the limits of the displacement measurement devices.

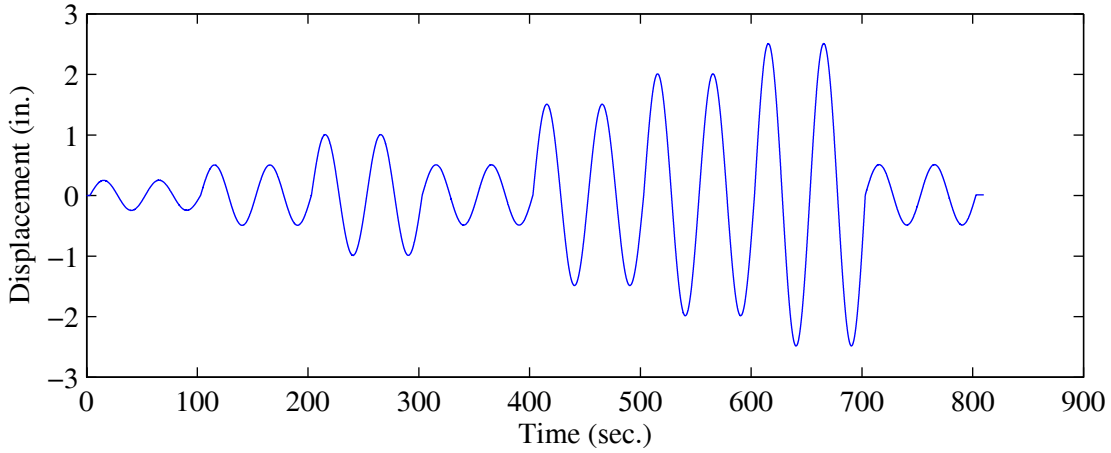

a. displacement history

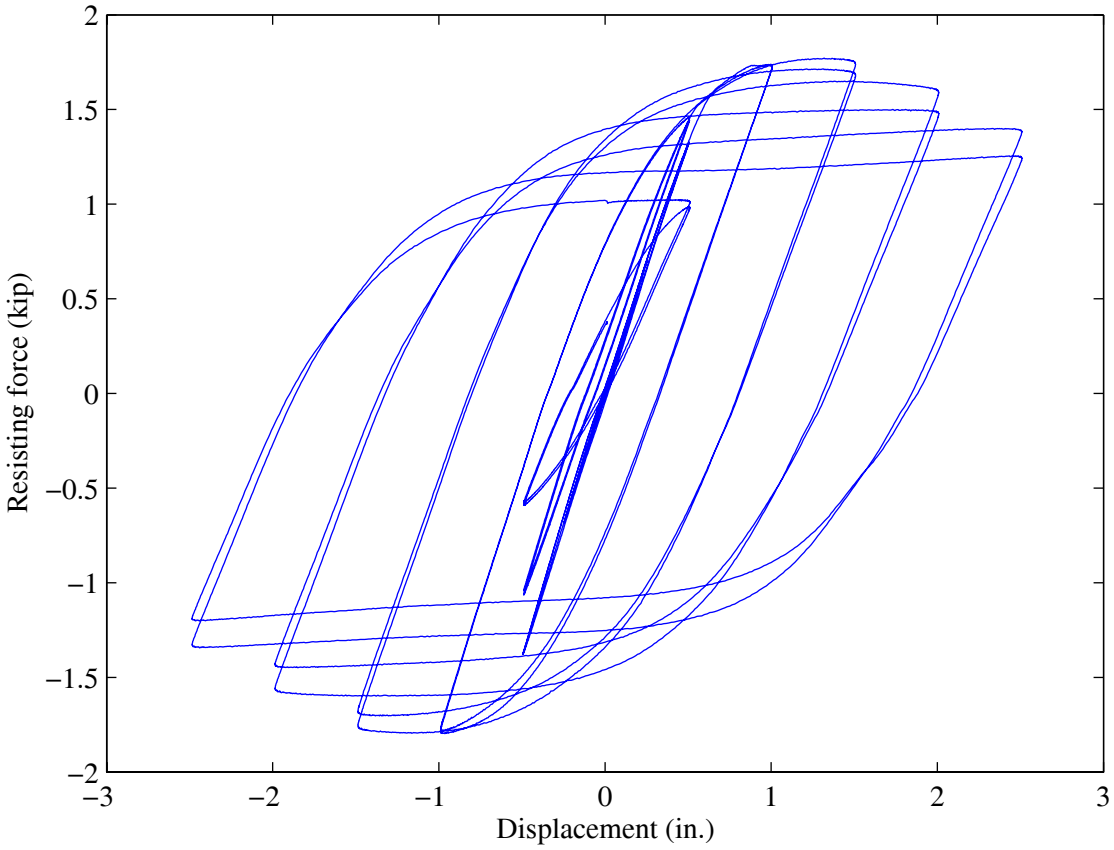

b. hysteresis

Figure 5-3. Behavior of cantilever column specimen subjected to cyclic loading

The measured resisting forces of the cantilever specimen subjected to the cyclic load history are shown in Figure 5-3b. Based on this data, the initial stiffness of the test specimen was estimated as 2.8 kip/in. with a peak resisting force of 1.8 kip. During the quasi-static test, the coupons buckled in compression as can be seen in Figure 5-4. The buckled shape of the coupons curve inwards towards the clevis as a result of the combined compression and rotational deformations at the top end restraints. The permanent damage to the coupons results in both strength and stiffness degradation evident in the measured resisting forces in Figure 5-3b.

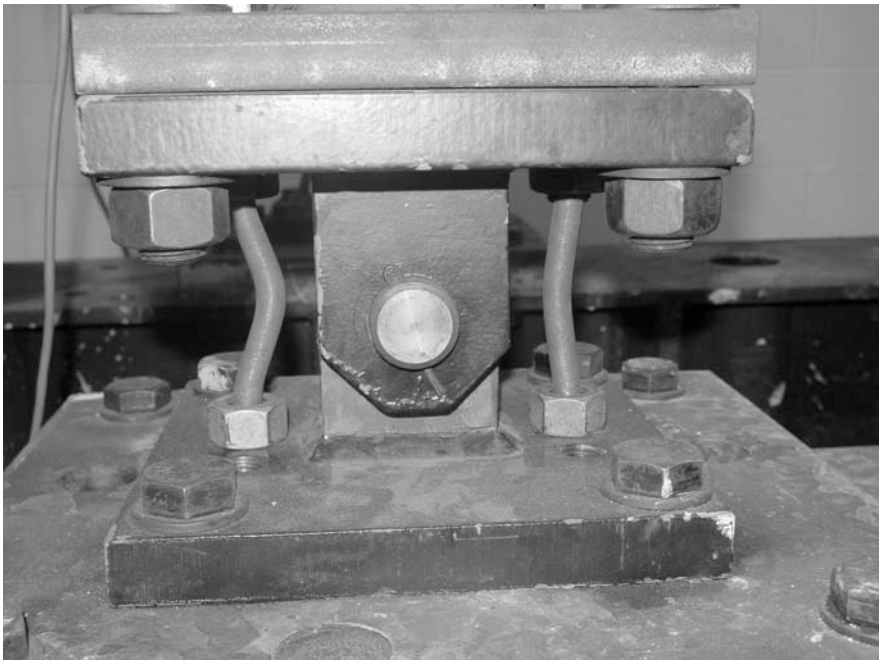

Figure 5-4. Buckled coupons in non-linear clevis connection

5.2.2 Servo-Hydraulic Actuators

The test specimens are loaded using two identical 12-kip servo-hydraulic actuator with a 15 in-stroke. The actuators have trunion mounts with a thru rod and are double acting, having equal areas of the piston subjected to hydraulic pressure when the actuator is moving in either direction. The effective piston area subjected to hydraulic pressure is 4.22 $in.^2$. The servo-valves are rated at 25 gallons per minute at 1000 psi and are connected to a hydraulic supply line maintained at 3000 psi by a local one-gallon accumulation system. The actuator is trunnion mounted to the reaction frame at the rear end of the cylinder body by fitted clamps tightened to allow rotation with minimal back-

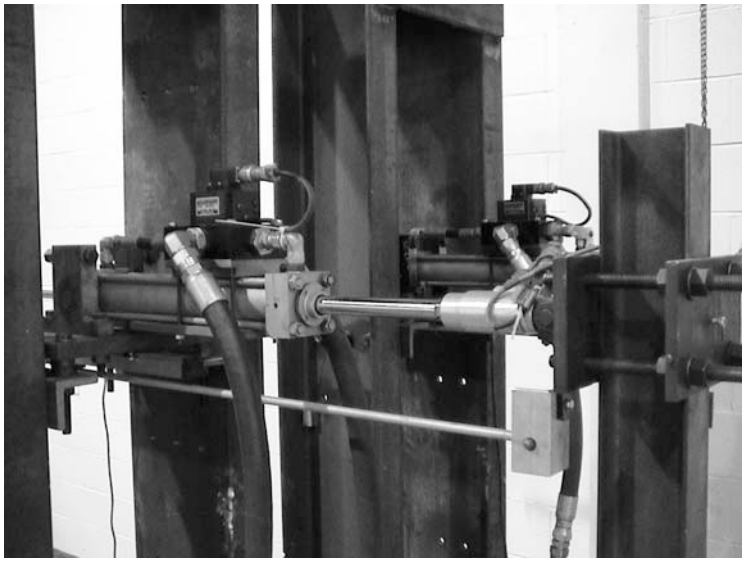

Figure 5-5. Photograph of servo-hydraulic actuator

lash in the connection. At the specimen end, the piston thru rod is screwed to an aluminum load cell followed by a uni-directional clevis. The clevis is bolted to the two plates clamping the cantilever specimen.

For identification purposes, the actuator near the back wall is labeled as Actuator1 and connected to channel 3 of the servo-controller. Actuator 2, shown at the forefront in Figure 5-5, is connected to channel 2 of the servo-controller.

5.2.3 Reaction Frame

A self-equilibrating reaction frame was designed to support the actuators and specimens under static and dynamic loading conditions. The frame was designed to remain elastic when loaded to full capacity with up to two 12-kip hydraulic actuators. However, some elastic deformations were permitted, mainly for future studies evaluating the dynamic interaction of the reaction wall with the actuator and specimen. Additionally, the test frames were designed to cover a range of stiffness and period ratios between the reaction frame and the specimen that are expected for large-scale testing. The expected dynamic properties of the reaction wall and specimen were obtained from an analysis of different wall configurations and sample specimens using the reconfigurable reaction wall of the Berkeley NEES facility (Stojadinovic et al. 2002).

The reaction frame base consists of an 8 ft. W14X176 beam with two through holes 6 ft. apart for post-tensioning to the strong floor. The web is reinforced by five 1-in. thick stiffener plates welded on each side. The reaction column consists of two MC12X40 channel sections providing for an effective moment of inertia of 468 in.^{4}. Each channel section is welded to the top and bottom flanges of the base beam and the two the stiffener plates positioned at the edges of the column. Additionally, the channel sections are welded to a 3/4 in. plate at the top to prevent the columns from twisting. The 27X27 in. top plate also serves as a platform for adding mass to the reaction frame to modify its dynamic properties.

System identification of the reaction frame by free and forced vibration tests determined the fundamental frequency to be 37 Hz, which is sufficiently higher than the frequency range of interest for seismic testing. It was also experimentally verified that the frequency of the frame can be reduced to 23 or 18 Hz by adding 0.5 kip or 1 kip of mass to the top plate.

5.2.4 Instrumentation

Instrumentation provides the feedback for the two inner closed loops shown in Figure 4-3. Displacement measurements are used for the servo-hydraulic control loop and force and displacement measurements are recorded by the local digital signal processor (DSP), which collects the data for the hybrid simulation algorithms. A list of the instrumentation used in the experimental setups and the corresponding channel numbers are listed in Table 5-1. The table lists the channels from the ATS servo-control system and the dSPACE DSP used for signal generation. It should be noted that the dSPACE channel listings correspond to the local testing configuration using a single on-line computer. The instrumentation and command channels corresponding to Actuator 2 are moved to the second on-line computer for distributed multi-substructure network testing.

Two principal instruments are used to measure the response of each cantilever specimen. A ± 12 kip load cell between the actuator and the specimen shown in Figure 5-5 measures the resisting force. A ± 3 in. displacement transducer located on the instrumentation frame shown in Figure 5-1 measures the absolute horizontal displacement. The free-standing instrumentation frame is used to remove the effect of backlash in the actuator clevis and flexibility in the reaction frame from the measured data by providing an absolute frame of reference. A secondary ± 10 in. displacement transducer attached to the reaction frame underneath the actuator also measures the

Table 5-1. List of instrumentation

Channel No.		*Instrument*			*Description*
ATS	*dSPACE*	*Type*[1]	*Range*	*Units*	
0		NOVO	*±10*	in.	axial displacement of actuator 1
1		NOVO	*±10*	in.	axial displacement of actuator 2
2	ADC2	LC	*±12*	kip	axial load in actuator 1
3	ADC4	LC	*±12*	kip	axial load in actuator 2
4	DAC1	D/A	*±3*	in.	command signal for actuator 1
5	DAC2	D/A	*±3*	in.	command signal for actuator 2
6	ADC1	DCDT	*±3*	in.	absolute displacement of cantilever specimen 1 at actuator elevation
7	ADC3	DCDT	*±3*	in.	absolute displacement of cantilever specimen 2 at actuator elevation
1. NOVO = Novotechnik position transducer, LC = load cell, D/A = digital to analog converter output from dSPACE, DCDT = direct current displacement transducer					

displacement of the actuator. The additional instrument is necessary to cover the complete 15 in. stroke of the actuator. If control of the actuator is lost and the ± 3 in. displacement limits of the primary device are exceeded, control of the actuator can be retained by switching the feedback device in the control loop to the ± 10 displacement transducer.

5.2.5 Servo-Hydraulic Control System

The basic system used for load controlled quasi-static testing at the UC Berkeley Earthquake Engineering Research Center was also utilized for hybrid simulation. The system consists of a 386 PC running Window 3.1 to conform to legacy software developed by ATS for management of the servo-control and data acquisition hardware. Through the D/A and A/D converters, the computer interfaces with a 4-channel analog servo-valve controller manufactured by MOOG and sixteen channels of data acquisition equipped with PACIFIC INSTRUMENTS signal conditioners. A picture of the servo-hydraulic control system is shown in Figure 5-6.

Primary control of the actuator is handled by the software through a digital implementation of a Proportional-Derivative control algorithm. The computer sends the control signal based on the error (difference between command and measured displacement) and its time derivative to the MOOG servo-controllers, which then generates the appropriate electrical signals to command the

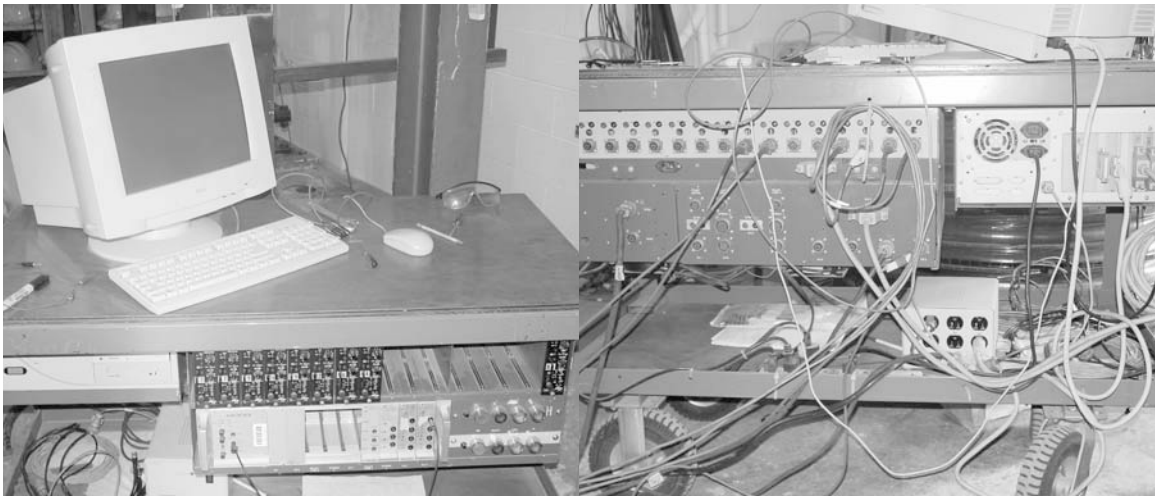

a. front view b. back panel

Figure 5-6. Photograph of servo-control computer and data acquisition system

servo-valve. A control strategy utilizing the time integral of the error signal is not implemented in this controller. The feedback signal for closed-loop control can be obtained from instruments attached to any of the sixteen data acquisition channels, including linear combinations of these channels. The servo-control software provides the necessary functions to safely run servo-hydraulic actuators such as limit detects with automatic hydraulic shutoff, a function generator for commanding load histories and a recorder for data acquisition. However, the test system does not include the capabilities for on-line computation necessary to implement hybrid simulation algorithms. A second computer (DSP) was integrated with this system to provide these capabilities.

5.2.6 On-Line Computer

The on-line computer consists of a PC running the Windows 2000 operating system and the Mathworks (2003) software: Matlab, Simulink, Stateflow and Real-Time Workshop. This computer is complemented by the dSPACE ACE KIT 1104, which includes a Texas Instruments DSP TMS3220F240 on a PCI board with a 250 MHz processor and 32 MB of RAM, software for communication and control of the DSP from the host computer, and software for downloading and running Simulink models for real-time applications. The DSP is able to interface with analog devices through an external connector panel with 8 D/A output channels, 8 A/D input channels. A photograph of the host computer and the dSPACE hardware is shown in Figure 5-7

a. two host computers b. DSP PCI card with connector panel

Figure 5-7. On-line computer with real-time capabilities for hybrid testing

The on-line computer was integrated with the existing servo-hydraulic control system using the least intrusive means, although not the most efficient. The difficulty in integrating the two systems is that the existing servo-controller is not equipped with an analog input for external function generation of actuator commands typical of many controllers. Instead of physically altering the internal wiring to obtain such and input, a different approach was taken to convert the existing load control test setup to a hybrid simulation enabled test system. The dSPACE command signals were calibrated to the same volt-displacement ratio as the feedback displacement transducer and this analog output was connected into the data acquisition channels on the servo-controller. The net feedback for the actuator was then selected as the difference of the displacement feedback measurement and the input command from dSPACE. As can be seen from the control feedback diagram in Figure 5-8, the resulting error signal will move the actuator according to dSPACE command signal while the ATS command remains constant. One drawback to this approach is that the command first goes through a signal conditioner where the filter process delays the signal. This testing setup was found to work well only for slow rates of testing.

To enable hybrid simulation with the on-line computer, measured data from the experimental setup is required as feedback. Analog signals of the measurements for all data channels are available through back panel connectors of the data acquisition system. These banana type connectors provide the filtered signals from the signal conditioners which were routed to the A/D inputs

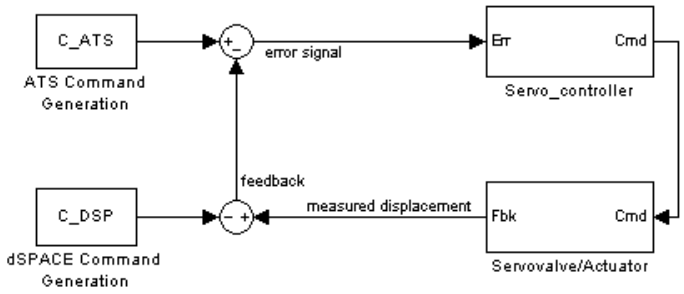

Figure 5-8. Feedback diagram for commanding actuators from the DSP.

in the DSP connector panel. A direct connection between the two systems resulted in an electrical noise signal being generated by dSPACE, resulting in large amplitude noise in the digitized measurements. To eliminate this effect, a second signal conditioner was added between the servo-control system and dSPACE, at the expense of additional filtering delays in the control loop.

5.3 EXPERIMENTAL SYSTEM FOR HYBRID SIMULATION

Using the experimental equipment described above, the hardware was configured based on the architecture described in Chapter 4. Using the three-loop control scheme, the ATS software and the MOOG analog servo-control cards carried out the servo-control loop, the signal generation task was executed in the dSPACE real-time DSP, and the integration task was handled by a standard PC (host to the DSP) running Matlab. Two different setups were configured: one for local testing and the other for distributed testing over the Internet. The two configurations are described in the sections that follow.

A third configuration was also implemented where the integration and signal generation tasks were both implemented in the real-time processor. This latter configuration, similar to that used by Nakashima and Masaoka (1999), allowed for faster rates of testing. Real-time testing rates were not possible with the existing actuators because of the cut-off frequency limit described later in Section 5.5.1. Only the three-loop configurations for local and network testing are described in this report.

5.3.1 Local Configuration

The configuration for local testing consists of single PC hosting the DSP, the servo-control and data acquisition system, and the two experimental test specimens. The integration of the equation of motion for the structural model is handled by the host PC processor and the signal generation task is handled by the DPS on the PCI bus. The integration algorithm running in Matlab can read and write directly to the memory of the DSP through the PCI bus interface. The DSP communicates with the servo-control system by sending analog command and receiving analog feedback signals as explained in Section 5.2.2. The hardware configuration layout for local testing is illustrated in Figure 5-9.

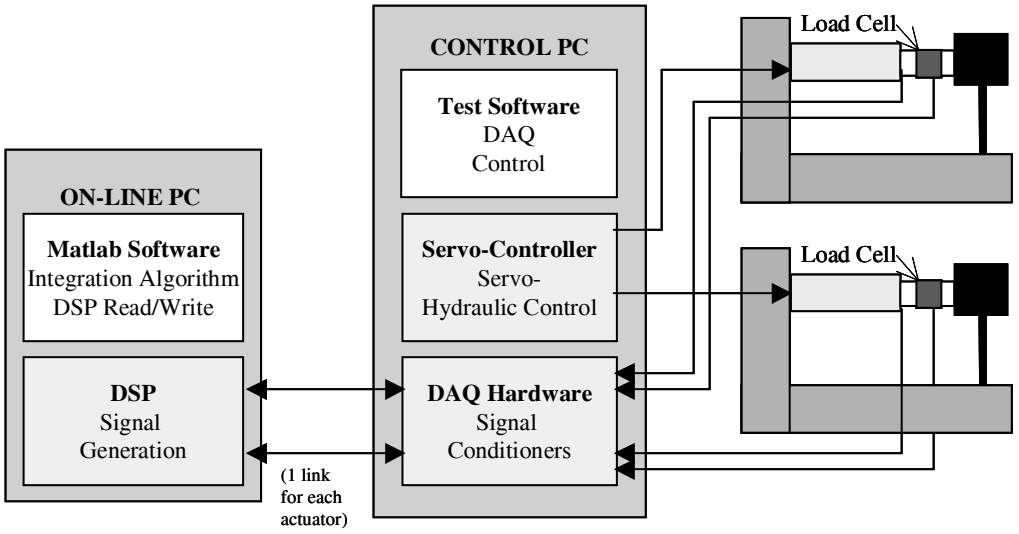

Figure 5-9. Hardware configuration for local testing

5.3.2 Network Configuration

For distributed network tests, it was necessary to modify the configuration of the on-line computer. The signal generation task remained in the local DSP to maintain deterministic update rates to the servo-controller. The host on-line PC served to relay information coming in from the remote analysis PC via Ethernet to the DSP. The integration algorithm was moved to a separate PC with Matlab and Ethernet capabilities. Thus, the host PC did not have an active role: this is the principle difference compared to the local test configuration. The communication link between the DPS and the servo-controller remained the same.

The hardware configuration layout for distributed testing is illustrated in Figure 5-10. At the experimental site, a second on-line computer was added to simulate a testing environment with multiple remote substructures. Each of the two on-line computers shown in Figure 5-10 control a single test specimen and communicate only with its corresponding substructure. Although the servo-control system is shared, each test setup uses different channels for control and data acquisition with no local coupling between the two. Each on-line computer has its own network identification IP number and, thus can be located anywhere on the Internet. Since the purpose of the research presented here is the development of a distributed control system, the single physical location for all the hardware simplified debugging of the network software. However, software developed in this local configuration can be directly applied to a hybrid simulation with multiple remote substructures. The details of the network protocol are discussed in the section that follows.

5.4 NETWORK PROTOCOL

A connection between the analysis computer and the computers controlling the remote substructures is established using a Matlab toolbox for distributed processes (Andrade 2001, Rydesater 2001). This software first opens a Transmission Control Protocol/Internet Protocol (TCP/IP) connection between one computer and multiple daemons in the Matlab environment. Once the connection has been established, the coordinating computer responsible for the numerical analysis of the structural model can send and receive data from multiple remote computers. This allows the analysis engine to send commands and receive measurements from the remote sites.

5.4.1 Description of Communication

For distributed hybrid simulation, the amount of data that needs to be exchanged through the network is relatively small, typically tens of double precision variables for multiple substructures. However, the amount of time required for a computer to send a small amount of data to a remote computer and receive a response can be substantial. In order to minimize the amount of time to run a test over the network, the number of data transactions within each simulation step should be reduced. Using TCP/IP for the transfer of data, a communication protocol was developed to manage the exchange of data between the analysis site and remote hosts of the experimental sim-

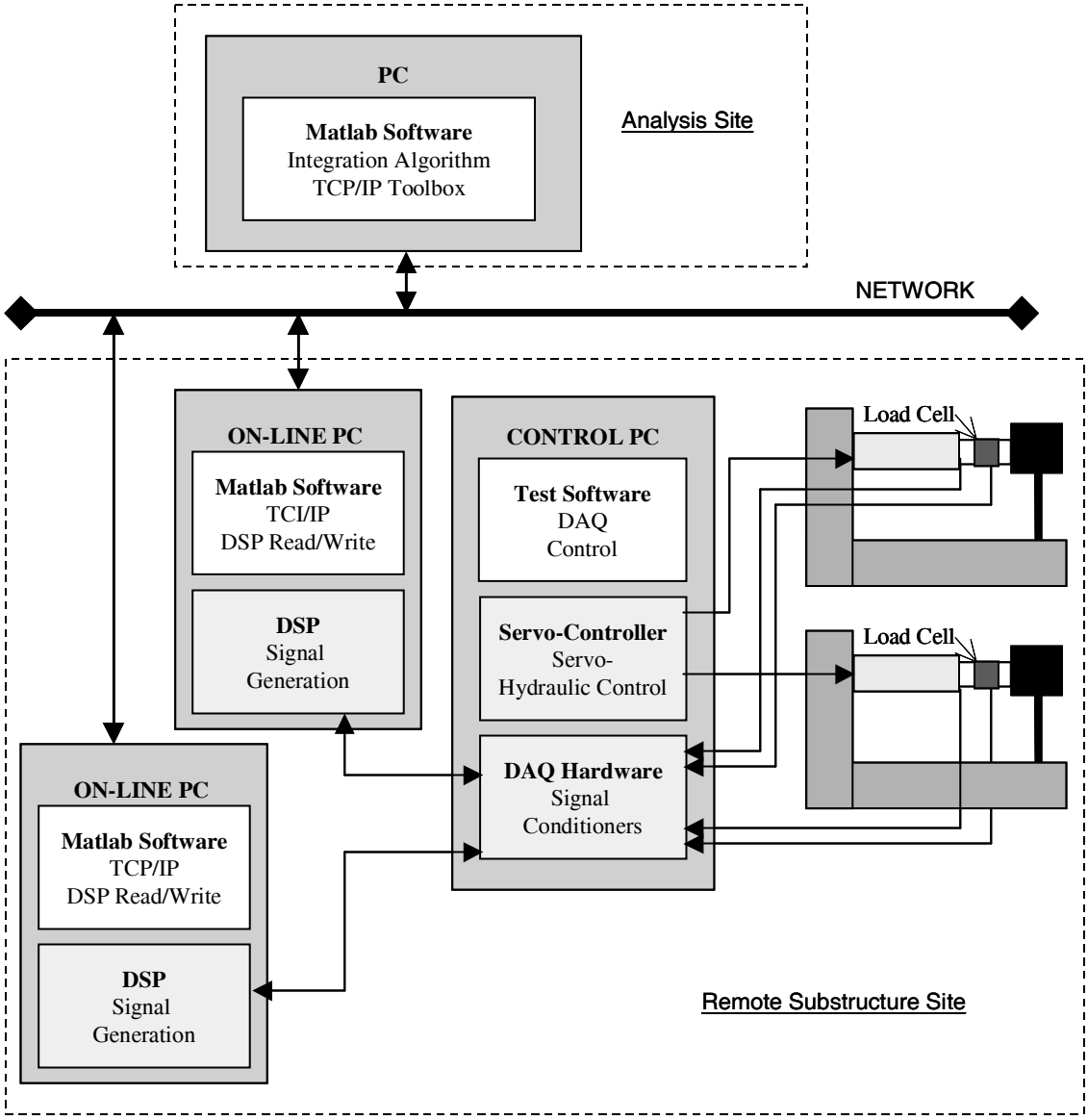

Figure 5-10. Hardware configuration for network testing

ulations. The purpose of this protocol is to attain a reliable working system and to test the effectiveness of the distributed event-driven control scheme.

The communication protocol is divided into three sections:

1. *Initialization*
2. *Execution of Test*
3. *Termination of Network Connections*

The major steps in each of these tasks are listed in Table 5-2 for the three computers involved in the distributed network configuration. The computer coordinating the overall simulation is the numerical simulation computer, which communicates through Ethernet with the host DSP computers at the remote sites. The host computer communicates with the DSP by reading and writing to its memory and relays information back to the integrator. The servo-controller is not included in the table since it plays a passive role in this process, accepting commands from the signal generator at all times.

In order to reduce the run-time of a simulation, the steps during the execution of the test are minimized since this process can be repeated thousands of times. To this end, several steps are involved in the initialization procedure to ensure that the network connection has been established with the correct remote hosts and the controller is ready to accept commands. The TCP/IP connections opened during the initialization phase are maintained opened for the remainder of the experiment.

For multiple remote substructures, the integration computer carries out a similar communication sequence with the other remote host computers starting with identifying the remote hosts based on its IP number. The integration computer must receive a confirmation from all remote experimental sites before moving on to the next step.

5.4.2 Characterization of Network

Simulations were carried out to characterize the behavior of the network for conducting distributed hybrid tests. Two computers connected on the Internet were used for this purpose: the first computer acted as the structural analysis site integrating the equation of motion and the second computer simulated a remote substructure. The integration computer computes the response of single degree of freedom linear structure using an explicit integration algorithm in the Matlab environment. The tasks of the remote computer are to receive a displacement value, multiply it by a given stiffness and return the force value to the integrator. The remote computer simulating the test specimen is also carrying out the computations in the MATLAB environment. Thus, this simulation captures the time required to complete the tasks of integration and network communication in each step. The tasks omitted from a real hybrid simulation include moving the actuators to the target displacement and taking measurements.

Table 5-2. Communication protocol for network tests

Integration PC *Analysis Site*	*Remote Host PC* *Experimental Site*	*Command Signal Generator* *Experimental Site*
INITIALIZATION		
load analytical structural model	initialize network.... search for port at integration PC IP	Start up hydraulic power to actuators and zero out loads. Start DSP...initialize set-point at current displacement and wait for command from host
initialize network... open ports and listen		
	found port... report own IP number... listen	
identify substructure based on IP... request controller status		
	forward controller status... listen	
if all controllers are ready... start		
EXECUTION OF TEST *(repeat until simulation time has elapsed)*		
compute d_{i+1} and send		
listen for update	write d_{i+1} to DPS memory	
	listen for update	interpolate towards d_{i+1}
		target reached... measure r_{i+1}
	read r_{i+1} from DSP memory and send to integrator	extrapolate towards predicted target and listen for update
read r_{i+1}, update structural response	listen for update	
TERMINATION OF NETWORK CONNECTIONS		
request to close connections		shut down hydraulic power
	close connections	
close port		

Communication between the analysis computer and the computer simulating the experimental substructure is established using the Matlab TCP/IP toolbox. For these simulations, the integration computer opens two communication ports with the single remote computer. One port is used for sending data and the second is used for receiving data throughout the simulation.

Network communication time measurements from a local area network configuration (LAN) and a wide area network configuration (WAN) are demonstrated. In the LAN configuration, both computers are on the same sub-network in RFS. In the WAN configuration, one computer is located at RFS and the other at the UC Berkeley campus. A network trace showed that three routers are used to link RFS and UC Berkeley. A baseline time was also established by directly connecting the two computers using a twisted-pair wire to cross-over their Ethernet ports. The direct cross-over configuration determines the time it takes for both computers to carry out their computational tasks and send and receive data through Ethernet. The use of additional network hardware, such as a hub, is also investigated in the LAN configuration.

The randomness associated with network transmission time and the Matlab environment is shown in Figure 5-11 for 500 simulation steps. The four plots demonstrate the different network configurations listed in the subtitles. The four subplots in Figure 5-12 show the histograms corresponding to the time histories plotted in Figure 5-11. The configuration used for Figure 5-11a is the Ethernet cross-over cable. Figure 5-11b shows that the same two computers connected over the LAN have a similar time distribution as the direct cross-over connection. The histograms in Figures 5-12a and 5-12b verify that there is negligible time delay within the LAN. The major delays result from Matlab and internal operations in the computer to transfer the data through Ethernet. For both configurations, the average step duration is 0.208 seconds.

The data in Figure 5-11c examines the effect of additional hardware in the network by repeating the LAN test with and additional NetGear DS108 Hub in the loop. For this case, an increase in delayed steps is evident from the histogram in Figure 5-12c when compared to Figure 5-12b.

Figure 5-11d demonstrates the behavior of a WAN, where one computer is located in RFS and the other in Davis Hall. The distribution of the step time is shown in Figure 5-12d. The effect of the additional three routers is that each simulation step takes longer on average and frequent excessive delays are experienced. The average step takes 0.286 seconds and range from a minimum of 0.16 to a maximum of 1.26 seconds. The minimum value is similar to the crossover cable configuration, which indicates that no delays are experienced in the routers for these steps and that communication over an uncongested WAN can be efficient.

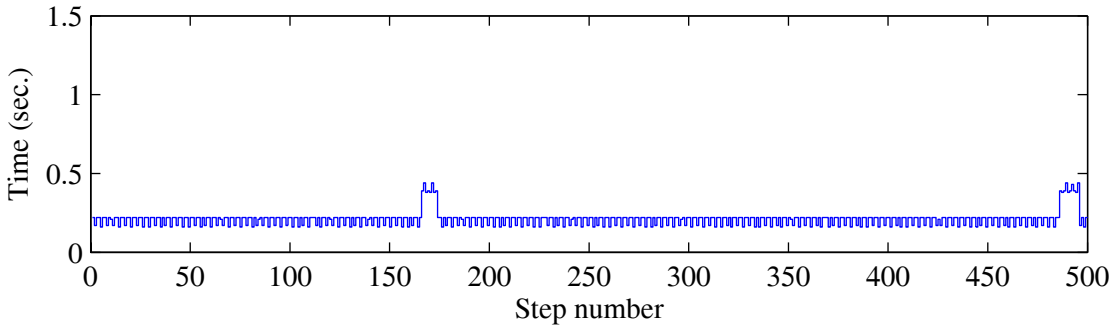

a. Ethernet crossover cable

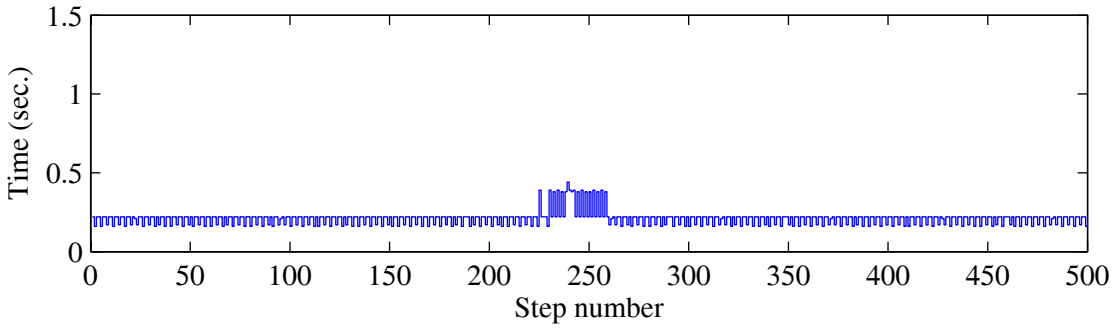

b. RFS LAN

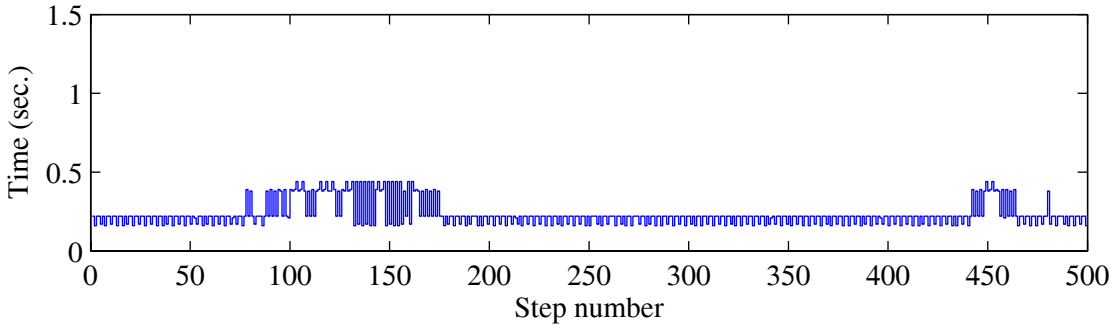

c. RFS LAN with Hub

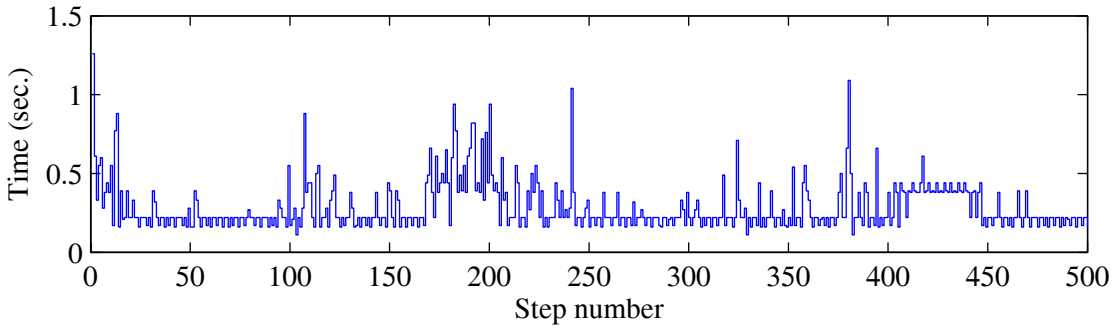

d. RFS and Davis Hall

Figure 5-11. Time duration of 500 steps of hybrid simulation using various network configurations

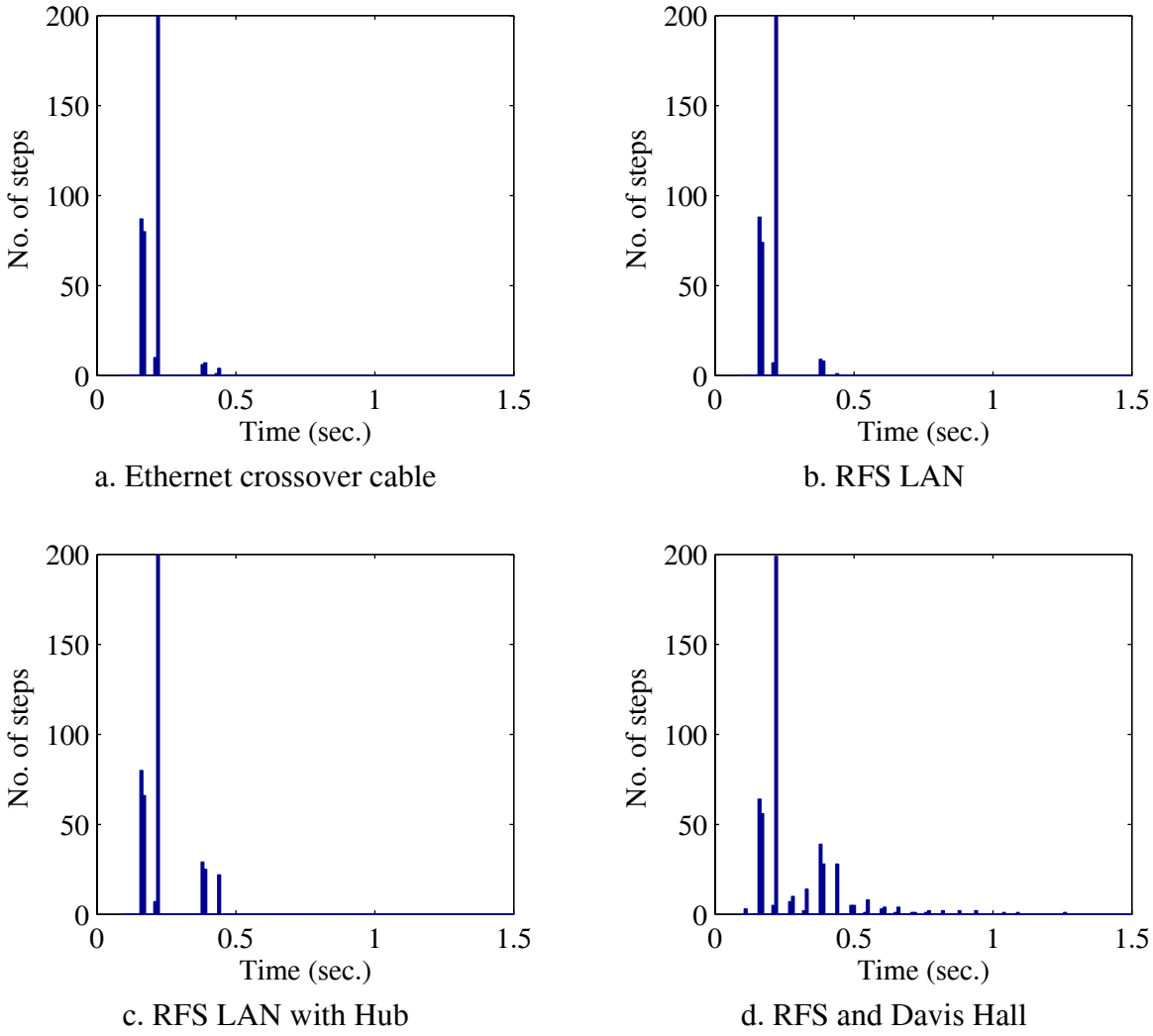

a. Ethernet crossover cable

b. RFS LAN

c. RFS LAN with Hub

d. RFS and Davis Hall

Figure 5-12. Histograms of data in Figure 5-11

The histograms can be used to derive or fit a statistical distribution to estimate the expected duration of a simulation step. However, the distribution is likely to vary with time and day, depending on the network congestions. As a result, a completely different set of parameter may be obtained from various trial run. Instead, a simpler approach is taken to model the random behavior of the network. Figure 5-13 plots the cumulative number of steps completed within a specified time for the test between RFS and the UC Berkeley campus. From this plot, a target percentage of steps that will be completed within an allowable time can be estimated. The timing scheme for the event-driven controller can be selected accordingly. For example, if the goal is to allow 95 percent of the steps to complete without having to slow down the actuator, then 0.6 seconds should be allocated

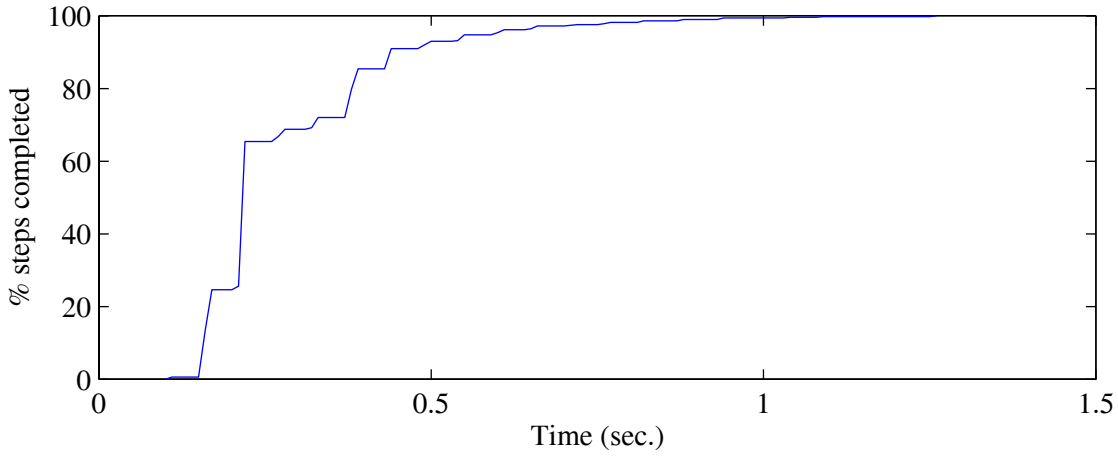

Figure 5-13. Cumulative number of completed simulation steps vs. time

for network communication. However, no guarantees can be made that during the actual experiment, the network and computers involved will complete the tasks as expected or within a maximum time. In fact, network delays as long as 20 seconds have been observed in one step.

A further statistical analysis of the network timing is not presented because the fitted distribution variables are trial-dependent. Also, sufficient data is not available at this time to reasonably characterize the network behavior. Experiments conducted within more distant facilities are likely to have a wider distribution since more routers will link the network travel path. The data presented here was obtained using computers located relatively close in terms of distance and the number of routers in the network path.

5.5 SYSTEM CHARACTERIZATION

The reliability of the results from a hybrid simulation are highly dependent on the performance of the experimental setup. The servo-hydraulic system should be able to correctly apply the command displacements or forces on the experimental substructures and obtain accurate measurements of the specimen response. The performance of the servo-hydraulic system depends on the flow capacity of the pumps, the accumulation system, and the size of the hydraulic actuators. Limitations imposed by the servo-hydraulic system play a significant role in selecting the scale size of the experimental specimen based on the maximum loads that can be applied. Also, the rate of testing is limited by the dynamic performance of the actuator, which can be characterized by its frequency

response function and maximum velocity. In order to conduct a real-time test, it is necessary for the actuator to track the command signal accurately within the entire frequency range containing the natural frequencies of the structural model and the input excitation. In addition, the the response lag of the actuator must be sufficiently small to effectively apply compensation techniques.

In order to determine the capabilities of the experimental setup, the dynamic response of the actuators were further investigated. To this end, the transfer function of the desired displacement to the measured displacement was estimated using experimental data. The data transfer rates between the different computers involved in the experimental setup were also examined. The characterization of the complete hybrid simulation test system provides the information necessary to determine the practical rates of testing using this setup.

5.5.1 Dynamic Response of Actuator

To determine the limitations of the experimental setup, the dynamic performance of the actuators to commands from the dSPACE DPS was characterized. The performance of the actuator is mainly dependent on the payload mass and the controller gain settings. Other servo-hydraulic equipment such as accumulators may also limit the system performance. In terms of tuning, the user adjustable settings for this system are the controller gains set in two places: (1) digital inputs in the software for proportional-derivative control and (2) an analog turn screws in the MOOG servo-valve driver cards, which serves as a proportional gain. The digital gains were set as follows: proportional gain $K_{pro} = 0.5$ and derivative gain $K_{der} = 0.25$. It was difficult to obtain a precise setting of the variable analog gains, so they cannot be exactly specified. In the configuration used for these tests, the MOOG servo-control cards were measured to give a servo-valve command signal of 0.0023 amp/volt. It should be noted that these gain setting were not tuned to optimize the dynamic performance of the actuator. The primary goal was to minimize overshooting to a command displacement, for example, to a step response. This criterion was selected to insure that the target command displacement was not exceeded during the hybrid simulations.

In the system identification of the actuator response, the input command signal was generated by the DSP and the output signal was measured from the absolute displacement transducer digitized by the DSP. The data collected by the DSP was used to estimate the transfer function of the actuator response since the DSP reports measurements back to the integrator. The DSP update

rate for the command generation and measurement sampling rate was set to 1000 Hz. Since the response of the actuator is sensitive to the payload mass, the cantilever specimen was attached to the actuator during the characterization tests. The coupons were omitted from the experimental setup in order to simulate the specimen mass without displacement-dependent resistance.

The transfer function describing the dynamic response of the actuator was estimated from measured data. The frequency response of the output command signal was divided by the frequency response of the input response measurement signal to determine both the amplitude ratio and phase between the input and output White noise and sine sweep command signals were used as the inputs for this purpose.

The transfer function for a white noise input is shown in Figure 5-14 for both actuators. The plots shown are the result of 32 averages of measured data sampled at 1000 Hz over a period of 100 seconds. The noise in the plot is the result of computing a transfer function from experimental data, largely due to the division operation on two numbers determined from measured data. The denominator can be close to zero if the computed Fourier amplitude of the signal is low at a particular frequency, resulting in a large transfer function amplitude ratio. The data also appears coarse because the plot is focused on a frequency range of 0-10 Hz whereas the complete range is 0-500 Hz for the 1000 Hz sampling rate.

A smoother transfer function is obtained from the measured response of the actuator to a sine sweep signal as shown in Figure 5-15. A comparison of Figures 5-14 and 5-15 shows that both sets of experimental data predict similar dynamic characteristics; the amplitude and phase have similar trends. The amplitude appears to decay from unity after 2 Hz, indicating that the actuator does not respond well to frequencies beyond this range. This limiting frequency indicated by the transfer functions is commonly referred to as the cutoff frequency. The measured cutoff frequency is relatively low for these actuators because of the low control gain settings and the limited flow capacity of the servo-valve.

5.5.2 Delay in Actuator Response

Critical to the results of hybrid simulation is the delay in the response of the actuator. For the setup described here, the total delay of interest is between a digital command generated by the DSP and

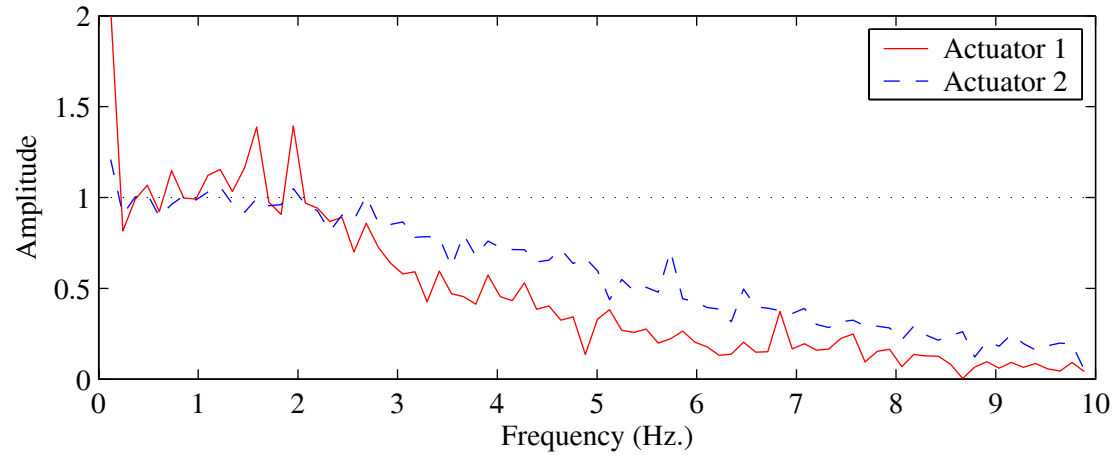

a. transfer function amplitude

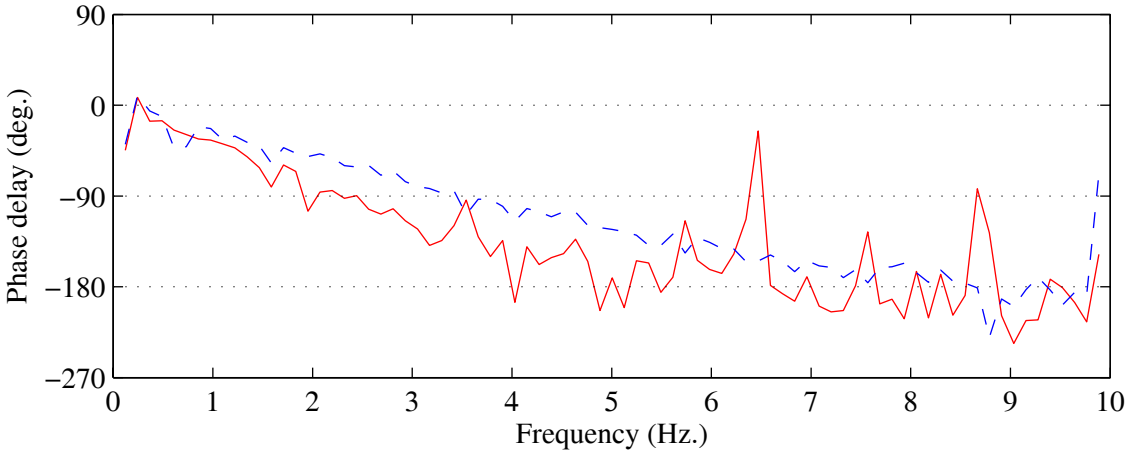

b. transfer function phase delay

Figure 5-14. Transfer function computed from white noise input

the digitized measurements correspond to the feedback. The following sources of delay were identified in the hardware configuration:

1. D/A conversion of command signal
2. signal conditioning filter delay of command delay
3. servo-valve and actuator response delay
4. signal conditioner filter delay of measurement
5. second signal conditioner filter delay of measurement (required for buffering)
6. A/D conversion

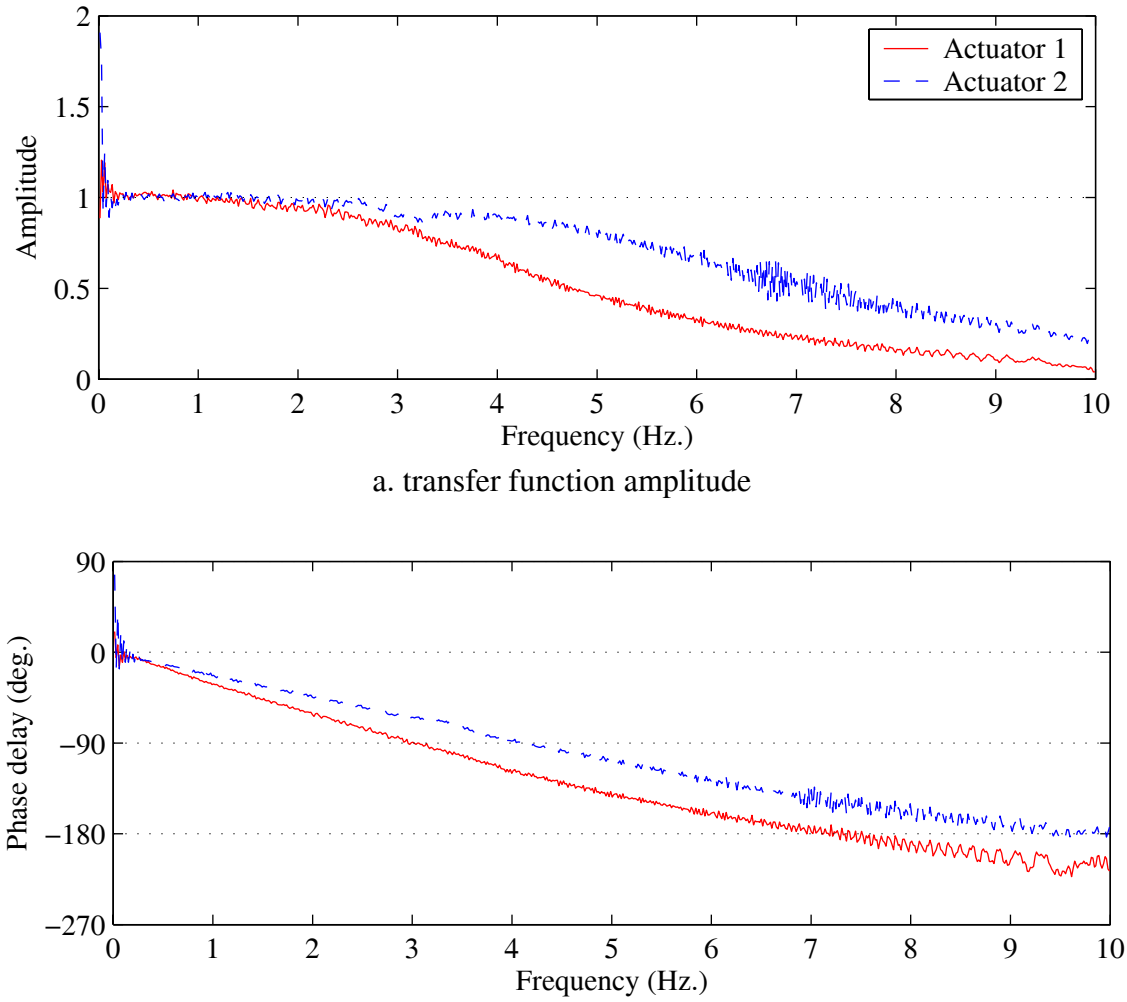

Figure 5-15. Transfer function computed from sine sweep input

As a result of wiring configuration between the DSP and the servo-control system in this setup, items 2 and 5 are additional delays that are not common in typical system.

To measure the actuator delay, a refined sine-sweep test was conducted. Figure 5-16 shows the experimental transfer function obtained from the measured response of Actuator 1 to a 100 second sine sweep signal with a 0.1 in. amplitude and frequencies ranging from 0.01 Hz to 2 Hz. The transfer function amplitude ratio shows a desirable response close to unity for the range of frequencies shown. As the loading frequency approaches 2 Hz, there is an undershooting error of approximately 10 percent. The angular phase delay between the input and output signals increases at a linear rate with frequency, which suggests a constant time delay in the response of the actuator.

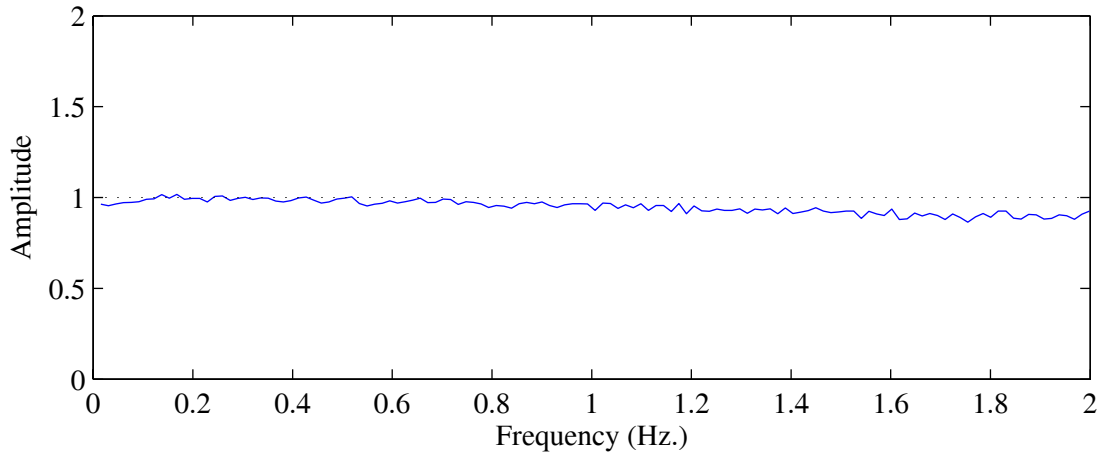

a. transfer function amplitude

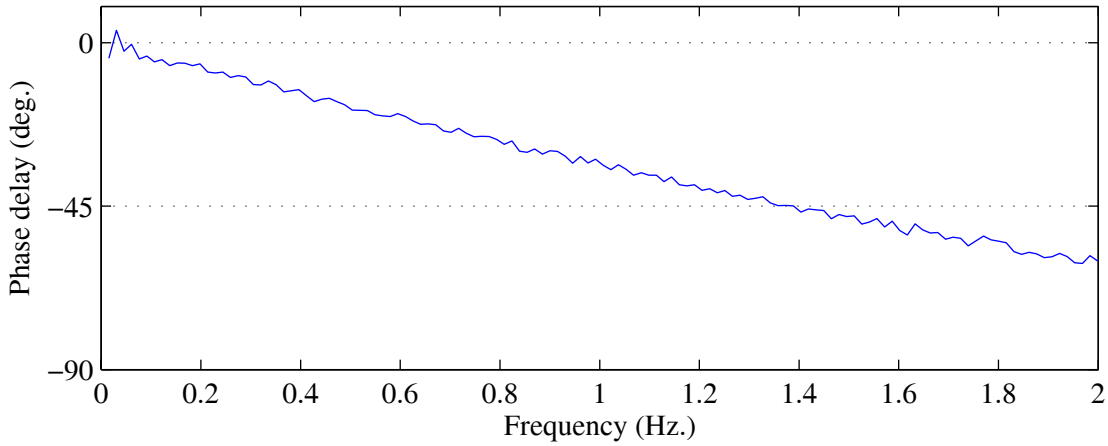

b. transfer function phase delay

Figure 5-16. Experimental transfer function of actuator with gains K_{pro}=0.5 and K_{der}=0.25

Using a least-squares fit, a first order polynomial was fitted to the phase delay, from which the time delay was estimated to be 90 milliseconds. A similar investigation on Actuator 2 resulted in a calibrated time delay of 78 milliseconds.

The measured delays in the response of the actuators are much larger than typically expected for a servo-hydraulic actuators. Values as low as 7 milliseconds have been reported by other researchers (Horiuchi et al. 1999). To further investigate the delays, the controller gains were tuned to improve the dynamic performance of the actuators. The digital gains were increased to $K_{pro} = 1.0$ and $K_{der} = 0.5$. The resulting transfer function is shown in Figure 5-17. The phase delay clearly shows an increase in performance with the time delay reduced from 90 to 38 milli-

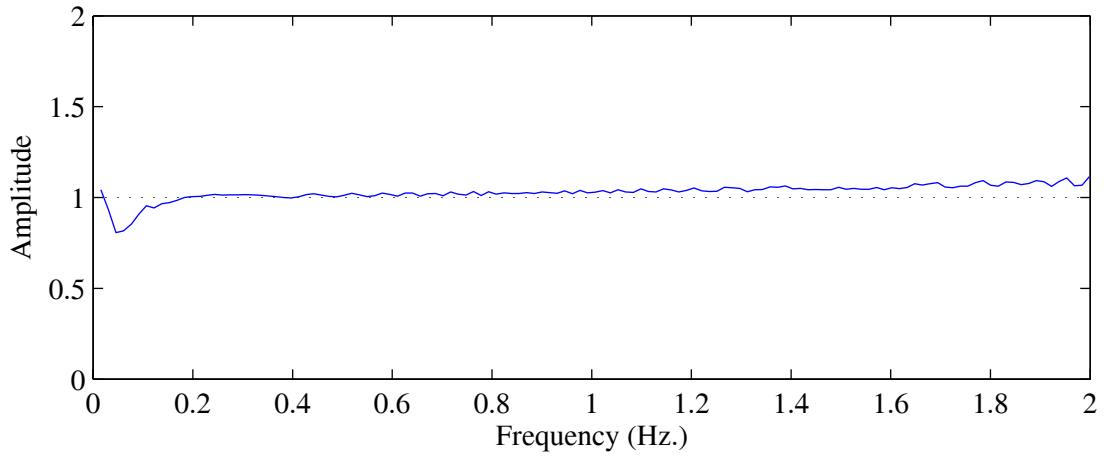

a. transfer function amplitude

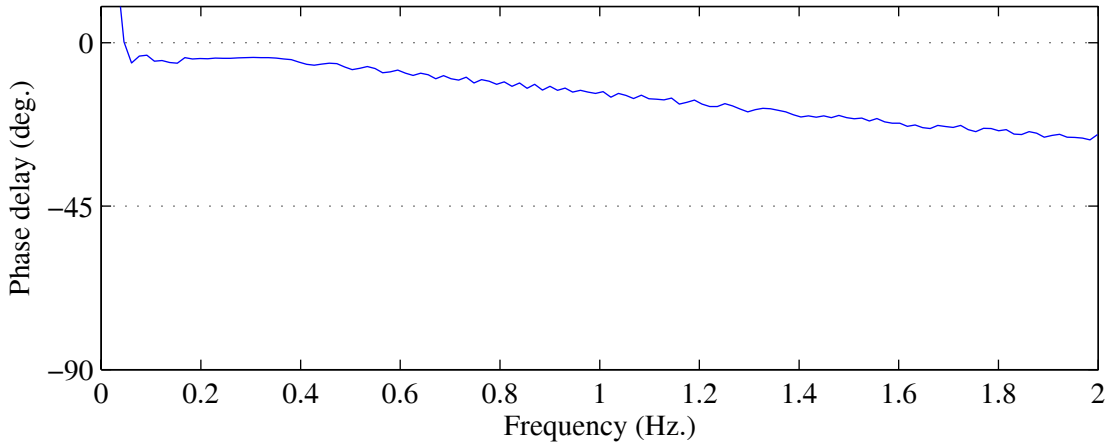

b. transfer function phase delay

Figure 5-17. Experimental transfer function of actuator with gains K_{pro}=1.0 and K_{der}=0.5

seconds. However, the amplitude of the transfer function increased to about 1.1 at 2 Hz. With these gain settings, the actuator is likely to overshoot a target displacement command. Additionally, the cutoff frequency of the actuator increased to approximately 5 Hz. Unfortunately, in some cases, the response of the actuator became unstable by responding with amplitude levels much greater than the input signal. To reduce the overshooting errors and, more importantly ensure stability, the initial gains ($K_{pro} = 0.5$ and $K_{der} = 0.25$) were reset prior to conducing hybrid experiments.

The measured delays correspond to a 1000 Hz command update and sampling rate in the DSP. Although 1000 Hz is significantly faster than necessary for the frequency response range of the actuators, a reduction in the sampling rate will increases the effective time delay of the actuator

measured by the DSP. It is worth mentioning that the data collected directly on the servo-control system predicted delays approximately 5 milliseconds less than those predicted by the data collected on the DSP. The difference is likely due to the additional signal conditioners necessary to transfer data between the DSP and the servo-controller.

5.5.3 Data Transfer Rates

The time delays and frequency response characteristics of the actuator limit the rate of testing for a hybrid simulation. There are also other tasks that must be considered in selecting the time scale for an experiment, namely computational time and the communication time between the numerical and experimental components. For hybrid simulations, the actuator commands are computed in the integration task and are transferred to the actuator controller. The experiments in Section 5.5.2 characterize the response of the actuator controlled from the DSP. In a single processor application where the integration algorithm and the signal generation tasks are programmed into a single DSP, the computational time and actuator characterization above provide sufficient data to characterize the total system delays. For the three loop architecture, the data transfer rate between the integrator and the DSP also needs to be considered.

In the local testing configuration, the integration algorithm is executed on the processor of the host PC. Therefore the transfer rate between the computer and the DSP located on the computer's PCI bus needs to be determined. Since the host computer is not based on a real-time operating system, the communication time can vary from step to step. Such timing depends on the particular PC architecture, the operating system, and concurrently running applications. For the PC's used in this experiment, it was found that data transfers required for one simulation steps can be completed within 0.1 seconds.

For the network configuration, the integration PC needs to send data to the remote host through Ethernet, then the host needs to relay the information to the DSP. Based on the characterization of the network in Section 5.4.1, the communication time using TCP/IP varies depending on the location of the two computers involved. For a test between RFS and the UC Berkeley campus, a time can be selected to accommodate a certain percent of the steps. It would be impractical to select the maximum communication time from the simulations in Section 5.4.1 since this value can vary from time to time. Steps with excessive delays can be handled by the event-driven controller.

After investigating the delays and task times involved in a hybrid simulation, the rate of testing can be determined. Note that the rate of testing is only important to the experimental simulations, particularly when the test specimens exhibit rate dependent behavior and force relaxation. Therefore, the critical time to be determined is the length of time it takes for the experimental site to receive a target displacement update after applying the last target value. This period determines the length of time the signal generation task predicts actuator commands before the additional *slow* and *hold* states need to be activated. Only the communication and computation tasks need to be considered; compensation techniques can be used to mitigate delays in the actuators. For the network setup described between RFS and the UC Berkeley Campus, about 95 percent of the steps can complete the required tasks within 0.7 seconds, including 0.6 seconds for computation and network transmission and 0.1 seconds to pass the data from the host computer to the DSP.

5.6 SUMMARY

The components of the experimental test setup were presented and the performance of the system was characterized. Of particular interest for hybrid simulation is the dynamic performance of the actuators and the communication delays between the different computers involved in a simulation. It was found that the actuators used in the experimental setup respond adequately to command signals with frequency content under 2 Hz. The time delay in the response of the actuators was determined to be 90 milliseconds for Actuator 1 and 78 milliseconds for Actuator 2. Based on the measured frequency response and time delays, the dynamic performance of the actuators is not satisfactory for real-time applications. Although the performance of the actuators can be improved by tuning the control gains, the dynamic response is not sufficiently stable.

The communication time between the different computers involved in a local and distributed hybrid test was also investigated, including communication through the PCI bus and network communication through Ethernet. For the DSP and the host computer considered, the time required to exchange data was estimated to be 0.1 seconds. The characteristic of the network were shown to be random and highly dependent on current usage. Based on the presented data, it was determined that 0.6 seconds should be allocated to the network communication task. The goal is to provide sufficient time to complete 95 percent of the steps using continuous testing methods; the remaining steps with longer delays are handled by the event-driven controller.

6 Geographically Distributed Network Tests

6.1 INTRODUCTION

The hybrid simulation test method for geographically distributed testing is experimentally verified through tests conducted with substructures located at the UC Berkeley Campus and the Structural Engineering Laboratory at the Richmond Field Station. The numerical analysis of a structural model is carried out on a computer located on Campus and is linked to two independent experimental substructures located at the structures laboratory using Ethernet and TCP/IP. The event-driven distributed control architecture is implemented to manage the random communication delays between the two sites. The results from the network tests are presented and compared to tests conducted using a local hardware configuration that does not involve Ethernet communication, and therefore has no large random delays.

6.2 STRUCTURAL MODEL

The structural model consists of an idealized two-degree of freedom shear-frame with two experimental substructures representing the columns. The beams are assumed rigid and the deformations are as shown in Figure 6-1. The columns have a point of inflection mid-height of the story under the assumed deformation constraints, allowing for the extraction of two simple experimental substructures. The resisting shear force for each story can be obtained experimentally by testing half of a column configured as a cantilever transversely loaded by an actuator. The other column in each story is assumed to behave the same as the tested column. The two identical test specimens described in Chapter 5 are used to represent the two experimental substructure columns.

The structural model is not intended to represent a real structure, instead this model was selected based on its ability to demonstrate the proposed test procedure and allow for the inexpensive repetition of linear and non-linear tests.

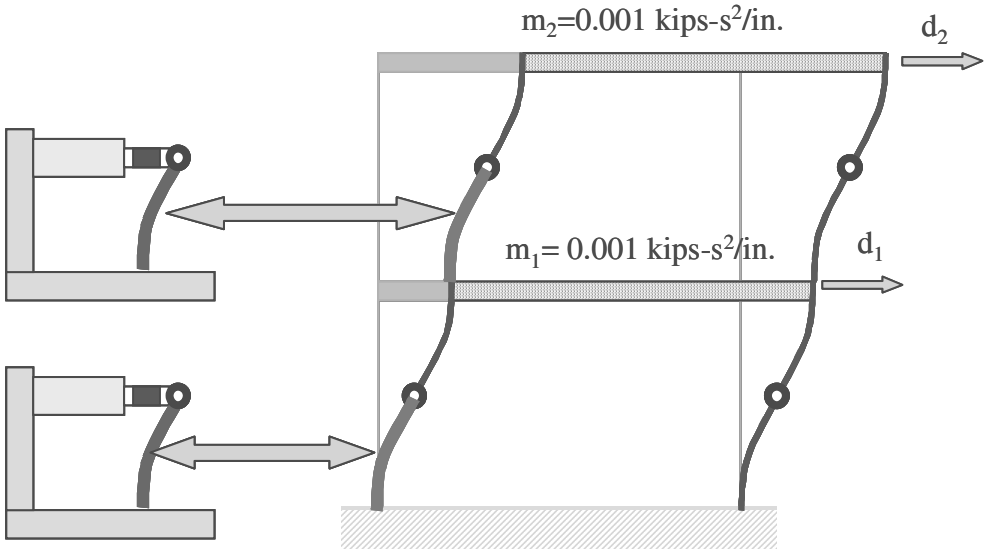

Figure 6-1. Idealized two-story shear frame with two experimental substructures

6.2.1 Equation of Motion

The equation of motion for the structural model subjected to a ground acceleration, $\ddot{u}_g$, is

$$\begin{bmatrix} m_1 & 0 \\ 0 & m_2 \end{bmatrix} \begin{bmatrix} \ddot{u}_1 \\ \ddot{u}_2 \end{bmatrix} + \begin{bmatrix} c_{11} & c_{12} \\ c_{21} & c_{22} \end{bmatrix} \begin{bmatrix} \dot{u}_1 \\ \dot{u}_2 \end{bmatrix} + \begin{bmatrix} r_1 \\ r_2 \end{bmatrix}^E = \begin{bmatrix} m_1 \\ m_2 \end{bmatrix} \ddot{u}_g \tag{6.1}$$

The restoring forces vector is obtained from experimental measurements of the two substructures. There are no numerical substructures providing displacement-dependent resisting forces. Preliminary characterization tests of the physical column models reveal that the initial stiffness is approximately 2.8 kips/in. Based on the properties of the experimental elements and the mass assigned to the shear frame in Figure 6-1, the resulting vibration periods of the structure are 0.62 seconds and 0.24 seconds for the first and second mode, respectively. The damping matrix is specified as stiffness proportional with 5 percent of critical damping in the first mode. This damping ratio was selected to quickly decay the free vibration response of the structure.

The equation of motion for the structural model is solved using Newmark's explicit integration algorithm implemented for hybrid testing (Section 2.4.1). This algorithm was selected because it is simple to implement and its stability limits are suitable for the structural model under consideration. For each simulation time step, the integration task computes the next target displacements,

carries out the transformation between the global degrees of freedom and the substructure degrees of freedom, sends the displacements to the experimental substructures, and waits until the restoring force measurements are returned. The transformation between the global degrees of freedom, $\boldsymbol{u} = \begin{bmatrix} u_1 & u_2 \end{bmatrix}^T$, and the actuator degrees of freedom, $\boldsymbol{u}^{ac} = \begin{bmatrix} u_1^{ac} & u_2^{ac} \end{bmatrix}^T$, is given by

$$\boldsymbol{u}^{ac} = \frac{1}{2}\boldsymbol{T}\boldsymbol{u} \tag{6.2}$$

where only half of the story displacements are applied to the half-column experimental models. The transformation matrix, $\boldsymbol{T}$, is given by

$$\boldsymbol{T} = \begin{bmatrix} 1 & 0 \\ -1 & 1 \end{bmatrix} \tag{6.3}$$

The DSP providing the local command generation to the experimental substructures receives the target displacements, $\boldsymbol{u}^{ac}$, from the integrator and sends a calibrated signal to the servo-hydraulic controller. The resisting forces are measured upon reaching the target displacement and sent to the integrator. The actuator forces are transformed to the global structural degrees of freedom by

$$\boldsymbol{r} = 2\boldsymbol{T}^T\boldsymbol{r}^{am} \tag{6.4}$$

The vector $\boldsymbol{r} = \begin{bmatrix} r_1 & r_2 \end{bmatrix}^T$ contains the restoring forces at the structural degrees of freedom and the measured actuator forces are contained in the vector $\boldsymbol{r}^{am}$. The measured shear forces are doubled to account for the relation between the cantilever column model and the two fixed-beam columns in the prototype model.

6.3 TEST PROTOCOL

The parameters specific to the tests presented here are the forces applied to the structural model and the actual time allotted for each simulation time step. The selected ground motions and time scale factors are discussed below.

6.3.1 Ground Motion

The combined experimental and analytical structural model was subjected to a cosine pulse and a historical earthquake acceleration record. The cosine pulse is useful to observe the behavior of the structure excited primarily in its first mode of vibration. The short duration of the pulse also allows for the examination of the response of the structure in forced and free vibration response phases. The cosine pulse has a period of 0.6 seconds, which is near the fundamental frequency of the structural model, and a peak acceleration of 0.15 g. The cosine pulse acceleration history is shown in Figure 6-2a.

The earthquake record serves to examine the performances of the hybrid simulation method to a realistic input excitation. The ground motion selected is the NF01 near fault record obtained from the SAC database (Somerville 1997). The ground motion was recorded during the 1978

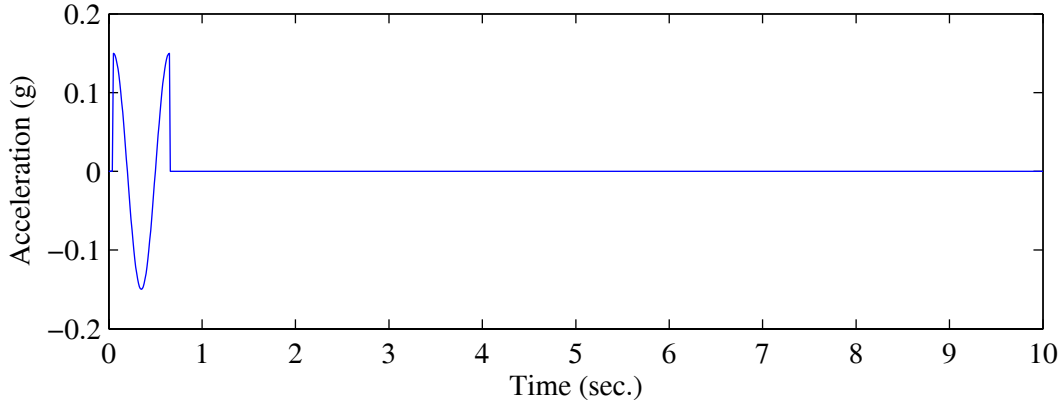

a. cosine pulse

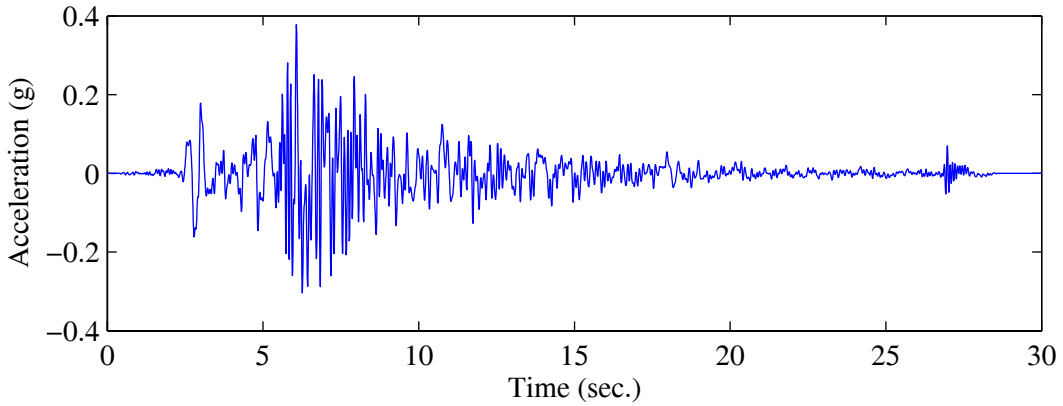

b. 1978 Tabas record scaled for elastic level simulation Tabas-50%

Figure 6-2. Ground acceleration records for hybrid simulations

Tabas, Iran earthquake and modified based on the SAC protocol to represent NEHRP soil type S_d. The acceleration record was further modified for these tests using the length scale factor of 3 (time scale factor of $\sqrt{3}$). The amplitude scale of the test was also modified by 50 percent to obtain an elastic level simulation (peak ground acceleration of 0.38 g) and by 150 percent to yield the specimens and obtain a non-linear response (peak-ground acceleration of 1.13 g). The Tabas acceleration history scaled to the elastic level simulation is shown in Figure 6-2b.

The response of the structural model to the cosine pulse was computed for 10 seconds at an integration time step of 0.01 seconds for a total of 1000 simulation steps. The earthquake simulation was allowed to run for 30 seconds using the same integration time step of 0.01 seconds. The sequence of tests listed in Table 6-1 was carried out using the network configuration and then repeated using the local hardware configuration. Since the experimental substructures were intended to remain in the elastic range for the first two simulations, only one set of coupons was used for the three simulations. After the three tests, the coupons were replaced before repeating the test sequence under a different hardware configuration.

Table 6-1. Test log for local hardware configuration and network configuration

Test label	*Excitation*			*Simulation time (sec.)*	*Description*
	Record	*Length scale*	*PGA (g)*		
Cosine Pulse	Pulse	-	0.150	10	elastic response to cosine pulse acceleration
Tabas-50%	NFO1	3	0.378	30	elastic response to 1978 Tabas, Iran ground acceleration
Tabas-150%	NFO1	3	1.133	30	non-linear response to 1978 Tabas, Iran ground acceleration

6.3.2 Task Timing

The overall experiment is coordinated by the integration task, but the rate of testing is managed by the event-driven signal generation task executed on real-time platform. The task coordination is shown in Figure 6-3 for the three tasks of integration, network communication and signal generation. The time scale at the top of the graph represents a single simulation step in the integration algorithm. The time scales shown at the bottoms of the figure provide the time assigned to each state in the event-driven controller for one integration time step. Note that the signal generation

task and the integration task are not completely synchronized in time, since the signal generation step *i+1* can start before the corresponding integration step *i+1*.

Both the integration and network communication tasks are executed as fast as possible using standard hardware. The integration tasks runs in the Windows-based Matlab environment and the network communication is through TCP/IP, neither of which are real-time environments. The DSP running the event-driven signal generation task runs in a real-time device and serves to interface with the experimental setup. The only process concerned with the actual time of the simulation is the signal generation task, which determines the duration of each simulation step.

Figure 6-3 includes the task times assigned to the four states in the signal generation algorithm. The total time for each step can vary depending on the allotted target time for each step, Δt_a, and the combined duration of the integration task and network communication, Δt_I. Δt_I is the time it takes for the real-time signal generation task to receive a displacement update after reaching the previous target displacement. For a smooth execution of the test, Δt_I should be less than the time allotted to the *extrapolate* state. Longer delays activate the supplemental *slow* and *hold* states, consequently extending the duration of the step.

The time scale factor for the event-driven tests was selected to insure that the experimental elements are only subjected to the hold phase during steps with excessive delays. Based on the system characterization in Chapter 5, each step was programmed for a desired actual run-time of $\Delta t_a = 1.2$ seconds. This time scale was selected with the goal of having approximately 95 percent of the steps execute without having to slow down the actuators. A step can take longer if delays are experienced during the network communication. The same time scale expansion factor of 120 was used for the local hardware configuration without an Ethernet network, although a much smaller time step can be accommodated by the hardware. A local test can execute a step as fast as 0.2 seconds without experiencing delays, but the same time scale was used to allow for a fair comparison between the two hardware configurations.

Within each step, the *extrapolation* state executes up to 60 percent of the time or 0.72 seconds. The *slow* state reduces the scaled velocity by half and runs until 80 percent of the step is complete. This allows a maximum of 0.48 seconds to the *slow* state since the actual time scale is further extended to twice the rate compared to the simulation time. The allowable time in the *slow* state is exhausted after a total wait time of 1.2 seconds, after which the actuator is forced to *hold* indefi-

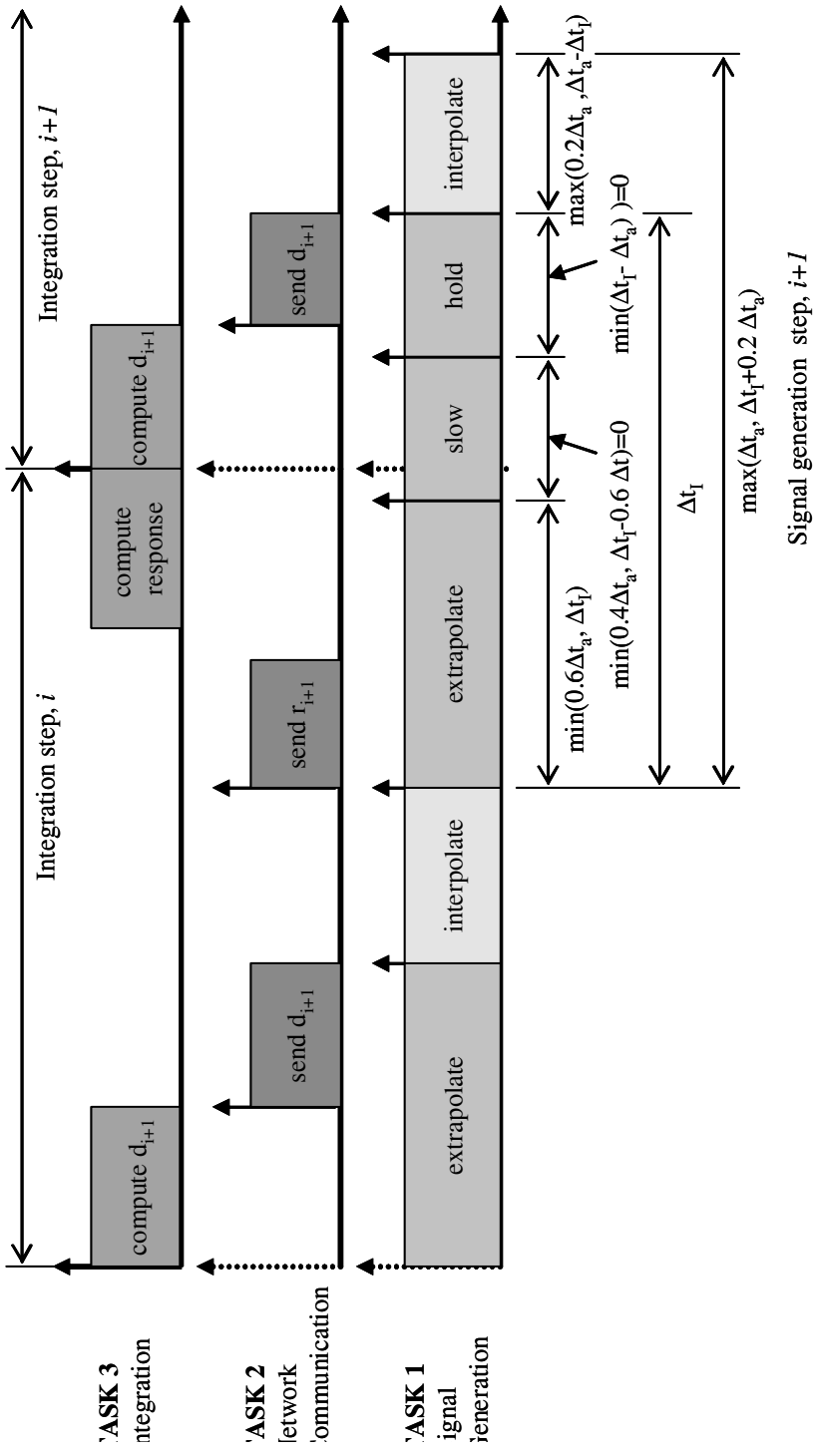

Figure 6-3. Task coordination for continuous testing over the Internet

nitely until an update becomes available. The *interpolation* state is activated for the remainder of the step after receiving updated data.

6.4 SOFTWARE FOR EVENT-DRIVEN CONTROL

The event-driven signal generation task is implemented in the Mathworks' (2003) Stateflow as a module in Simulink. The finite state chart implementation of the event-driven scheme is show in Figure 6-4. The real-time execution of the state chart is accomplished by setting the module to run on a trigger activated by a real-time clock at a rate of 1000 Hz. Each time the event-driven process is executed, the commands to the actuators are updated and measurements are digitized. The update rate of 1000 Hz is sufficiently fast to obtain a smooth response from the actuators and minimize time delays in the measurements.

The finite state chart in Figure 6-4 is composed of two main parallel states, *Counter* and *Command*, each of which has several sub-states. Both parent states are executed each time the finite state chart is triggered by the real-time clock. The *Counter* state has the following functions: increment the step counter, k, each time the chart is executed; check for displacement updates; and broadcast events to the *Command* state. The *Command* state generates the actuator commands based on its current sub-state and the step counter, k. Events to change the *Command* sub-state are generated in the *Counter* state based on the counter, k.

The number of signal generation update steps in each integration time step is determined by the parameter k_{max}, set to 1200 for the present application. Since the finite state chart is triggered by a real-time clock at a rate of 1000 Hz, the counter, k, keeps track of the clock ticks in units of milliseconds, thus the length of the integration step is 1200 milliseconds. The counter, k, is increased by one each time the *extrapolate* state or *interpolate* state is executed and is reset to one upon entry into the *extrapolate* state. The step counter is increased by 0.5 during the *slow* state and remains constant in the *hold* state. This approach allows the counter to functions as a real-time clock for generating a continuous command signal with the ability to slow down and pause to accommodate the delays.

The command signal is generated using the polynomial prediction/correction procedure based on the sub-step counter, k, and the maximum number of sub-steps k_{max}. The extrapolation procedure is

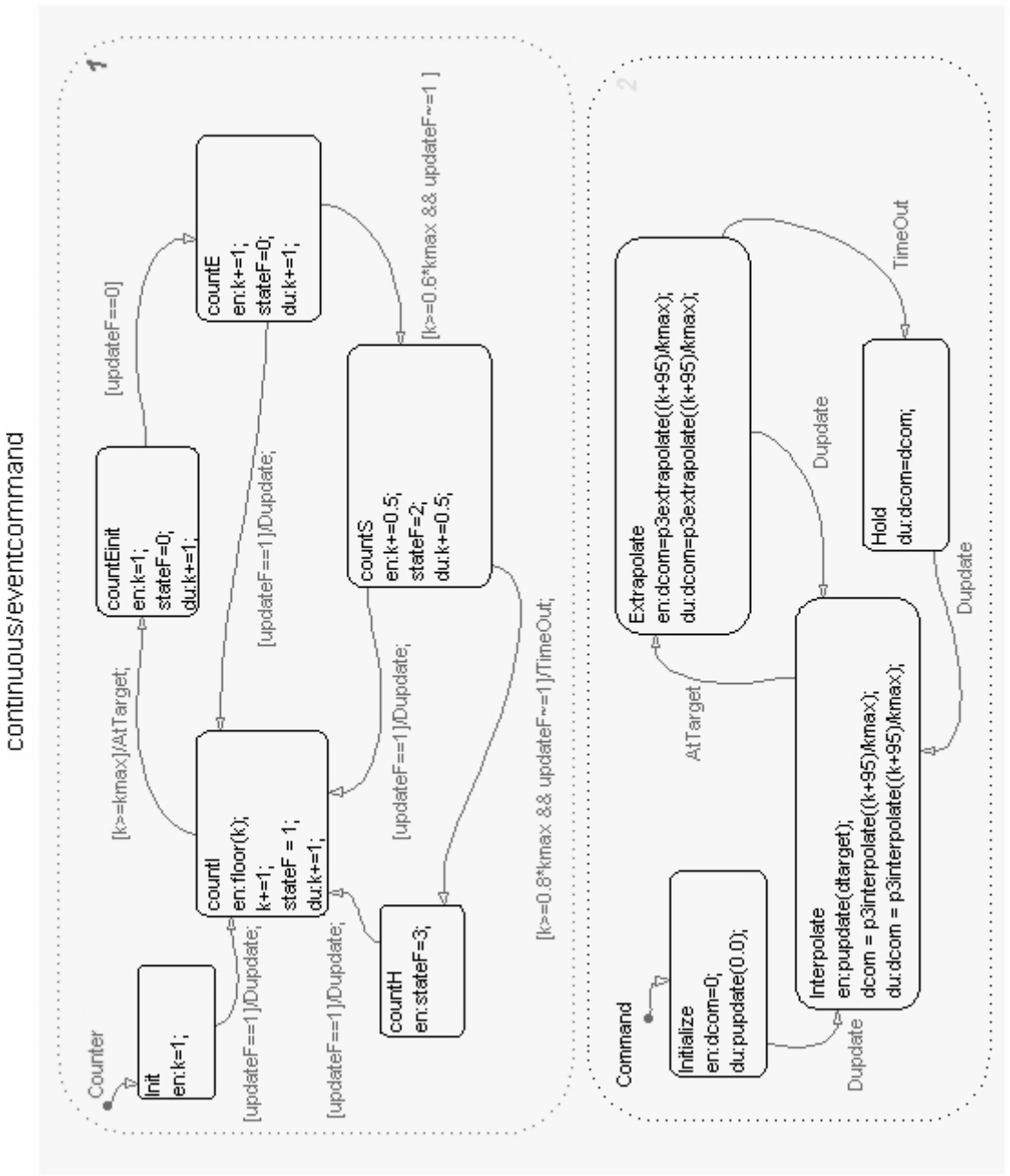

Figure 6-4. Finite state chart program in Stateflow for event-driven control

$$d^{k}_{i+1}(t_k) = \frac{d_i}{6}(1+t_k)(2+t_k)(3+t_k) - \frac{d_{i-1}}{2}(t_k)(2+t_k)(3+t_k) \tag{6.5}$$
$$+ \frac{d_{i-2}}{2}(t_k)(1+t_k)(3+t_k) - \frac{d_{i-3}}{6}(t_k)(1+t_k)(2+t_k)$$

and the interpolation procedure is

$$d^{k}_{i+1}(t_k) = \frac{d_{i+1}}{6}(t_k)(1+t_k)(2+t_k) - \frac{d_i}{2}(-1+t_k)(1+t_k)(2+t_k) \tag{6.6}$$
$$+ \frac{d_{i-1}}{2}(t_k)(-1+t_k)(2+t_k) - \frac{d_{i-2}}{6}(t_k)(-1+t_k)(1+t_k)$$

where

$$t_k = \frac{k + k_{comp}}{k_{max}} \tag{6.7}$$

The constant k_{comp} is used to compensate for the actuator time lag in units of milliseconds. For the specific test setup used here k_{comp} is set to 95 for Actuator 1 and 85 for Actuator 2. These values are about five percent higher than the measured lag in the actuators, but these settings were found to best minimize the actuator tracking errors.

6.5 TEST RESULTS

The results from the hybrid simulations conducted locally and using the distributed hardware architecture are presented for the three selected input ground motions. The network tests are compared to the local tests to verify the performance of the event-driven controller with and without delays.

6.5.1 Cosine Pulse Simulation

The computed displacement response of the two story shear frame subjected to the cosine pulse acceleration record is shown in Figure 6-5. The displacement history computed during the network simulation is compared to the results from the local test. The second story response is identical for both test, but there is a small deviation between the two displacement histories at the first story level. The first story drift computed during the network test has a greater amplitude at the negative peak displacements, which propagates throughout the remainder of the simulation as a permanent offset. There is also a progressively increasing phase shift between the two signals, suggesting a

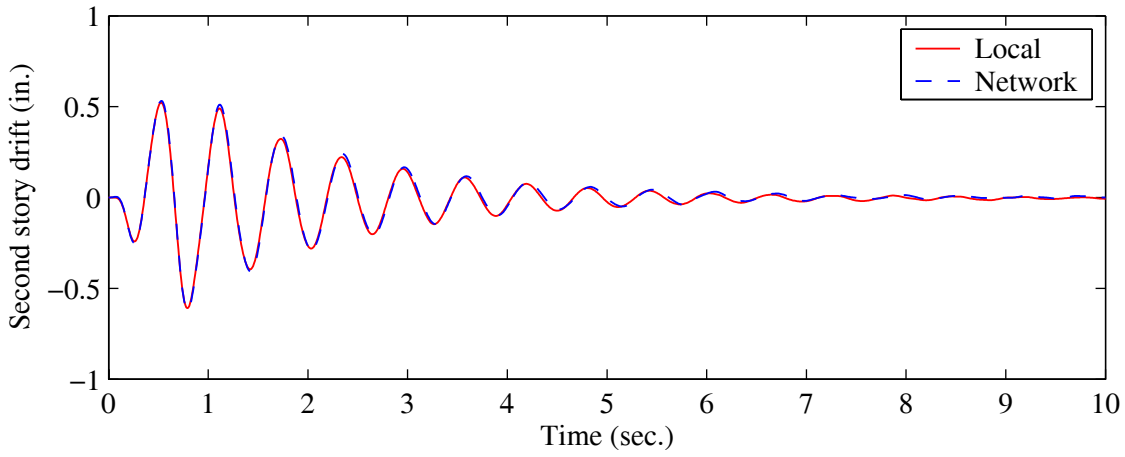

a. second story relative displacement history

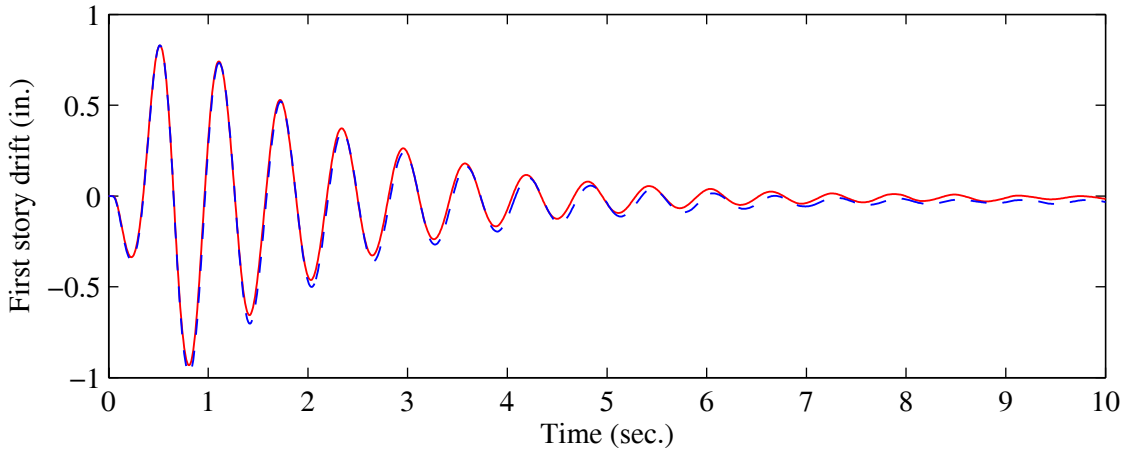

b. first story relative displacement history

Figure 6-5. Displacement response of two story shear frame subjected to Cosine Pulse for local and network simulations

longer period for the structural model in the network simulation. A Fourier Transform of the two displacement histories indicates that the first-mode periods are 0.615 seconds and 0.619 seconds for the local and network tests, respectively. A one percent change in stiffness is required to cause this change in period for a linear system. To examine the difference in response in more detail, the behavior of the experimental substructures is examined.

The measured restoring forces are plotted as a function of the command displacement in Figure 6-6 for both the local and the network tests. The data is scaled to the global structure degrees of freedom, representing the inter-story drift and the story resisting shear forces. The second story substructure model remains linear but there is a small amount of hysteresis in the first story sub-

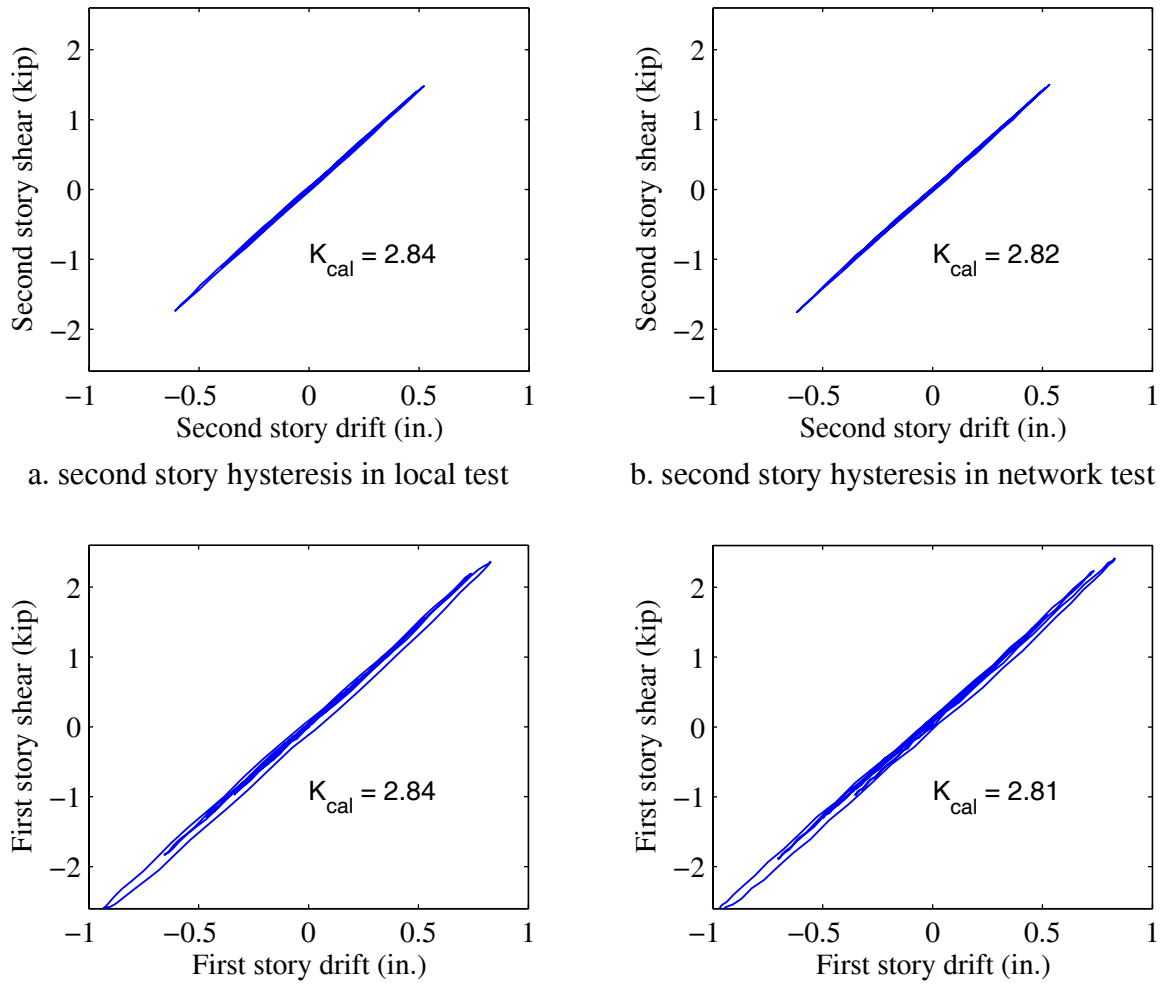

Figure 6-6. Measured shear vs. drift for two-story frame subjected to Cosine Pulse

structure model for both the local and the network simulations. The apparent offset in first story drift between the two simulations is likely due to localized yielding in the experimental substructures. The response of the building structure is sensitive to the stiffness of the experimental substructures because the computed response is in free vibration after 0.60 seconds.

The stiffness calibrated from a least-squares fit of the measured data (measured force vs. measured displacement) are shown in the corresponding figures. The coupons used for the local test resulted in a slightly stiffer cantilever specimen compared to the specimen in the distributed configuration. The variation in specimen stiffness is likely responsible for the longer natural period observed for the network test in Figure 6-5.

6.5.2 Elastic-Level Earthquake Simulation Tabas-50%

The resulting displacements response of the two-story shear frame structure subjected to the ground acceleration record Tabas-50% is shown in Figure 6-7. A direct comparison of the displacement histories for the local test and the network test verifies that the distributed controller functions effectively in the presences of communication delays. Figure 6-8 displays the measured shear forces versus commanded displacements for both stories. The stiffness calibrated to the measured data are shown in the corresponding figures. There is less than 1.2 percent variation in the column stiffness. Unlike the cosine pulse test, the resulting displacement histories are very similar for both stories. The effects of specimen variability is less pronounced for the earthquake excitation as com-

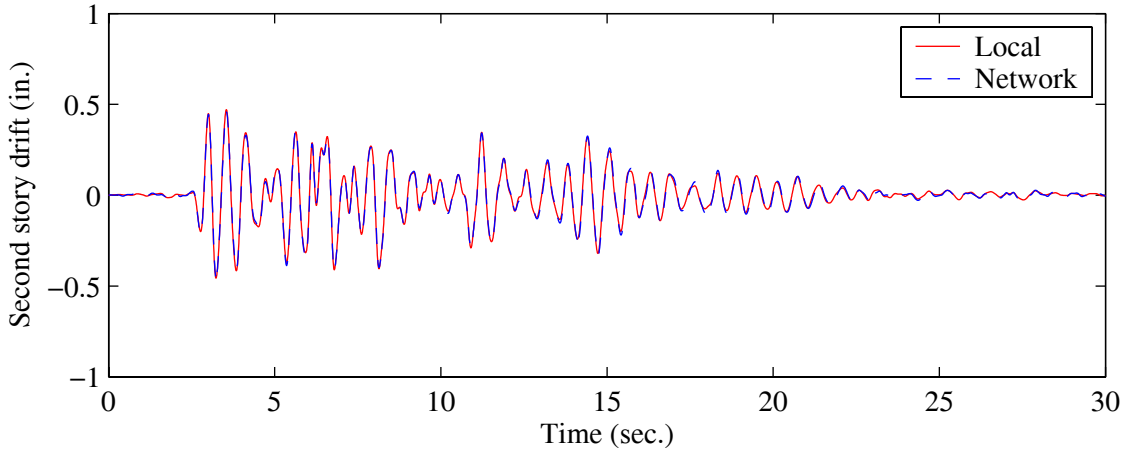

a. second story relative displacement history

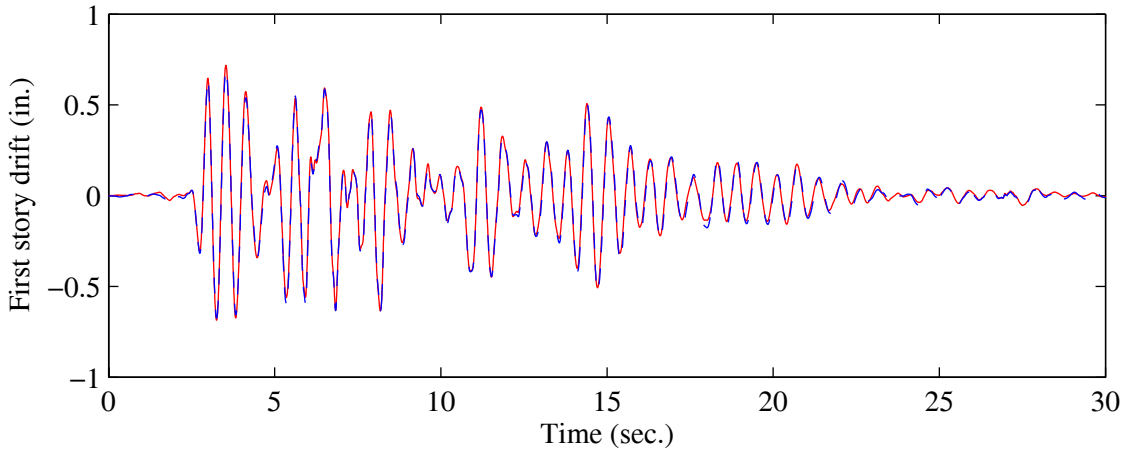

b. first story relative displacement history

Figure 6-7. Displacement response of two story shear frame subjected to Tabas-50% for local and network simulations

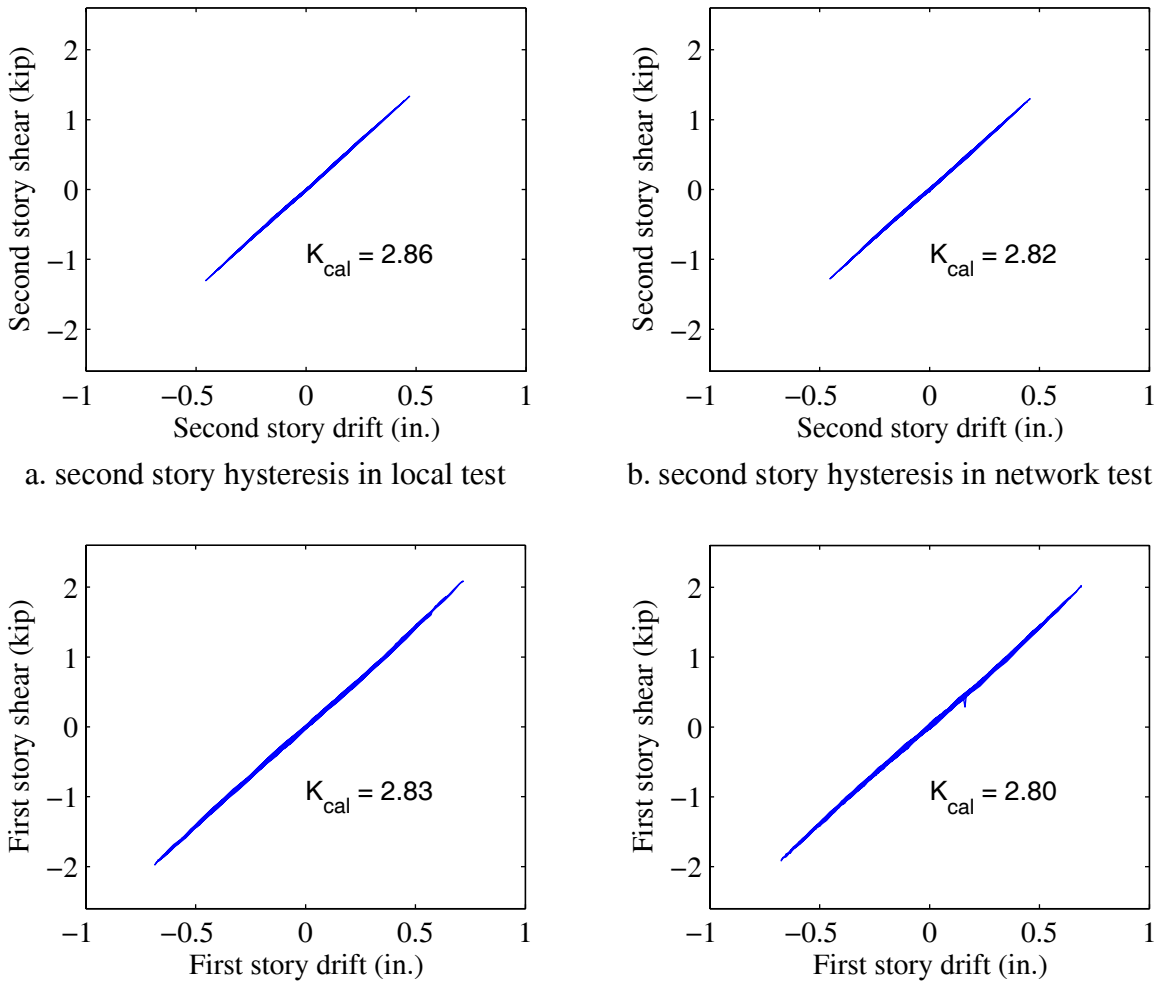

Figure 6-8. Measured shear vs. drift for two-story shear frame subjected to Tabas-50%

pared to the pulse because the pulse response is predominantly in free vibration. Also, material variability plays an insignificant role in the results for these tests because all four of the experimental substructures remained fully in the elastic range.

6.5.3 Non-Linear-Level Earthquake Simulation Tabas-150%

The results from the simulated response of the model structure subjected to the Tabas-150% ground acceleration are shown in a similar format in Figure 6-9 and Figure 6-10. The first story substructure was subjected to non-linear drift levels while the second story remained linear. A comparison of the second story drifts for the local and network tests shows that the two time histories are practically identical. The first story has a substantially larger permanent drift of 1.8 in.

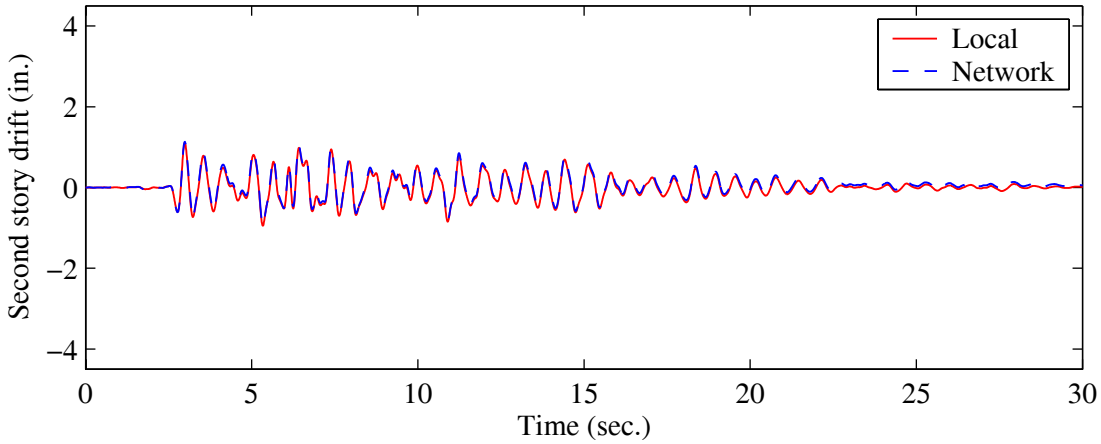

a. second story relative displacement history

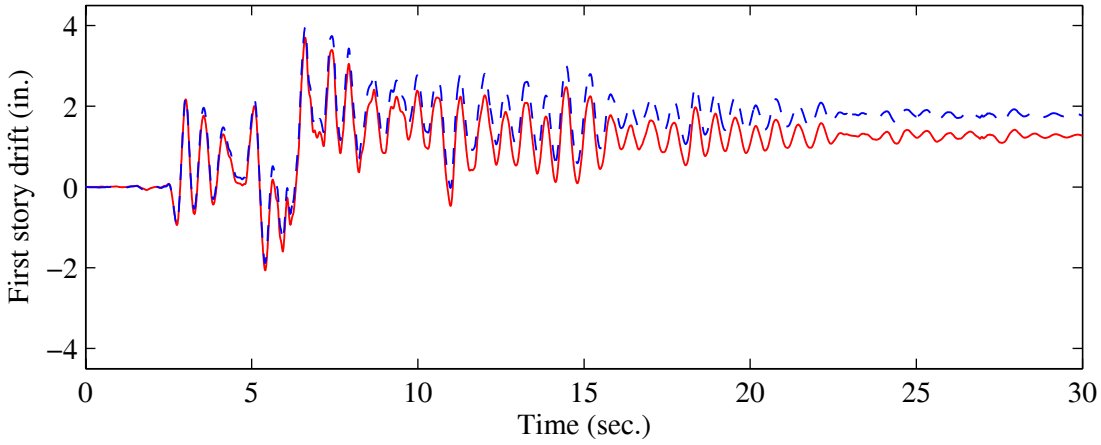

b. first story relative displacement history

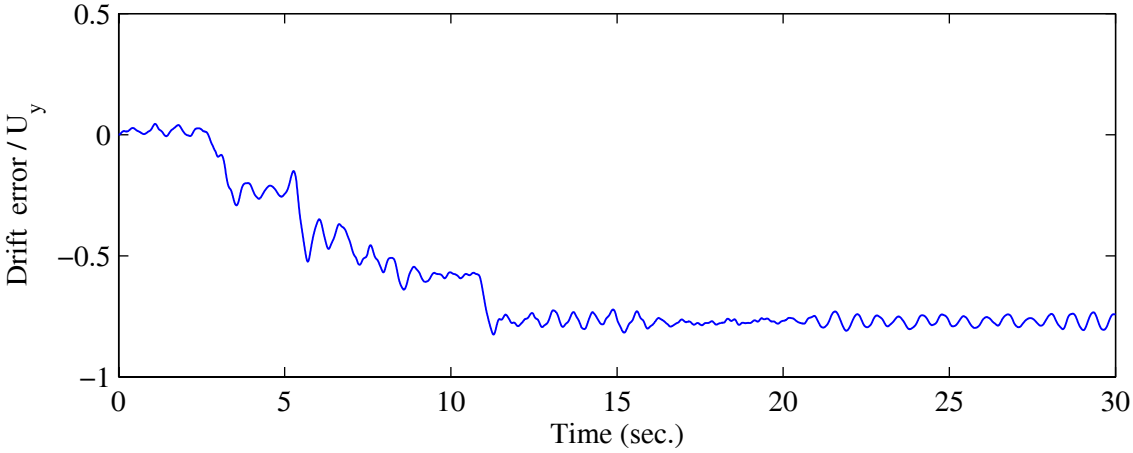

c. difference in first story drift between the local and network tests

Figure 6-9. Displacement response of two story shear frame subjected to Tabas-150% for local and network simulations

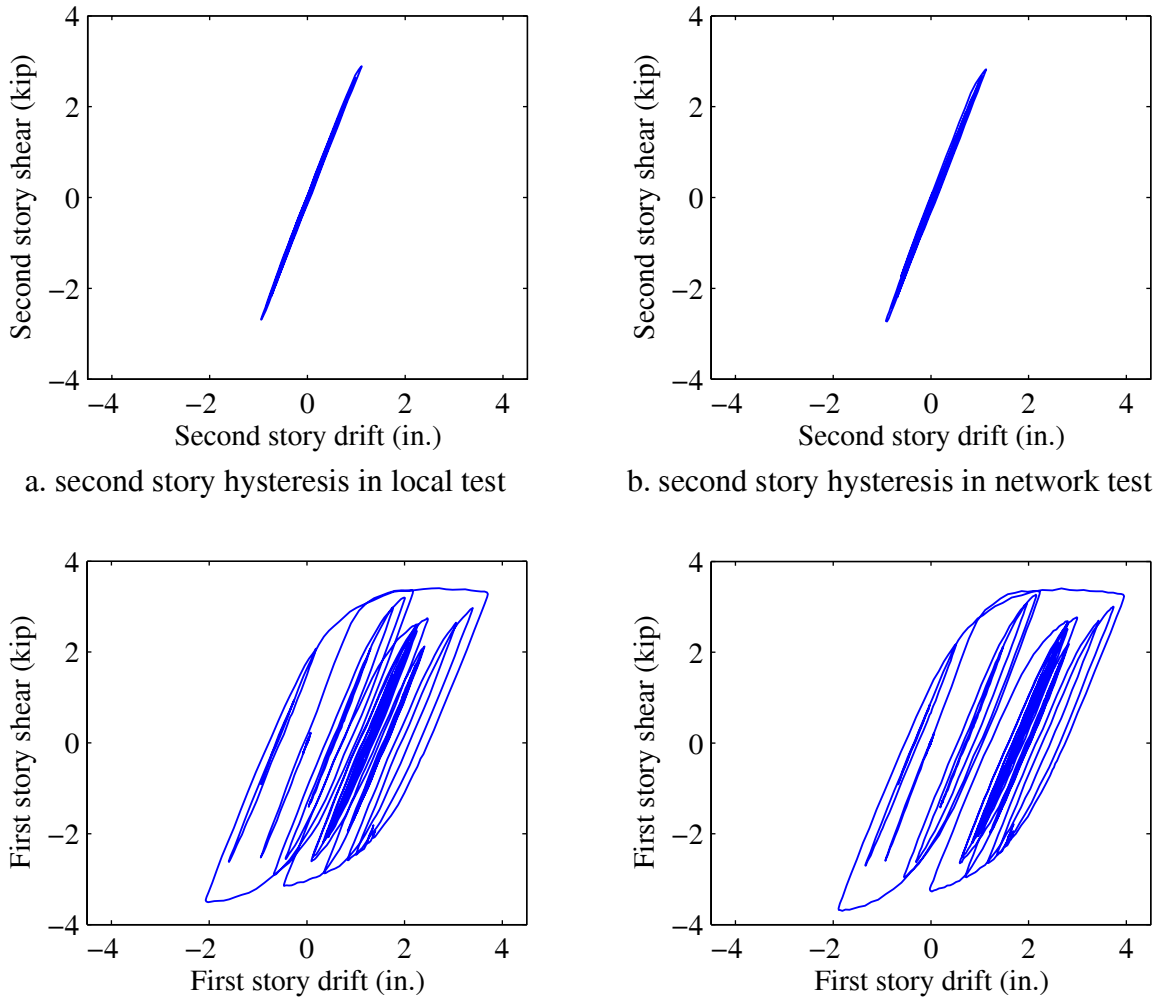

Figure 6-10. Measured shear vs. drift for two-story shear frame subjected to Tabas-150%

for the network test compared to 1.3 in. for the local test. The difference in the computed first story drift between the local and the network tests is shown in Figure 6-9c. The relative difference in drift grows in a step-wise fashion with three major increments. The largest step increment in the relative offset occurs between 5 and 6 seconds, corresponding to the maximum negative displacement. In this region, larger forces are evident in the force-displacement response of the first story experimental model for the network test in Figures 6-10c and 6-10d. The maximum first story shear force recorded for the network test is approximately five percent greater than the corresponding force for the local test. The observed difference in drift response is likely due to the variation in the strength between the experimental specimens used for both simulations. It is well known that the non-linear

dynamic response of structures is sensitive to the yield strength of the structural components (Chopra 1996). Apart from the permanent drift offset, the overall characteristics of the response are in phase and exhibit similar relative characteristics.

It is important to note that the difference in specimen behavior shown in Figure 6-10 is not a result of delays in the network test. The rate-effects and force relaxation caused by delays are known to decrease the maximum stresses developed in steel structures (Shing and Mahin 1988, Harris and Sabnis 1999). The opposite trend is show here, indicating that this phenomenon is likely the result of variability in the installation of the coupons and material properties.

6.5.4 Performance of Event-Driven Controller

During the network tests, there were several instances when the DSP did not receive data from the integrator by the required time and activated the supplemental *slow* and *hold* states. Figure 6-11 shows the distribution of the time taken for the DPS to receive data from the integrator after reaching the last target displacement. The length of time captured in the figure is the integration task time and the network communication time, shown in Figure 6-3 as Δt_I. The results of the network tests are shown for the 1000 steps of the Cosine Pulse and the 3000 steps of both earthquake simulations. The dashed lines in the figure represent the limits where the *slow* and *hold* states were activated according to the selected timing scheme in Figure 6-3. Table 6-2 summarizes some statistics of the network delays including the percentage of the steps in which the *slow* and *hold* states were activated, the maximum delay during the test, and the total run time for the test.

It is interesting to note from Table 6-2 that the test with the most delays (Tabas-50%) overran the total target simulation time of 3600 seconds by only 67 seconds. More importantly, the actuators subjected the experimental specimens to a hold phase for less than two percent of the simulation steps. The simulation Tabas-150% had less than half of the delayed steps compared to Tabas-50%. The variation of delays between the two earthquake simulations is characteristic of the network behavior and is likely due to variations in network congestion during the time the test was executed.

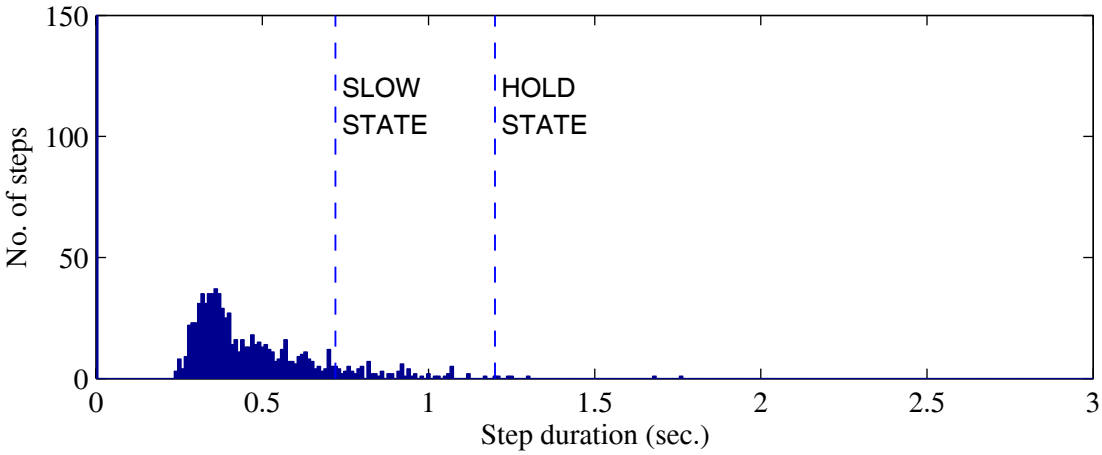

a. cosine

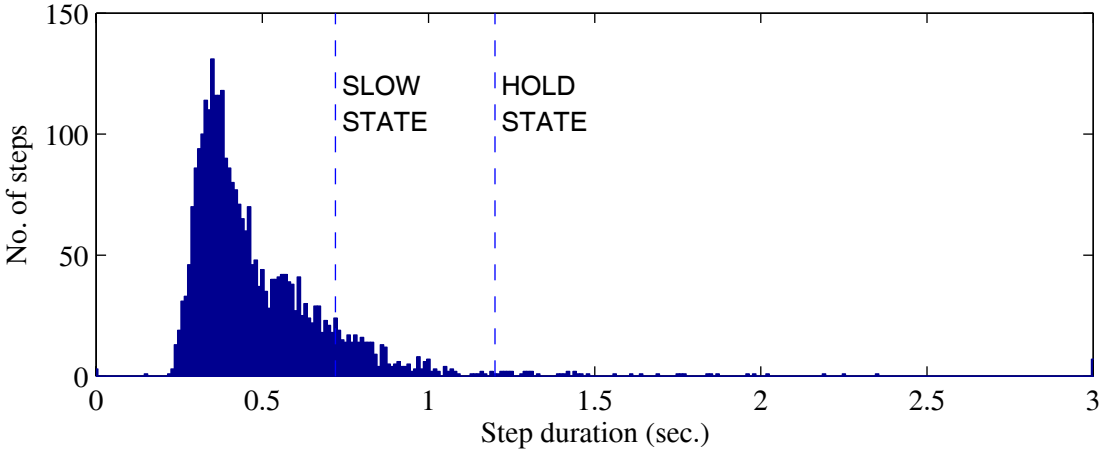

b. 50% NFO1

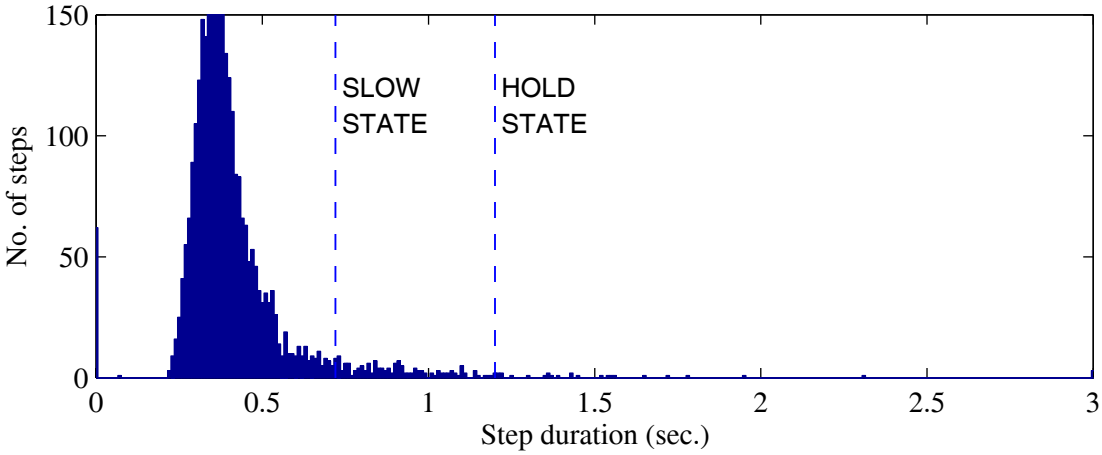

c. 150% NFO1

Figure 6-11. Histogram of step duration during network tests

Table 6-2. Results of delays for network tests based on the measured task times for integration and network communication, Δt_I

Test label	*No. of steps*	*% of delayed steps*		$max(\Delta t_I)$ *(s)*	*Total run time (s)*
		slow state $\Delta t_I < 0.72$	*hold state* $\Delta t_I < 1.2$		
Cosine Pulse	1000	9.2	0.6	1.76	1210
Tabas-50%	3000	12.4	1.7	6.59	3667
Tabas-150%	3000	5.9	0.9	5.90	3638

6.5.5 Effects of Delays

Figure 6-12 provides a close look at the behavior of the yielded first-story substructure during the network test Tabas-150% for steps that experienced delays. The complete displacement history is repeated in Figure 6-12a as a function of the DSP real-time clock as opposed to the simulation time scale shown in Figure 6-9a. Note that the data recorded by the DSP is sampled at 100 Hz, or once every ten execution steps. Figure 6-12b shows the measured force versus measured displacement data recorded by the DPS at the actuator degrees of freedom. The bold segment in the displacement history near 1800 seconds and the bold segment in the corresponding force-displacement plot indicate the region of interest. The remaining figures concentrate on the 20 seconds of simulation highlighted in these two plots.

The state of the event-driven algorithm is shown in Figure 6-12c. The Y-axis marks the *(E)xtrapolate*, *(I)nterpolate*, *(S)low* and *(H)old* states for 20 seconds of real-time. As indicated in Figure 6-12c, the first few steps executed smoothly by switching directly from *extrapolate* to *interpolate*. At approximately 1785 seconds into the test, two short delays occurred followed by two longer delays. The length of the delays are identified by the amount of time spent in the *(H)old* state. The measured displacement history and force history are show for the same 20 seconds of DSP clock time in Figure 6-12d and Figure 6-12e, respectively. The measured force history together with the force-displacement data in Figure 6-12f illustrate the consequences of a hold phase on the behavior of the experimental substructures. During the hold period, the displacement remained constant as expected, but the force decreased in magnitude. The corresponding segment of the hysteresis provides further evidence of force relaxation, particularly during the two long delays. The circular markers on subplots c-f indicate the end of the simulation step where measure-

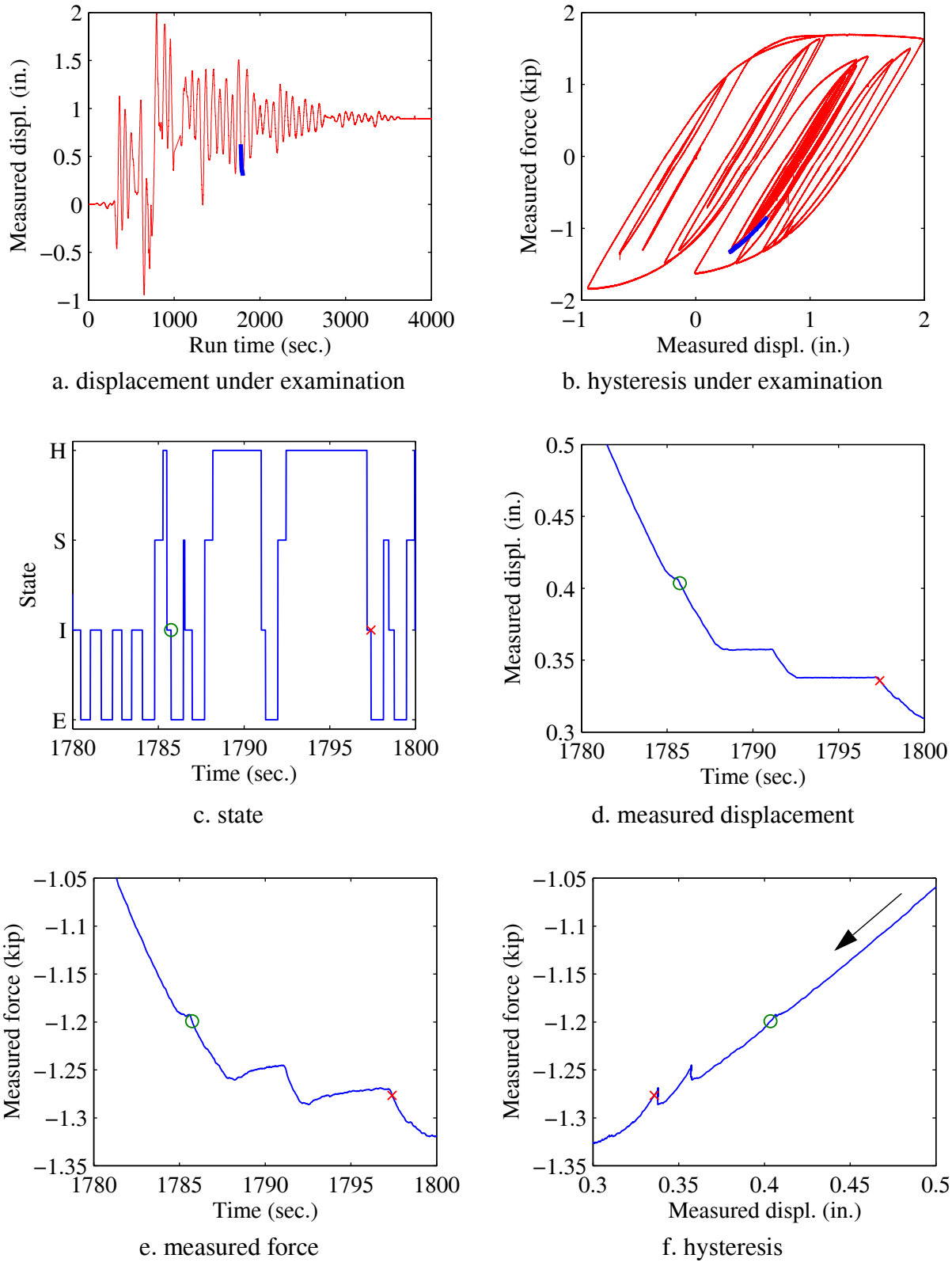

Figure 6-12. Behavior of experimental substructure during hold phase

ments were taken for a step with a 0.2 seconds hold period. In this case, there is negligible force relaxation and sufficiently accurate measurements were obtained. The 'x' marker notes the end of the step with a much longer delay, resulting in a 4.7 seconds hold phase. Note from the force displacement data in Figure 6-12f that the measured force value was taken while the specimen recovered from the force relaxation. Consequently, the measured force used in the integration algorithm includes errors. Steps in which the *hold* state was not activated provide a smooth force-displacement response, including the delayed steps in which the specimen was only subjected to the *slow* state.

6.6 SUMMARY

A hybrid simulation procedure for continuous real-time-based testing applications in the presences of random network delays was implemented. The test method was verified using a two degree of freedom structural model with two remote experimental substructures connected using the Internet. The three loop distributed hardware architecture with an event-driven control scheme was utilized to provide a fault-tolerant mechanism that minimizes force relaxation and rate-related errors in the experiments.

An evaluation of the hybrid simulation results confirms that the distributed hardware architectures is able to adequately execute a test on a distributed structural model. The elastic-level network test results using the Cosine Pulse and a historical earthquake record compare well to results obtained using a traditional local testing configuration. The differences in the results from the non-linear tests are a consequence of specimen variability in yield strength, and not necessarily a deficiency in the test method. The non-linear dynamic response of structures is sensitive to the strength of the structural elements, an important characteristic that this test procedure is able to reproduce.

The effectiveness of the event-driven scheme was demonstrated, particularly in minimizing the hold phase in the experimental element load history and maintaining the duration of the test within a reasonable time frame. The test results also indicate the importance of moving form ramp-and-hold to continuous loading methods. Although the event-driven procedure presented here is not able to completely eliminate the hold phase during a distributed hybrid tests, more than 99 percent of the steps experience a continuous load trajectory during the non-linear earthquake simulation. The minimization of the hold phase can improve the results of a hybrid simulation by

eliminating errors in measured forces resulting from force relaxation. The few instances of excessive network delays would have resulted in the catastrophic failure of previously developed continuous testing procedures.

7 Evaluation of Hybrid Simulation Results

7.1 INTRODUCTION

Hybrid simulations have been shown to provide realistic results by comparison to shake table tests (Takanashi and Nakashima 1987, Magonette and Negro 1998, Mahin et al. 1989) and pure numerical simulations (Shing et al 1996, Darby et al. 1999, Blakeborough 2001). The conclusions from these studies indicate that reliable results can be obtained only if the propagation of experimental errors is properly mitigated. In the case that shake table test data is available, the numerical models in the hybrid simulation also need to be sufficiently accurate to obtain comparable results. Another notable procedure used to estimate the quality of the test results consists of examining the energy errors that accumulate in the experimental substructures (Thewalt and Roman 1994).

In this chapter, the results of the hybrid simulations presented in Chapter 6 are evaluated. The following three procedures are carried out for this purpose: (1) an investigation of the actuator displacement control errors, (2) a comparison of the results with a pure numerical simulation, and (3) an examination of the energy input into the structural model resulting from actuator control errors. In addition, a simple formulation is proposed to compute the energy errors in the experimental substructures. Since similar experimental results were obtained from the hybrid simulations using the local and the network hardware configuration, only the results from the network experiments are evaluated here.

7.2 ACTUATOR CONTROL ERRORS

Experimental errors have been shown to be critical to the reliability of the hybrid simulation results. For this reason, displacement control errors in the actuators, defined as the difference in command displacement and measured displacement are examined. The error histories for the three network tests are shown in Figures 7-1, 7-2 and 7-3 for the hybrid simulations presented in Sections

6.5.1, 6.5.2 and 6.5.3 respectively. The errors in Actuator 2 applying the loads on the second story substructure are shown in subplot *a* and the errors in Actuator 1 applying the loads on the first story substructure are shown in subplot *b*. The power spectral densities of the error histories are shown in subplots *c* and *d*. The displacement error histories are normalized by the maximum stroke of the actuators in the test setup, which is limited to 3 inches by the displacement transducer stroke limit. This limit is referred to as the test setup displacement capacity in the following discussion.

An examination of the error signal reveals trends that indicate the presence of systematic errors in the tests. For example, in Figure 7-1a, the error signal corresponding to the Cosine Pulse simulation has a predominant sinusoidal history for the first two seconds. The amplitude and frequency of the error signal has similar characteristics to the command displacement show in Figure 6-5. The dominant sinusoidal error history is more evident in the first two seconds of the test because the amplitude of the command signal is larger. The amplitude of the sinusoidal signal decays and becomes more difficult to identify within the random noise that is also present in the error signal. The power spectral density of the error signal in Figure 7-1c confirms the presence of a dominant frequency around 1.6 Hz, corresponding the fundamental mode of vibration of the structural model. The power spectral density of the error signal corresponding to Actuator 1 in Figure 7-1d also shows the same dominant frequency, although this frequency is not evident from examining the error history in Figure 7-1b. The displacement errors and the power spectral density for the two earthquake simulations also show the presence of a dominant frequency at 1.6 Hz.

The presences of the structural model's fundamental frequency in the error signal for all three tests suggests that systematic overshooting or undershooting errors may be present (Thewalt and Roman 1994). Table 7-1 lists the absolute maximum errors normalized by the capacity of the test setup and the maximum errors normalized by the absolute maximum displacement command during the test. A review of Table 7-1 concludes that the magnitude of the displacement errors are small compared to the displacement demands for all three tests. The magnitude of the errors is less than 0.2 percent of the test setup displacement capacity, and less than 1 percent of the maximum displacement demand. Even though systematic errors are present in the displacement control of the actuators, these errors are small and not expected to have a significant impact on the structural response compared to all other sources of error.

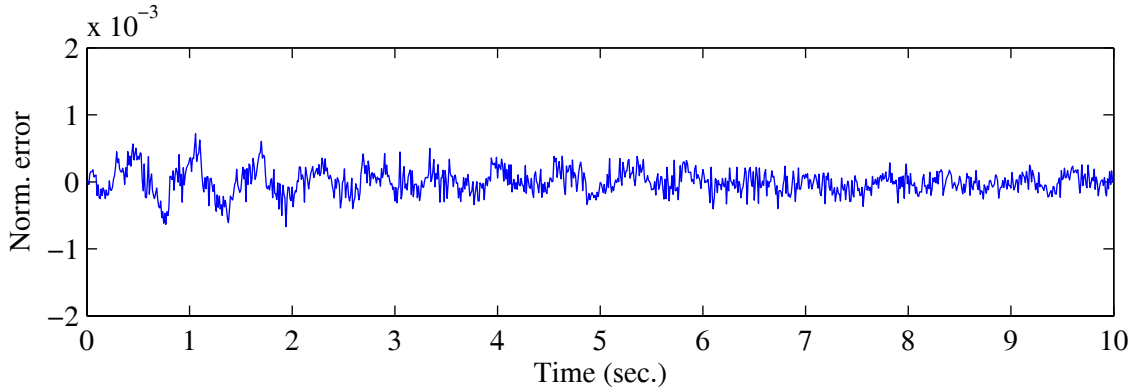

a. Actuator 2 error: second story substructure

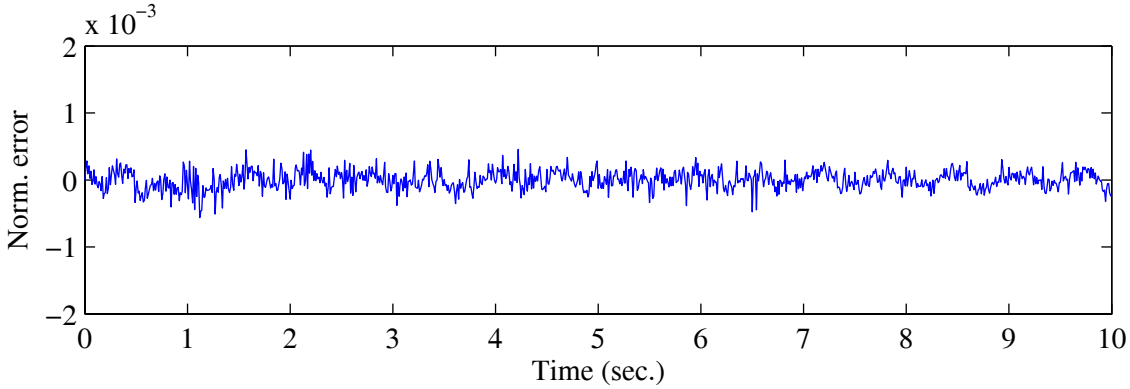

b. Actuator 1 error: first story substructure

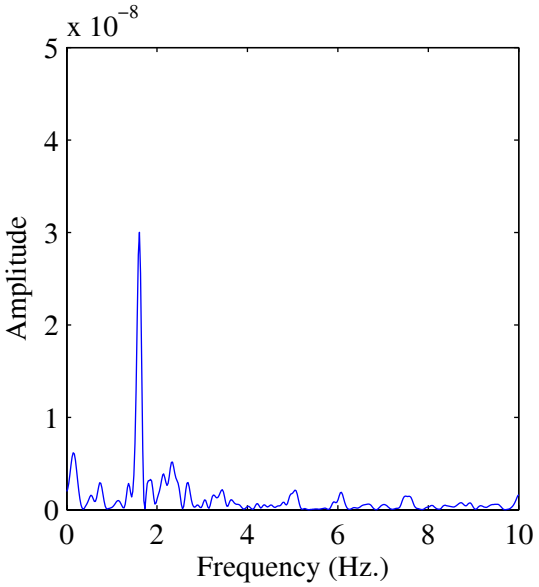

c. PSD of Actuator 2 error

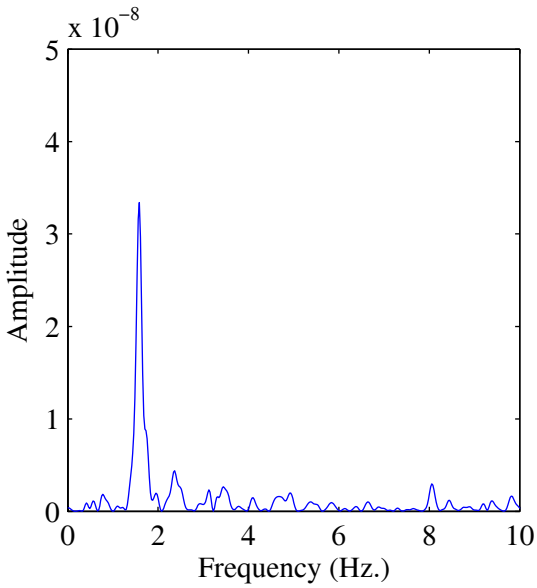

d. PSD of Actuator 1 error

Figure 7-1. Actuator displacement error (command-measured) time histories and power spectral density (PSD) for Cosine Pulse

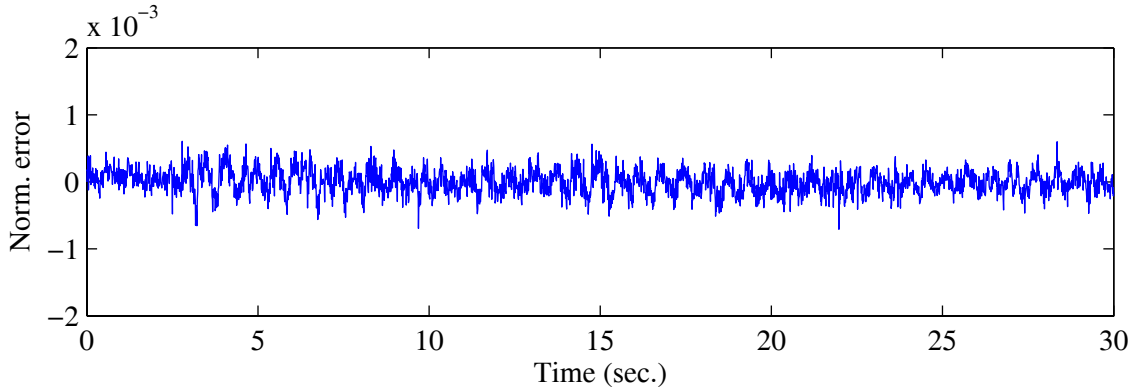

a. Actuator 2 error: second story substructure

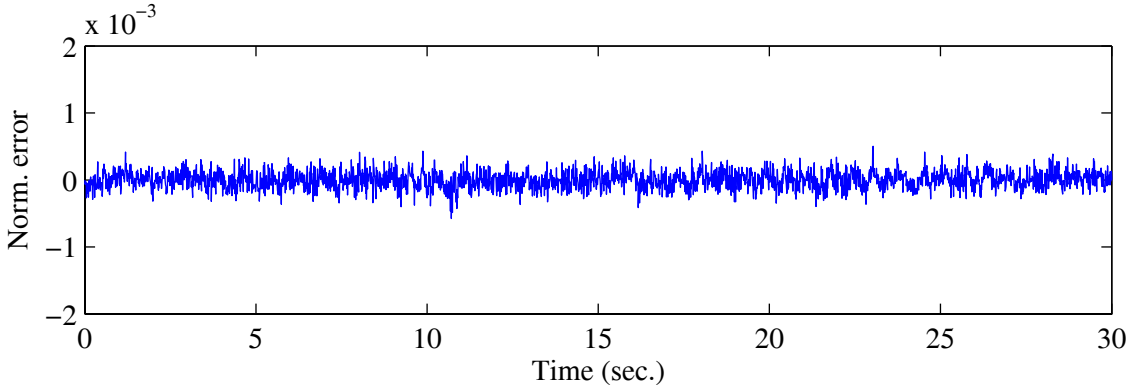

b. Actuator 1 error: first story substructure

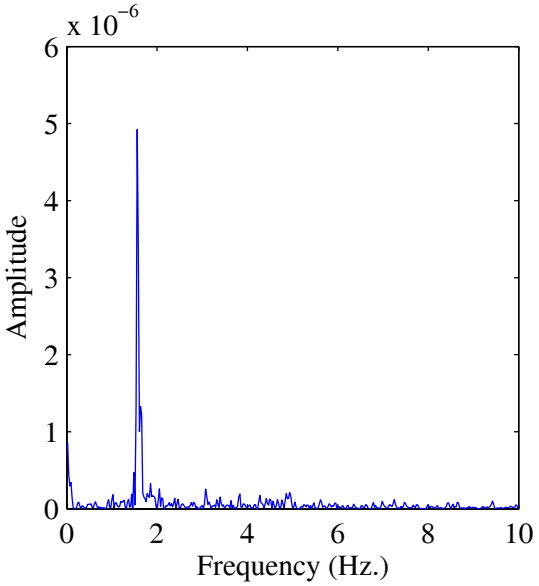

c. PSD of Actuator 2 error

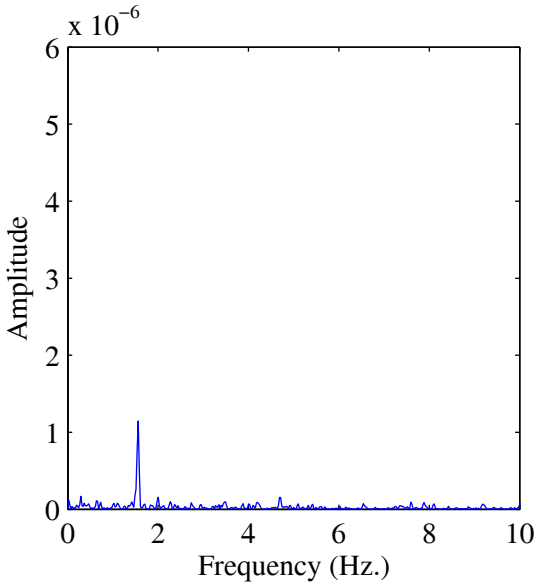

d. PSD of Actuator 1 error

Figure 7-2. Actuator displacement error (command-measured) time histories and power spectral density (PSD) for Tabas-50%

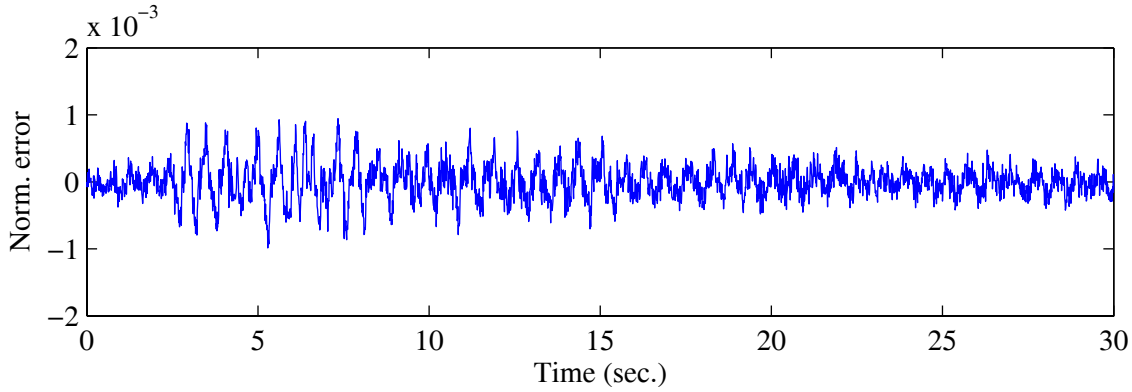

a. Actuator 2 error: second story substructure

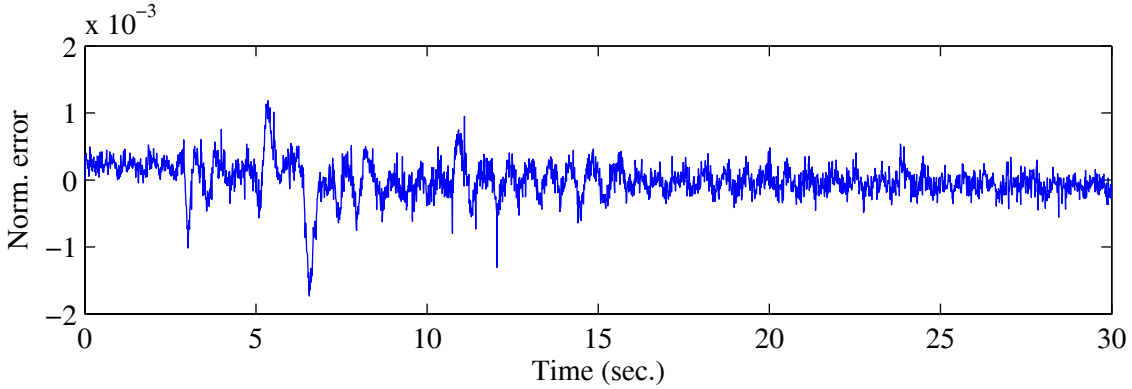

b. Actuator 1 error: first story substructure

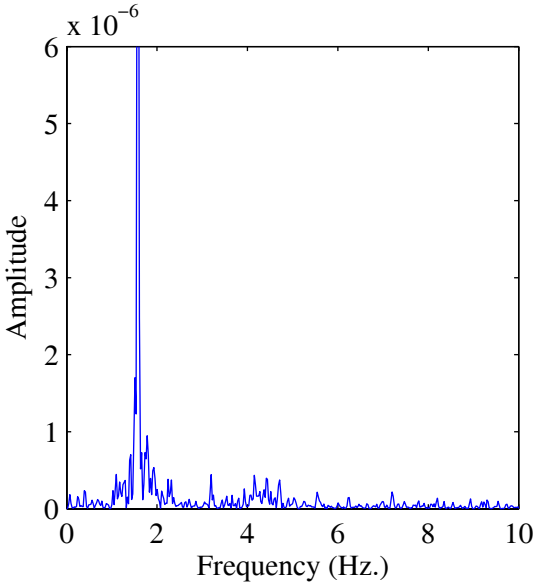

c. PSD of Actuator 2 error

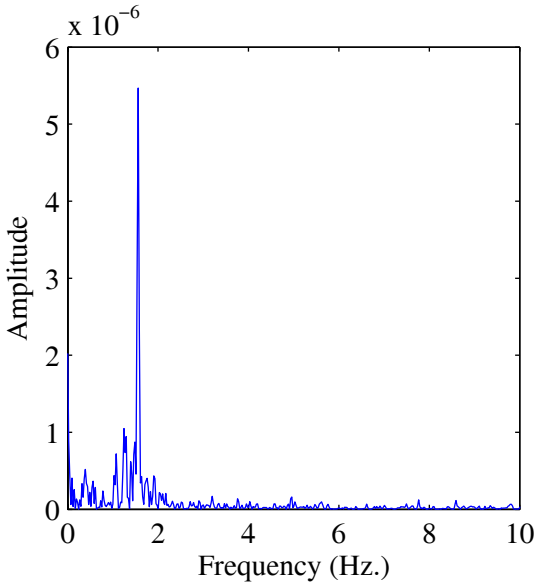

d. PSD of Actuator 1 error

Figure 7-3. Actuator displacement error (command-measured) time histories and power spectral density (PSD) for Tabas-150%

Table 7-1. Summary of measured errors in actuators during hybrid simulations

Test	*norm. by max. actuator disp.*		*norm. by max. measured disp.*	
	Actuator 1	*Actuator 2*	*Actuator 1*	*Actuator 2*
Pulse	0.0006	0.0007	0.0035	0.0070
50% NF01	0.0006	0.0007	0.0049	0.0093
150% NF01	0.0017	0.0010	0.0026	0.0052

7.3 COMPARISON TO PURE NUMERICAL MODELS

The experimental results from the distributed network hybrid simulations are evaluated by a comparison to a pure numerical simulation. The exact same structural model and numerical algorithms are used in both the hybrid simulations and the pure numerical simulations. The main difference is that experimental elements are used in the hybrid simulation, which can include measurement errors and actuator tracking errors. In the numerical simulation, the experimental elements are replaced by numerical models calibrated to the measured force and measured displacement data from the corresponding experiment. In a hybrid simulation involving experimental substructures, the numerical integration algorithm uses the measured force versus command displacement to capture the behavior of the experimental elements. The use of the measured displacement instead of the command displacement for model calibration eliminates the effect of actuator control errors in the purely numerical simulations.

7.3.1 Numerical Models of Experimental Elements

Two different numerical models are used to capture the behavior of the experimental elements at the macroscopic level. These two models are the linear elastic spring model and the non-linear Bouc-Wen model (Bouc 1975, Wen 1976). The linear model computes the restoring force as

$$r(t) = k_{cal} u(t) \tag{7.1}$$

where k_{cal} is the calibrated stiffness and u is the applied displacement. The stiffness is calibrated based on a least-squares fit of the measured restoring force and measured displacement for the experimental elements that respond with a predominantly linear behavior.

The Bouc-Wen model is a smoothed plasticity model that provides the non-linear restoring force using displacement related parameters as:

$$r(t) = \alpha k_{cal} u(t) + (1-\alpha) k_{cal} u_y z(t) \tag{7.2}$$

where u_y is the yield displacement and α is the ratio of the post- to pre-yield stiffness. The stiffness k_{cal} is the initial stiffness calibrated similar to the linear elastic spring model, using only the measured data prior to yielding. The evolutionary parameter $z(t)$ models the smooth hysteretic behavior and is governed by the following differential equation:

$$u_y \dot{z}(t) + \gamma |\dot{u}(t)| z(t) |z(t)|^{n-1} + \beta \dot{u}(t) |z(t)|^n - \dot{u}(t) = 0 \tag{7.3}$$

The dimensionless parameters γ, β, and n control the shape of the hysteretic loop.

7.3.2 Cosine Pulse Simulation

A comparison between the hybrid simulation and the calibrated numerical simulation is shown in Figure 7-4 for the Cosine Pulse input excitation. The response is mostly in free vibration, with the input excitation lasting for the first 0.60 seconds of the simulation. In the numerical simulation, the experimental specimens are replaced by the linear elastic spring models calibrated to a stiffness of 2.81 kip/in. and 2.82 kip/in. for the first and second story, respectively. The drifts computed in the purely numerical simulation are greater in amplitude for both stories compared to the hybrid simulation results. The difference in response is likely due to the energy dissipated at below-yield deformation levels due to friction and other sources of energy dissipation in the test setup, including the measured hysteretic response shown in Figure 6-6. Further, the unintentional yielding in the first story specimen results in the permanent offset between the numerical and hybrid displacement histories in Figure 7-4b.

7.3.3 Elastic-Level Earthquake Simulation Tabas-50%

The linear spring model is also used to compute the substructure resisting forces for the numerical simulation to Tabas-50%. In the corresponding hybrid simulation, the experimental specimen response is linear with calibrated stiffness values of 2.80 kip/in. for the first story and 2.82 kip/in. for the second story. A comparison of the inter-story drifts in Figure 7-5 shows that both the numerical and the hybrid simulation provide similar results. The results are in better agreement here than in the previous case because the linear model is more appropriate for the observed specimen behav-

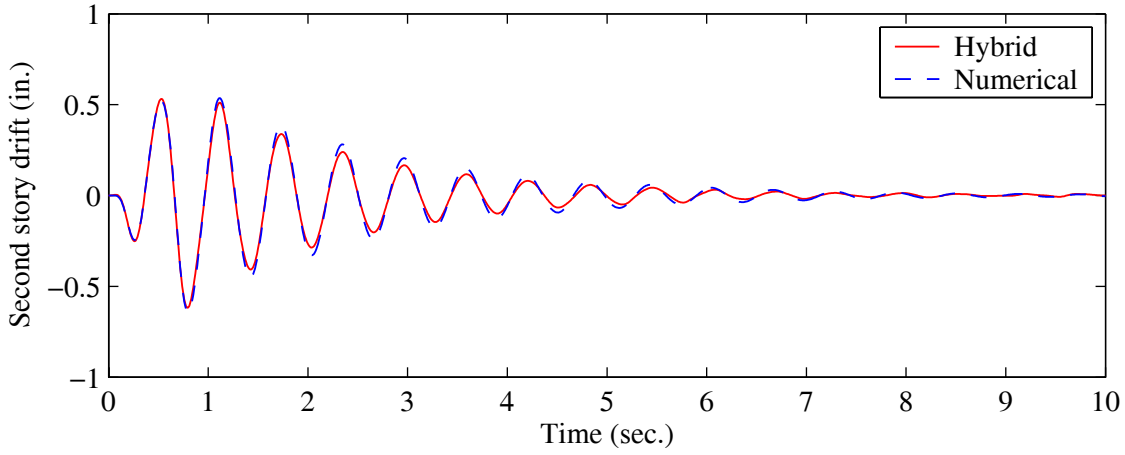

a. second story relative displacement history

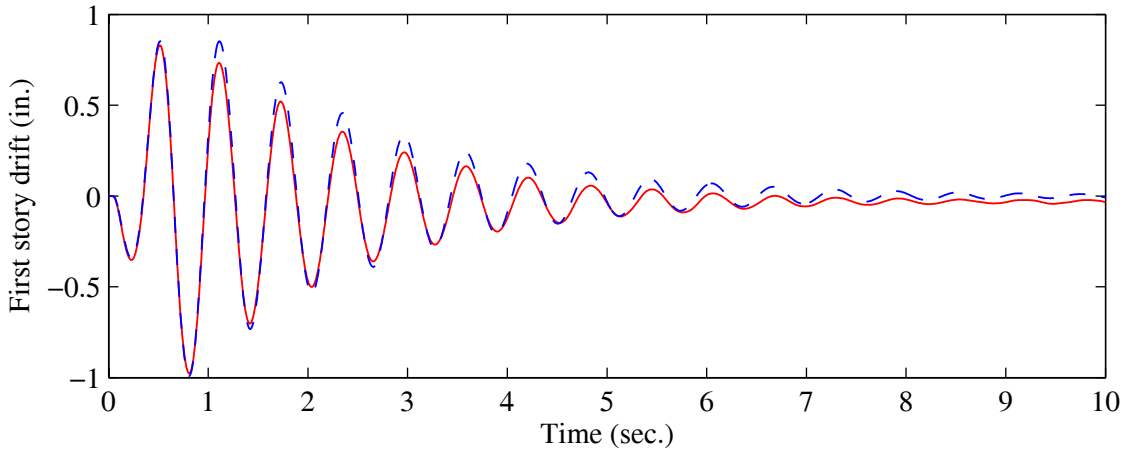

b. first story relative displacement history

Figure 7-4. Displacement response of two story shear frame subjected to Cosine Pulse for distributed hybrid simulation and numerical simulation

ior. In the hybrid simulation Tabas-50%, the experimental elements did not show evidence of yielding (see Figure 6-8).

7.3.4 Non-Linear-Level Earthquake Simulation Tabas-150%

For the hybrid simulation using the input ground motion record Tabas-150%, the response of the second story substructure remains linear, but the first story substructure behavior is non-linear. Accordingly, the linear model replaces the second story substructure and the non-linear Bouc-Wen model replaces the first story substructure in the purely numerical simulation.

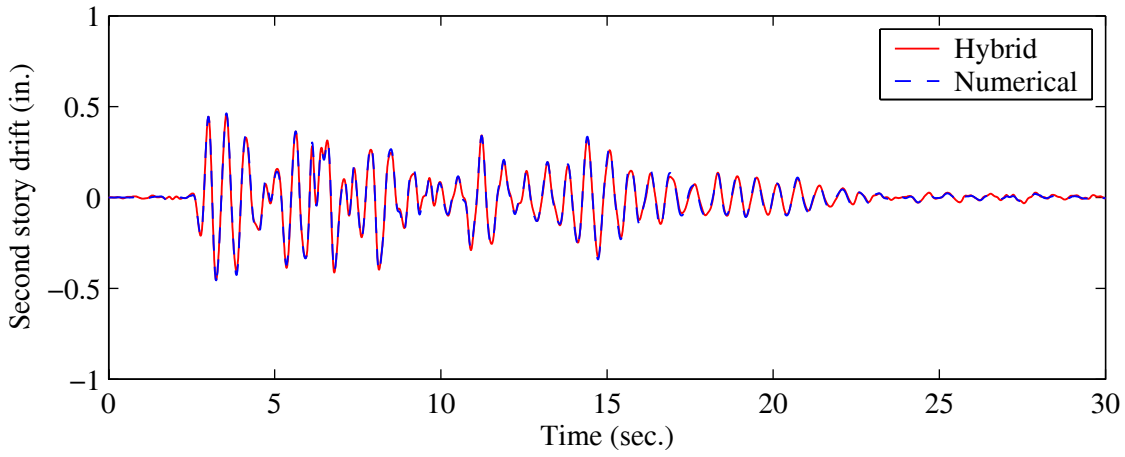

a. second story relative displacement history

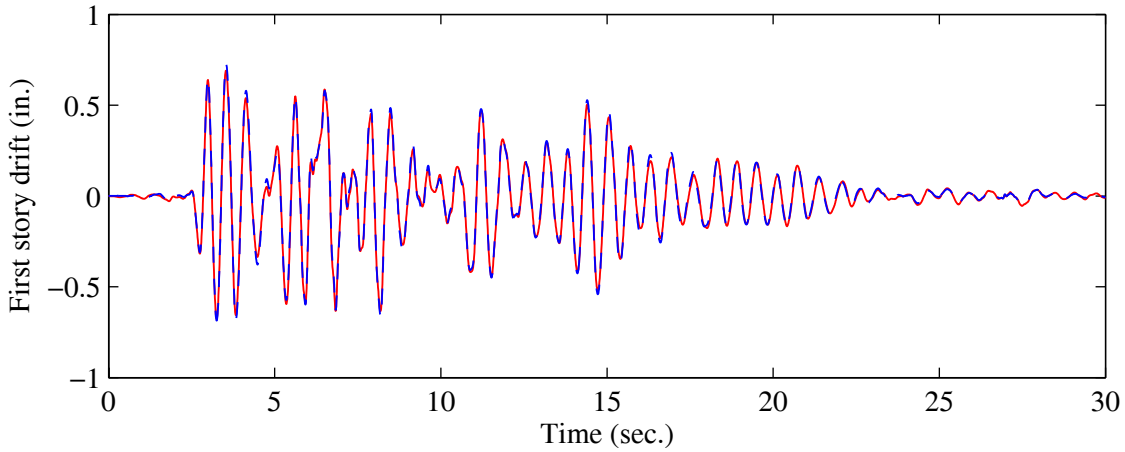

b. first story relative displacement history

Figure 7-5. Displacement response of two story shear frame subjected to Tabas-50% for distributed hybrid simulation and numerical simulation

The second story linear stiffness calibrated to the measured specimen response is 2.74 kip/in. The Bouc-Wen parameters for the first story model are listed in Table 7-2. The initial elastic stiffness is calibrated using the measured response of the experimental element prior to yielding. The yield displacement is estimated as the peak force divided by the elastic stiffness and is given by

$$u_y = \frac{max|r(t)|}{k_{cal}} \tag{7.4}$$

where the maximum measured resisting force is 1.85 kips at the local element (or actuator) degrees of freedom. The post-yield stiffness ratio is estimated to be zero and the remaining parameters in

Table 7-2. Parameters used in the Bouc-Wen model for numerical simulation Tabas-150%

Parameter	*Description*	*Value*
k_{cal}	initial elastic stiffness	2.74 kip/in.
u_y	yield displacement	0.675 in.
α	post-yield/elastic stiffness	0
γ	Bouc-Wen parameter	.45
β	Bouc-Wen parameter	.55
n	Bouc-Wen parameter	2

Table 7-2 are selected to obtain the shape of the hysteresis loop similar to the recorded response of the experimental elements. Based on the relationship between the experimental half column model and the two fixed end columns in each story, the maximum first story shear force and the first story yield drift at the global structure degrees of freedom are twice the values listed in Table 7-2.

A comparison of the earthquake simulation results to Tabas-150% is presented in Figure 7-6. The experimental results from the hybrid simulation correlate well with the numerical simulation, particularly at the second story level. The maximum drift error between the two simulations occurs at the first story level and is 10 percent of the absolute maximum drift.

Figure 7-7 compares the measured resisting forces to the forces predicted by the numerical models. The Bouc-Wen model captures the dominant characteristics of the first-story experimental substructure in Figure 7-7c as can be seen by the numerical simulation of the hysteresis in Figure 7-7d. The negative peaks forces are similar for both simulations, but the Bouc-Wen model predicts a larger positive peak force. The positive peak force is smaller for the experimental element because its strength degrades after yielding, while the strength of the numerical model does not degrade. Nonetheless, the numerical simulation and the hybrid simulation provide similar results for the two-story structural model subjected to Tabas-150%.

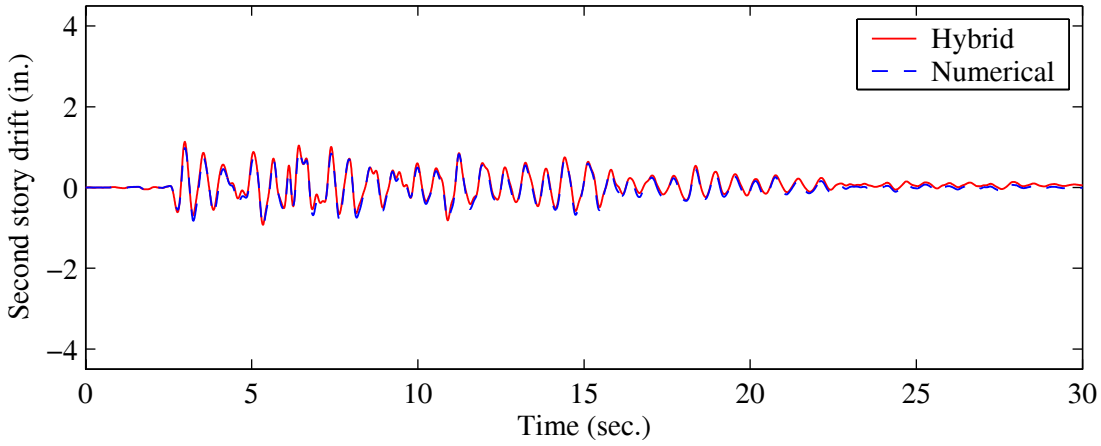

a. second story relative displacement history

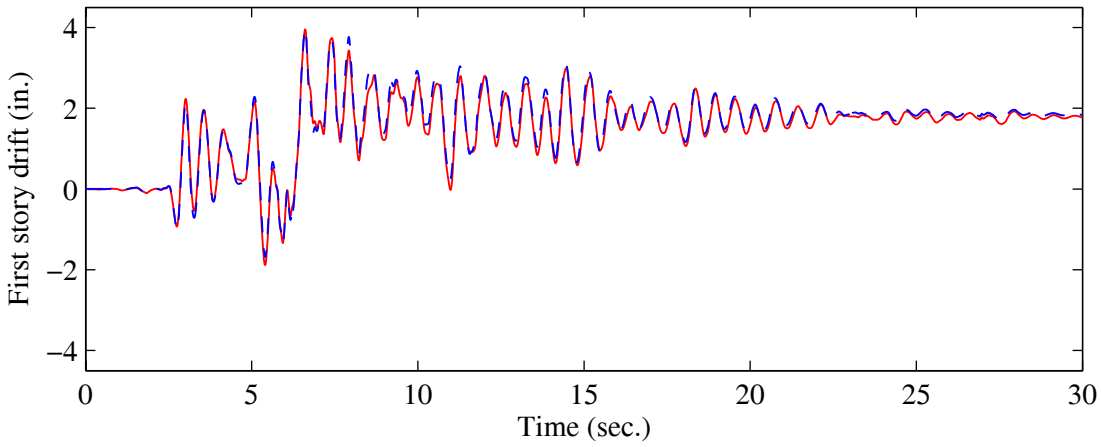

b. first story relative displacement history

Figure 7-6. Displacement response of two story shear frame subjected to Tabas-150% for distributed hybrid simulation and numerical simulation

7.4 ENERGY ERRORS IN EXPERIMENTAL SUBSTRUCTURES

In the examination of displacement control errors, evidence of systematic errors was found, but the effects of these errors on the test results could not be precisely determined. Thewalt and Roman (1994) showed that systematic experimental errors can be detected by the cumulative growth of energy errors resulting from the displacement control of the actuators. Further, the sign of the energy error indicates if energy is being added or dissipated as a result of the experimental errors. Thewalt and Roman presented a technique for computing energy errors during a test but their formulation requires the use of the tangent stiffness matrix. Although a method was proposed to esti-

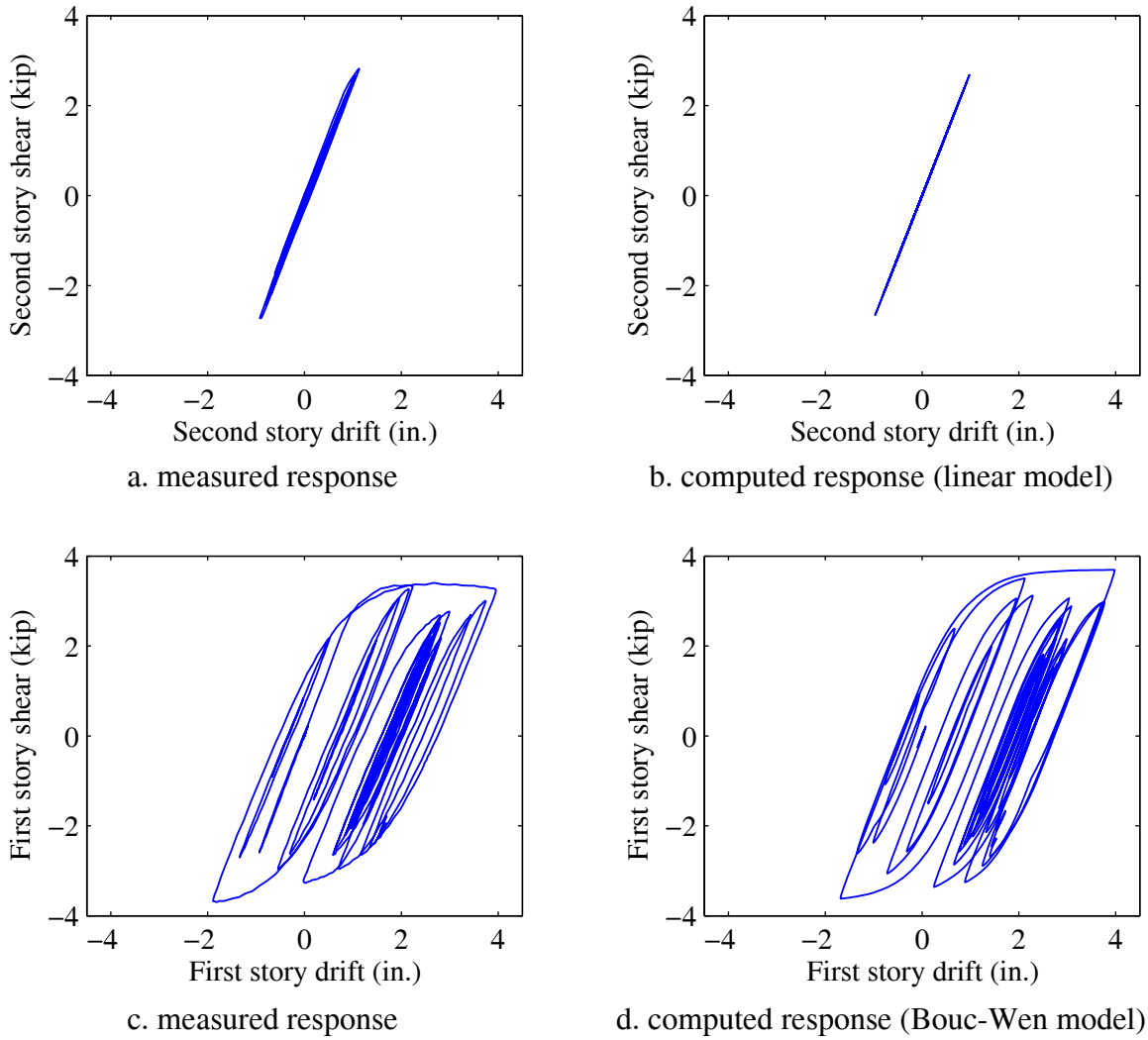

Figure 7-7. Hysteresis of two story shear frame subjected to Tabas-150% for distributed hybrid simulation (a and c) and numerical simulation (b and d)

mate the tangent stiffness matrix using measured test data and initial stiffness data, the procedure appears cumbersome. A simpler approach to measure the cumulative energy error based on displacement control errors is developed here that does not require the tangent stiffness matrix. The proposed procedure in employed to verify that the energy errors generated by the test setup during the distributed hybrid simulations are within reasonable limits.

7.4.1 Energy Balance Equation for Hybrid Simulation

The generalized equation of motion for a hybrid simulation with experimental and numerical substructures is described in Chapter 2. The equation of motion is repeated here for convenience.

$$M^A \ddot{u} + C^A \dot{u} + R^A_{i+1} + R^E_{i+1} = f_{i+1} \tag{7.5}$$

In this equation, superscript *A* refers to the numerical (analytical) substructures, while superscript *E* refers to the experimental substructures. The energy associated with each term in Equation (7.5) is derived by computing the work done by each of the forces in the equation. Integrating each component with respect to the displacement *u* of the structure results in:

$$\int (M^A \ddot{u})^T du + \int (C^A \dot{u})^T du + \int (R^A)^T du + \int (R^E)^T du = \int f^T du \tag{7.6}$$

The above equation states that the energy input from the applied forces *f* is accounted for by the (1) kinetic energy stored in the moving mass, (2) energy dissipated by viscous damping, and (3) strain energy stored by the deformed structural members and hysteretic energy dissipated in the structural members. For a hybrid simulation, energy can be stored and dissipated by both experimental and numerical substructures.

The energy associated with the experimental substructures, E^E, is of particular interest to this discussion. This energy is captured by the work done by the measured resisting forces, R^E, on the structural displacement and can be expressed as

$$E^E = \int (R^E)^T du \tag{7.7}$$

The experimental substructure energy, E^E, accounts for the energy that is stored as strain energy and the energy absorbed by hysteretic dissipation in the experimental substructures only. The remainder of the terms in Equation (7.6) remain unchanged compared to a pure numerical simulation, such as a conventional finite element analysis. Methods to compute the energy balance terms in a pure numerical simulation can be found elsewhere (Uang and Bertero 1990).

As will be demonstrated in the discussion that follows, the experimental substructure energy, E^E, can be contaminated by experimental errors, E^{error}, that may add or dissipate additional energy into the structural model. These errors are introduced into the energy balance equation and can be moved to the right-hand side as shown below.

$$\int (M^A \ddot{u})^T du + \int (C^A \dot{u})^T du + \int (R^A)^T du + \int (R^E)^T du = \int f^T du - E^{error} \tag{7.8}$$

The negative sign on the experimental substructure energy error, E^{error}, indicates that a negative error inputs energy into the structural model. It is important to consider the sign of E^{error} since positive or negative energy errors will have a different effect on the structural response. The following section examines the sources of the experimental energy errors.

7.4.2 Source of Energy Errors in the Test Setup

In the experimental setup, the displacements are imposed at the actuator degrees of freedom and the forces are typically measured by load cells on the actuators. Therefore, it is useful to express the energy in the experimental substructures in terms of the actuator degrees of freedom. This approach allows for the energy errors to be computed separately for each actuator and related to the energy in the global structural model using geometric transformations from conventional finite element models (Fillipou 2002). Further, the energy errors can be examined for each individual actuator.

The geometric transformation matrix T is obtained by transforming the global structural degrees of freedom, u, to the actuator degrees of freedom

$$u^{ac} = Tu \tag{7.9}$$

where u^{ac} is a vector containing the displacement command signals for the actuators. A similar transformation is used in Chapter 6 to relate the global degrees of freedom with the actuator degrees of freedom. The transformation

$$R^E = T^T r^{am} \tag{7.10}$$

can then be used to transform the measured forces at the actuator degrees of freedom, r^{am}, to the global degrees of freedom in the restoring force vector R^E. Substituting Equation (7.10) into Equation (7.7) results in

$$E^E = \int (r^{am})^T T du \tag{7.11}$$

Differentiating both sides of Equation (7.9)

$$du^{am} = Tdu \tag{7.12}$$

and substituting directly into Equation (7.11), an expression of the energy in the experimental substructures in terms of the actuator degrees of freedom is obtained.

$$E^{E} = \int (r^{am})^{T} du^{am} \tag{7.13}$$

In the above expression, the vector multiplication suggests that the energy in the experimental substructures is simply the sum of the energy contributions produced by each individual actuator. The actuators are decoupled in the energy formulation since the energy in each individual actuator can be identified and computed separately. For cases with two or more actuators applying loads on the same physical substructure, the actuators are naturally decoupled for the energy computations, even though the resisting forces are coupled and dependent on the actions of the other actuators. The force coupling is considered in the measured forces used to compute the energy.

Equation (7.13) states that the numerical integration algorithm considers the response of the experimental elements as the measured restoring forces resulting from the command displacements. However, since the command displacement is not necessarily the same as the applied or measured displacement, the behavior of the specimen is not captured accurately. This source of error in a hybrid simulation was discussed in Chapter 3.

A more exact representation of the experimental substructure behavior can be obtained from the measured displacement and the measured force data. This set of data is the best representation of the experimental substructure available and is typically used to evaluate a structure after a quasi-static test. The best estimate of energy stored and dissipated by the experimental substructure is

$$E^{BE} = \int (r^{am})^{T} du^{am} \tag{7.14}$$

where u^{am} is the measured displacement of the specimen at the actuator degree of freedom. It is important to consider that in a hybrid simulation, the load path of the experimental element should coincide with the computed response of the structural model. Consequently, E^{BE} is not necessarily the best estimate with respect to computed response. However, the energy error introduced into a hybrid simulation can be estimated as

$$E^{error} = E^{BE} - E^{E} \tag{7.15}$$

Equation (7.15) captures the difference between the energy that is actually dissipated by the experimental substructures and the energy dissipation that is accounted for in the numerical integration algorithm. The energy error, E^{error}, should be close to zero if the displacement control errors are small. Numerical methods to compute the total energy and the energy errors in the experimental substructures are discussed in the section that follows.

It is important to note that Equation (7.14) does not account for scaling factors between the numerical model (global degrees of freedom) and the experimental substructure (actuator degrees of freedom). Such factors, if not included in the transformation matrix, should be applied to the energy calculations so that a fair comparison can be made between the computed energy errors and relevant energy measures in the global structure expressed by Equation (7.6). Here, the appropriate scaling factors are applied to the energy measures shown later in Section 7.4.4 to account for the relationship between the global structural degrees of freedom and the actuator degrees of freedom.

7.4.3 Computation of Energy Errors

The energy can be computed in each integration time step as

$$E_i = \int_{t_{i-1}}^{t_i} r\,du \approx \frac{1}{2}(r_i + r_{i-1})^T (u_i - u_{i-1}) \tag{7.16}$$

by approximating the integration within a time-step using the trapezoid rule. This formulation implicitly assumes a linear force-displacement relation in the step. The cumulative sum of the energy represents the total energy at time t_j

$$E(t_j) = \sum_{i=1}^{j} E_i \tag{7.17}$$

Using the same approximation as in Equation (7.16), Thewalt and Roman (1994) compute the energy error in each integration time step as

$$E_i^{error} = \frac{1}{2}(K_i u_i^{error} + K_{i-1} u_{i-1}^{error})(u_i^{ac} - u_{i-1}^{ac}) \tag{7.18}$$

where K_i is the tangent stiffness matrix and u_i^{error} is the measured displacement error at step i defined as

$$u_i^{error} = u_i^{ac} - u_i^{am} \tag{7.19}$$

Using the definition of the energy error derived in Equation (7.15), another approach to computing the errors generated by the experimental setup is

$$E_i^{error} = E_i^{BE} - E_i^{E} \tag{7.20}$$

where

$$E_i^{BE} = \frac{1}{2}(r_{i-1}^{am} + r_i^{am})^T(u_i^{am} - u_{i-1}^{am}) \tag{7.21}$$

is the best estimate of the energy in the experimental substructure and

$$E_i^{E} = -\frac{1}{2}(r_{i-1}^{am} + r_i^{am})^T(u_i^{ac} - u_{i-1}^{ac}) \tag{7.22}$$

is the energy in the experimental substructure observed by the numerical integrator in the hybrid simulation. This procedure requires only information that is known at the end of the integration time step and does not require the use of the tangent stiffness matrix. A comparison between the numerical estimation proposed by Thewalt and Roman in Equation (7.18) and the estimation proposed here in Equation (7.20) is shown in the section that follows.

7.4.4 Application to Hybrid Simulation Test Data

The energy-based formulation to detect the growth of experimental errors is applied to the experimental data obtained from the distributed hybrid simulations. Both, the formulation proposed by Thewalt and Roman and the formulation proposed here are used for this purpose. The energy errors for each actuator and the total energy in the structural model are show in Figures 7-8, 7-9, and 7-10 for the three simulations: Cosine Pulse, Tabas-50% and Tabas-150%.

The computed energy error histories using the data from the Cosine Pulse hybrid simulation are shown in Figure 7-8. The energy errors for the individual actuators using Thewalt and Roman's formulation and the proposed method are shown in Figure 7-8a for the second story substructure and Figure 7-8b for the first story substructure. The error histories display the growth of negative

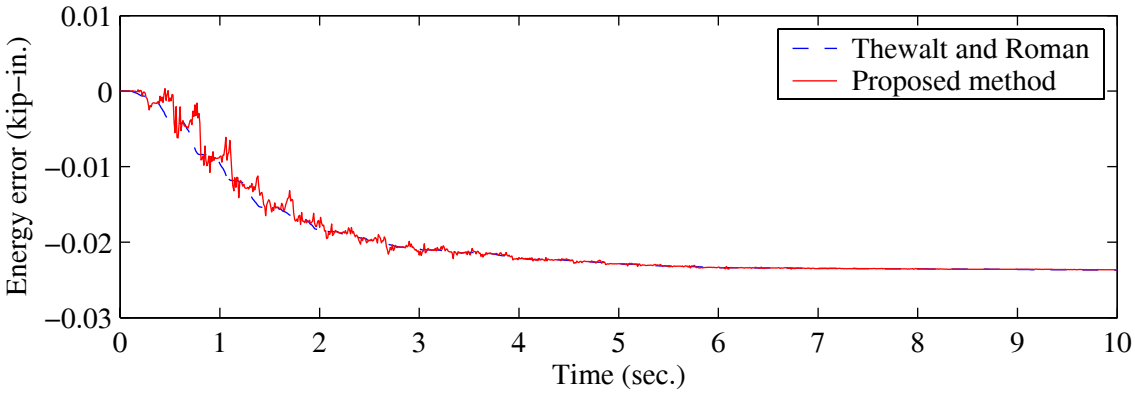

a. energy error in Actuator 2: second story experimental substructure

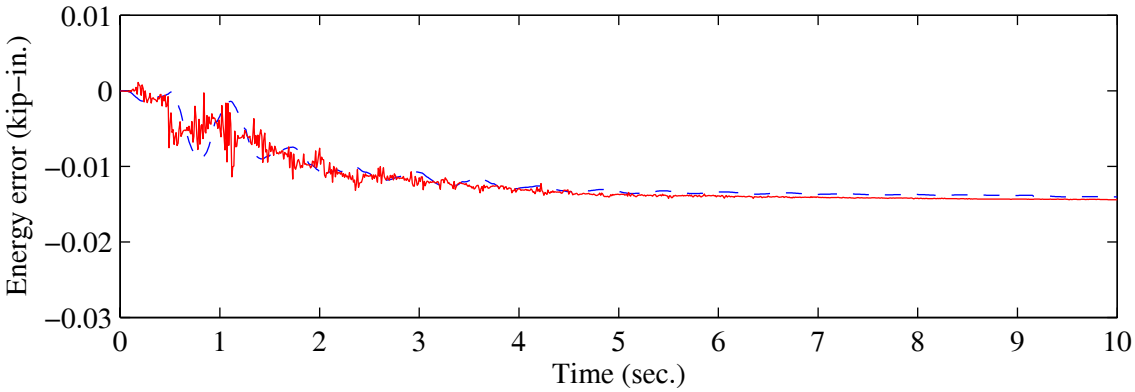

b. energy error in Actuator 1: first story experimental substructure

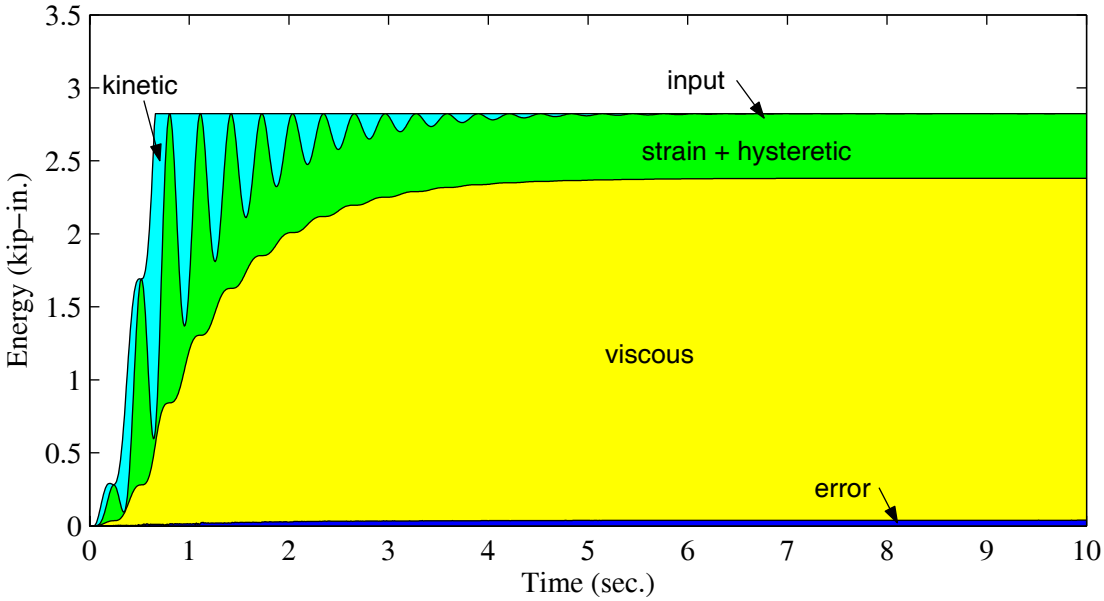

c. distribution of total energy input

Figure 7-8. Energy error and total energy history for simulation Cosine Pulse

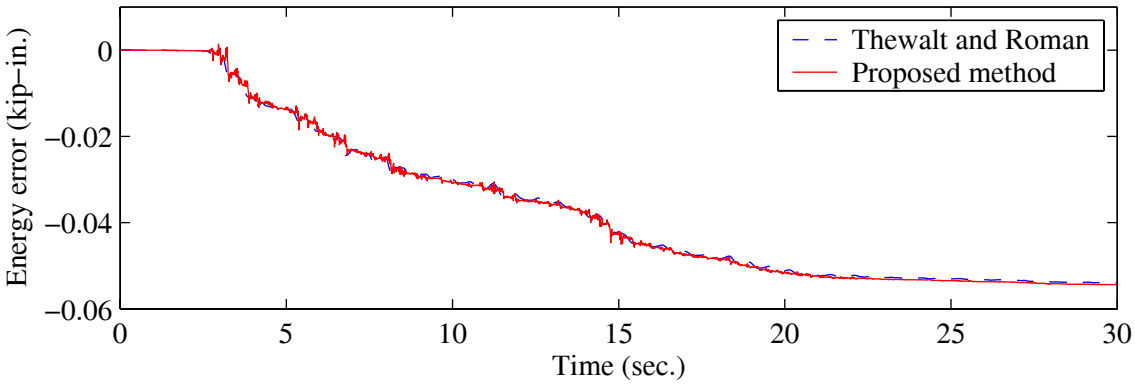

a. energy error in first story experimental substructure

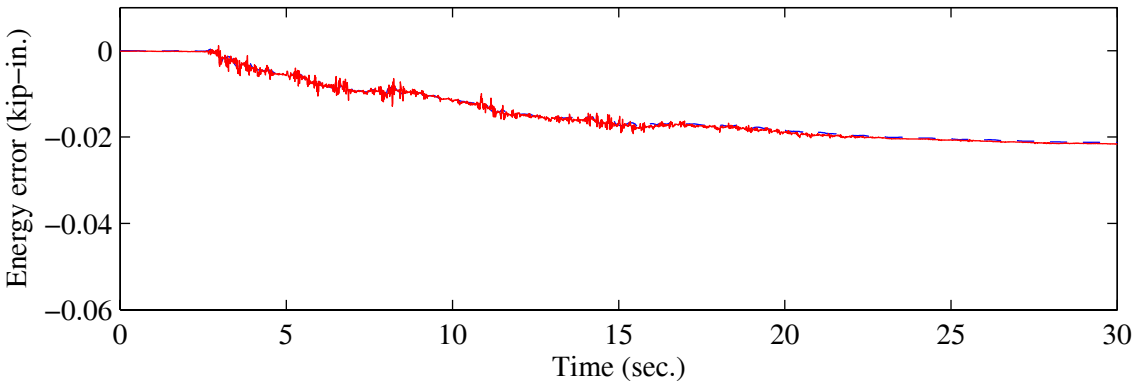

a. energy error in second story experimental substructure

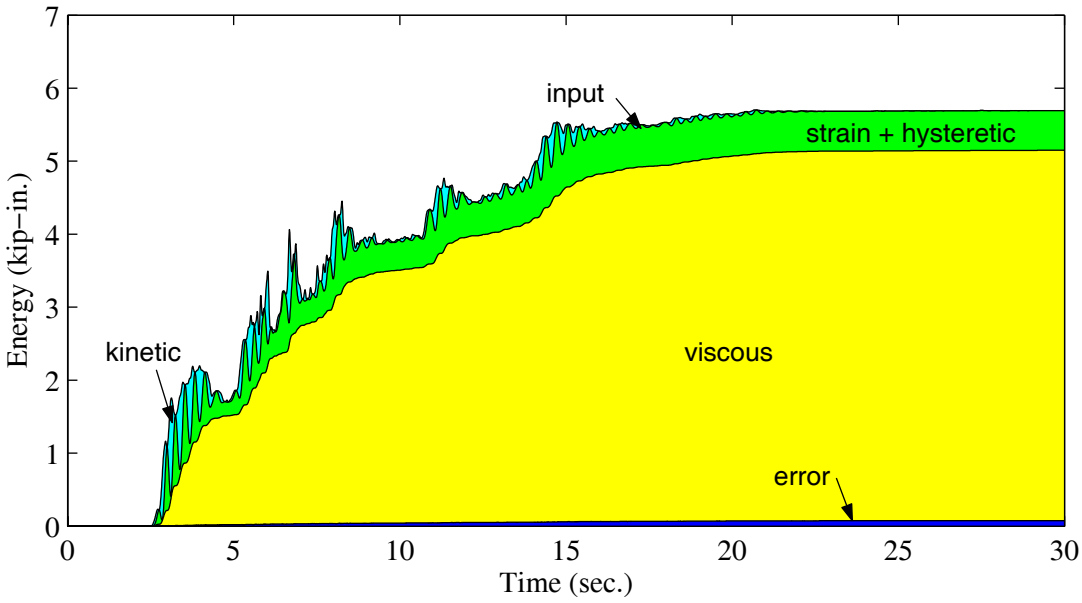

c. distribution of total energy input

Figure 7-9. Energy errors and total energy history for simulation Tabas-50%

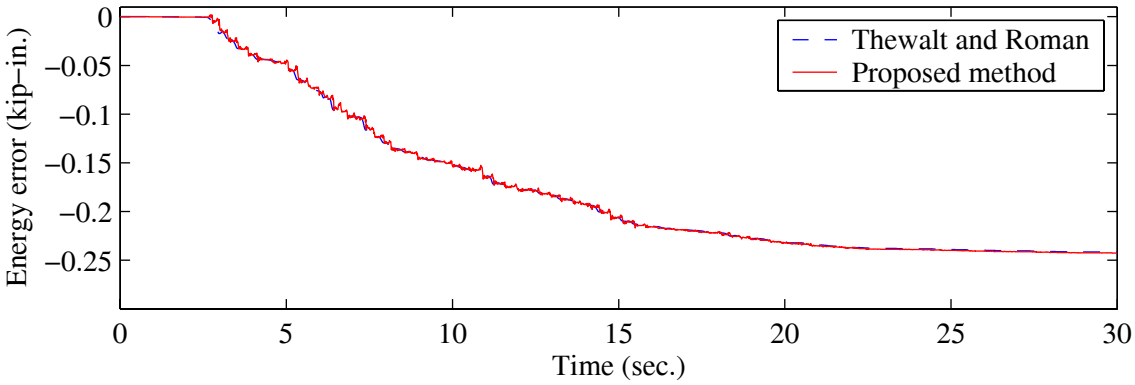

a. energy error in first story experimental substructure

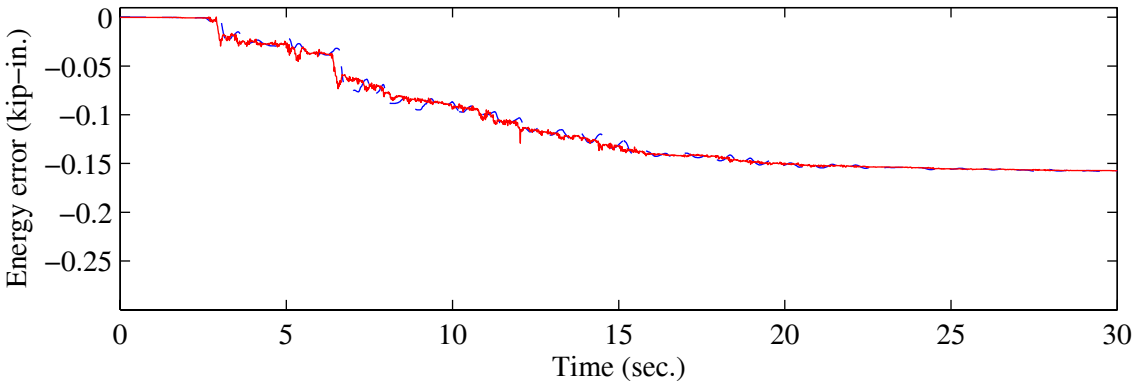

b. energy error in second story experimental substructure

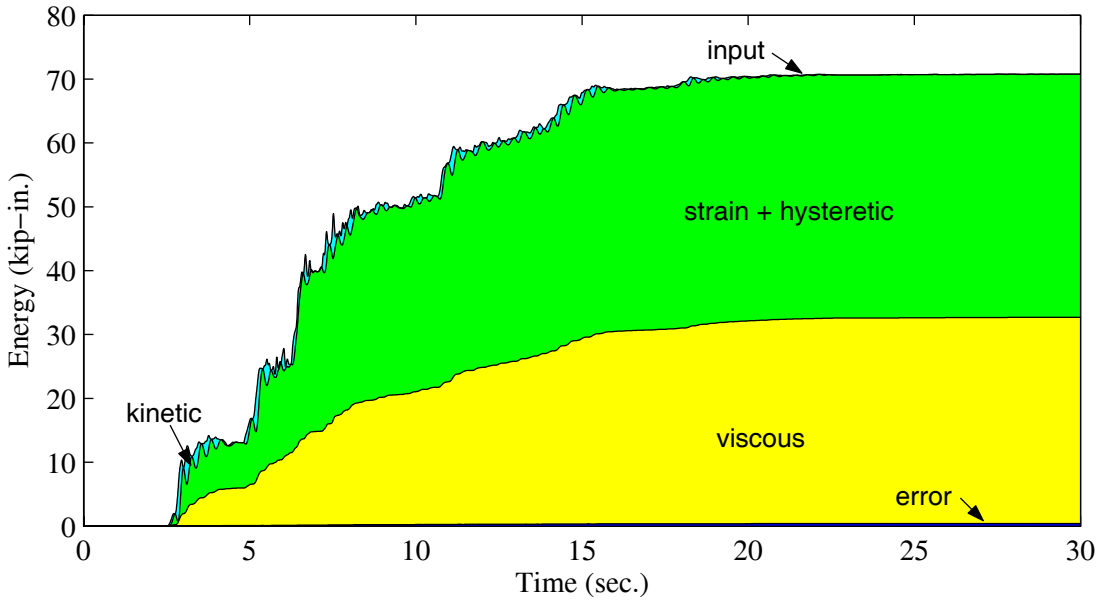

c. distribution of total energy input

Figure 7-10. Energy errors and total energy history for simulation Tabas-150%

energy errors as the simulation progresses. The negative sign indicates that energy is being added to the structural model as a result of undershooting or a lag in the response of the actuator. It appears that the method proposed here is more sensitive to noise in the experimental data, as can be seen by the high frequency oscillations in the energy error histories. High frequency noise in not apparent in the error histories computed using Thewalt and Roman's formulation. However, both methods estimate similar magnitudes for the energy error, which determines their severity.

To compare the magnitude of the energy errors to the total energy in the structural model, Figure 7-8c plots the energy input from the applied loads. The input energy is divided into the different components including: kinetic energy in the mass, viscous dissipation, and strain and hysteretic energy in the structural members. The total energy error, computed as the sum of the energy errors in both actuators is also included in Figure 7-8c. The measured errors in the actuators supply an additional 0.038 kip-in. of input energy to the structural model. This energy is, in reality, dissipated by the experimental substructures, but is not captured by the numerical integration algorithm. The energy error accounts for only 1.6 percent of the total energy input from the applied loads. About 85 percent of the earthquake input energy is dissipated through viscous damping while the remaining 15 percent is dissipated by the hysteretic response of the experimental substructures.

Similar results are shown for the earthquake simulations Tabas-50% in Figure 7-9 and Tabas-150% in Figure 7-10. Table 7-3 lists the numeric values of the energy measures for the three hybrid simulations, including a comparison between the energy errors and the total earthquake energy input at the end of the simulations. The total energy error input into the structural model is small compared to the energy input from the applied load for all three cases. The dissipation of the energy error through viscous and hysteretic damping does not appear to cause a significant difference in the response. In fact, the magnitude of the energy error is within the normal estimates on viscous damping and hysteretic properties in the numerical model.

Table 7-3. Summary of energy input and energy dissipation

Test	*Energy error*		*Hysteretic dissipation (kip-in.)*	*Viscous damping (kip-in.)*	*EQ input energy (kip-in.)*
	Input (kip-in.)	*% of EQ input*			
Pulse	-0.0381	1.6	.442	2.38	2.82
50% NF01	-0.0760	1.3	.542	5.15	5.70
150% NF01	-0.3999	0.57	38.06	32.69	70.77

7.5 SUMMARY

The experimental results from the hybrid simulations using a distributed network architecture were evaluated using three different approaches. An examination of the errors in the experimental substructures showed the presences of systematic errors, but the magnitude of these errors was less than one percent compared to the maximum displacement demands on the actuators. Errors of this magnitude are not expected to have a significant impact on the results of a hybrid simulation. The results from the hybrid simulations were also compared to a pure numerical simulation with calibrated numerical models replacing the experimental substructures. Especially for the elastic level earthquake simulation, the numerical and the hybrid approach gave identical results. The third evaluation procedure examined the energy errors in the experimental substructures. For this purpose, a simple method was derived to compute the cumulative energy associated with the actuator displacement control errors. The resulting energy errors were found to be at most 1.6 percent of the energy input from the earthquake excitation. All three verification procedures indicate that the hybrid simulations presented in Chapter 6 provide reliable results and that the errors introduced from the experimental substructures were reasonably small.

8 Hybrid Simulation Error Indicators

8.1 INTRODUCTION

In the previous chapter, the hybrid simulation results were evaluated after the test had been completed. If the evaluations concluded that the experimental errors were unacceptable, it would be necessary to repeat the hybrid simulations to obtain reliable results. The cost associated with repeating a test is prohibited in most applications.

In this chapter, a technique based on the cumulative energy errors in the experimental substructures (Section 7.4) is used to monitor the hybrid simulations as the test progresses. Hybrid Simulation Error Indicators (HSEI) are proposed to predict the quality of the hybrid simulation results and detect unacceptable levels of experimental errors, preferably before the experimental substructures are damaged. Warning signals from the HSEI can be beneficial in that the simulation can be paused and corrective measures taken to minimize the source of the errors prior to continuing with the simulation. Moreover, the additional information supplied by the HSEI provides a level of confidence to the researcher that the simulation is progressing within allowable tolerances.

Thewalt and Roman (1994) suggested that cumulative energy errors in the experimental substructures can be used to measure the performance of a hybrid simulation. However, they did not develop a relationship between their proposed performance parameters and the accuracy of the simulation. Such a relationship is necessary to justify the use of HSEI based on energy errors. To fill this need, a numerical study is conducted here to relate the proposed HSEI to accepted performance measures of accuracy for structural simulations.

The proposed HSEI are based on the cumulative energy error history normalized by the properties of the structural model and the input excitation. As was shown in Section 7.4, the data necessary to compute the energy error history is available during the simulation, hence the HSEI can be computed up to the current simulation time. However, the accuracy of a real hybrid simu-

lation cannot be determined since the exact solution is not known. Therefore, the use of HSEI as a performance measure is evaluated using purely numerical models for which the exact solution can be determined. Based on these numerical simulations, a relationship is established between HSEI and acceptable accuracy measures that can provide, for example, an estimate of displacement errors in terms of the magnitude of HSEI. Further, the suitability of HSEI as a direct measure of accuracy can be determined. An example application using HSEI is provided and suggested actions are recommended based on the predetermined tolerance specified in terms of the HSEI. First, HSEI and accepted performance measures describing the accuracy of the simulation are defined. Then, the HSEI are compared to the accepted performance measures using data from the numerical simulations. Several definitions are proposed for both the HSEI and the performance measures to examine the correlation between the various definitions considered.

8.2 DEFINITION OF HSEI

The use of HSEI to asses the quality of a hybrid simulation requires that a threshold value be specified as the level of unacceptable error, anticipating that the accuracy of results is exceeding the allowable tolerance limits. The threshold value should relate the energy error to parameters specific to the hybrid simulation under consideration. Two different norms are examined here based on (1) the maximum recoverable strain energy and (2) the input energy from the earthquake excitation. Both definitions are based on characteristics of the structural model and response parameters that are known in a hybrid simulation.

8.2.1 Recoverable Strain Energy

Thewalt and Roman (1994) recommended the use of performance measure based on the experimental energy error compared to the recoverable strain energy in the structural system. This normalization relates the error strictly to parameters of the structural model under investigation and can be defined as

$$HSEI^{S} = \frac{E^{error}}{E^{strain}} \tag{8.1}$$

where

$$E^{strain} = \frac{1}{2} u_y^T K u_y \tag{8.2}$$

Assuming elasto-plastic behavior, the maximum recoverable strain energy E^{strain} is constant for a given structure. Therefore, the error is normalized by a constant value and $HSEI^S$ does not capture the amplitude or the duration of the input excitation.

8.2.2 Input Earthquake Energy

A global view of the experimental substructure energy errors is given by the energy balance Equation (7.8) of the entire structure repeated below

$$\int (M^A \ddot{u})^T du + \int (C^A \dot{u})^T du + \int (R^A)^T du + \int (R^E)^T du = \int f^T du - E^{error} \tag{8.3}$$

Based on Equation (8.3), the magnitude of E^{error} relative to the input energy

$$E^{input} = \int f^T du \tag{8.4}$$

appears to be an important factor in determining the impact of the errors on the structural response. A measure of energy error relative to the input energy can be defined as follows

$$HSEI^I = \frac{E^{error}}{E^{input}} \tag{8.5}$$

At the beginning of a simulation, the input energy is zero, which can result in an infinite value of $HSEI^I$. In order to define the normalized energy error in the structure throughout the simulation, Equation (8.5) is re-formulated as follows

$$HSEI^I = \frac{E^{error}}{E^{strain} + E^{input}} \tag{8.6}$$

8.3 HYBRID SIMULATION PERFORMANCE PARAMETERS

A relationship between the proposed HSEI and the dynamic response of structures is established using performance measures describing the accuracy of the simulation. The performance parameters presented here cannot be used directly as HSEI because they are generally available only after the test has been completed or are not available at all; the exact solution is required to compute

these values. In the forthcoming numerical studies, the use of HSEI to predict these performance parameters is investigated.

Two measures of accuracy are proposed based on the errors between the displacement results of the simulation with experimental errors, u^{sim}, and the exact displacement results determined from an identical simulation without errors, u^{exact}.

$$\varepsilon^{max} = \frac{MAX\left|u^{exact} - u^{sim}\right|}{MAX\left|u^{exact}\right|} \tag{8.7}$$

$$\varepsilon^{rms} = \frac{RMS\left|u^{exact} - u^{sim}\right|}{MAX\left|u^{exact}\right|} \tag{8.8}$$

The normalized measure of accuracy of the simulation ε^{max} captures the maximum error between the exact simulation and the simulation with induced errors, while the performance measure ε^{rms} captures the root-mean-square of the error throughout the simulation. Since each measure captures different aspects of the error history, both measures are considered in the analysis that follows.

A third performance measure is considered based on the input energy into the structural model. The normalized measure based on energy input from the applied loading is

$$\varepsilon^{enr} = \frac{\left|\int f^T du^{exact} - \int f^T du^{sim}\right|}{\int f^T du^{exact}} \tag{8.9}$$

Since the energy input is dependent on the displacement response of the structure, this energy input will be different for the exact simulation and the simulation with errors. This performance measure is not entirely dependent on the displacement response of the structure, and therefore might be useful to detect errors for structures with a displacement response that is not sensitive to the applied loading.

8.4 HYBRID SIMULATION WITH ERRORS

To asses the use of HSEI as performance measures, a relationship is developed between the proposed HSEI and the performance parameters, ε, typically used to measure the accuracy of simulations. This relationship is established using data from numerical simulations of a hybrid

experiment, since the exact solution is, strictly speaking, not known for hybrid simulation involving experimental substructures. In the numerical models, the experimental errors can be completely eliminated and the exact solution can be determined within the accuracy of the numerical model. Moreover, the magnitude of the errors can be incrementally modified to observe the changes in the structural response and the performance parameters along with the changes in the HSEI.

8.4.1 Numerical Models

A Simulink (Mathworks 2003) model of a hybrid simulation algorithm with induced systematic errors was presented in Section 3.4.2. This model was previously used to demonstrate the effects of errors on the dynamic response of structures. The same Simulink model is used here to generate data to examine the relationship between the performance measures and the HSEI.

Three different structural models and two ground motions are considered in this study. The structural models are: (1) a single degree of freedom (SDOF) system with a period of 1.0 seconds and 5 percent viscous damping; (2) a SDOF with a period of 0.33 seconds and 5 percent viscous damping; and (3) a 2-DOF structure with periods of 1.0 and 0.38 seconds with 5 percent viscous damping for both modes of vibration. The two ground motions considered are the 1940 El Centro N-S component and the 1978 Tabas record. Both records are maintained at their original length scale, but the amplitude scale is modified to obtain a linear level simulation and a non-linear level simulation. As reported in Section 3.4, a linear resisting force model is used in the linear simulations and an elastoplastic model is used in the non-linear simulations. Five structure and ground motion pairs are considered in this study and are listed in Table 8-10, including the amplitude scale factors for the ground motions. The structural model and ground motion listed as Case 1 was previously examined in Section 3.4.2.

The ground motion amplitude scales were selected to obtain a maximum displacement just under the yield displacement (corresponding to the non-linear model) for the linear simulation and a ductility of four in the non-linear simulation. The two amplitudes are intended to resemble the typical test sequence for shake table and hybrid simulations consisting of an elastic-level simulation followed by a destructive high intensity simulation.

The earthquake time histories and the linear displacement and acceleration response spectra are shown in Figure 8-1 for El Centro and in Figure 8-2 for the Tabas record. The spectra are plot-

Table 8-10. Pairs of structural models and ground motions used to examine the relationship between HSEI and performance parameters

Case	*Structural model*		*Ground motion*		
	Degrees of freedom	*Natural period (sec.)*	*Record*	*Amplitude scale for linear model*	*Amplitude scale for non-linear model*
1	1	1.0	El Centro	0.2	1.0
2	1	1.0	Tabas	5	1.5
3	1	0.33	El Centro	1.0	5.0
4	1	0.33	Tabas	0.13	0.35
5	2	1.0, 0.38	El Centro	0.2	1.0

ted for damping ratios of 0, 2 and 5 percent of critical damping to examine the influence of damping in the regions corresponding to the structural models examined. The circular markers in the figure show the location of the SDOF structures listed in Table 8-10 within the spectra. The 2-DOF system has natural periods close to the periods of the two individual SDOF systems.

A total of 22 simulations were carried out for each of the five cases listed in Table 8-10. As an example, the complete sequence of simulations is listed in Table 8-11 for Case 1. The eleven linear and eleven non-linear simulations were executed with systematic errors of various intensities to observe the change in structural response with increasing errors. Systematic errors were introduced into the simulation as displacement control errors, generated as the product of a random number and the step displacement increment (See Figure 3-5). The mean of the random number generator varied between 0 and 1 with increments of 0.1. The variance of the random number generator remained constant at 0.1 for all cases. The systematic errors resulted in a simulated delay in the response of the actuator varying from approximately 0 to 10 milliseconds in increments of 1 millisecond. The mean of the random number generator along with the time delay calibrated from a comparison between the command displacement and the command displacement plus the error are listed in Table 8-11. The same sequence of tests was repeated for the other four cases in Table 8-10. For Case 5, errors were added to the displacements of both actuator degrees of freedom (story drifts) prior to computing the story resisting shear forces.

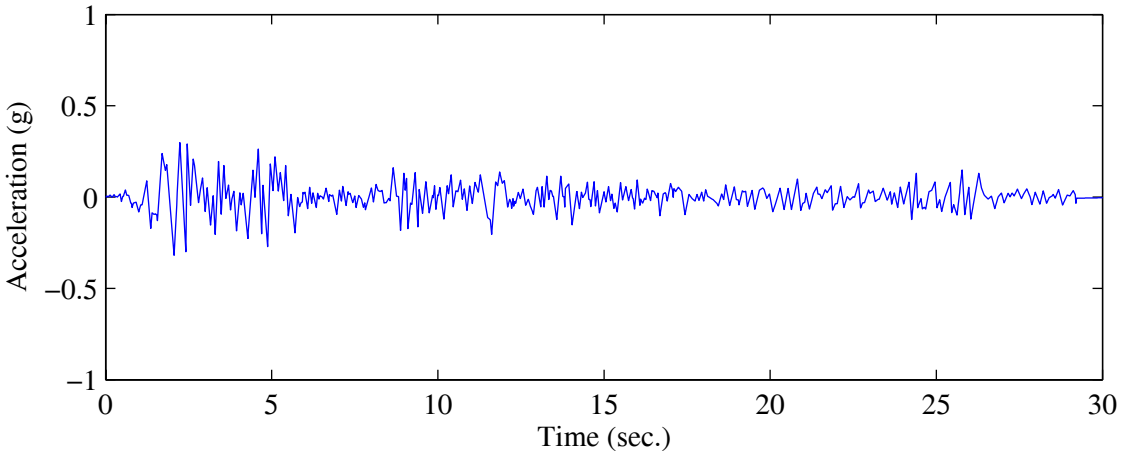

a. acceleration history

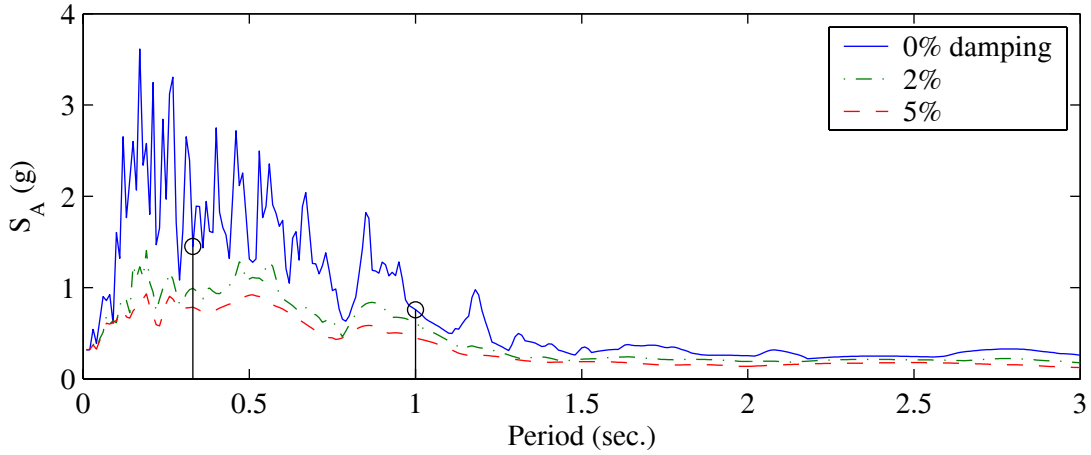

b. pseudo-acceleration response spectra

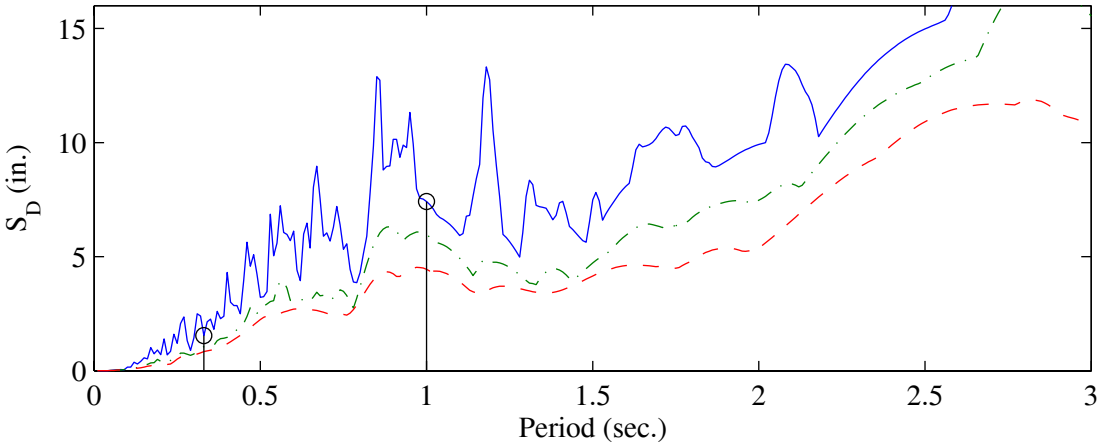

c. displacement response spectra

Figure 8-1. Ground motion record and response spectra for 1940 El Centro

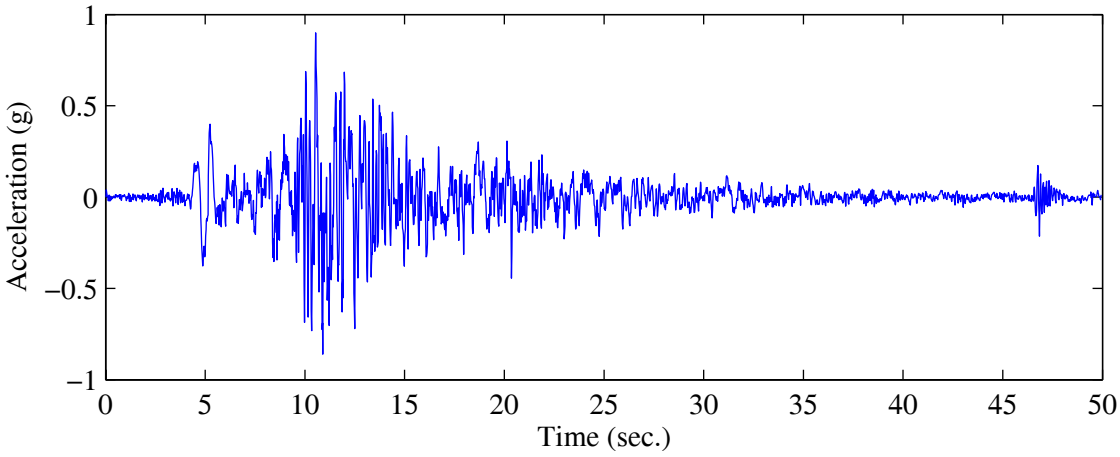

a. acceleration history

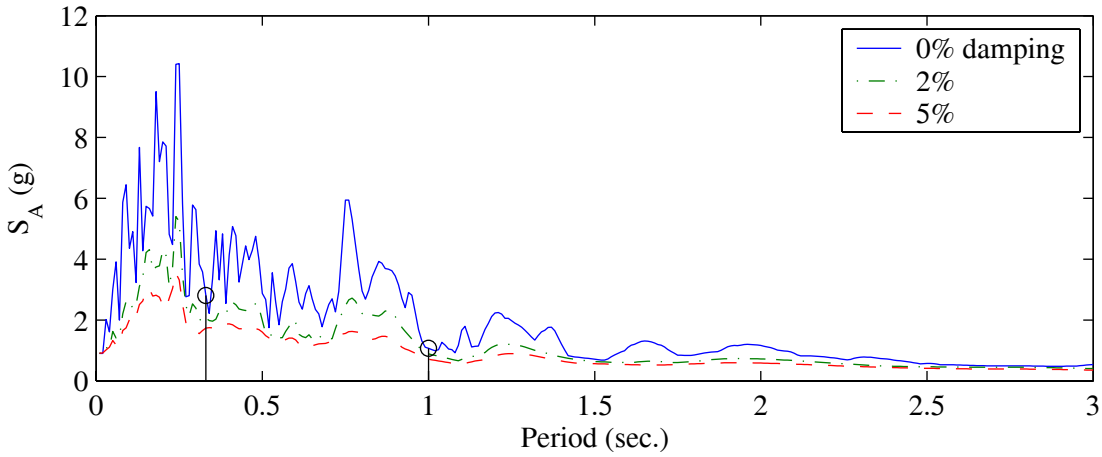

b. pseudo-acceleration response spectra

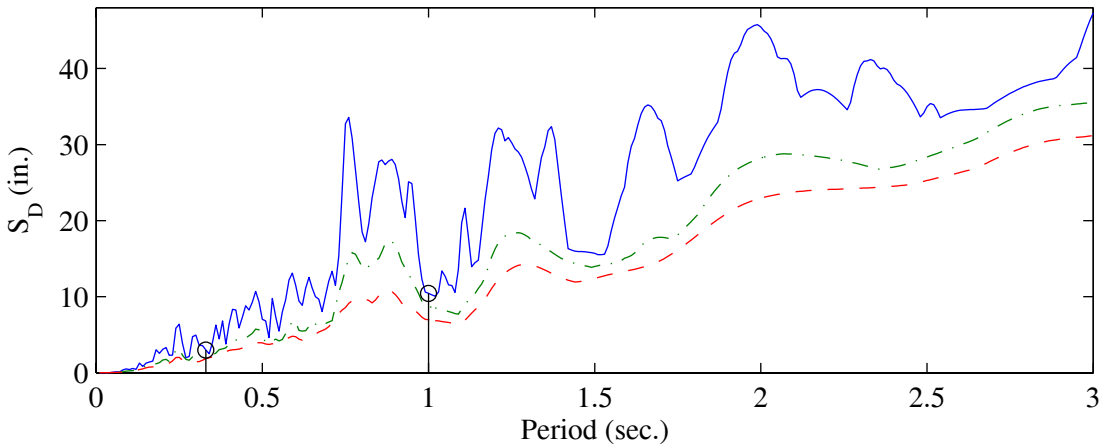

c. displacement response spectra

Figure 8-2. Ground motion record and response spectra for 1978 Tabas

Table 8-11. Sequence of simulations for evaluation of HSEI using Case 1: SDF with 1.0 second period subjected to El Centro

Test run	*Ground motion amplitdue*	*structural model*	*Simulated error*	
			Mean of random error	*Effective delay (msec.)*
1	.20	linear	0.0	0
2	.20	linear	0.1	1.0
3	.20	linear	0.2	2.0
4	.20	linear	0.3	2.9
5	.20	linear	0.4	3.9
6	.20	linear	0.5	4.9
7	.20	linear	0.6	5.9
8	.20	linear	0.7	6.9
9	.20	linear	0.8	7.9
10	.20	linear	0.9	8.9
11	.20	linear	1.0	9.9
12	1.0	non-linear	0.0	0
13	1.0	non-linear	0.1	1.0
14	1.0	non-linear	0.2	2.0
15	1.0	non-linear	0.3	2.9
16	1.0	non-linear	0.4	3.9
17	1.0	non-linear	0.5	4.9
18	1.0	non-linear	0.6	5.8
19	1.0	non-linear	0.7	6.8
20	1.0	non-linear	0.8	7.8
21	1.0	non-linear	0.9	8.7
22	1.0	non-linear	1.0	9.7

8.4.1 Result of Numerical Simulations

The simulation model listed as the first case in Table 8-10 was previously examined in Section 3.4.2. Detailed results of the simulations are shown for the linear and the non-linear simulations, corresponding to test runs 3 (Figure 3-6), 11 (Figure 3-7), 14 (Figure 3-8), and 22 (Figure 3-9) in Table 8-11. The resulting displacement error history and the two proposed HSEI are shown in Figure 8-3 for a simulated actuator lag of 2 milliseconds. The subplots on the left (*a*, *c*, and *e*) correspond to the linear simulation and the subplots on the right (*b*, *d*, and *f*) are for the non-linear sim-

ulation. The negative value of HSEI indicates that the energy error is negative and, as a result, energy is added to the simulation.

For the linear simulation, the largest rate of increase in displacement error occurs between 3 and 5 seconds in Figure 8-3a. At around the same time, there is a substantial increase in the energy error for both HSEI in Figures 8-3c and 8-3e. It appears that the slope of the HSEI is related to the amplitude growth of the error signal. This trend is evident for the linear simulation, and is more subtle for the non-linear simulation. The ability to capture a rapid increase in displacement errors is an attractive feature of the error monitor.

The displacement error history and the HSEI are repeated for the linear and non-linear simulations with a 10 millisecond actuator lag in Figure 8-4. Only the magnitude of the error and HSEI histories change as the actuator lag is increased. The same trends exist between the growth of the displacement errors and slope of the HSEI.

Figure 8-5 presents a summary of the performance parameters, ε, and HSEI for the 22 simulations listed in Table 8-11. The data presented in the figure corresponds to the final values computed at the end of the simulation as a function of the simulated time lag in the actuator. Different markers are used to distinguish between the linear and the non-linear simulations as shown in the legend. An examination of the three performance measures considered in Figure 8-5a shows that the simulation errors grow with increasing actuator lag as expected. Also, the errors in the linear simulations are greater in magnitude compared to the nonlinear simulation for the same actuator lag.

In Figure 8-5b, the energy error measure normalized by strain energy, $HSEI^S$, increases at a much faster rate for the non-linear simulation compared to the linear simulations. This measure does not capture the intensity of the applied loading, and therefore, does not correlate well with the performance measures. Larger errors should be expected and allowed for increased actuator velocity demands or longer simulations. The second energy measure, $HSEI^I$, shows that the linear simulations are more sensitive to systematic errors than the non-linear simulations and correlates best with the performance measures considered in Figure 8-5a,

A direct comparison between the HSEI and the performance measures is shown in Figure 8-6. The three performance measures, separated into linear and non-linear simulations, are compared to $HSEI^I$ in Figure 8-6a and to $HSEI^S$ in Figure 8-6b. In Figure 8-6a, the data for the linear

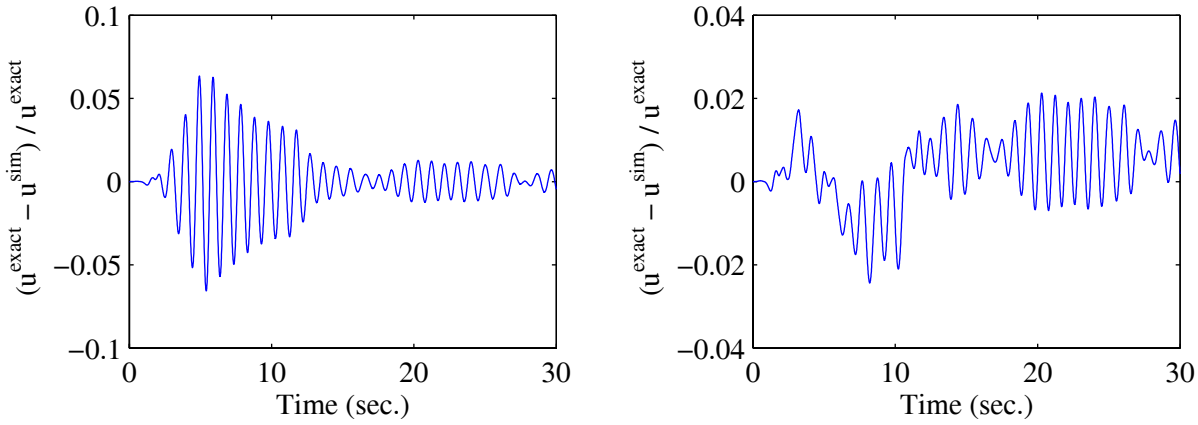

a. displacement error for linear model

b. displacement error for nonlinear model

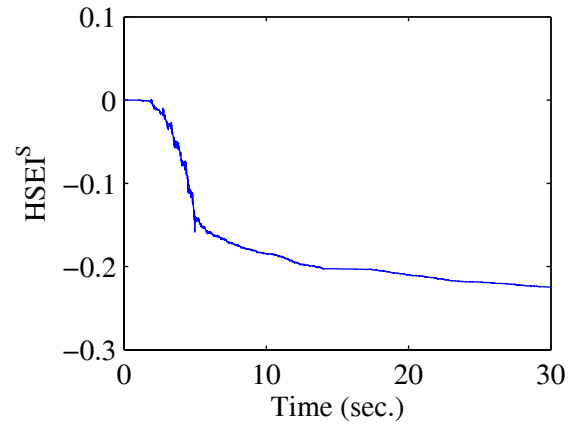

c. HSEI for linear model

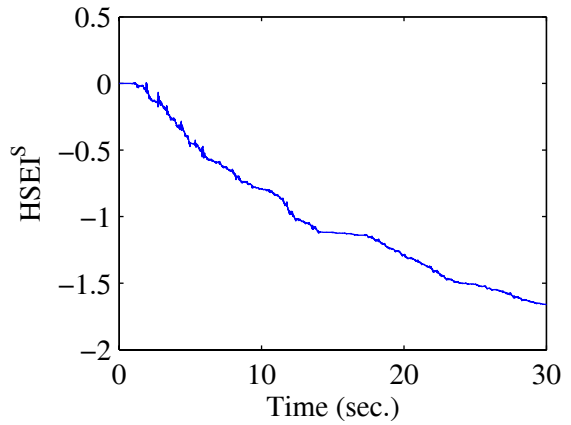

d. HSEI for non-linear model

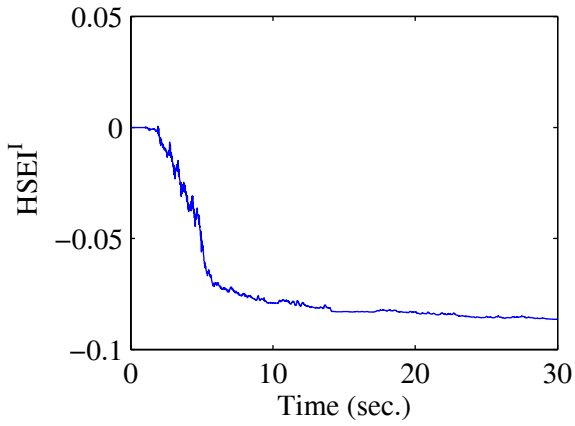

e. HSEI for linear model

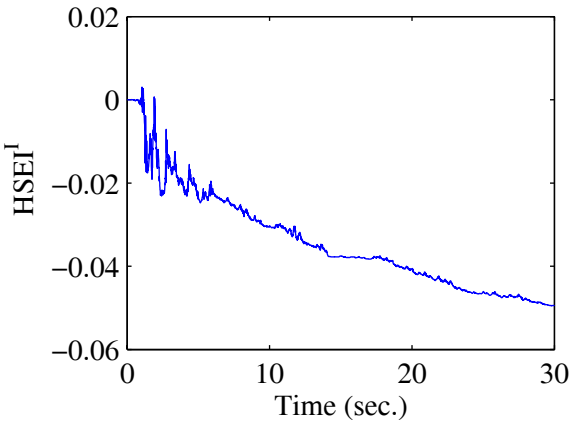

f. HSEI for non-linear model

Figure 8-3. Displacement response errors and HSEI with simulated actuator lag of 2 msec. for structure with 1.0 second period subjected El Centro ground motion

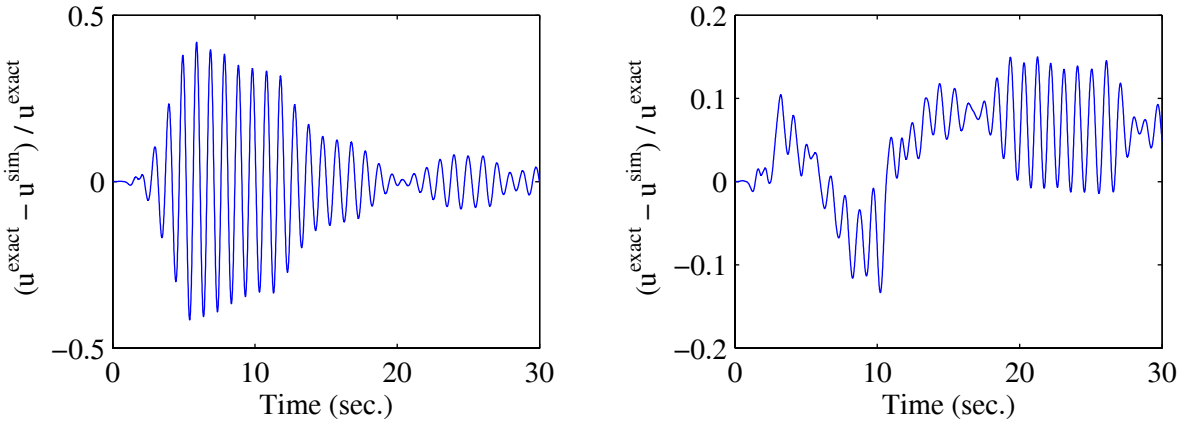

a. displacement error for linear model

b. displacement error for nonlinear model

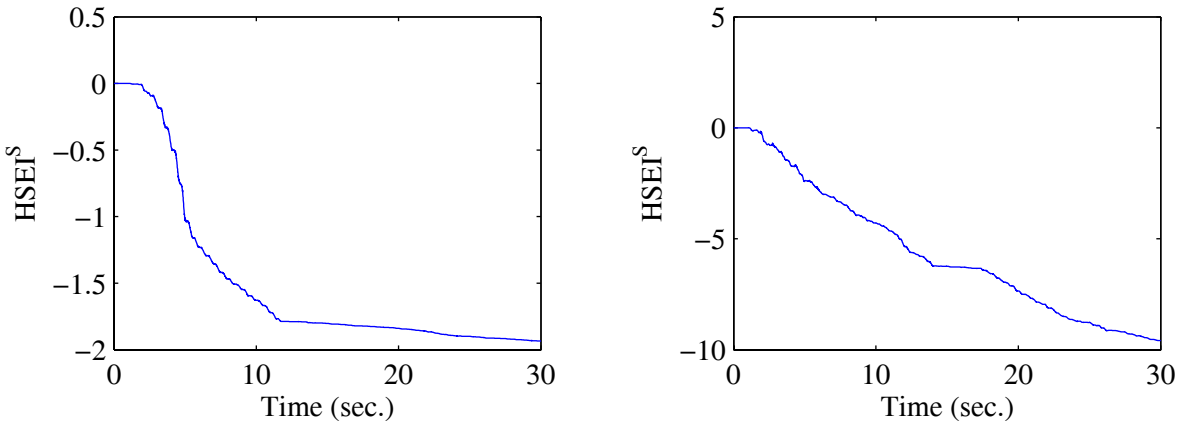

c. normalized energy for linear model

d. normalized energy for nonlinear model

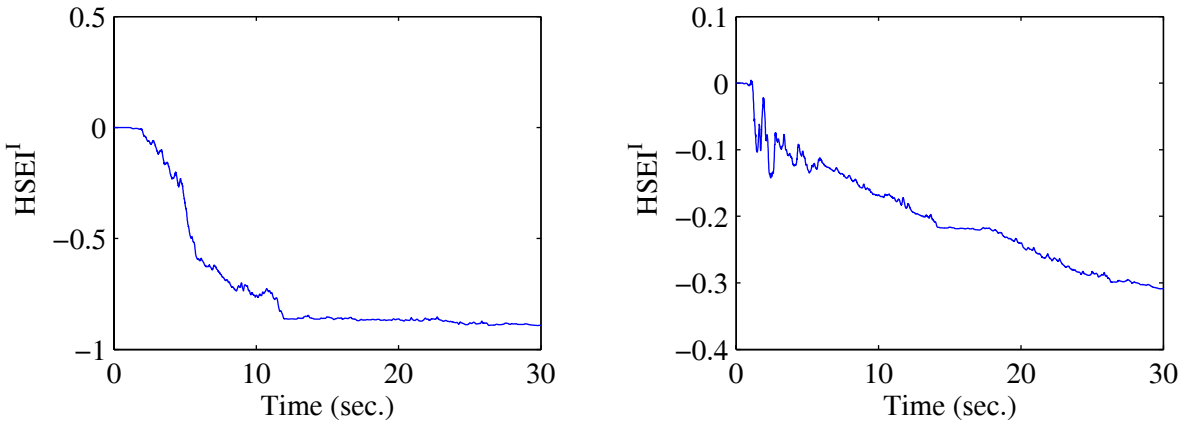

e. normalized energy for linear model

f. normalized energy for nonlinear model

Figure 8-4. Displacement response errors and HSEI with simulated actuator lag of 10 msec. for structure with 1.0 second period subjected El Centro ground motion

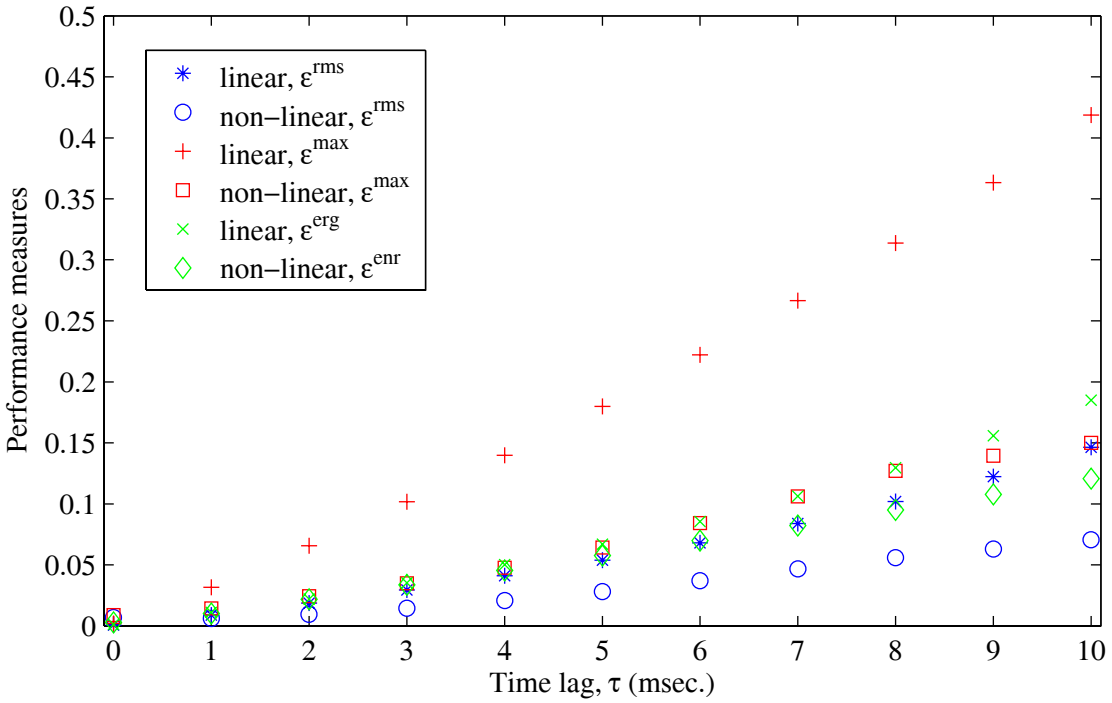

a. variation in performance measures with simulated actuator lag

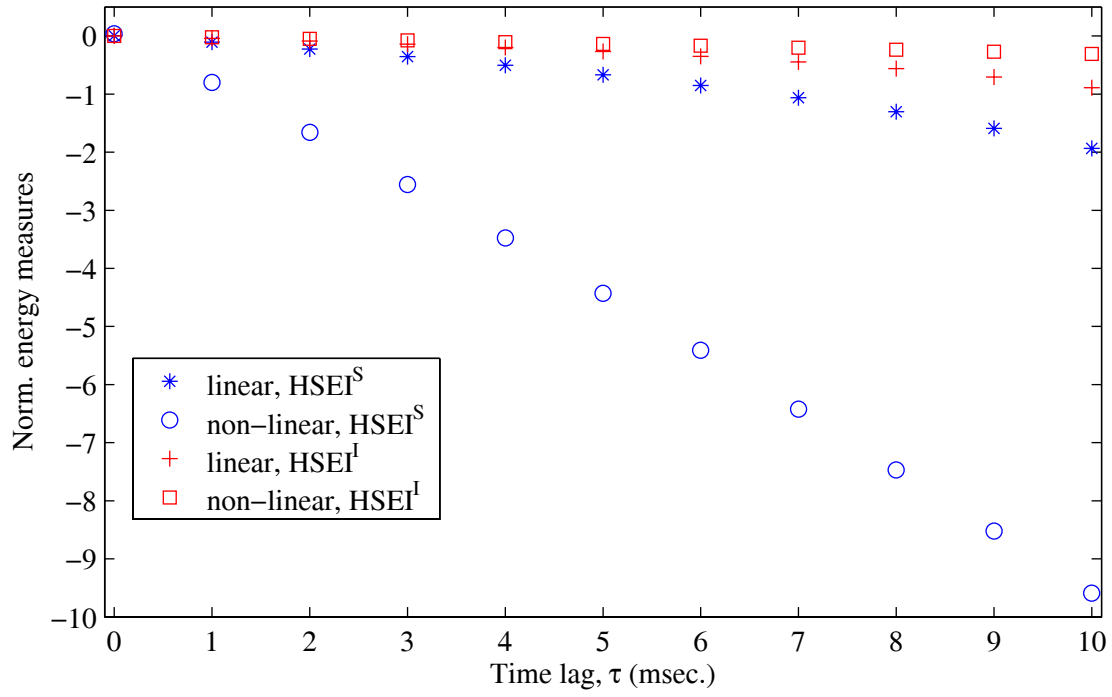

b. variation in HSEI with simulated actuator lag

Figure 8-5. Effects of systematic errors on structural response performance measures and HSEI

simulations range is [-0.9, 0] along the X-axis and the non-linear simulation data range is [-0.3,0] because the data was collected based on similar actuator lags. The difference in the resulting values of HSEI for the linear and non-linear simulations is shown in Figure 8-5b.

The data in Figure 8-6a shows that a linear relationship exists between the performance measures and the HSEI for the structural model considered. Also, equal values of $HSEI^I$ provides the same value of performance ε^{rms} for both the linear and the non-linear simulations. This characteristic is desirable so that the performance of a non-linear simulation can be predicted from a linear simulation. Figure 8-6b shows a large disparity between the linear and the non-linear simulations for the three performance measures compared to $HSEI^S$. The performance measures grow at a much faster rate for the linear simulations in Figure 8-6b.

Figure 8-7 presents a summary of the data collected for Case 2 in Table 8-10, which consists of the same structural model subjected to a different ground motion. An examination of the data supports the linear trends observed in Case 1. The main difference is that the normalized performance measure ε^{enr} increases at a faster rate compared to $HSEI^I$ and $HSEI^S$ for the non-linear simulations using the Tabas record. The other displacement-based performance measures decrease slightly for the Tabas record based on the same value of HSEI. The response spectra in Figures 8-1 and 8-2 show that the displacement response of a structure with a 1.0 second period is more sensitive to damping for the El Centro record than Tabas. Therefore, it is not surprising that the performance measures are less for Tabas since the simulated actuator lag causes a negative damping effect. A comparison of the relationship between performance measures and HSEI for the two ground motions indicates that this relationship is sensitive to the input excitation.

In Cases 3 and 4, the natural period of the structure is reduced to 0.33 seconds and subject to the same two ground motions. A summary of the data for Case 3 is shown in Figure 8-8 and the results of Case 4 are shown in Figure 8-9. The actuator lag is also simulated from 0 to 10 milliseconds in increments of 1 millisecond. It was concluded in Section 3.5 that the effects of restoring force lag on the structural response are dependent on the magnitude of the lag relative to the natural period of the structure. Therefore, the effects of the simulated errors are expected to be much worse for Cases 3 and 4 since the structural period is smaller. In fact, the linear simulations became unstable after the delay was increased above 5 milliseconds. This is why fewer data points are shown for the linear simulations in Figures 8-8 and 8-9. Also note that the X-axis scale has been increases

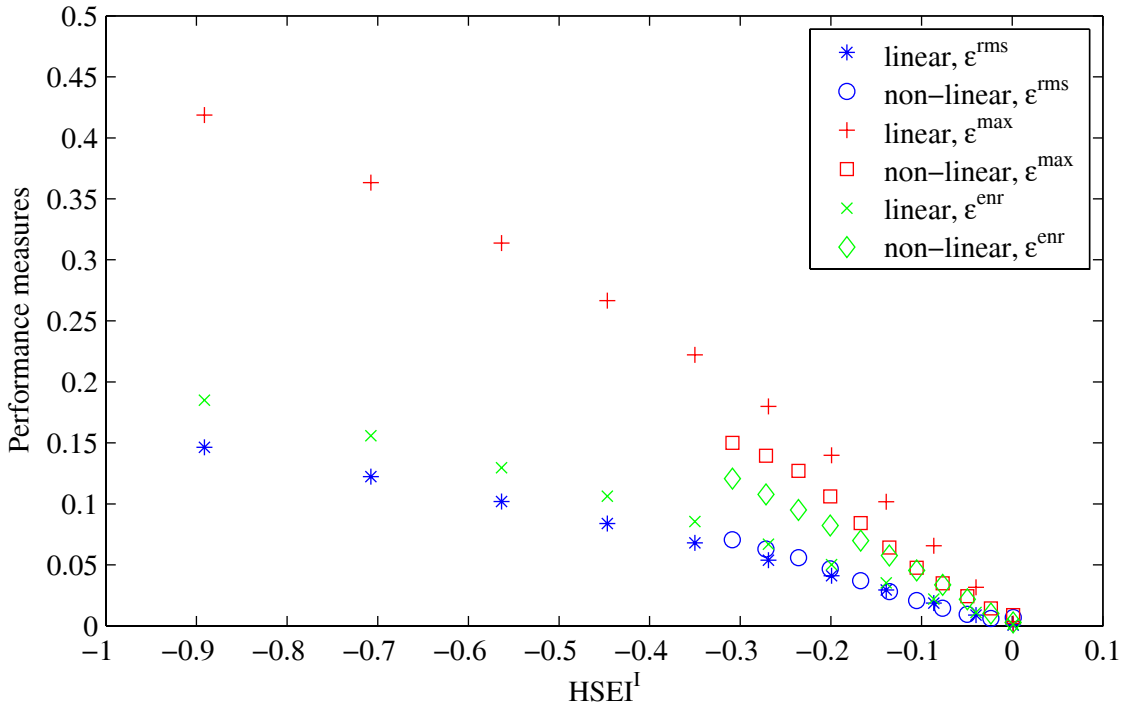

a. relationship between performance measures and $HSEI^I$

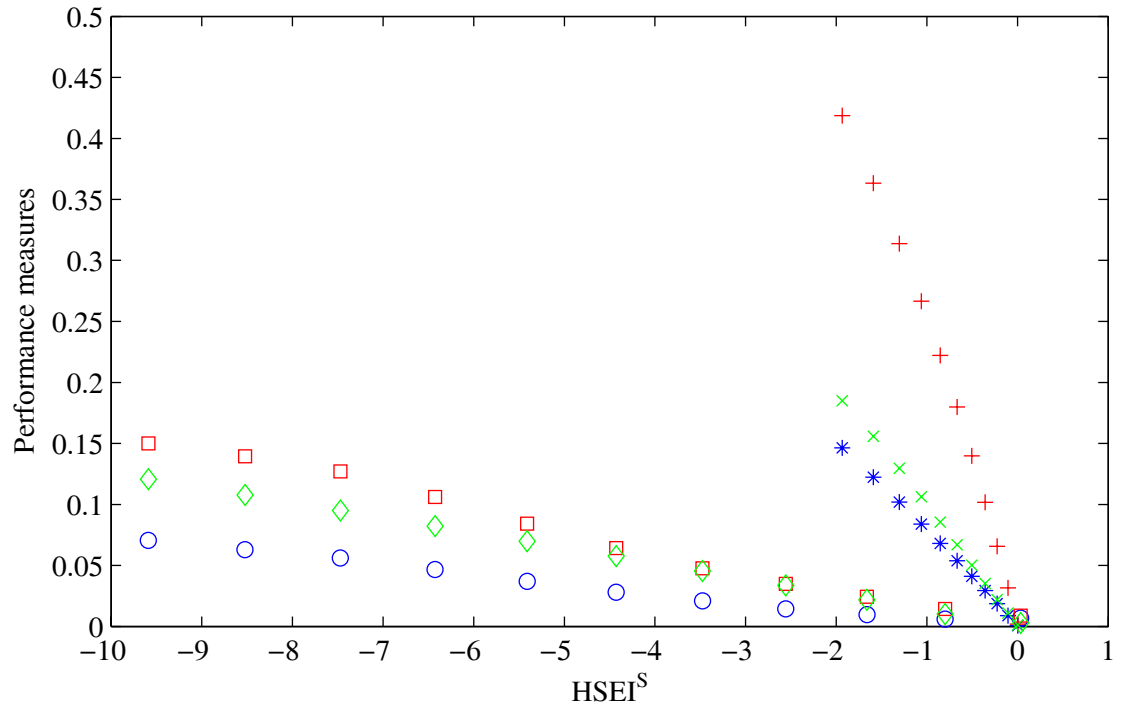

a. relationship between performance measures and $HSEI^S$

Figure 8-6. Evaluation of HSEI for Case 1 in Table 8-10: SDF with 1.0 sec. period subjected to El Centro

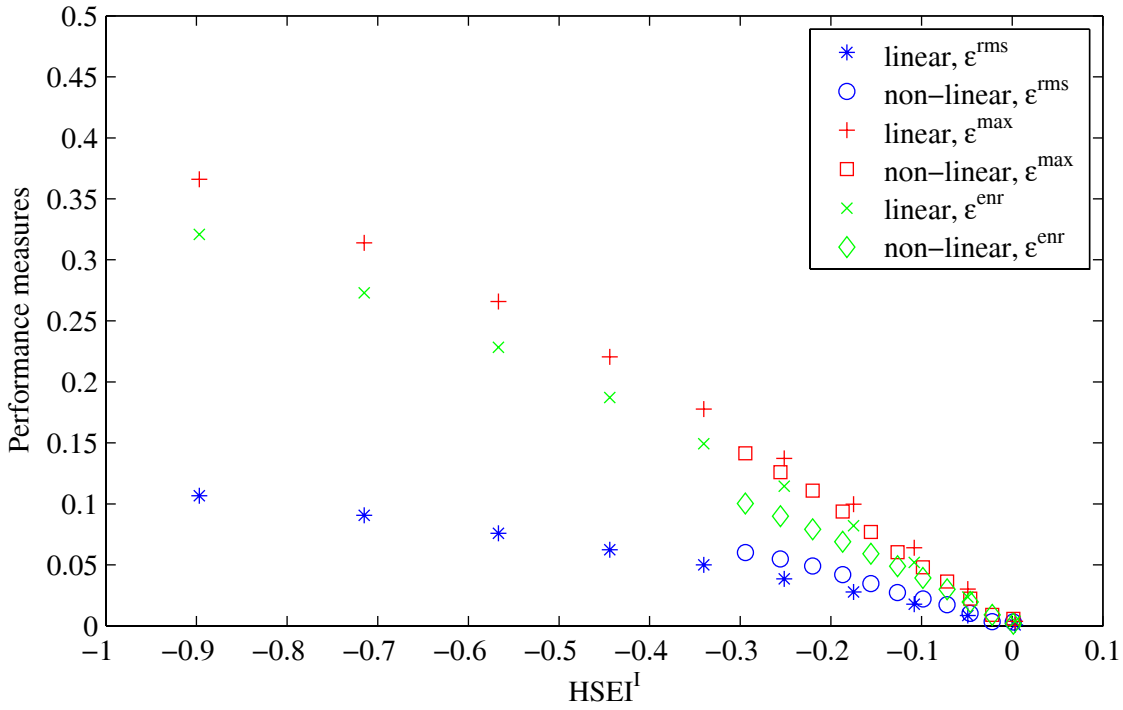

a. relationship between performance measures and $HSEI^I$

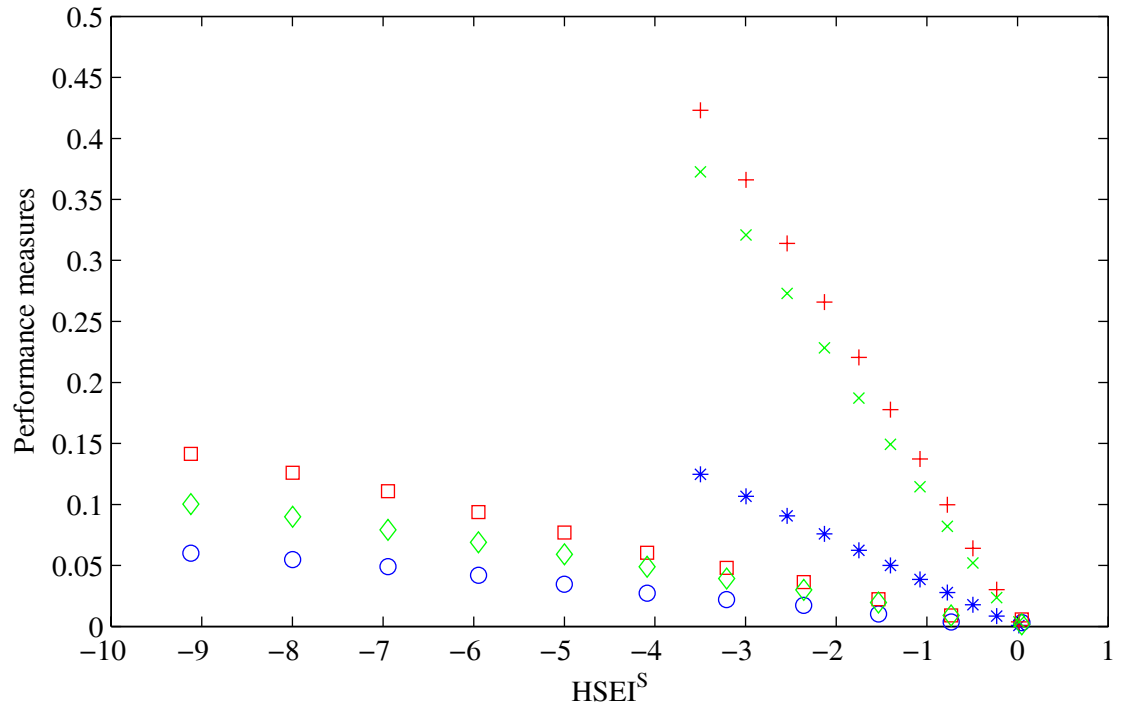

b. relationship between performance measures and $HSEI^S$

Figure 8-7. Evaluation of HSEI for Case 2 in Table 8-10: SDF with 1.0 sec. period subjected to Tabas

by a factor of five for $HSEI^I$ and by a factor of four for $HSEI^S$ compared to the plots for Cases 1 and 2. For $HSEI^I$ less than (-1), the input energy from errors in the experimental setup is greater than the input energy from the applied loads, and should be unacceptable regardless of the value of performance measures.

The comparison between the performance measures and $HSEI^I$ for the structure with a 0.33 second period in Figures 8-8 and 8-9 do not show the same linear trends as in Cases 1 and 2. There is a large disparity between the two ground motions, supporting an earlier observation that the relationship between performance measures and HSEI is sensitive to the input forces. The variation in the relationship between the performance parameters and $HSEI^I$ is likely due to the change in structural response and earthquake energy that is absorbed by the structural model. A more clear relationship exists between the performance parameters and $HSEI^S$ since the energy error is normalized by a constant value.

Similar to viscous damping, energy errors are likely to have a different effect on the structural response as the natural period of the structure is modified. Based on the response spectra for both records, the displacement response of the structural model with a 0.33 second period is less sensitive to damping compared to a structure with a 1.0 second period. The structure with a 0.33 second period falls in the acceleration-sensitive region of the spectra. Therefore, the displacement-based performance parameters are not sensitive as sensitive to the simulated errors. Note that ε^{enr} is the only performance parameter that is monotonically increasing compared to $HSEI^I$ for Case 3 and 4.

A summary of the results for Case 5 using a two degree of freedom structural model subjected to El Centro are shown in Figure 8-10. In this case, the linear simulations also resulted in an unstable response for a simulated actuator lag greater than 5 milliseconds. An evaluation of the displacement history and its frequency content showed that the instability resulted from the growth of the second mode of vibration. For the non-linear structural model, the second mode also dominated the overall response at the larger values of actuator lag, but the amplitude of the response remained bounded within reasonable limits of the response without errors. The response is bounded in the non-linear simulations because the additional hysteretic energy dissipation counterbalance the energy errors.

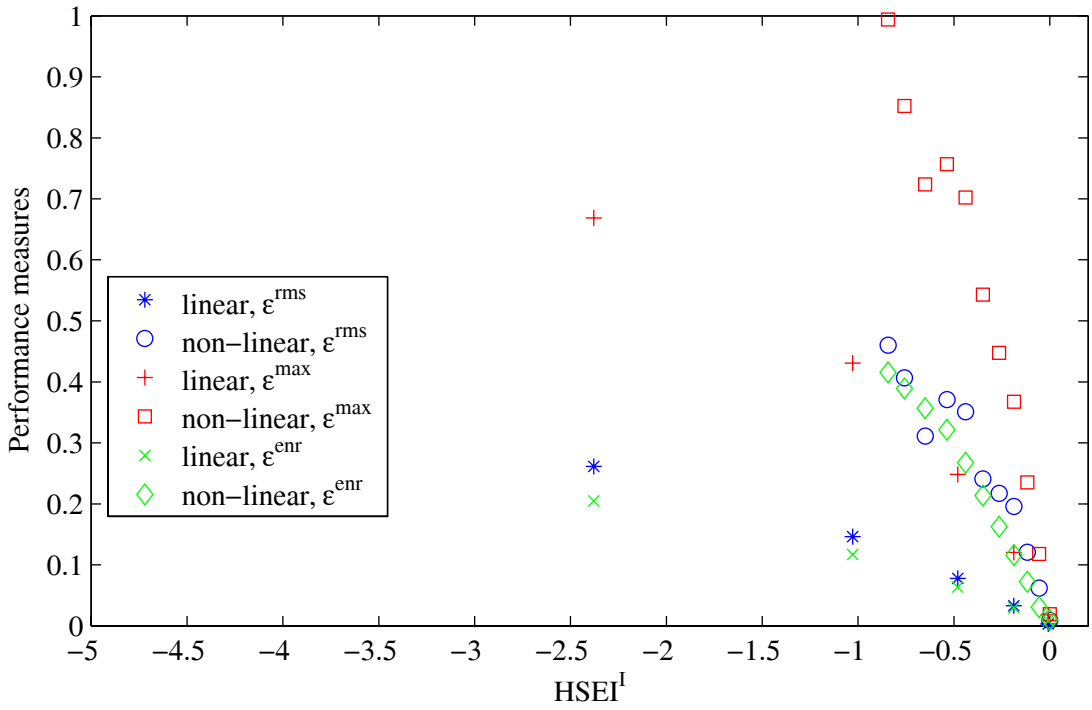

a. relationship between performance measures and $HSEI^I$

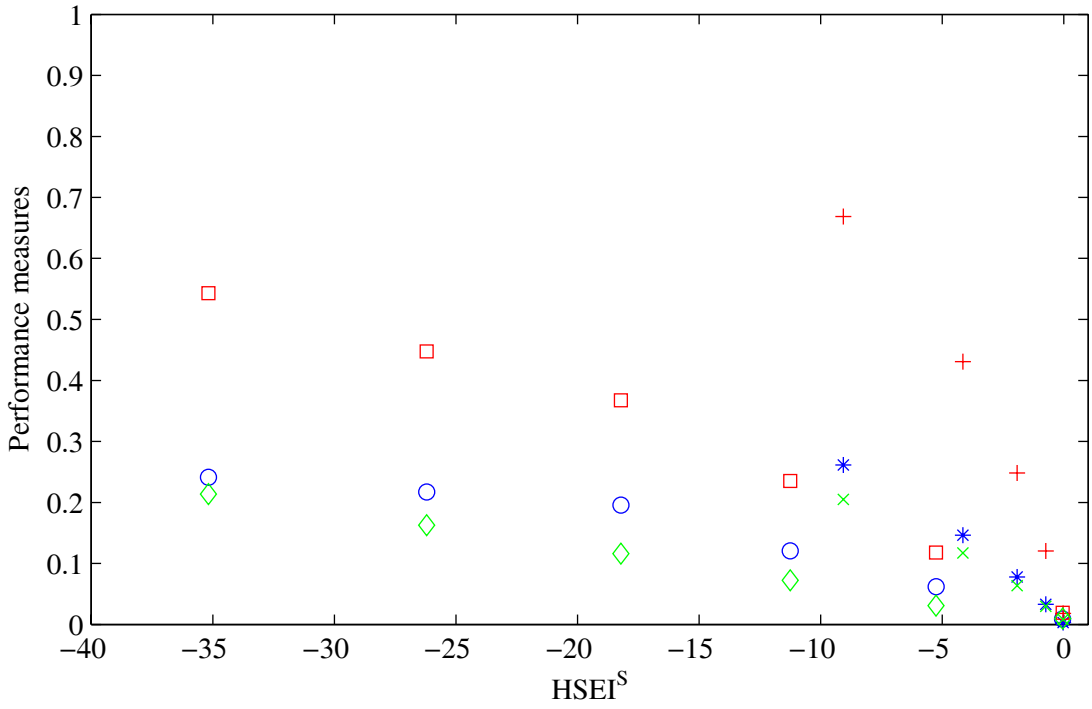

b. relationship between performance measures and $HSEI^S$

Figure 8-8. Evaluation of HSEI for Case 3 in Table 8-10: SDF with 0.33 sec. period subjected to El Centro

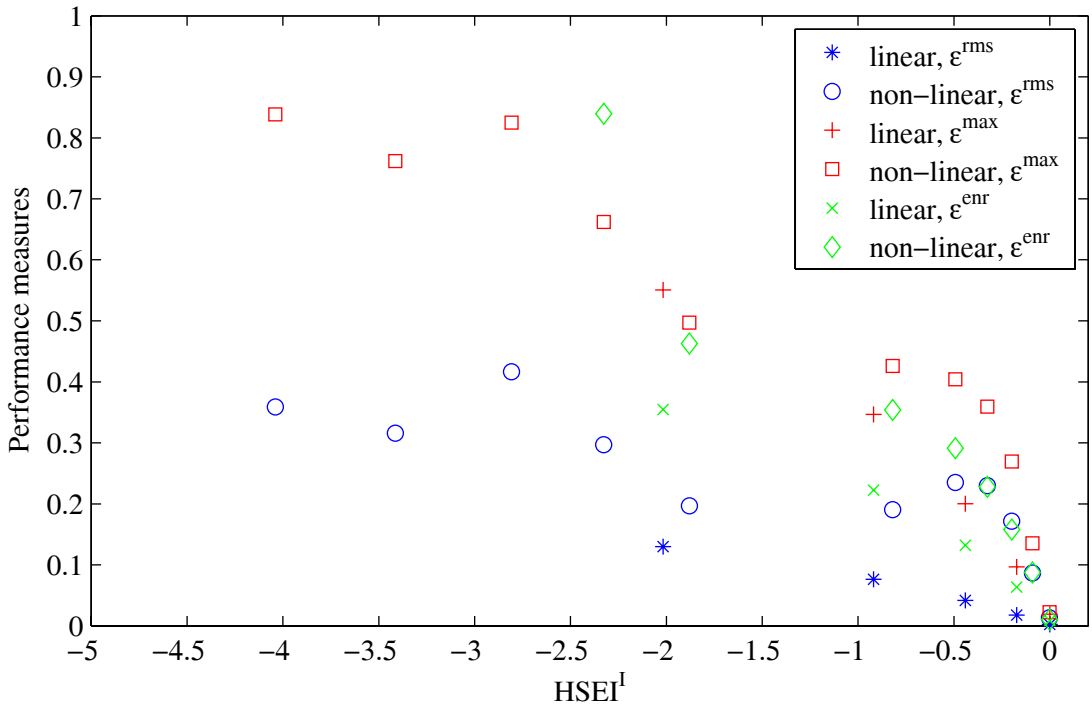

a. relationship between performance measures and $HSEI^I$

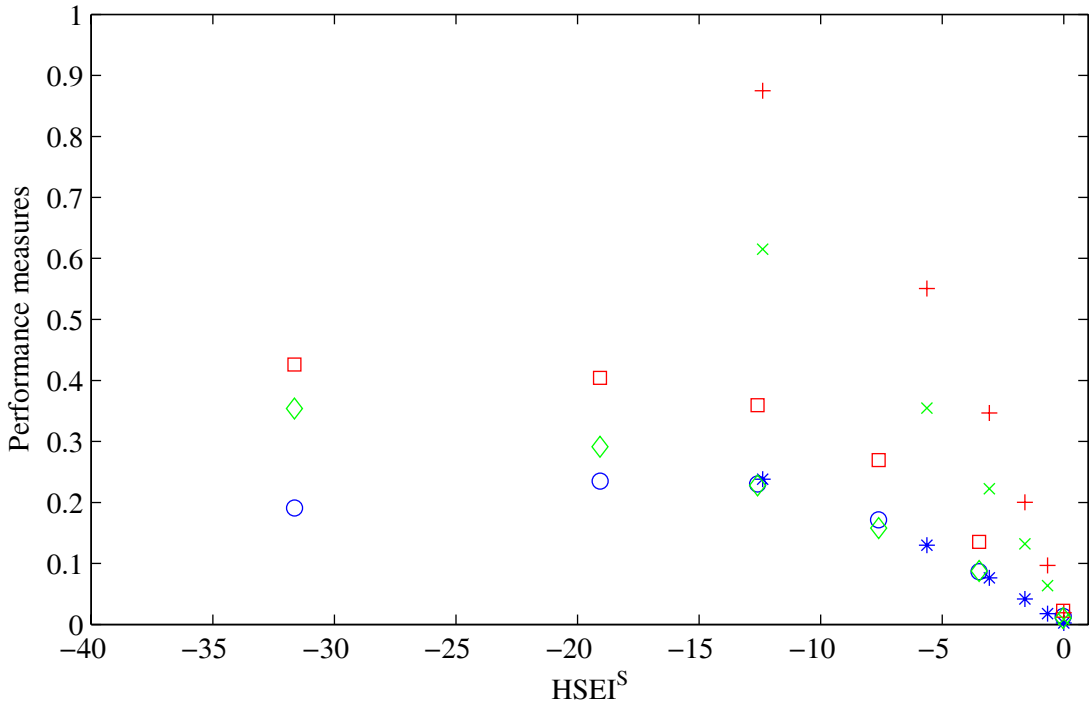

b. relationship between performance measures and $HSEI^S$

Figure 8-9. Evaluation of HSEI for Case 4 in Table 8-10: SDF with 0.33 sec. period subjected to Tabas

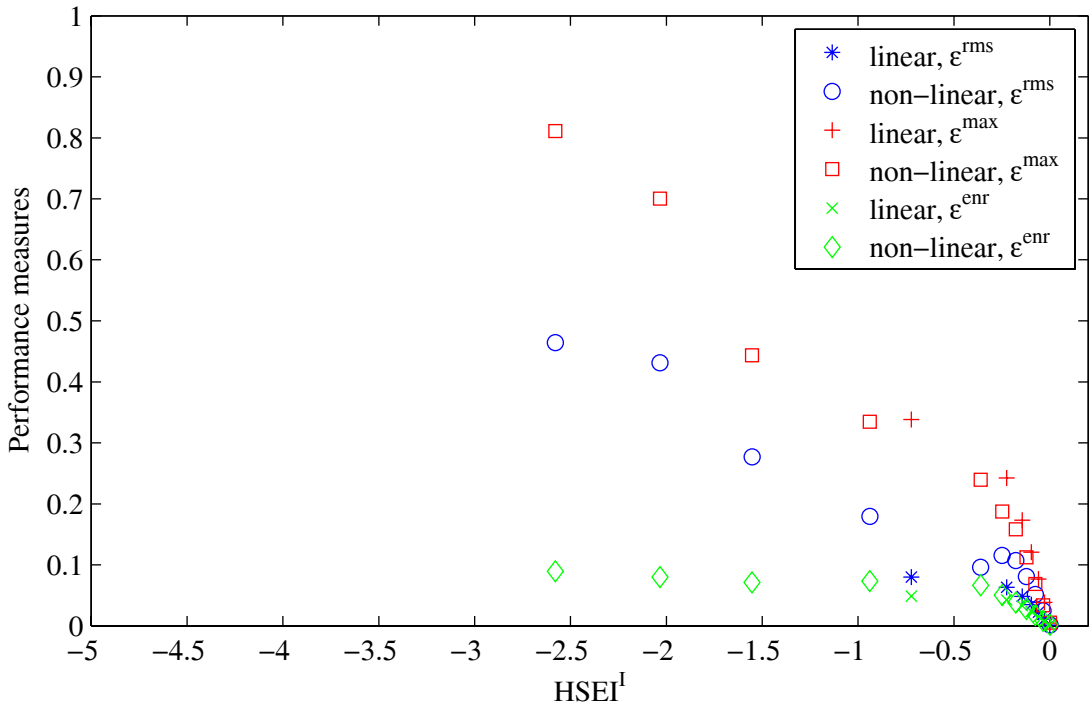

a. relationship between performance measures and $HSEI^I$

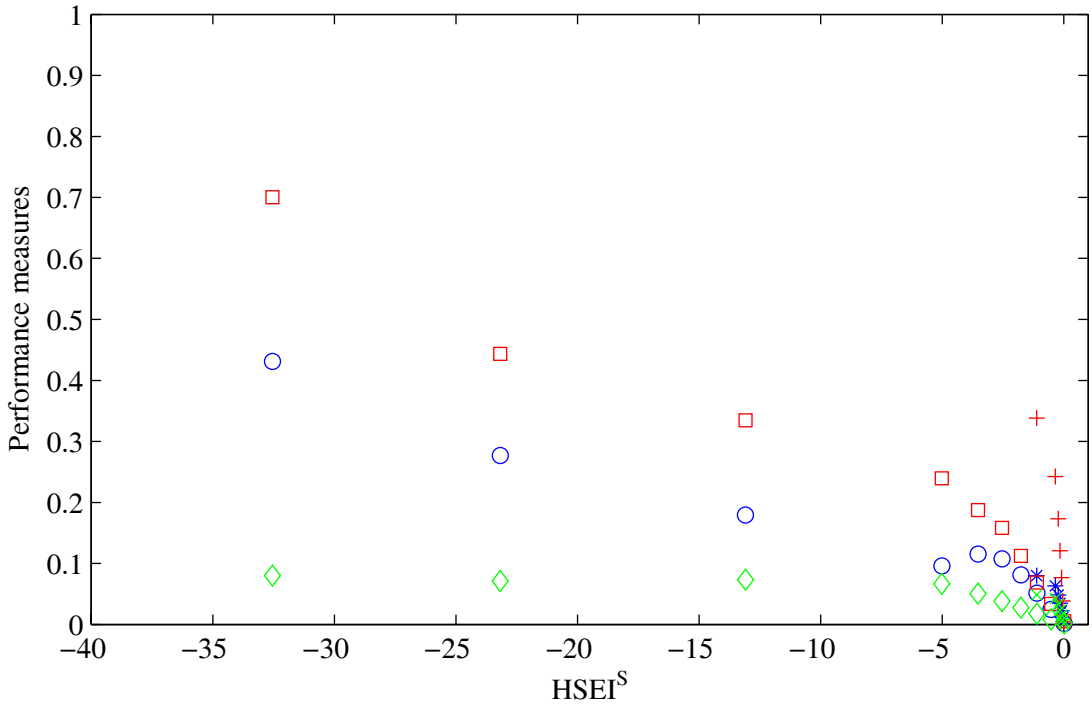

b. relationship between performance measures and $HSEI^S$

Figure 8-10. Evaluation of HSEI for Case 5 in Table 8-10: two-DOF with 1.0 sec. and 0.38 periods subjected to El Centro

The data in Figure 8-10 shows that the performance measures monotonically increase with increasing magnitudes of both HSEI. For the same actuator lag, the HSEI are greater for the 2-DOF model than the SDOF model with a period of 1 second, but are on same order of magnitude for the SDOF structure with a period of 0.33 seconds. In the 2-DOF model, the second mode is excited the most by the induced errors and dominates the response.

It is interesting to note that as the magnitude of the HSEI increases, the performance measure ε^{enr} remains constant at approximately 0.1. A constant performance measure ε^{enr} indicates that the energy input from the earthquake loads remains constant as the actuator lag is increased. However, there is a substantial increase in the energy input from experimental errors. This trend is evident by the increasing magnitude of both HSEI, due to the increase in energy error input relative to the constant strain energy and the input earthquake energy. The dominant response of the second mode is clearly a result of the energy input from errors in the experimental setup.

8.4.2 HSEI as Performance Parameters

Based on the simulation results of the three structural models with systematic errors and two ground motions, it appears that the relationship between the HSEI and the three observed performance parameters ε^{max}, ε^{rms}, ε^{enr}, is dependent on the applied loading. Particularly for Cases 3 through 5, the data presented includes large values of performance parameters and HSEI. The practical range of interest for the performance parameters is likely limited to values below 0.2. For example, if the performance parameter ε^{max} is considered, the maximum displacement is 20 percent larger or smaller than the expected displacement without errors. This is a reasonable upper limit of accuracy for reliable experimental tests results; larger errors should be unacceptable. Similarly, the practical range of interest for the absolute magnitude of HSEI should be less than unity, and even less for $HSEI^I$ since the primary source of energy into the structural model should be from the applied loads and not from experimental errors.

Figure 8-11 shows the data from Figure 8-10a zoomed to a range of practical interest. The X-axis for $HSEI^I$ is reduced to the range [-1.0, 0.1] and the Y-axis for the performance measures is reduced to the range [0, 0.2]. In this region, there is a dominant trend indicating that the growth of energy errors in the experimental substructures results in larger errors in the computed response of structures for both the linear and non-linear simulations. With the exception of ε^{rms} for the non-

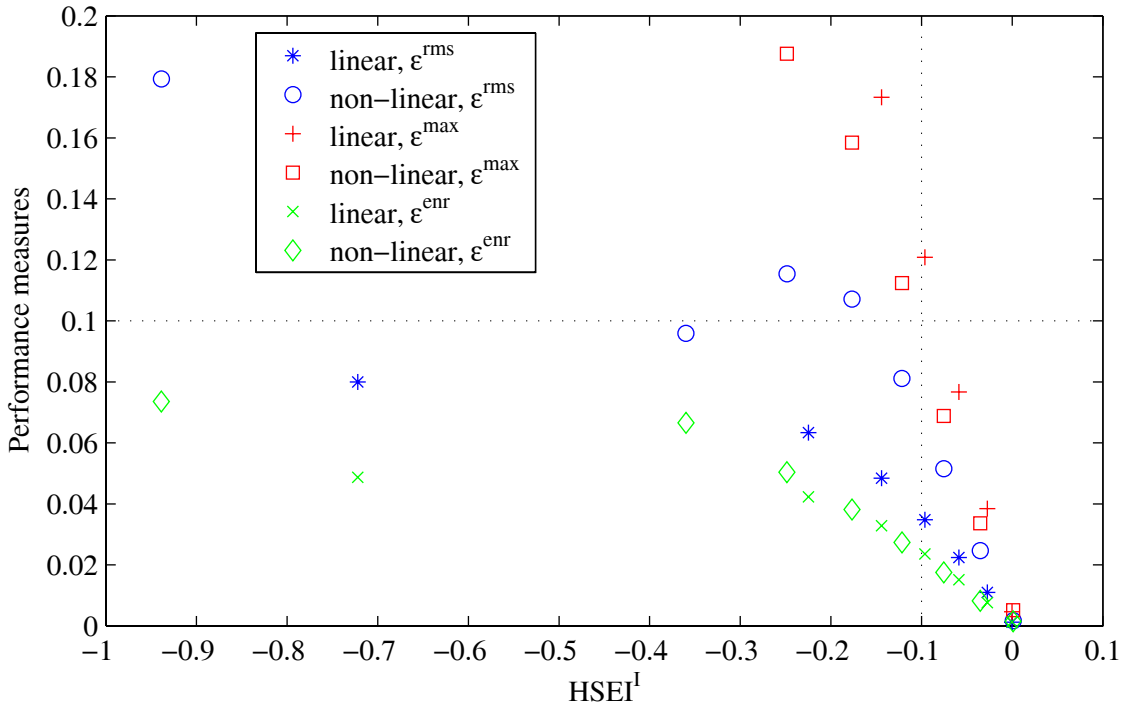

Figure 8-11. Relationship between performance measures and $HSEI^I$ for Case 5 in Table 8-10: 2-DOF with 1.0 sec. and 0.38 periods subjected to El Centro

linear simulations, all of the remaining performance measures are monotonically increasing with HSEI.

As an example of application using HSEI, a hybrid simulation is considered for the structural model examined in Case 5 of Table 8-10. The relationship between the performance measures and the HSEI is shown in Figure 8-11. If the tolerance limit is specified as 10 percent accuracy based on the performance measure ε^{max}, then the threshold values for $HSEI^I$ can be set to -0.1 for both a linear and a non-linear simulation. $HSEI^I$ can be computed during the simulation, providing a real-time measure of the performance of the test. Errors exceeding the predetermined limits of -0.1 can trigger a warning, allowing the opportunity to pause or stop the experiment meanwhile the experimental setup is examined. After verifying that the performance of the actuators is accurate, the test may be continued with improved confidence in the results.

8.5 SUMMARY

A simple method was devised to estimate the severity of errors in experimental substructures during a hybrid simulation. HSEI were proposed based on the computed energy errors normalized by the maximum recoverable strain energy and the input earthquake energy. A relationship between the HSEI and accepted performance parameters describing the accuracy of the simulation was developed using three different structural models and two ground motions. The results of this study indicate that HSEI can be used to detect the severity of errors in a simulation, and can therefore be used as performance parameters to predict accuracy of the results. However, the relationship between the HSEI and conventional performance parameters needs to be examined for each particular structure and the ground motions under consideration since the magnitude of HSEI depend on the structural model and input excitation. Once the sensitivity of the structural response to experimental errors has been established, the appropriate threshold values can be determined for the HSEI to monitor and insure the quality of the hybrid simulation results. A significant advantage of the proposed use of HSEI is that errors can be monitored in real-time as the simulation is in progress.

The use of HSEI is particularly useful to geographically distributed hybrid simulations. In such tests, the principal investigator cannot be present at all of the experimental sites to verify that the performance of the test equipment is adequate. HSEI can be used during the hybrid simulation to predict the severity of the errors on the test results or to identify the source of errors. Depending on the magnitude of the HSEI, the principal investigator may decide to pause the experiment while the source of error is inspected.

9 Summary and Conclusions

The experimental studies described in this report are the first-ever geographically distributed hybrid simulations using real-time based continuous algorithms. To conduct these tests and improve the quality of the result, a review of integration algorithms and implementation techniques for hybrid simulation was conducted. The sources of error in the test setup were identified and methods to evaluate and mitigate the effect of these errors were examined. Several needs were identified and techniques were proposed to improve the reliability of the results for geographically distributed hybrid simulations. The key contributions and findings presented in this dissertation are listed below.

1. A review of algorithms used to integrate the equation of motion showed that non-iterative methods, including explicit and operator partitioning methods, are much easier to implement than iterative implicit methods. Implicit methods can provide improved accuracy and stability, but integration methods that are simple to implement without a significant loss of accuracy are more convenient, particularly in geographically distributed hybrid simulations.
2. Mitigation of experimental errors is crucial to the results of a hybrid simulation. Various simulations and analytical models were used to demonstrate the effects of errors on the dynamic response of structures.

3. Several techniques have been employed to load the experimental substructures in a hybrid simulation, including ramp-and-hold, slow continuous testing, and real-time testing methods. Force relaxation that occurs during the hold phase in the conventional ramp-and-hold technique can introduce force measurement errors into the test. Continuous testing methods at slow and fast rates can improve the simulation results.

4. A distributed hardware architecture based on event-driven controllers that allows for the implementation of various hybrid simulation algorithms was presented. This architecture permits real-time testing, continuous testing, and multiple substructure testing in a local or distributed configuration using the Internet.

5. A notable advantage of the proposed event-driven controller is that continuous testing techniques based on real-time algorithms can be implemented for geographically distributed applications where communication and other tasks may have random completions times.

6. The effectiveness of the proposed hardware architecture based on an event-driven scheme was demonstrated in a series of experiments. The response of a structural model was determined using hybrid simulation, where the integration of the equation of motion was carried out at a remote location relative to the location of two experimental substructures. All connections were established using the TCP/IP Internet communication protocol. The test results verified a continuous load history on the experimental substructures for a majority of integration time steps. The continuity of the tests was jeopardized in a few steps with severe network delays. As a result, the experimental substructures where subjected to a hold phase, but this occurred in less than two percent of the steps.

7. An evaluation of the test results showed that accurate and reliable results were obtained from the geographically distributed hybrid simulations. The test results compared well to hybrid simulations using a conventional local testing configuration and to purely numerical simulations.

8. A simple formulation was developed to estimate the severity of experimental errors. The errors in the test setup were characterized in terms of the energy that is added or dissipated by the experimental substructures as a result of displacement control errors in the actuators.

9. Hybrid Simulation Error Indicators (HSEI) were proposed to monitor the quality of a hybrid simulation as the test progresses. The HSEI are based on normalized measures of the energy errors in the experimental substructures. It was shown the HSEI can be used to detect the severity of the experimental errors during the hybrid simulation and predict the quality of the simulation results.

References

[1] Anderson, E.L. and Mahin, S.A.(2002). Influence of substructure yielding on seismically isolated bridges designed according to the AASHTO Guide Specification for Seismic Isolation Design. *Proceedings, Seventh U.S. National Conference on Earthquake Engineering*, EERI.

[2] Andrade, L. (2001). Parmatlab: Distributed processes over matlab workers. *Matlab Central File Exchange*, http://www.mathworks.com/matlabcentral/.

[3] Bathe, K.-J. (1996). *Finite Element Procedures*. Prentice Hall.

[4] Blakeborough, A., Williams, M.S., Darby, A.P. and WIlliams, D.M. (2001). The development of real-time substructure testing. *Dynamic Testing of Structures: Papers of a Theme, Philosophical Transactions of the Royal Society: Mathematical, Physical and Engineering Sciences*, 359:1869-1891.

[5] Campbell, S. and Stojadinovic, B. (1996). A system for simultaneous pseudodynamic testing of multiple substructures. *Proceedings, Sixth U.S. National Conference on Earthquake Engineering*, EERI.

[6] Chang, S.-Y. (1997). Improved numerical dissipation for explicit methods in pseudodynamic tests. *Earthquake Engineering and Structural Dynamics*, Wiley, 26(9):917-929.

[7] Chang, S.-Y., Tsai, K.-C. and Chen, K.-C. (1999). Improved time integration for pseudodynamic tests. *Earthquake Engineering and Structural Dynamics*, Wiley, 27(7):711-730.

[8] Chang, S.-Y. (2002). Explicit pseudodynamic algorithm with unconditional stability. *Journal of Engineering Mechanics*, ASCE, 128(9):935-947.

[9] Chopra, A.K. (1995). *Dynamics of Structures*. Prentice-Hall, Inc.

[10] Clough, R.W. and Penzien, J. (1993). *Dynamics of Structures, Second Edition*. McGraw Hill.

[11] Combescure, D. and Pegon, P. (1997). Alpha-operator splitting time integration technique for pseudodynamic testing error propagation analysis. *Soil Dynamics and Earthquake Engineering*, Elsvier, 16(7-8):427-443.

[12] Constantinou, M.C. et al. (1993). NCEER-Taisei Corporation research program on sliding seismic isolation systems for bridges: experimental and analytical study of a

friction pendulum system (FPS). *Report NCEER-93-0020*, National Center for Earthquake Engineering Research, State University of New York, Buffalo.

[13] Conte, J.P. and Trombetti, T.L. (2000). Linear dynamic modeling of a uni-axial shaking table system. *Earthquake Engineering and Structural Dynamics*, Wiley, 29(9):1375-1404.

[14] Darby, A.P., Blakeborough, A. and Williams, M.S. (1999). Real-time substructure test using hydraulic actuator. *Journal of Engineering Mechanics*, ASCE, 125(10):1133-1139.

[15] Darby, A.P., Blakeborough, A. and Williams, M.S.(2001). Improved control algorithm for real-time substructure testing. *Earthquake Engineering and Structural Dynamics*, Wiley, 30(3):431-448.

[16] Dermitzakis, S.N. and Mahin, S.A. (1985). Development of substructuring techniques for on-line computer controlled seismic performance testing. *Report UCB/ EERC-85/04*, Earthquake Engineering Research Center, University of California, Berkeley.

[17] dSPACE. (2001). *dSPACE GmbH*. http://www.dspaceinc.com/

[18] Fenves, G.L., McKenna, F.M., Scott, M.H. and Takahashi, Y. (2004). An object oriented software environment for collaborative network simulation. *Proceedings, 13th World Conference on Earthquake Engineering,* Paper No. 1492.

[19] Fillipou, F. (2002). *CE220 Course Notes*. Department of Civil and Environmental Engineering. University of California, Berkeley.

[20] Harel. D. (1987). Statecharts: A visual formalism for complex systems. *Science of Computer Programming*, 8:231-274.

[21] Harris, H.G. and Sabnis, G.M. (1999). *Structural Modeling and Experimental Techniques, Second Edition*. CRC Press.

[22] Hilber, H.M., Hughes, T.J.R. and Taylor, R.L. (1977). Improved numerical dissipation for time integration algorithms in structural dynamics. *Earthquake Engineering and Structural Dynamics*, Wiley, 5(3):283-292.

[23] Horiuchi, T., Nakagawa, M., Sugano, M. and Konno, T. (1996). Development of a real-time hybrid experimental system with actuator delay compensation. *Eleventh World Conference on Earthquake Engineering,* Elsevier Science Ltd, Paper No. 660.

[24] Horiuchi, T., Inoue, M., Konno, T. and Namita. Y. (1999). Real-time hybrid experimental system with actuator delay compensation and its application to a piping system with energy absorber. *Earthquake Engineering and Structural Dynamics*, Wiley, 28(10):1121-1141.

[25] Hughes, T.J.R. and Liu, W.K. (1978). Implicit-explicit finite elements in transient analysis: stability theory. *Journal of Applied Mechanics*, ASME, 45(2):371-374.

[26] Kelly, J.M., Buckle, I.G. and Tsai, H.-C. (1985). Earthquake simulator testing of a base-isolated bridge deck. *Report UCB/EERC-85/09*, Earthquake Engineering Research Center, University of California, Berkeley.

[27] Kelly, J.M. (1985). Aseismic base isolation. *The Shock and Vibration Digest*, 17(7):3-14.

[28] Mahin S.A., Shing, P.B., Thewalt, C.R. and Hanson, R.D. (1989). Pseudodynamic test method - Current status and future direction. *Journal of Structural Engineering*, ASCE, 115(8):2113-2128.

[29] Magonette, G.E. and Negro, P. (1998). Verification of the pseudodynamic test method. *European Earthquake Engineering*, PUB 40-50.

[30] Magonette, G. (2001). Development and application of large-scale continuous pseudo-dynamic testing techniques. *Dynamic Testing of Structures: Papers of a Theme, Philosophical Transactions of the Royal Society: Mathematical, Physical and Engineering Sciences*, 359:1771-1799.

[31] Mathworks (2003). *MATLAB, The language of technical computing*. The Mathworks Inc., Natick, MA.

[32] Merritt, H.E. (1967). *Hydraulic Control Systems*. Wiley.

[33] Molina, F.G., Verzeletti, G., Magonette, G., Buchet, P.H. and Geradin, M. (1998). Bi-directional pseudodynamic test of a full-size three-story building. *Earthquake Engineering and Structural Dynamics*, Wiley, 28(12):1541-1566.

[34] Molina, F.G., Verzeletti, G., Magonette, G., Buchet, P.H., Renda, M., Geradin, M., Parducci, A., Mezzi, M., Pacchiarotti, A., Federici, L., and Mascelloni, S. (2002). Pseudodynamic tests on rubber base isolators with numerical substructuring of the superstructure and strain-rate effect compensation. *Earthquake Engineering and Structural Dynamics*, Wiley, 31(98):1563-1582.

[35] MOST (2003). Multisite on-line simulation test. *NEESgrid*, http://www.neesgrid.org/most/.

[36] Nakashima, M., Kaminosono, T., Ishida, I. and Ando, K. (1990). Integration techniques for substructure pseudo dynamic test. *Proceedings*, *Fourth U.S. National Conference on Earthquake Engineering*, EERI.

[37] Nakashima M., Kato, M. and Takaoka, E. (1992). Development of real-time pseudo dynamic testing. *Earthquake Engineering and Structural Dynamics*, Wiley, 21(1):79-92.

[38] Nakashima M. and Masaoka, N. (1999). Real-time on-line test for MDOF systems. *Earthquake Engineering and Structural Dynamics*, Wiley, 28(4):393-420.

[39] Newmark, N.M. (1959). A method of computation for structural dynamics. *Journal of Engineering Mechanics*, ASCE, VOL:67-949.

[40] OpenSees (2003). *Open System for Earthquake Engineering Simulation*. Pacific Earthquake Engineering Research Center. http://opensees.berkeley.edu/.

[41] Pegon, P, and Pinto, A.V. (2000). Pseudo-dynamic testing with substructuring applications at the ELSA Laboratory. *Earthquake Engineering and Structural Dynamics*, Wiley, 29(7):905-925.

[42] Pinto, A., Pegon, P., Magonnete, G., Molina, J., Buchet. G. and Tsionis, G. (2002). Pseudodynamic test on a large-scale model of an existing RC bridge using non-linear substructuring and asynchronous motion. *EUR 20525 EN*, European Laboratory for Structural Assessment. Ispra, Italy.

[43] Rodgers, J.E. and Mahin S.A. (2002). Shaking Table Tests Examining Effects of Connection Behavior on a Steel Moment Frame System with Idealized Connections. *Proceedings, Seventh U.S. National Conference on Earthquake Engineering*, EERI.

[44] Royal Society (2001). Dynamic testing of structures: Papers of a theme. *Philosophical Transactions of the Royal Society: Mathematical, Physical and Engineering Science*, 359.

[45] Rydesater, P. (2001). TCP/UDP/IP Toolbox 2.0.4. *Matlab Central File Exchange*, http://www.mathworks.com/matlabcentral/.

[46] Shing, P.B. and Mahin, S.A. (1983). Experimental error propagation in pseudodynamic testing. *Report UCB/EERC-83/12*, Earthquake Engineering Research Center, University of California, Berkeley.

[47] Shing, P.B. and Mahin, S.A. (1984). Pseudodynamic test method for seismic performance evaluation: theory and implementation. *Report UCB/EERC-84/01*, Earthquake Engineering Research Center, University of California, Berkeley.

[48] Shing, P.B. and Mahin, S.A. (1988). Rate-of-loading effects on pseudodynamic tests. *Journal of Structural Engineering*, ASCE, 114(11):2403-2420.

[49] Shing P.B., Vannan, M.T. and Cater, E. (1991). Implicit time integration for pseudodynamic tests. *Earthquake Engineering and Structural Dynamics*, Wiley, 20(6):551-576.

[50] Shing, P.B., Bursi, O.S. and Vannan, M.T. (1994). Pseudodynamic tests of a concentrically braced frame using substructuring techniques. *Journal of Construction Steel Research*, 29(1-3):121-148.

[51] Shing, P.B., Nakashima, M. and Bursi, O.S. (1996). Application of pseudodynamic test method to structural research. *Earthquake Spectra*, EERI, 12(1):29-54

[52] Shing, P.B., Spacone, E. and Stauffer, E. (2002). Conceptual design of fast hybrid test system at the University of Colorado. *Proceedings, Seventh U.S. National Conference on Earthquake Engineering*, Boston.

[53] Schneider, S.P. and Roeder, C.W. (1994). An inelastic substructure technique for the pseudodynamic test method. *Earthquake Engineering and Structural Dynamics*, Wiley, 23(7):761-775.

[54] Sommervile, P. (1997). Suite of earthquake ground motions for analysis of steel moment frame structures. *Report SAC/BD-97/03*, Woodward-Clyde Federal Services, SAC Steel Project.

[55] Stojadinovic, B., Mosalam, K., Mahin, S.A. and Moehle, J.P. (2002). Reconfigurable Reaction Wall Seismic Testing Facility. *Proceedings, Seventh U.S. National Conference on Earthquake Engineering*, EERI.

[56] Stoten, D. and Magonette, G. (2001). Developments in the automatic control of experimental facilities. *ECOEST2-ICONS Report No. 9*. Laboratorio Nacional de Engenharia Civil, Lisboa, Port.

[57] Systran (2003). SCRAMNet Network. http://www.systran.com/scmain.html.

[58] Takanashi, K. (1975). Non-linear earthquake response analysis of structures by a computer-actuator on-line system.

[59] Takanashi, K. and Nakashima, M. (1987). Japanese activities on on-line testing. *Journal of Engineering Mechanics*, ASCE, 113(7):1014-1032.

[60] Thewalt, C.R. and Mahin, S.A. (1987). Hybrid solutions techniques for generalized pseudodynamic testing. *Report UCB/EERC-87/09*, Earthquake Engineering Research Center, University of California, Berkeley.

[61] Thewalt, C.R. and Roman, M. (1994). Performance parameters for pseudodynamic tests. *Journal of Structural Engineering*, ASCE, 120(9):2768-2781.

[62] Thoen, B. (2003) Personal Communication. MTS Staff Scientist.

[63] Tsai, K.-C., Yeh, C.-C., Yang, Y.-S. Wang, K.-J., Wang, S.-J. and Chen, P.-C. (2003). Seismic Hazard Mitigation: Internet-based hybrid testing framework and examples. *International Colloquium on Natural Hazard Mitigation: Methods and Applications*, France, May 2003.

[64] Uang C.-M. and Bertero, V.V. (1990). Evaluation of Seismic Energy in Structures. *Earthquake Engineering and Structural Dynamics*, Wiley, 19(1):77-90.

[65] van Dam, M. (2000). Effects of hysteretic degradation on seismic response of steel structures. M.Eng Thesis, Dept. of Civil and Environmental Engineering, University of California, Berkeley.

[66] Watanabe, E., Kitada, T., Kunitomo, S. and Nagata, K. (2001). Parallel pseudo-dynamic seismic loading test on elevated bridge system through the Internet. *The Eight East Asia-Pacific Conference on Structural Engineering and Construction*, Singapore, December 2001.